EARTHQUAKE LOCATIONS AND THREE-DIMENSIONAL SEISMIC STRUCTURE OF SOUTHERN PERU

by

Paul S. Cunningham

S.B., Massachusetts Institute of Technology
(1984)

SUBMITTED TO THE DEPARTMENT OF EARTH, ATMOSPHERIC, AND PLANETARY SCIENCES IN PARTIAL FULFILLMENT OF THE REQUIREMENTS FOR THE DEGREE OF

MASTER OF SCIENCE

in

Earth and Planetary Science

at the

MASSACHUSETTS INSTITUTE OF TECHNOLOGY

May, 1984

Signature of Author .....
Department of Earth, Atmospheric, and Planetary Sciences
May 24, 1984

Certified by ...
Steven W. Roecker
Thesis Advisor

Accepted by .....
Theodore R. Madden
Chairman
Departmental Committee on Graduate Students

EARTHQUAKE LOCATIONS AND THREE-DIMENSIONAL SEISMIC STRUCTURE OF SOUTHERN PERU

by

Paul S. Cunningham

Submitted to the Department of Earth, Atmospheric, and Planetary Sciences in partial fulfillment of the requirements for the Degree of Master of Science in Earth and Planetary Science

ABSTRACT

Arrival time data, acquired in southern Peru during the summer of 1981, were used to relocated microearthquakes using three-dimensional structures to model lateral heterogeneities of the crust and upper mantle. The results of these relocations were very similar to the original hypocentral solutions computed by Grange(1983), indicating that the simple flat layered structures which he used were reasonable approximations to the actual structure. The tectonic characteristics of southern Peru were equally well defined with either set of earthquake locations. The most prominent feature, the bend in the Nazca plate as it is subducted under southern Peru, was located beneath the northern end of the volcanic arc in the region. North of the bend, the slab is being subducted at a shallow angle ($10^{\circ}-15^{\circ}$), while south of the bend, the slab is descending at a steeper angle ($25^{\circ}-30^{\circ}$). These observations corroborated the theory of Barazangi and Isacks (1976;1979) that a wedge of aesthenosphere is required between the overridding and subducted plates, for subduction-related volcanism to occur. It was also shown that the contorted zone of the Nazca plate is parallel to the plate's direction of motion with respect to the South American plate.

A subset of the well located events was then used to perform three-dimensional velocity inversions in an attempt to model the seismic structure of the region. Criteria established by Roecker (1982) to aid in the interpretation of the inversion results were used. The features that appear from these results are the following: First, a velocity gradient seems to exist perpendicular to the coast. The velocities are higher in the southwest crossing the Moho under the coast, and decrease under the Western Cordillera of the Andes and the Altiplano. Second, the Moho at its deepest point under the Altiplano, seems to be at a depth of about 70 km. Third, the upper mantle seems to be a region where P and S velocities are gradually increasing with depth, with the exception of a few P velocity anomalies between 70 and maybe as much as 130 km depth. The average velocities for this region seem to be in the range of 7.5 to 8.0 km/s for the P, and 3.9 to 4.6 km/s for the S. The velocities for the anomalies were greater than 8.0 km/s and less than 7.5 km/s. Finally, an S wave low-velocity zone is seen between 100 and 130 km depth. However, it does not seem to be as pronounced as it was originally thought to be, when Wadati plots were made to determine V_P to V_S ratios for different depth slices.

Thesis Supervisor: Dr. Steven W. Roecker

Title: Research Associate

ACKNOWLEDGEMENTS

This thesis is dedicated to my parents and to the friends I have made during my years at MIT, especially the brothers at the Pi and the FWFW women.

Special thanks go to Peter Molnar who aroused my interest in this project; to Steve Roecker without whose help and guidance I would not have been able to do this paper; and to Debby Roecker for her help in eliminating many of the bureaucratic hurdles at MIT.

TABLE OF CONTENTS

CHAPTER 1

INTRODUCTION

The subduction of the Nazca plate beneath the western margin of South America, is the archtypical example of subduction of an oceanic plate beneath a continental plate. It is the object of many studies, not only to understand what is occurring along the western edge of South America (the "Andean " margin), but to gain insight into the processes which followed this same model in other parts of the world in past eras. Being a seismically active region, information can be gathered about the tectonic deformation from the crust down to hundreds of kilometers within the mantle. Distinctive features of the region can be recognized, an example being the deformation of the Nazca plate as it is subducted under southern Peru. By analyzing shallow and intermediate depth microearthquakes, the geometry of this particular feature as well as the patterns of deformation occurring within the crust can be better understood.

Temporary seismic networks were installed in central and southern Peru during the summers of 1980 and 1981 to record microearthquakes. The recorded P and S arrival times were used by Grange (1983) to study the deformation of the crust and of the Nazca plate subducting beneath South America. In the study carried out by this author, only the arrival times recorded in 1981 were used. With this data, earthquakes were relocated using three-dimensional models of the crust and upper mantle. Next, three-dimensional velocity inversions were carried out to determine the velocity structure of the region. The results were then analyzed in terms of the tectonics and seismic characteristics of the region.

This project was carried out be faculty members and students of the Massachusetts Institute of Technology and of the Université de Grenoble with help from staff of the Instituto Geofisico del Peru and other individuals.

This paper begins with a brief overview of the tectonics of southern Peru, a large portion of the information being based on work described in papers by members of this project (Grange (1983), Grange et al., (1984a;1984b)). Next, a review of the problem of determining earthquake hypocenters and inverting for the velocity structure is carried out in chapter 3. Chapter 4 describes the manner in which initial velocity structures were determined and the earthquakes relocated, along with an analysis of the seismicity patterns. The velocity inversions and the implications of their results are described in chapter 5. Appendix A contains a list of 396 events considered to be well located used in the velocity inversion. Appendix B contains the computer printouts of the inversion runs.

CHAPTER 2

THE TECTONICS OF SOUTHERN PERU

Earthquakes that occur at intermediate and deep depths within the subducted oceanic lithospheres define the geometry of the downgoing slabs. These seismic zones generally outline simple, inclined planes, but often show that the subducted lithosphere is contorted or discontinuous. For example, profiles of different parts of the subducted portion of the Nazca plate beneath South America show that the dip of the seimic zone varies between 10°–15° and 25°–30° [Swift and Carr (1974); Barazangi and Isacks (1976;1979)]. Under northern and central Peru, and again under central Chile, the seismic zone dips at a gentle angle (10°–15°), while under southern Peru, Bolivia and northern Chile the dip of the seismic zone is steeper (25°–30°).

Barazangi and Isacks (1976;1979) made profiles perpendicular to the coast, using data from the International Seismological Center. They inferred the existence of a discontinuity in the seismic zone trending northeast through 16° *S*, 72° *W*, and implied a tear in the slab (Figure 1). However, Hasegawa and Sacks (1981), using earthquake locations based on data from a local network of stations, pointed out that any discontinuity of the seismic zone would be small, the prominent feature being a contortion in the slab and not a tear (Figure 2). Corroborating this result, Grange (1983) and Grange et al. (1984a;1984b), using microearthquake data collected in 1980 and 1981, showed that profiles perpendicular to the coast had the same dips as those of Hasegawa and Sacks (1981), gradually becoming shallower towards the northwest (Figure 3). The focal depths of these earthquakes were as great as 250 km in the southeast but

no deeper than 130 km in the northwest. Profiles made parallel to the coast also showed a bend in the seismic zone with no offset of the seismic activity that would imply a tear between the two parts of the slab (Figure 4). Morever, maps of the earthquake epicenters at different depth intervals show a gradual broadening of the seismic zone to the northeast for depths greater than 100 km (Figure 5).

Grange (1983) and Grange et al. (1984a;1984b), also showed that the transition zone is parallel to the direction of motion of the Nazca plate relative to the South American plate (approximately $N80°E$) and not perpendicular to the coast as both Barazangi and Isacks (1976;1979) and Hasegawa and Sacks (1981) had implied. This can be clearly seen by observing that profiles perpendicular to the coast flatten out towards the northeast at large depths, while profiles parallel to $N80°E$ do not show any change in the dip of the seismic zone for each profile (Figure 6). This feature can also be seen if contours of the events at different depth ranges are made on a map (Figure 7). Because of this orientation, it is not necessary for the transition zone within the Nazca plate to migrate with respect to the South American plate.

Barazangi and Isacks (1976;1979) pointed out the lack of Quaternary volcanism of the South American plate in areas where the Nazca plate is being subducted at a shallow angle, and its occurrence where the subduction of the Nazca plate is at a steeper angle. They inferred that a wedge of aesthenospheric material must exist between the overriding plate and the subducted plate for subduction-related volcanism to occur. They also estimated the "tear" in the Nazca plate to be about 100 km southeast of the northernmost volcanoes. But the results of Grange et al. (1984a;1984b) show that the bending of the Nazca plate actually seems to occur under the northern

edge of the volcanic arc in southern Peru. This would further support Barazangi and Isacks's reasoning for the need of a wedge of aesthenosphere to exist between the plates.

The locations of shallow microearthquakes within the South American plate were divided into three belts parallel to the coast by Grange (1983), and Grange et al. (1984b): a group offshore between the trench and the coast following the 1800 m bathymetric contour, another beneath the coast, and a third under the Western Cordillera of the Andes. In addition, a few scattered microearthquakes were located within the Altiplano.

Both the offshore belt of activity and the belt beneath the coast, despite being separated by a gap, seem to be associated with the slip between the Nazca and South American plates. The offshore group appears to occur below the South American crust at the interface between the two plate. The group under the coast, though, does not seem to occur at the base of the crust, but between slabs of mantle lithosphere. The fault plane solutions for this last group do not show simple underthrusting, but a variety of deformation styles (Figure 8). Although each solution can be explained in terms of plate deformations, no clear interpretation for the group as a whole could be made. No fault plane solutions could be made for the offshore group due to the distribution of the recording stations.

The belt of earthquakes located under the Western Cordillera is situated 60 to 100 km from the coast, and occurs in both the crust and the mantle. The belt seems to terminate at about $16°S$ in the northwest direction, and in the seismicity maps of Grange (1983), extends only as far south as $17°S$. However, this does not appear to be the actual southern limit of the belt, but the result of the elimination of poorly located events in the region. The fault plane

solutions for some of these events show a rather unexpected deformation style. Thrust faulting is predominant towards the northwest end of the belt, while earthquakes towards the southeast, have large components of strike slip faulting. For both cases, neither nodal plane for most of the events parallels the seismic zone. However, the P axes for both types of faulting do parallel the zone, thus suggesting some crustal shortening in the southeast-northwest direction.

The fault plane solutions for the few events within the Altiplano indicate mostly normal faulting. These last few events are characteristic of the present tectonic state of the Altiplano, as described by Suarez et al. (1983) and others.

The low level of seismicity of the crust and upper mantle under the coast, coupled with the fault plane solutions for the events under the Western Cordillera give no indication of any active "tectonic erosion" of the leading edge of South America. This concept of tectonic erosion has been used by a number of authors [e.g. Plafker (1972); Rutland (1971)] to explain the exposure of Precambrian rocks near the coast of Peru and the inland migration of volcanism over the last 100 m.y. If such erosion of the plate does occur, it seems to be aseismic, and any crustal thickening perpendicular to the Andes takes place along its eastern edge [Suarez et al. (1983;1984)].

A few other points of interest were noted by Grange et al. (1984b). First, there is an apparent gap in seismicity in the southernmost part of the area studied between depths of approximately 130 and 180 km (Figure 3). Since the station networks were recording only for short periods of time during the summers of 1980 and 1981, one cannot conclude that this gap is permanent. But its existence does not seem to be due to poor locations. Second, there seems to be a small decrease in the seismic activity within the steeply dipping

zone when compared to the contortion zone. This is in agreement with the idea that there are greater stresses and more rapidly occuring deformations within the contorted part of the downgoing slab. The third point concerns the shallow events under the Western Cordillera whose northern limit is close to the zone of bending of the Nazca plate. Since this zone is actually slightly farther north, and at a greater depth than the shallow events, one cannot directly correlate the stresses associated with these events with the bend. But it seems entirely plausable that these earthquakes may be related to the occurrence of active volcanoes, which in turn are linked to the existence of a wedge of aesthenospheric material between the plates.

CHAPTER 3

SEISMIC DATA INVERSION THEORY

I. The Inversion Problem

The inversion problem under consideration involves matching observed and calculated travel time data by simultaneously determining the hypocentral parameters (origin time, latitude, longitude and depth) for each event, and the velocities of elastic waves in a three-dimensionally varying structure. We proceed by formulating the problem in the following fashion:

A set of observed arrival times of waves from r earthquakes recorded at s stations can be described by

$$t_{ij} = t_{ij}\left(x_{1i}, x_{2i}, x_{3i}, x_{4i}, y_1, y_2, \ldots y_k\right) \qquad (1)$$

$$\text{for } i = 1, 2, \ldots, r \text{ and } j = 1, 2, \ldots, s$$

where x_{1i} through x_{4i} represent the hypocentral parameters and y_1 through y_k represent the k parameters used to describe the velocity model used. For the sake of clarity we will describe this entire set of parameters by a vector $\vec{\mathbf{X}}$ with n components ($n = 4r + k$).

Given an initial set of model and hypocentral parameters $\vec{\mathbf{X}}_0$, we can calculate a travel time for each hypocenter (the forward problem), and compare it with the observed travel time. The difference between these times - the travel time residual - is then minimized in a least squares sense by making

adjustments to the initial solution. The travel time functions are nonlinear functions of the hypocentral and model parameters, which we can estimate by a linear system of simultaneous equations using a Taylor series expansion. The travel time residuals can now be described by

$$t_{ij}^{obs} - t_{ij}^{calc} = \sum_{l=1}^{n} \left(\frac{\partial t_{ij}}{\partial x_l} \right) \Delta x_l + \varepsilon_{ij} = \Delta t_{ij} \tag{2}$$

Here

$$\Delta x_l = x_l - x_{l0} \quad and \quad \Delta t_{ij} = t_{ij} - t_{ij0} \tag{3}$$

where the subscript o denotes values calculated using the initial set of parameters. The variable ε_{ij} represents the contribution of noise and higher order terms. Using matrix notation, (2) becomes

$$\mathbf{G}\vec{\mathbf{m}} = \vec{\mathbf{d}} + \vec{\mathbf{n}} \tag{4}$$

where $\mathbf{G}$ is an $m \times n$ matrix of partial derivatives, $\vec{\mathbf{m}}$ is a "correction" vector $(= \vec{\mathbf{X}} - \vec{\mathbf{X}}_o)$, and $\vec{\mathbf{d}}$ is a vector of travel time residuals. The vector $\vec{\mathbf{n}}$, whose elements are the ε_{ij}, represents the error found in the data. The "correction" vector is determined by minimizing $||\vec{\mathbf{d}} - \mathbf{G}\vec{\mathbf{m}}||^2$. Thus the changes in travel time needed to eliminate the residuals can be expressed in terms of corrections to the initial model and hypocentral parameters to obtain a "best fit" solution. The actual solution, $\vec{\mathbf{m}}$, of the least squares problem is approximated by a generalized inverse solution, $\hat{\mathbf{m}}$ (Aki and Richards, 1980) through the operation

$$\hat{\mathbf{m}} = \left[\mathbf{G}^T\mathbf{G}\right]^{-1} \mathbf{G}^T \vec{\mathbf{d}} \tag{5}$$

However, because $\mathbf{G}^T\mathbf{G}$ may have small eigenvalues, a stochastic inversion is used instead. The stochastic inverse provides a damping factor which prevents

a solution from becoming unstable. Furthermore, this inverse requires only relatively simple matrix operations, while the generalized inverse requires a complete eigenvector analysis. The solution described here, a special case of the stochastic inverse, is of the least squares variety (Franklin, 1970; Aki and Richards, 1980):

$$\hat{\mathbf{m}} = L\mathbf{G}\hat{\mathbf{m}} \tag{6}$$

where the stochastic inverse operator is

$$L = \left(\mathbf{G}^T\mathbf{G} + \vartheta^2\mathbf{I}\right)^{-1}\mathbf{G}^T \tag{7}$$

The damping term ϑ^2 is the ratio of the variance of the data to the variance of the model, $\frac{\sigma_n^2}{\sigma_m^2}$, and $\mathbf{I}$ is the identity matrix. In this inversion, contributions due to eigenvectors with small eigenvalues ($\lambda < \vartheta^2$) are suppressed. As discussed in the next section, although $\hat{\mathbf{m}}$ does not satisfy (4) exactly, it represents a smoothed version of the true model.

As shown by Lanczos (1961), any rectangular matrix can be decomposed into three matrices:

$$\mathbf{G} = \mathbf{U}\Lambda\mathbf{V}^T \tag{8}$$

where $\mathbf{U}$ is an $m \times m$ matrix whose columns span the data space of $\mathbf{G}$, Λ is an $m \times n$ diagonal matrix containing the singular values of $\mathbf{G}$, and $\mathbf{V}^T$ is the transpose of an $n \times n$ matrix $\mathbf{V}$ whose columns span the model space of $\mathbf{G}$. We can divide $\mathbf{V}$ into two parts, $\mathbf{V}_p$ and $\mathbf{V}_0$, where $\mathbf{V}_p$ consists of the eigenvectors with nonzero singular values and $\mathbf{V}_0$ is made up of eigenvectors with zero singular values. Here, p, the number of nonzero singular values found in Λ, is the number of

independent parameters used to determine the solution. In the same fashion, we can divide the matrix **U** into two parts: $\mathbf{U}_q$, representing the nonzero eigenvalues, and $\mathbf{U}_0$, representing the zero eigenvalues. $\mathbf{U}_q$ can be further divided as shown below $\left[\mathbf{U}_q = \left[\mathbf{U}_1, \mathbf{U}_2\right]\right]$.

We are working with an overdetermined system of m equations ($m = rs$), n unknowns ($n = 4r + l$) and p independent parameters. Our data space, then, consists of p pertinent bits of data and m-p bits of excess data. Thus we can say that part of $\mathbf{U}_q$, which we will call $\mathbf{U}_1$, spans the pertinent data space, while the remainder of $\mathbf{U}_q$, call it $\mathbf{U}_2$, will span the excess data space along with $\mathbf{U}_0$. Schematically we have

$$\mathbf{G} = \begin{matrix} \overset{\longleftarrow m \longrightarrow}{\left[\begin{array}{ccc} \mathbf{U}_1 & \mathbf{U}_2 & \mathbf{U}_0 \end{array}\right]} \\ m \end{matrix} \begin{matrix} \overset{\longleftarrow n \longrightarrow}{\left[\begin{array}{c|c} \lambda_1 \cdots \lambda_p & 0 \\ \hline 0 & \end{array}\right]} \\ n \end{matrix} \begin{matrix} \overset{\longleftarrow n \longrightarrow}{\left[\begin{array}{c} \mathbf{V}_p^T \\ \hline \mathbf{V}_0^T \end{array}\right]} \\ n \end{matrix} \tag{9}$$

II. The Stochastic Inverse vs. the Generalized Inverse

The reason for using the stochastic inverse can be illustrated as follows. As we noted earlier, the solution to the generalized inverse is described by (5). We can then take the decomposition of (8) one step further, as shown by Lanczos (1961), where

$$\mathbf{G} = \mathbf{U}_p \Lambda_p \mathbf{V}_p^T \tag{10}$$

This is possible as the $\mathbf{U}_0$ and $\mathbf{V}_0$ spaces are not mapped by the operator **G**. By

substituting (10) into (5), we then have

$$\hat{\mathbf{m}} = \mathbf{V}_p \Lambda_p^{-1} \mathbf{U}_p^T \vec{\mathbf{d}} \tag{11}$$

where

$$\Lambda_p^{-1} = \begin{bmatrix} \lambda_1^{-1} & & & \\ & \lambda_2^{-1} & & \\ & & \ddots & \\ & & & \lambda_p^{-1} \end{bmatrix} \tag{12}$$

In the neighbourhood of any singularity, one or more small eigenvalues mapped through (11) would produce large changes in the parameters contained in $\hat{\mathbf{m}}$. These small eigenvalues then become a source of instability by reducing the precision of the calculations when the inversion of large matrices are carried out, as well as causing an amplification of the noise within the data. In addition, this instability could cause the solution to diverge as the calculations proceed from one iteration to another.

Because of this problem in the neighbourhood of singularities, a method that suppresses large changes due to small eigenvalues is desirable. The stochastic inverse introduced by Franklin (1970) performs this stabilizing function for small eigenvalues. By substituting the stochastic inverse operator (7) and the matrix decomposition (10) into the stochastic inverse solution (6) we have

$$\hat{\mathbf{m}} = \mathbf{V}_p \frac{\Lambda_p}{\Lambda_p^2 + \vartheta^2 \mathbf{I}} \mathbf{U}_p^T \vec{\mathbf{d}} \tag{13}$$

Here each element of the diagonal matrix is given by $\frac{\lambda_i}{\lambda_i^2 + \vartheta^2}$.

As we can see, small eigenvalues, specifically those smaller than the damping term ϑ^2, cause the changes in the parameters to decrease. As the eigenvalues decrease, the changes approach zero smoothly, instead of approaching infinity, as in the case of the generalized inverse. This process is illustrated in the figure below:

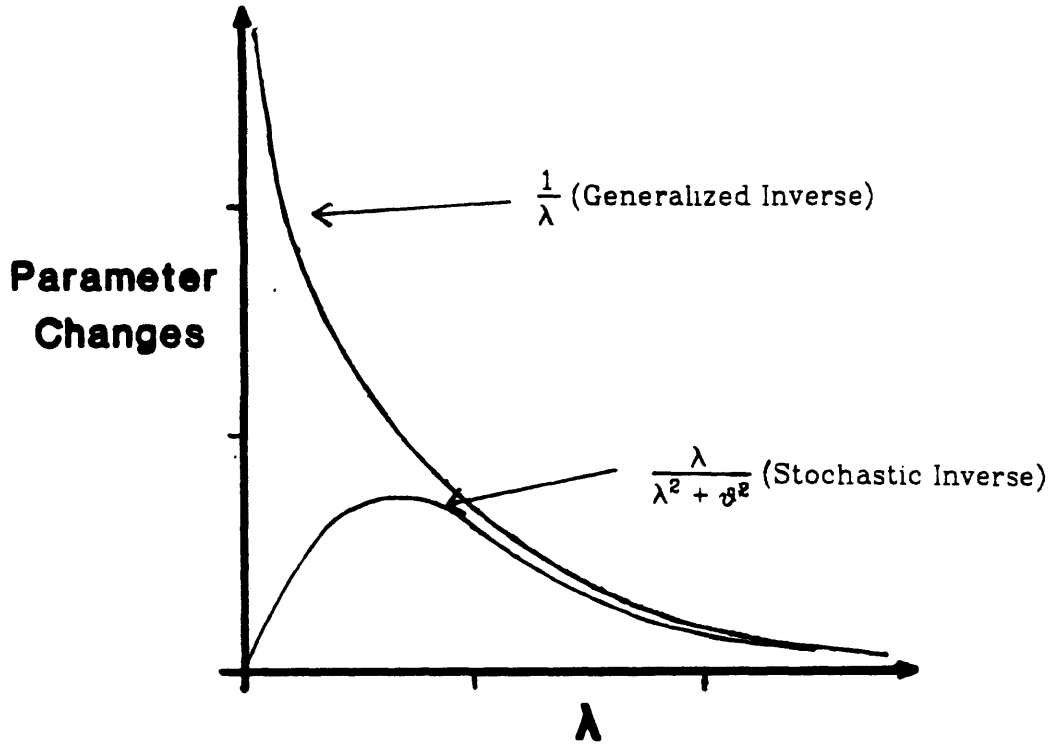

Comparison of the influence of small eigenvalues on the behavior of parameter changes for the generalized and stochastic inverse methods.

III. Decoupling the Hypocenter and Velocity Solutions

As noted earlier, these inversion methods solve for the changes made to the model and hypocentral parameters. However, by including the hypocenter for each event four rows and columns are added on to the matrix of partial derivatives. This leads to difficult storage and computational problems when carrying out the calculations. On the other hand, if perturbations to the hypocenters are not considered - that is, the hypocenters are fixed - we are assuming that there is no coupling between the hypocentral and the model parameter solutions. To overcome this problem, Pavlis and Booker (1980) and Spencer and Gubbins (1980) proposed methods of solving an equivalent inversion problem in which the hypocenter parameters are separated from the velocity parameters. With the notation of (4), this is

$$\vec{\mathbf{d}} = \mathbf{G}\vec{\mathbf{H}} + \mathbf{B}\vec{\mathbf{V}} + \vec{\mathbf{n}} \tag{14}$$

where $\vec{\mathbf{H}}$ is the vector containing changes in hypocentral parameters, and $\vec{\mathbf{V}}$ is the vector containing the velocity changes. As before, we can decompose $\mathbf{G}$ into the form of (9), where $\mathbf{U}_1$ spans the pertinent data space of $\mathbf{G}$. Now the elements of the residual vector, which map into $\mathbf{U}_1$ will determine the hypocenters, while the remaining elements will determine the velocity parameters or be considered noise.

Since the system of equations is overdetermined, $\mathbf{U}_2$ is assured to exist. Its columns will be orthogonal to $\mathbf{U}_1$ so that if we premultiply (14) by $\mathbf{U}_2^T$, the hypocentral solution will be detached from the velocity solution because

$$\mathbf{U}_2^T \vec{\mathbf{d}} = \mathbf{U}_2^T \mathbf{B}\vec{\mathbf{V}} + \mathbf{U}_2^T \vec{\mathbf{n}} \tag{15}$$

By this method, as much data as is desired can be utilized while only a number

of columns and rows equal to the number of parameters being solved for is stored.

The inclusion of S wave velocities in the solution increases the accuracy of the earthquake location. Although increasing the number of parameters used to describe the model, the hypocenter locations become more stable, being less susceptible to changes in the velocity structure than when only P waves are used [Chatelain et al. (1980)]. As stated by Roecker (1982) "the S waves appear to rotate the $\mathbf{U}_1$ space of the hypocenter matrix out of the $\mathbf{U}_1$ space of the velocity matrix, thereby uncoupling the solutions". If both P and S waves are used for the locations, both also have to be used when solving for the velocity structure. Otherwise, we would be working with different **U** spaces, each of which would cause different residual components to project onto the hypocentral solution.

If both types of waves are used simultaneously, it is reasonable to assume that some amount of coupling may occur between the velocity parameters. Then, it would be best if the solutions for the P and for the S wave velocities could be decoupled in the same fashion as the hypocenter and velocity solutions were. This being a difficult task however, we cannot hold the S velocities fixed, but must let them vary in the same manner as the P velocities.

IV. Obtaining Solutions and Estimating their Reliability

To avoid nonlinearity effects when trying to obtain stable solutions, either the partial derivatives in **G** must be nearly constant, or the corrections in $\hat{\mathbf{m}}$ must small. To avoid violating these conditions of linearity, we can vary the

parameters in a sequential fashion. This is done by beginning the inversion with the least sensitive parameter ,i.e., the one with the smallest partial derivative. In this manner, with each successive step, the residuals are reduced making subsequent corrections smaller. The sequence in which the parameters are allowed to vary begins with the hypocentral latitude and longitude, followed by the focal depth and origin time, phase velocities of the blocks, and the changes in the fractional slowness (1/velocity) of the structure. This procedure was called a "progressive" inversion by Roecker (1982).

The confidence we have in our solutions can be measured through two reliability estimators: the covariance matrix **C**, which gives us an estimate of the standard error of the solution, and the resolution matrix **R**, which indicates the degree to which our calculated solution approximates the true least squares solution.

The error within the data, $\Delta\vec{d}$, will produce an error Δm in our solutions which can be expressed through the covariance matrix (Aki and Richards, 1980) as

$$\mathbf{C} = \langle \Delta m \Delta m^T \rangle = \sigma_d^2 L L^T$$

$$= \sigma_d^2 \mathbf{V}_p \frac{\Lambda_p^2}{\Lambda_p^2 + \vartheta^2 \mathbf{I}^2} \mathbf{V}_p^T \qquad (16)$$

where σ_d^2 is the estimated variance of the data.

The resolution matrix is given by $\hat{\mathbf{m}} = \mathbf{R}\vec{\mathbf{m}}$ or

$$\mathbf{R} = L\mathbf{G}$$

$$= \mathbf{V}_p \frac{\Lambda_p^2}{\Lambda_p^2 + \vartheta^2 \mathbf{I}} \mathbf{V}_p^T \qquad (17)$$

(Aki and Richards, 1980).

Should any diagonal of $\mathbf{R}$ be zero, the corresponding parameter cannot be resolved. If, on the other hand, $\mathbf{R}$ is the identity matrix, then the solution is perfectly resolved and we have calculated the true solution ($\hat{\mathbf{m}} = \tilde{\mathbf{m}}$). The manner in which one interprets $\mathbf{R}$ for values between zero and one is rather subjective, but it often allows us to separate what we consider to be reliable solutions from unreliable solutions.

CHAPTER 4

MICROEARTHQUAKE LOCATIONS IN SOUTHERN PERU

The data used for this paper were acquired during the summer of 1981 in southern Peru. A temporary network of smoked paper recorders was installed in a dense array, the stations being within or close to the Western Cordillera of the Andes (Figure 9). In addition, data from station ARE of the World Wide Standardized Seismograph Network (WWSSN) and two stations installed by the Department of Terrestrial Magnetism of the Carnegie Institution in Washington (ONG and AYE) were used.

Over 20,000 P and S arrival times from approximately 3,000 events were read using a digitizing table. The uncertainties of these data, taking into account the uncertainties of the measurements, drifts of the recorders's internal clocks and variations in drum rotations, were estimated to be less than 0.1 seconds for P arrival times and about 0.8 seconds for S arrivals.

I. Original Hypocentral Solutions

Over 1200 events were initially located by Grange (1983) using the program HYPOINVERSE [Klein (1978)] after it had been modified to include elevation corrections. This correction was necessary since the altitude of the stations varied from sea level to 4,900 m. A series of tests was carried out to evaluate the quality of the locations so that the results could be discriminated between more or less reliable locations. Further tests were made to determine whether

or not it was valid to use flat layered structures, and to see if any lateral heterogeneities could be approximated by these methods. The results of the locations and tests were described in detail by Grange (1983) and Grange et al. (1984b), and are summarized here. It was decided that a reasonable approximation of the probable structure could be made by using three different simple layered models together. The three models corresponded roughly to the region between the trench and the Peruvian coast, the coastal region, and the region under the Western Cordillera and the Altiplano (Figure 10). Different stations were assigned to each model. The criteria arrived at to determine good locations were the following:

(1) A minimum of eight phase arrivals, at least one being an S-wave arrival.

(2) A root mean square value of travel time residuals (RMS) less than 0.40 sec. for events with 20 or more arrival times (N), an RMS less than 0.35 sec. for $15 < N < 20$, and an RMS less than 0.30 sec. for $8 < N < 15$.

(3) Estimated epicentral and focal depth errors of less than 10 km.

(4) Events with a maximum azimuthal aperture without stations (GAP) measured from the epicenter greater than 300^0, must have an epicentral distance to the nearest station (DMIN) less than one-half the calculated focal depth. For events with a GAP less than 300^0, DMIN must be smaller than the calculated focal depth for events deeper than 60 km, and less than twice the calculated focal depth for events shallower than 60 km.

To minimize bias in locations introduced by erroneous choices of velocity structure, the only events that were retained were those whose locations did not change by more than 10 km when relocated using different velocity structures. 592 events met these criteria, and the errors for depth and

epicentral coordinates were estimated to be no more than 5 km and 7 km, respectively. An additional 296 events were retained, since they had stable solutions, although they did not fulfill all the criteria above.

II. 3-D Hypocentral Relocations - The Initial Model

For the purposes of this study, the work done by Grange (1983), (described in the previous section) provided us with a set of events with stable solutions. These events were relocated using three-dimensional velocity models, which are presumably a more realistic approximation of the probable structure than that used by Grange. By relocating these events in a realistic structure, any errors due to lateral heterogeneities would be reduced. Also, the events would be located within a structure that could be used as an initial model for a three-dimensional velocity inversion. Assuming that the relocations were reasonably accurate, any changes of the hypocentral parameters made during the inversion would be relatively small. This was a necessary condition to avoid instabilities due to the nonlinearity of the inversion problem. Both the set of events retained by Grange and a portion of the set he discarded for having failed his reliability criteria were relocated.

The initial three-dimensional model was set up by taking a rectangular prism, aligned parallel to the Peruvian coast, centered about 16° *S*, 72° *W*. The dimensions of the rectangle, within which all the events are located, are 440 km in length by 330 km in width, or approximately 4° by 3° of arc. Next, a cross-section of the layers was taken perpendicular to the Peruvian coast. Each layer was divided up into blocks in a southwest to northeast direction. This profile was then extended in a southeast-northwest direction, producing a three-

dimensional structure (Figure 11). The geometry and assigned velocities, based on work by Grange (1983) (Figure 10), James (1971), and Ocola and Meyer (1973) (Figure 12), modeled a crust that thickened from the trench towards the Western Cordillera, and then thinned towards the Brazilian Shield. In this first relocation, the mantle below 70 km depth was modeled by one homogeneous block.

Once the relocation run was completed, the first step taken to pick the more reliably located events was to remove those events whose matrix of partial derivatives produced small eigenvalues. (Small eigenvalues were defined as those whose ratio to the largest eigenvalues was less than 0.01). Next, the events that showed some degree of instability - that is, those whose hypocentral parameters oscillated by large amounts from one iteration to the next - were discarded. The limits imposed on the oscillations were on the order of 2 to 3 km for latitude and longitude, 3 to 4 km for focal depth, and 1.0 sec for origin time. We noted that a few events with large changes in the hypocentral parameters required several iterations before converging. The criteria used by Grange (1983) was then applied, and 467 of the approximately 1,100 earthquakes satisfied all conditions. When the RMS criterion was relaxed, an additional 109 relocated events were considered reliable. This relaxation of the rule was the following:

(1) For number of phases (N) less than 15, the RMS had to be less than 0.5 seconds.

(2) For $15 < N < 20$, an RMS of less than 0.6 was required.

(3) For $N > 20$, the RMS could not be greater than 0.7 seconds.

Over ninety percent of the chosen relocations were among those events determined by Grange to be more reliable. A closer comparison of the results showed that most of the new locations tended to be slightly farther northeast and shallower than Grange's locations, and the origin time occured about 1 second later. The changes in locations were on the average no greater than 10 km. This appears to indicate that the data favors the parts of the model having slower than average crustal velocities. The estimated precision of the relocated events is approximately the same as those from Grange (1983). Few events located at depths greater than about 90 km satisfied all the criteria, suggesting that it is not sufficient to model the upper mantle by using one homogeneous block.

III. 3-D Hypocentral Relocations - Refining the Crustal Model

A second relocation was carried out, the purpose being to detect a few of the characteristics of the crustal structure on a smaller scale (e.g., tens of kilometers). Also, the events would then be located within a model that would then be used as an initial solution for the three-dimensional velocity inversion.

The principal aim was to try to determine the approximate location and shape of the Mohorovičic discontinuity (the Moho), across which the phase velocities should increase substantially. Previous studies (for example, Anzoleaga (1964), James (1971), Ocola et al. (1971), Ocola and Meyer (1973)) seem to agree on a Moho increasing from the coast towards the Andes. It appears to reach a maximum of 70±10 km under the Altiplano and then gradually becomes shallower towards the Brazilian shield (Figure 12).

Another important consideration in setting up the model, was the existence of low velocity zones (LVZ). Based on large amplitude secondary arrivals from refraction studies in the Altiplano, Ocola and Meyer (1972) stated that there existed two thin LVZs within the crust. However, since the dimensions of these low velocity zones were too small to be resolved, they were not included in the model. The remaining major boundary across which a change in velocity could perhaps be modeled was the LVZ that occurs within the mantle. According to James (1971), there did not appear to be any significant LVZ for shear waves in the upper 150 km of mantle beneath the continental crust, although it seemed that both P and S velocities were somewhat low. Yet, a major S wave LVZ was required under the oceanic crust in the area to satisfy phase and group velocity data. He set the upper boundary of this LVZ between 50 and 60 km depth, and the lower boundary at a depth greater than 200 km.

To determine whether the existence of a LVZ could be resolved, a series of Wadati plots was made to calculate the V_P to V_S ratio for different depth slices (Figure 13). This was done by ploting V_P minus V_S arrival times versus V_P arrivals. The slope of this graph minus one is equal to the average V_P to V_S ratio down to that depth slice. Since the ray paths for the events in any one slice passed through the layers above it, the resulting V_P to V_S ratios were an average of all ratios down to that respective slice. Thus, the ratio for each individual depth slice was calculated by eliminating the averaging effect due to any overlaying layers. The arrival times used for these calculations were from the events considered to be well located. Whether a layer boundary representing the Moho was assumed to be at 60 km, 80 km, or any other depth in that neighbourhood was immaterial, since the calculated V_P to V_S values were 1.74±0.01 for all layers down to about 100 km. At this depth a large increase in the ratio was noted, to 1.84±0.01. Even after taking into

consideration an increase in the P wave velocity, a pronounced S wave LVZ was required to fit the results. Trying different upper and lower boundaries in the calculations seemed to put this layer between 100±10 km and 130±10 km. Despite not having a large number of events located below 130 km depth, all layers below this point had V_P to V_S ratios of about 1.72±0.02.

The next step was to determine the parameters of the model, which were governed by two factors. First, the total number of blocks was limited by computational storage requirements, so that a large number of small blocks was ruled out. Besides, blocks with small dimensions (less than 20 km to a side) are poorly resolved in the inversion process. The second factor had to do with the number of ray paths through each block, also an indication of how well a block will be resolved. 20 rays through each block was set as the necessary minimum of samplings needed to "see" it. On the other hand, it would have been rather useless to use a small number of large blocks, each of which would be sampled a very large number of times (e.g., a thousand or more times), thus providing only redundant information. This was especially true for the region in the center of the structure, an area with a high concentration of earthquakes. To determine the number of ray path segments passing through each block, part of the three-dimensional velocity inversion program was used. This was repeated using different block arrangements, until a satisfactory balance in the number of samplings per block and their dimensions was obtained. The locations of the events from the first relocation run were used as the initial solutions for the partial velocity inversion runs. This procedure is valid since stable solutions do not vary significantly from one model to another. The block structure was extended to a greater depth in this run, so that the upper mantle, including the S wave LVZ, could be adequately modeled. In this manner, a larger number of intermediate depth events could be better located.

The resulting model is depicted in Figure 14.

Using the same selection criteria that were used for the first relocation run, 442 events were considered to be well located. Nearly a hundred additional events were considered to have good stable solutions under the relaxed criteria. This set of relocations showed the same trends as the previous set when compared to the locations by Grange. However, the changes were smaller in magnitude: on the average, the differences in latitude and longitude were of about 5 km, approximately 7 km for the depths, and the new relocations indicated that the origin times were about 0.5 to 1.0 sec later. Also, the RMS values were about 0.1 sec less on the average. Once again, the errors in the hypocentral locations were about the same as Grange's. In this set of relocations, 92 percent of the reliable locations were among the events chosen by Grange.

IV. Final Observations

As a final comment on the relocations of these microearthquakes, it should be pointed out that the simple models used by Grange were a valid approximation of a three-dimensional structure. The results he attained were often very near the hypocenters calculated for the relocations, usually close enough so that the uncertainty margins of both solutions overlapped. Also, it should be noted that the few additional locations picked despite their larger RMS, are valid solutions. The RMS residual is an indication of the effect of noise within the data on the solution, and of the bias due to the model being used. Since the RMS in all the flat layered and three-dimensional locations were about the same size for most of the well located events, the bias due to the models

could be considered to be small. Since we then knew that the noise in the data was the major source of the RMS residual, we could relax the criterion established by Grange for this parameter, provided that these solutions converged and were stable for all models.

As could then be expected, the same seismicity patterns observed by Grange (1983), described here in chapter 2, were noted. Despite having a smaller set of earthquakes, the contortion zone of the Nazca plate could be easily identified in cross-sections parallel to the Peruvian coast (Figure 15), and in others parallel to the direction of motion of the Nazca plate (Figure 16). The location of the bend clearly matched the northern end of the volcanic arc in southern Peru. All three shallow seismicity belts were seen. The belts beneath the coast and beneath the Western Cordillera were the most prominent due to a greater number of events in these areas.

CHAPTER 5

THREE-DIMENSIONAL VELOCITY INVERSIONS

The work done by Grange (1983) and by this author, show that the velocity models used to relocate the earthquakes are reasonable approximations of the crust and upper mantle under southern Peru. Nevertheless, these models were somewhat limited. Grange's locations and subsequent tests provided only velocity models varying with depth. The relocations performed with more complex block structures were essentially only two-dimensionally varying models. That is, the wave velocities changed only with depth and across the profile made perpendicularly to the Peruvian coast. Thus we felt that performing a three-dimensional velocity inversion was the best method with which we could gain some insight into the complexities due to lateral heterogeneities of the Earth's crust.

I. Procedure and Estimated Confidence Indicators

The inversions performed here used for starting models, the same block structures and velocities used for relocating the microearthquakes. Simultaneously solving for the velocity structure and hypocentral solutions, these calculations proceeded in an iterative fashion by making the changes in the block's fractional slowness which best fit the residuals (see Chapter 3 and Roecker (1982) for details).

The arrivals used in these inversions were from the 442 events considered to be well located, and from 61 events with higher RMS. Besides having stable solutions these additional events were chosen because they had a large number of arrival times recorded, and most were located at depths greater than 70 km. Before proceeding with the inversions, however, the first group of 442 events was screened for events with less than 10 recorded phase arrivals located within regions of high seismic activity. These events, while occupying the same number of elements of the G matrix as events with a greater number of arrivals, only provide small amounts of redundant information. When this selection process was finished, 396 events were kept for the inversions. A list of these events is found in Appendix A and plotted in Figure 17.

Three velocity inversions were carried out. The first used the same model previously used in the second earthquake relocation. The second inversion used a slightly modified strucutre, in which the block interfaces parallel to the coast were shifted inland in a northeast direction. This shift allowed a greater number of blocks on the northeast side of the model with a sufficient number of ray paths through them to be resolved. The final inversion was carried out using a model in which the boundaries between the layers of blocks were changed so that the Moho could be determined with greater accuracy.

A simplified map of the area was made as a template (Figure 18). The results for each layer of blocks were then overlayed on the map in four different formats. First, the calculated P and the percent change from the initial model velocities were shown superimposed on the map. Second, a map was made which included the resolution and the standard deviation of the calculated P velocity. The third and fourth formats were similar to the first two, except that they used the calculated S velocities.

Before proceeding with the analysis, some degree of confidence in the results had to be established. A series of tests was performed by Roecker (1982) to determine to what extent problems such as nonlinearity and improper parameterization of the block structures affected the solutions to the inverse problems. The data used in these tests were microearthquakes recorded in the Pamir-Hindu Kush region of Central Asia. A summary of the criteria Roecker established to interpret the inversion results follows:

(1) The inferred velocities should be contourable. Trends should occur across several blocks instead of being defined by the fluctuation of any one block. This criterion is not only valid for variations within a layer, but from one layer to another as well.

(2) Large velocities at the edges of layers with few events are unreliable, and extreme variations in regions of low seismic activity could be exaggerated.

(3) A reasonable cut-off value for resolution is about 0.6 for P velocities. For the S velocities, the cut-off is about 0.5 since the S arrivals are assigned a smaller weighting.

(4) For the array and types of anomalies studied by Roecker, variations in the velocities smaller than 2% were probably insignificant.

Since the dimensions of the array and the magnitude of the anomalies being studied in southern Peru were roughly the same as those in the Pamir-Hindu Kush region, the same lower limit on velocity variations was adopted.

Roecker estimated that the velocity variations for a given layer were mainly due to the data from the events in that layer. Morever, one can usually be confident that the large scale variations of the calculated velocities

reasonably describe the actual structure. It should be kept in mind, however, that any structural features presented by the initial model will usually be present in the inversion results. The amount of change in the velocities between the initial and resulting models is a more appropriate indicator of whether the initial assumptions of the structure were reasonable or not.

II. Analysis of the Inversion Results

Overall, the results of the inversions were similar to one another. Several characteristics stand out: First, there was good correlation between the P and S velocities in each inversion down to about 70 km. Second, a velocity gradient trending southwest-northeast exists within the crustal layers. Third, the resolution deteriorated with depth due to the decrease in the number of events, especially below 100 km. Fourth, the data variance was considerably reduced (by approximately 60 %), with the resulting variance being about equal to the assumed noise level in the data (0.1 s). Finally, no resovable change in velocity could be associated with the contortion in the Nazca plate.

The Crust

The top layer of the crust showed scattered results and low resolution because of the geometry of the station network (Figures 19,20,33,34,47,48). For the layers between about 20 km and 70 km depth, a gradient for both P and S velocities was seen, with isovelocity contours roughly parallel to the alignment of the model and the coast. Compared to the initial model, the gradient in the results was smaller towards the edges of the structure and larger in the center. The velocities decreased towards the northeast, under the Altiplano, and

increased towards the southwest because of the effect of the oceanic and thinner continental crusts. The largest change noticed in the P and S velocities occured under the Western Cordillera of the Andes. The P velocities were in the range of 6.1 to 7.0 km/s to the northeast of the Cordillera, and were in the range of 6.6 to 7.6 km/s to the southwest. The results for these layers are shown in Figures 21-26, 35-40, and 49-52.

The Upper Mantle

Below about 70 km depth, the velocity gradient disappeared. Instead, there seemed to be a zone in which the P velocity increased with depth interspersed with regions of higher velocities (V_P>8.0 km/s) and lower velocities (V_S<7.5 km/s) (Figures 27-32, 41-46, and 53-58). Poor resolution did not permit any interpretations below 130 km depth. Nevertheless, the smaller regions of anomalous P velocities only stood out down to about 100 km. Below this point there did not appear to be any large changes in P velocities. But one should remember that poor resolution and the large scale of the blocks at this depth may not have allowed us to resolve any small scale features that may exist.

Within the mantle, the P and S velocities are not well correlated. The S velocities did not show any small scale velocity anomalies, but only gradual lateral changes in velocity with a high in the middle of the layers. Vertically, a low-velocity zone could be noted in the layer between 100 and 130 km depth. However, the velocity changes were such that no LVZ of the magnitude indicated by the Wadati plots was noted. Poor resolution of the calculated S velocities at depths greater than 130 km again did not permit any further interpretations.

The Mohorovicic Discontinuity

As mentioned above, the initial model for the third velocity inversion was designed so that a larger velocity contrast across the Moho could be detected, at a maximum depth under the Altiplano of either 60 or 80 km. In the previous inversions, a significant velocity contrast associated with the Moho could be seen at about 70 km depth under the Altiplano, and at shallower depths under the coastal region (Figures 25-28 and 39-42). The P velocities were at most about 7.0 km/s above this boundary, and about 7.6 km/s or more below.

The results of the third inversion did not reflect any changes at either 60 or 80 km under the Altiplano as markedly as the two previous inversions. Instead, it showed gradual velocity changes across these boundaries (Figure 51-56). This appears to indicate that under the Altiplano, the Moho is at about 70 km depth, and that the result of the third inversion is a consequence of averaging the velocities above and below this depth.

The Bend in the Nazca Plate

Because of the small size of the three-dimensional structures used, only a portion of the bend was included in our model. Unfortunately, this portion was located in the northern part of the structure, a region of poor resolution. For this reason, a small low velocity anomaly that could possibly be associated with the bend was only resolved to a reasonable degree between depths of about 70 and 100 km. Since only a few blocks with lower velocities matched the approximate location of the bend, no definite correlation could be made.

The last two criteria established by Roecker (1982), summarized earlier, were used to make contour maps of the percent change in P and S velocities

with the epicenters of the earthquakes for layers 3 through 6 (Figures 57-60). In addition, a few profiles parallel to the direction of motion of the Nazca plate were made and contoured in the same fashion (Figures 61-64). These figures highlight the velocity anomalies within the crust and upper mantle beneath southern Peru.

CHAPTER 6

SUMMARY AND CONCLUSIONS

The arrival time data set acquired in southern Peru during the summer of 1981 was used by Grange (1983) to locate a number of microearthquakes. This author, using the same data, relocated these events using three-dimensional structures to model lateral heterogeneities of the crust and upper mantle. The results of these relocations were very similar to the original hypocentral solutions computed by Grange, indicating that the simple flat layered structures which he used were reasonable approximations to the actual structure. The tectonic characteristics of southern Peru were equally well defined with either set of earthquake locations. The most prominent feature, the bend in the Nazca plate as it is subducted under southern Peru, was located beneath the northern end of the volcanic arc in the region. North of the bend, the slab is being subducted at a shallow angle ($10°-15°$), while south of the bend, the slab is descending at a steeper angle ($25°-30°$). These observations corroborated the theory of Barazangi and Isacks (1976;1979) that a wedge of aesthenosphere is required between the overridding and subducted plates, for subduction-related volcanism to occur. It was also shown that the contorted zone of the Nazca plate is parallel to the plate's direction of motion with respect to the South American plate.

A subset of the well located events was then used to perform three-dimensional velocity inversions in an attempt to model the seismic structure of the region. Criteria established by Roecker (1982) to aid in the interpretation of the inversion results were used. The features that appear from these results

are the following: First, a velocity gradient seems to exist perpendicular to the coast. The velocities are higher in the southwest crossing the Moho under the coast, and decrease under the Western Cordillera of the Andes and the Altiplano. Second, the Moho at its deepest point under the Altiplano, seems to be at a depth of about 70 km. Third, the upper mantle seems to be a region where P and S velocities are gradually increasing with depth, with the exception of a few P velocity anomalies between 70 and maybe as much as 130 km depth. The average velocities for this region seem to be in the range of 7.5 to 8.0 km/s for the P, and 3.9 to 4.6 km/s for the S. The velocities for the anomalies were greater than 8.0 km/s and less than 7.5 km/s. Finally, an S wave low-velocity zone is seen between 100 and 130 km depth. However, it does not seem to be as pronounced as it was originally thought to be, when Wadati plots were made to determine V_P to V_S ratios for different depth slices.

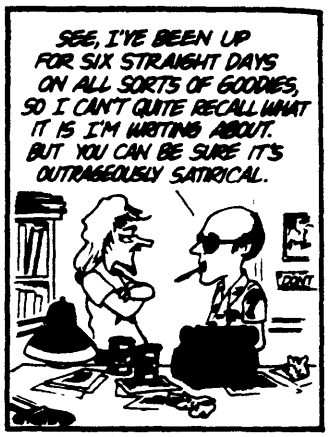

Trudeau (1975)

BIBLIOGRAPHY

Aki, K., and P.G. Richards, *Quantitative Seismology*, W.H. Freeman and Co., San Francisco, 1980.

Anzoleaga, R., *Algunas consideraciones sobre la Corteza Terrestre debajo de los Andes*, Licentia Thesis, Universidad Mayor de San Andres, La Paz, Bolivia,1964.

Barazangi, M., and B.L. Isacks, Spatial distribution of earthquakes and subduction of the Nazca plate beneath South America, *Geology, 4*, 686-693,1976.

Barazangi, M., and B.L. Isacks, Subduction of the Nazca plate beneath Peru: evidence from the spatial distribution of earthquakes, *Geophys. J. R. astr. Soc.,57*, 537-555, 1979.

Chatelain, J.L., S.W. Roecker, D. Hatzfeld, P. Molnar, Microearthquake seismicity and fault plane solutions in the Hindu Kush region and their tectonic inplications, *J. Geophys. Res., 85*, 1365-1387, 1980.

Couch, R., R.M. Whitsett, B. Huehn, and L. Briceno-Guarupe, Structure of the continental margin of Peru and Chile: Kulm et al., eds. *Nazca Plate: Geological Society of America Memoir 154*, 703-726, 1981.

Coulbourn, W.T., Tectonics of the Nazca plate and the continental margin of western South America, 18°*S* to 23°*S*: Kulm et al., eds. *Nazca Plate: Geological Society of America Memoir 154*, 587-618, 1980.

Crosson, R.S., Crustal structure modeling of earthquake data, 1, Simultaneous least squares estimation of hypocentre and velocity parameters, *J. Geophys. Res., 81*, 3036-3046, 1976.

Dalmayrac, B., and P. Molnar, Parallel thrust and normal faulting in Peru and constraints on the state of stree, *Earth & Plan. Sci. Lett., 55*, 473-481, 1981.

Franklin, J.N., Well-posed stochastic extensions of ill-posed linear problems, *J. Math. Anal. Appl., 31* 3682-3716, 1970.

Grange, F., Etude sismotectonique détaillée de la subduction lithospherique au Sud Perou, These pour docteur 3*eme* Cycle, I.R.I.G.M., Grenoble, 168 pp., 1983.

Grange, F., P.S. Cunningham, J. Gagnepain, D. Hatzfeld, P. Molnar, L. Ocola, A. Rodriguez, S.W. Roecker, J.M. Stock, and G. Suarez, The configuration of the seismic zone and the downgoing slab in southern Peru, *Geophys. Res. Lett., 11*, 38-41, 1984a.

Grange, F., D. Hatzfeld, P.S. Cunningham, P. Molnar, S.W. Roecker, G. Suarez, A. Rodriguez, L. Ocola, Tectonic implications of the microearthquake seismicity and fault plane solutions in southern Peru, *J. Geophys. Res.*, in press, 1984b.

Hasegawa, A., and J.S. Sacks, Subduction of the Nazca plate beneath Peru as

determined from seismic observations, *J. Geophys. Res.*, *86*, 4971-4980, 1981.

Isacks, B., and M. Barazangi, Geometry of Benioff zones: lateral segmentation and downwards bending of the subducted lithosphere: Talwani, M., and Pitman, W.C., III, eds. *Island arcs, deep sea trenches and back-arc basins: American Geophysical Union Maurice Ewing Series*, 99-114.

James, D., Andean crustal and upper mantle structure, *J. Geophys. Res.*, *76*, 3246-3271, 1971.

James, D., Plate tectonic model for the evolution of the Central Andes, *Geol. Soc. Am. Bull.*, *82*, 3325-3346, 1971.

James, D., Subduction of the Nazca plate beneath Central Peru, *Geology*, *6*, 174-178, 1978.

Johnson, S.H., and G. Ness, Shallow structures of the Peru margin: Kulm et al., eds., *Nazca Plate: Geological Society of America Memoir 154*, 525-544, 1980.

Klein, F.W., Hypocenter location program HYPOINVERSE, *U.S. Geological Survey Open File Report*, 78-694, 1978.

Lanczos, C., *Linear Differential Operators*, Van-Nostrand Co. Ltd., London, 564 pp., 1961.

Lee, W.H.K., R.G. Bennett, and K.L. Megaher, A method of estimating magnitude of local earthquakes from signal durations, *U.S. Geological Survey Open File Report*, 1972

Mammerickx, J., R.N. Anderson, H.W. Menard, S.M. Smith, Morphology and tectonic evolution of the East-Central Pacific, *Geol. Soc. Am. Bull.*, *86*, 111-118, 1975.

Ocola, L.C., R.P. Meyer, and L.T. Aldrich, Gross crustal structure under Peru-Bolivia Altiplano, *Earthquake Notes*, *42*, 33-48, 1971.

Ocola, L.C., and R.P. Meyer, Crustal low-velocity zones under the Peru-Bolivia Altiplano, *Geophys. J. R. astr. Soc.*, *30*, 199-209, 1972.

Ocola, L.C., and R.P. Meyer, Crustal structure from the Pacific basin to the Brazilian shield between 12° and 30° south latitude, *Geol. Soc. Am. Bull.*, *84*, 3387-3404, 1973.

Pavlis, G.L., and J.R. Booker, The mixed discrete-continuous inverse problem: Application to the simultaneous determination of earthquake hypocenters and velocity structure, *J. Geophys. Res.*, *85*, 4801-4810, 1980.

Plafker, G., Alaskan earthquake of 1964 and Chilean earthquke of 1960: implication for arc tectonics, *J. Geophys. Res.*, *77*, 901-925, 1972.

Roecker, S.W., Velocity Structure of the Pamir-Hindu Kush region: possible evidence of subducted crust, *J. Geophys., Res.*, *87*, 945-959, 1982.

Rutland, R.W.R., Andean orogeny and ocean floor spreading, *Nature*, *233*, 252-255, 1971.

Spencer, C., and D. Gubbins, Travel time inversion for simultaneous earthquake location and velocity structure determination in laterally varying media, *Geophys. J. R. astr. Soc.*, *63*, 95-116, 1980.

Suarez, G., Seismicity, tectonics, and surface wave propagation in the Central Andes, Ph.D. Thesis, M.I.T., 260 pp., 1982.

Suarez, G., P. Molnar, and B.C Burchfiel, Seismicity, fault plane solutions, depth of faulting, and active tectonics of the Central Andes, *J. Geophys. Res.*, *88*, 10,403-10,428, 1983.

Suarez, G., J Gagnepain, A Cisternas, D. Hatzfeld, P. Molnar, L. Ocola, S.W Roecker, and J P. Viode, Tectonic deformation of the Andes and the configuration of the subducted slab in central Peru: results from a microseismic experiment, submitted to *Geophys. J. R. astr. Soc.*, 1984.

Swift, S.A., and M.J. Carr, The segmented nature of the Chilean seismic zone, *Phys Earth & Planet. Int.*, *9*, 183-191, 1974.

Thurber, C.H., Earthquake locations and three-dimensional crustal structure in the Coyote Lake area, central California, *J. Geophys. Res.*, *88*, 8226-8236, 1983.

Trudeau, G.B., *Wouldn't a Gremlin Have Been More Sensible*?, Bantam Books, New York, 1975.

FIGURE CAPTIONS

Figure 1. Earthquake locations used by Barazangi and Isacks to infer a tear in the Nazca plate as it is subducted under southern Peru. From Isacks and Barazangi (1976), and Barazangi and Isacks (1979).

Figure 2. a) Vertical cross sections of earthquakes relocated by Hasegawa and Sacks inside rectangles shown in the inserted map. Solid line is the assumed shape of the seismic zone inferred from the seismicity below a depth of 50 km.

b) Map of local seismic network used by Hasegawa and Sacks.

c) Subduction model proposed by Hasegawa and Sacks. From Hasegawa and Sacks (1981).

Figure 3. Vertical cross sections of earthquakes perpendicular to the trench, and their locations on a map. All earthquakes were located by Grange (1983) and are considered to be reliable. Fault plane solutions are back hemisphere projections with dark compressional and light extensional quadrants. "T" indicates the position of the trench, "C" the position of the coast. Triangles at the top of some sections indicate the position of active (open triangles) and dormant (closed triangles) volcanoes. In some sections the Mohorovičic discontinuity, as inferred from the model of Couch et al., (1981), appears as a dotted line. From Grange (1983).

Figure 4. Vertical cross sections of earthquakes parallel to the trench, and their locations on a map. Symbols are the same as in figure 3. From Grange (1983).

Figure 5. Maps of reliably located earthquakes at different depth intervals. From Grange (1983).

Figure 6. Vertical cross sections of earthquakes parallel to the direction of underthrusting of the Nazca plate, and their locations on a map. From Grange (1983).

Figure 7. Map of all epicenters with contours for events in different depth ranges. Note the change in orientation of contours from being parallel to the coast to more northerly trends near 15° to 15.5° S. Open triangles show locations of active volcanoes, closed triangles dormant ones. The arrow to the left gives the direction of relative plate motion between the Nazca and South American plates. From Grange et al., (1984b).

Figure 8. Maps of reliably located earthquakes at different depth intervals with fault plane solutions. Fault plane solutions are lower hemisphere projections with dark compressional quadrants and light dilatational quadrants. From Grange (1983).

Figure 9. Map with locations of seismic stations in southern Peru. Latitude, longitude and depth for each station is listed.

Figure 10. Configuration of three-layered structures used by Grange (1983). The sections labelled 1, 2, and 3 show the limits of the three simplified structures used to approximate the thickening of the crust. Note that these limits depend on the relative postition of the event and the station.

Figure 11. Profile of first model used to relocate microearthquakes. Numbers are P and S velocities of different parts of the model.

Figure 12. a) Structure proposed by James (1971) for Bolivia and southern Peru.
b) Depth contours for the Moho proposed by James (1971).

Figure 13. Wadati plots for different depth intervals. Plotted points are P minus S arrival times vs. P arrival times.

Figure 14. Profile of second model used to relocate microearthquakes. Also used as the initial model for velocity inversions. Numbers are P and S velocities.

Figure 15. Vertical cross sections of relocated earthquakes, parallel to the trench, and their locations on a map. These earthquakes are considered to be reliably located.

Figure 16. Vertical cross sections of relocated earthquakes parallel to the direction of underthrusting of the Nazca plate, and their locations on a map.

Figure 17. a) Map of all relocated earthquakes used in the velocity inversions.
b) Maps of relocated earthquakes at different depth intervals with an outline of the three-dimensional structure used in the velocity inversions.

Figure 18. Simplified map used as a template to display the the calculated three-dimensional velocity structures.

Figures 19 - 58. Maps displaying calculated values for P and S velocity structure. On each page, the top map shows the calculate velocity and the percent change from the initial model for each block in the specified layer, and the bottom map shows the resolution and the standard deviation of the calculated velocity for each block. At the

bottom of each page the number of the inversion run, the upper and lower bounds of the layer, and the type of phase used (P or S) are specified.

Figures 59 - 61. Contour maps of the percent changes in P and S wave velocities for the first inversion. The configuration of the blocks used in the inversion is superimposed upon the seismicity maps.

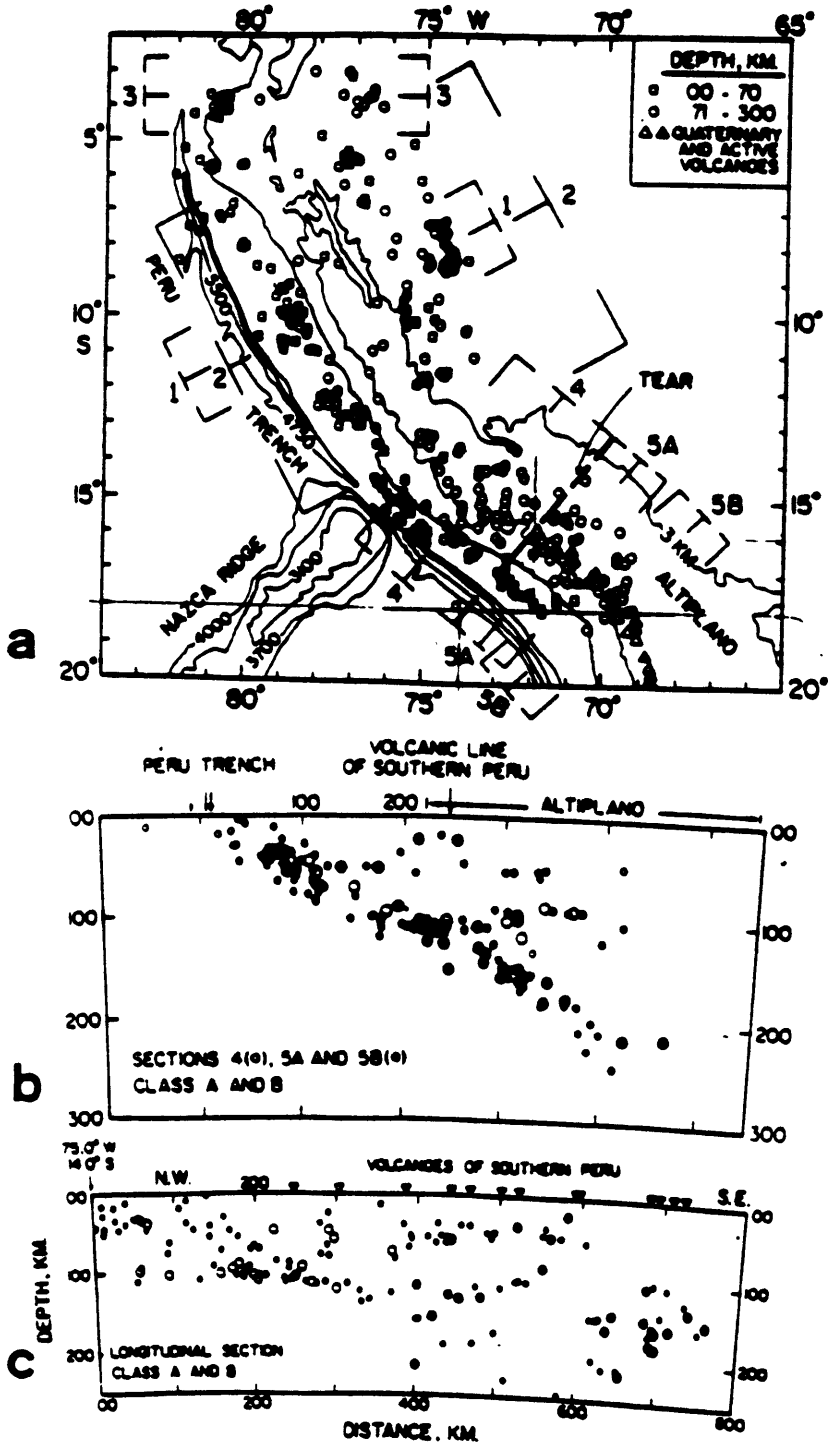
a
80°
75° W
70°
65°
DEPTH, KM.
00 - 70
71 - 300
QUATERNARY AND ACTIVE VOLCANOES
5°
10° S
15°
20°
PERU
TRENCH
NAZCA RIDGE
TEAR
ALTIPLANO
3 KM.
b
PERU TRENCH
VOLCANIC LINE OF SOUTHERN PERU
ALTIPLANO
100
200
SECTIONS 4(o), 5A AND 5B(o)
CLASS A AND B
c
N.W.
VOLCANOES OF SOUTHERN PERU
S.E.
DEPTH, KM.
LONGITUDINAL SECTION
CLASS A AND B
DISTANCE, KM.

Figure 1.

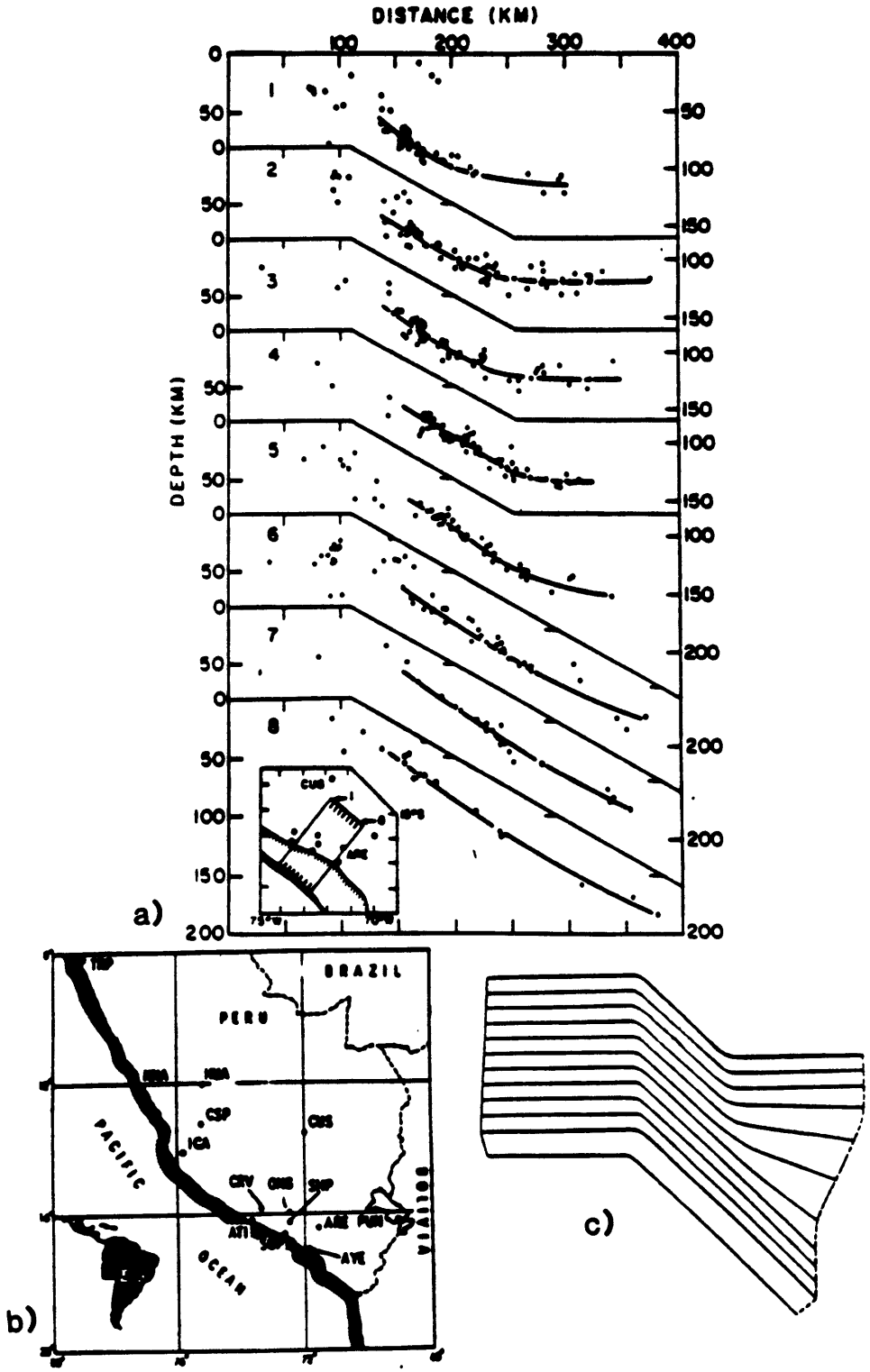
DISTANCE (KM)
DEPTH (KM)
a)
b)
c)
BRAZIL
PERU
PACIFIC
OCEAN

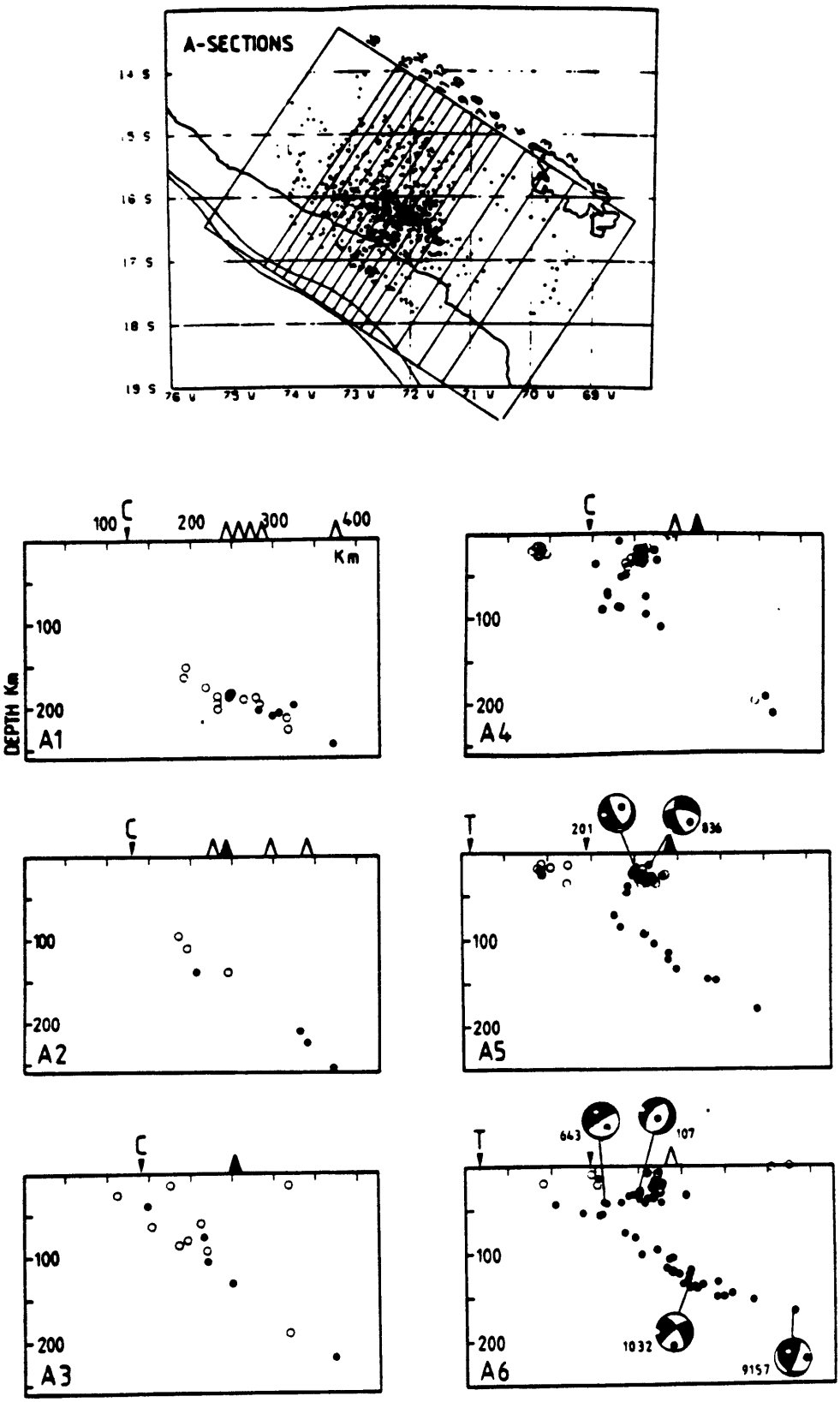
A-SECTIONS
14 S
15 S
16 S
17 S
18 S
19 S
76 W
75 W
74 W
73 W
72 W
71 W
70 W
69 W
C
100
200
300
400
Km
DEPTH Km
A1
A2
A3
A4
A5
A6
T
201
836
643
107
1032
9157

Figure 3.

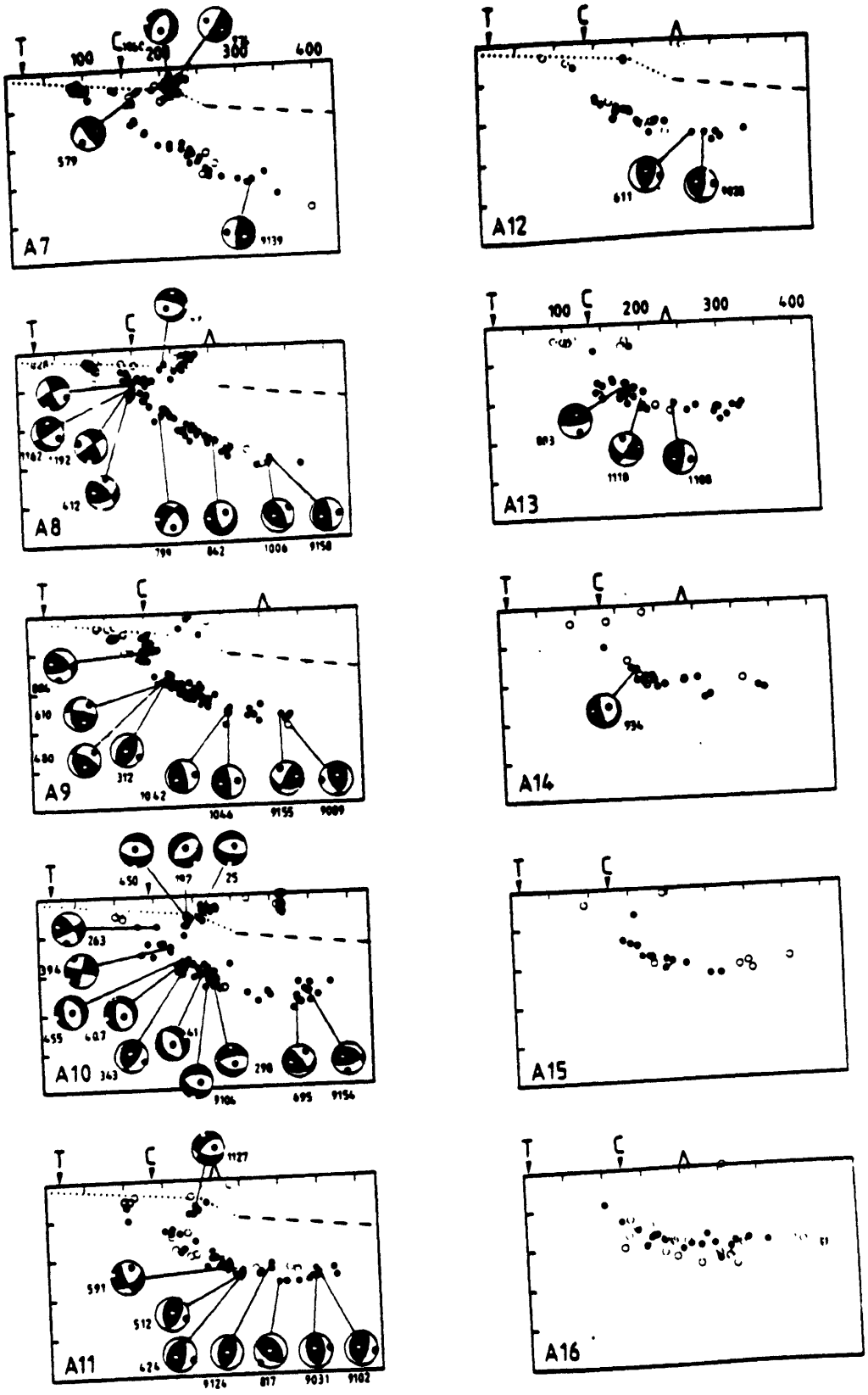

Figure 3(cont.).

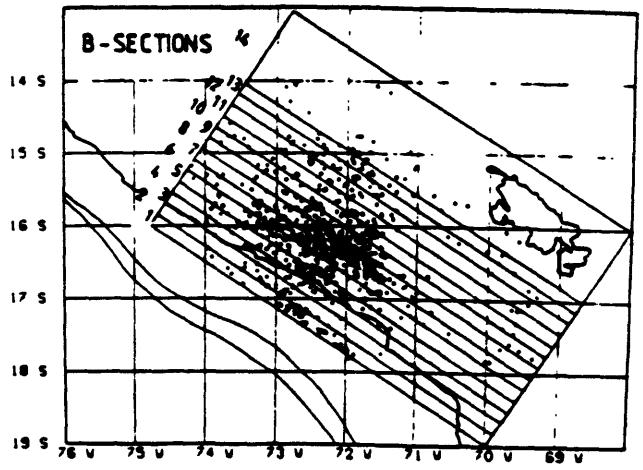
B-SECTIONS
14 S
15 S
16 S
17 S
18 S
19 S
76 W
75 W
74 W
73 W
72 W
71 W
70 W
69 W

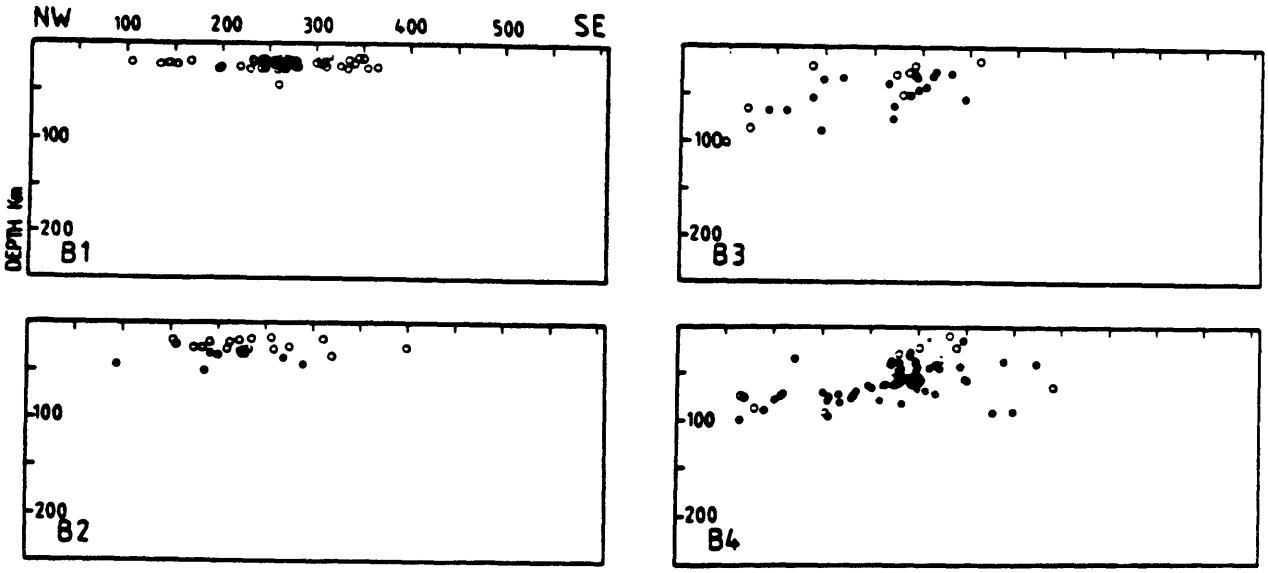
NW
100
200
300
400
500
SE
DEPTH Km
100
200
B1
100
200
B3
100
200
B2
100
200
B4

Figure 4.

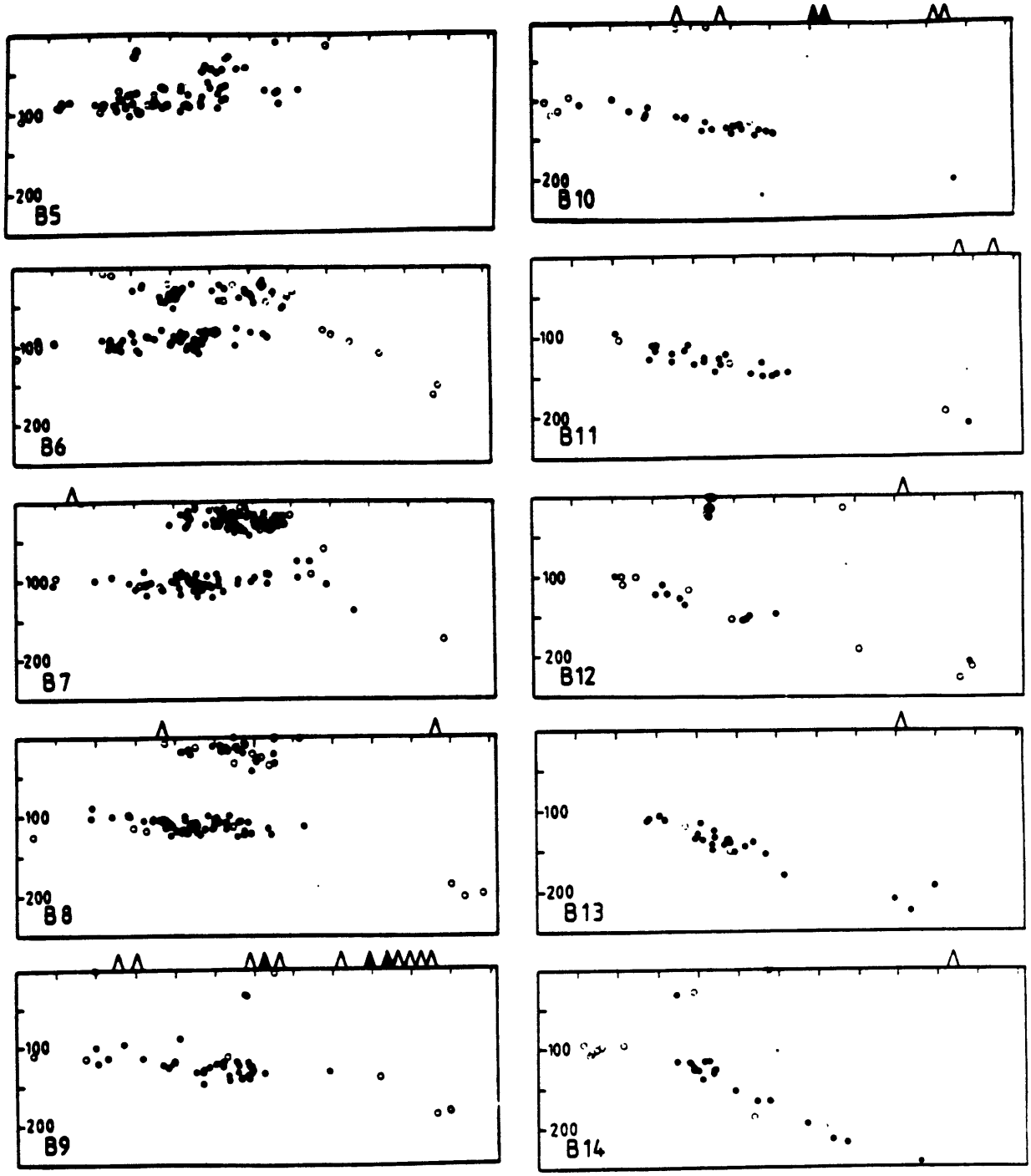

Figure 4(cont.).

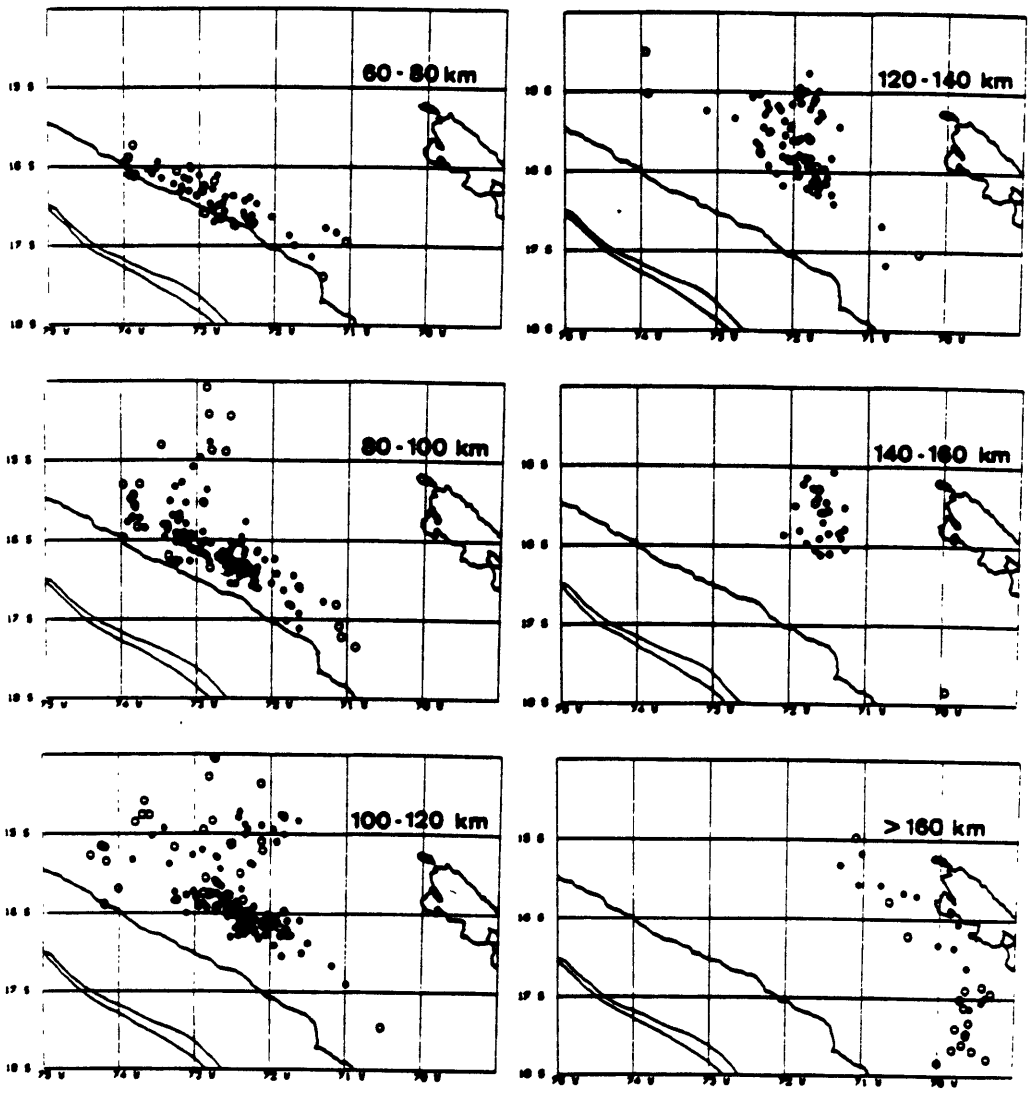

Figure 5.

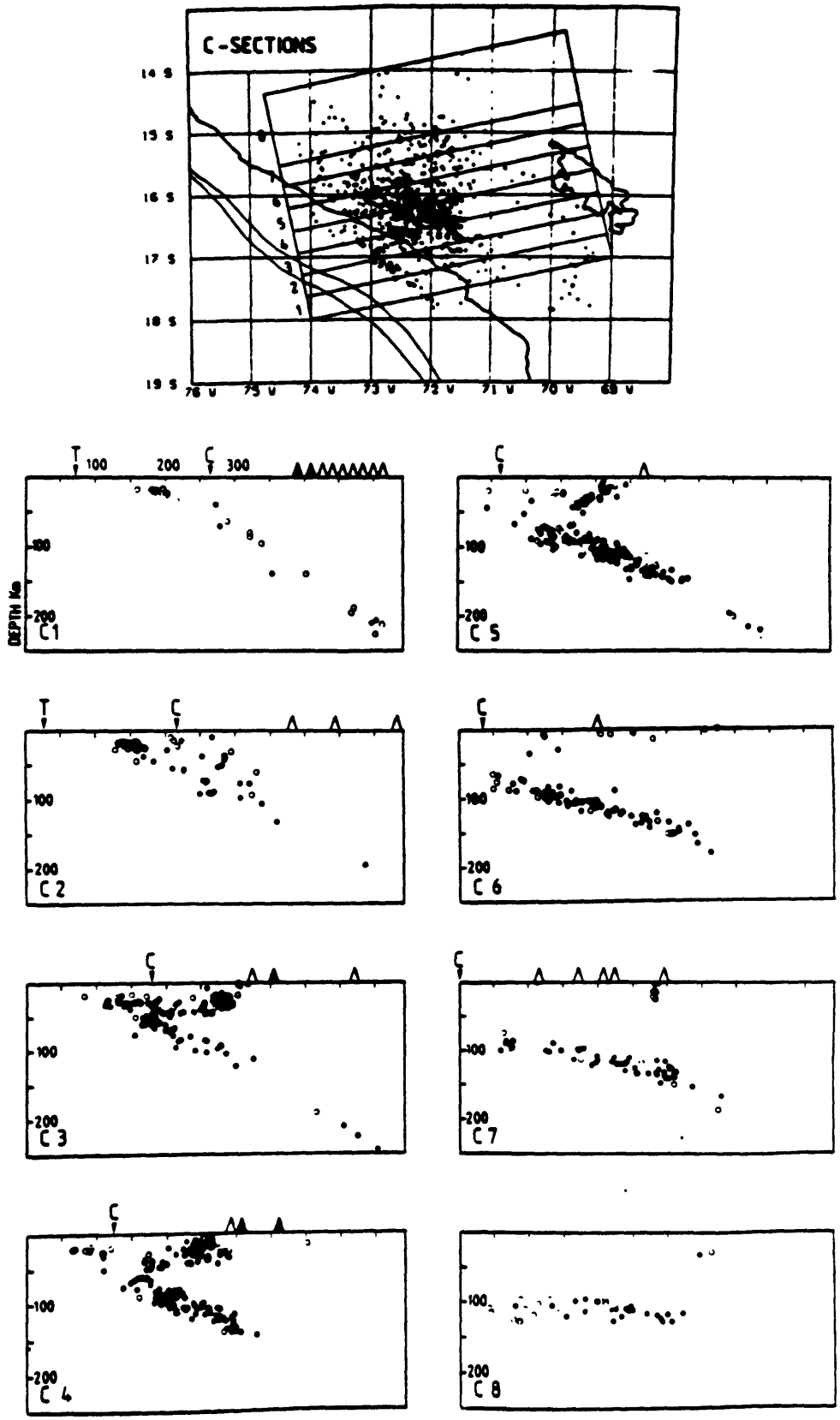
C-SECTIONS
14 S
15 S
16 S
17 S
18 S
19 S
76 W
75 W
74 W
73 W
72 W
71 W
70 W
69 W
T
C
100
200
300
DEPTH Km
C1
C2
C3
C4
C5
C6
C7
C8

Figure 6.

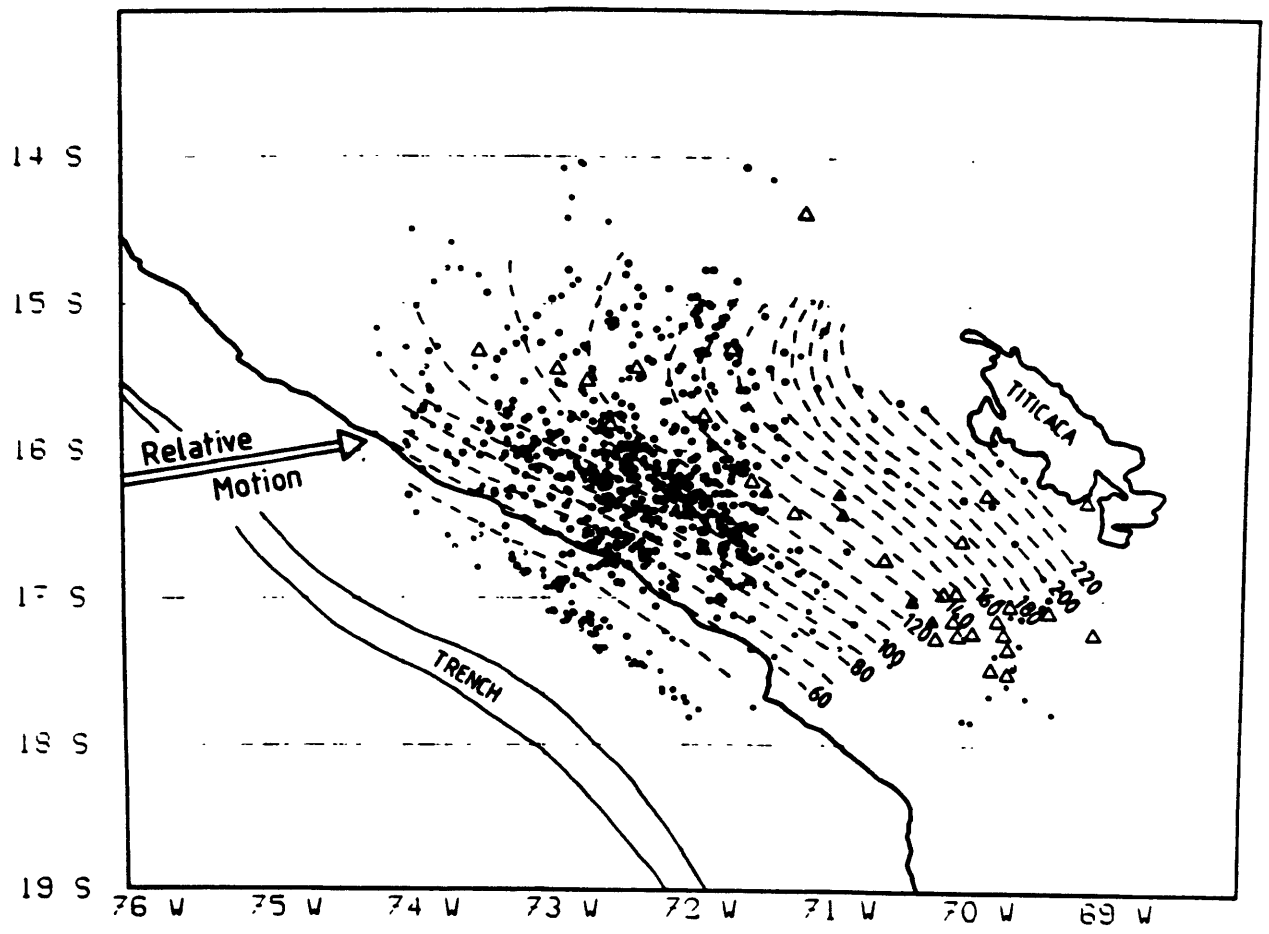
14 S
15 S
16 S
17 S
18 S
19 S
76 W
75 W
74 W
73 W
72 W
71 W
70 W
69 W
Relative
Motion
TRENCH
TITICACA
60
80
100
120
140
160
180
200
220

Figure 7.

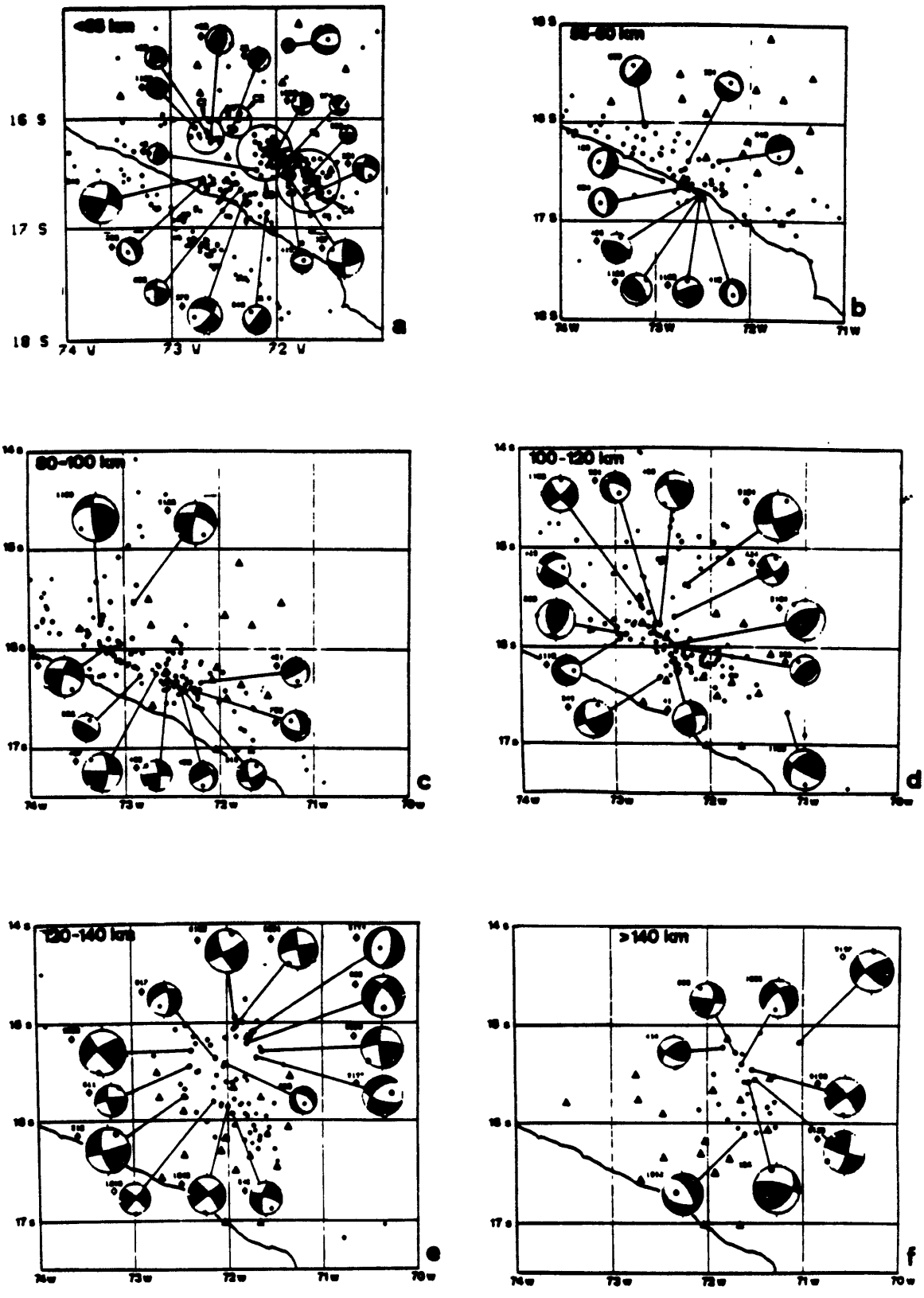
16 S
17 S
18 S
74 W
73 W
72 W
a
b
80-100 km
c
100-120 km
d
120-140 km
e
>140 km
f

Figure 8.

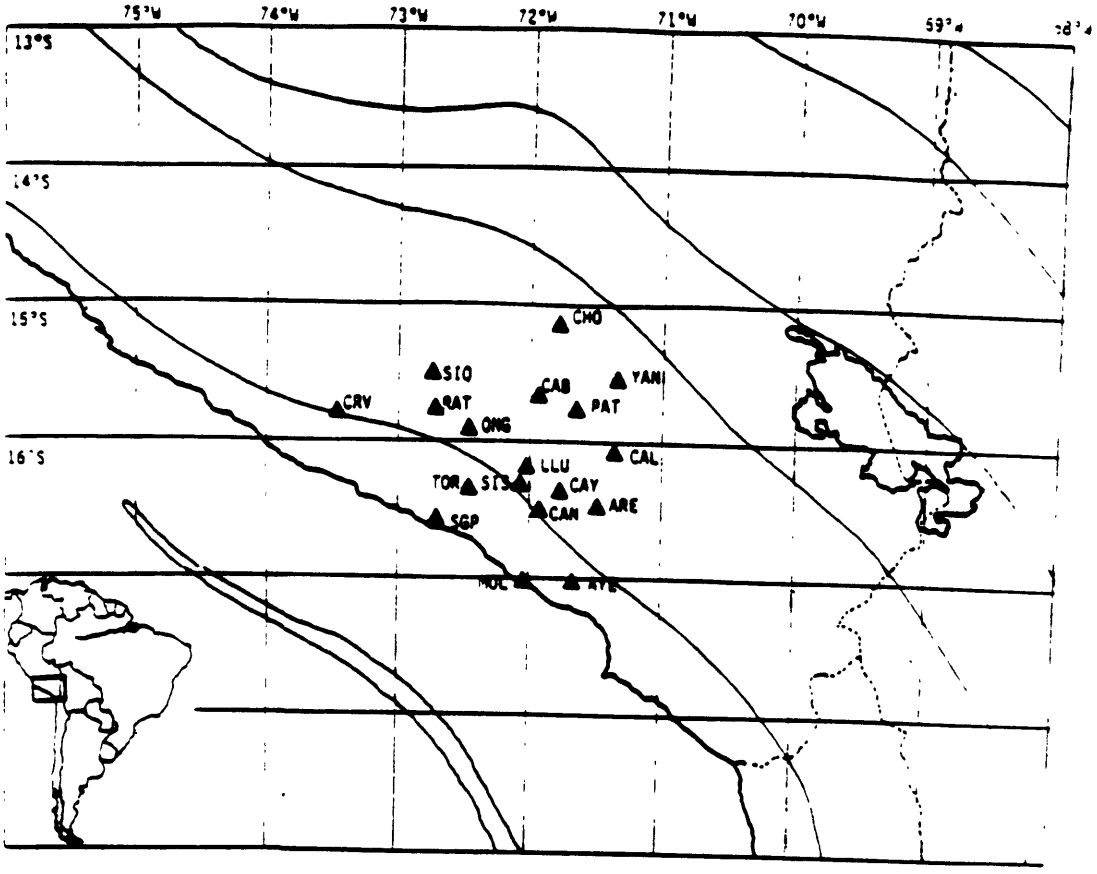

Station	Latitude S	Longitude W	Altitude
YAN	15° 32.09'	71° 21.03'	4050 m
CAL	16° 03.74'	71° 22.21'	3950 m
CHO	15° 08.00'	71° 47.71'	4500 m
PAT	15° 45.47'	71° 39.44'	4900 m
CAB	15° 39.62'	71° 56.66'	3770 m
LLU	16° 10.65'	72° 02.11'	1800 m
CRV	15° 47.07'	73° 28.38'	1780 m
ARE	16° 27.73'	71° 29.48'	2452 m
AYE	17° 00.80'	71° 40.31'	240 m
ONG	15° 53.94'	72° 28.39'	880 m
TOR	16° 20.46'	72° 28.25'	350 m
SIS	16° 18.13'	72° 04.85'	1475 m
CAY	16° 21.25'	71° 66.45'	1700 m
MOL	17° 00.52'	72° 02.88'	50 m
RAT	15° 45.33'	72° 43.62'	4000 m
SIQ	15° 29.89'	72° 45.06'	4550 m
CAN	16° 29.62'	71° 55.79'	1200 m
SGP	16° 33.87'	72° 42.75'	140 m

Figure 9.

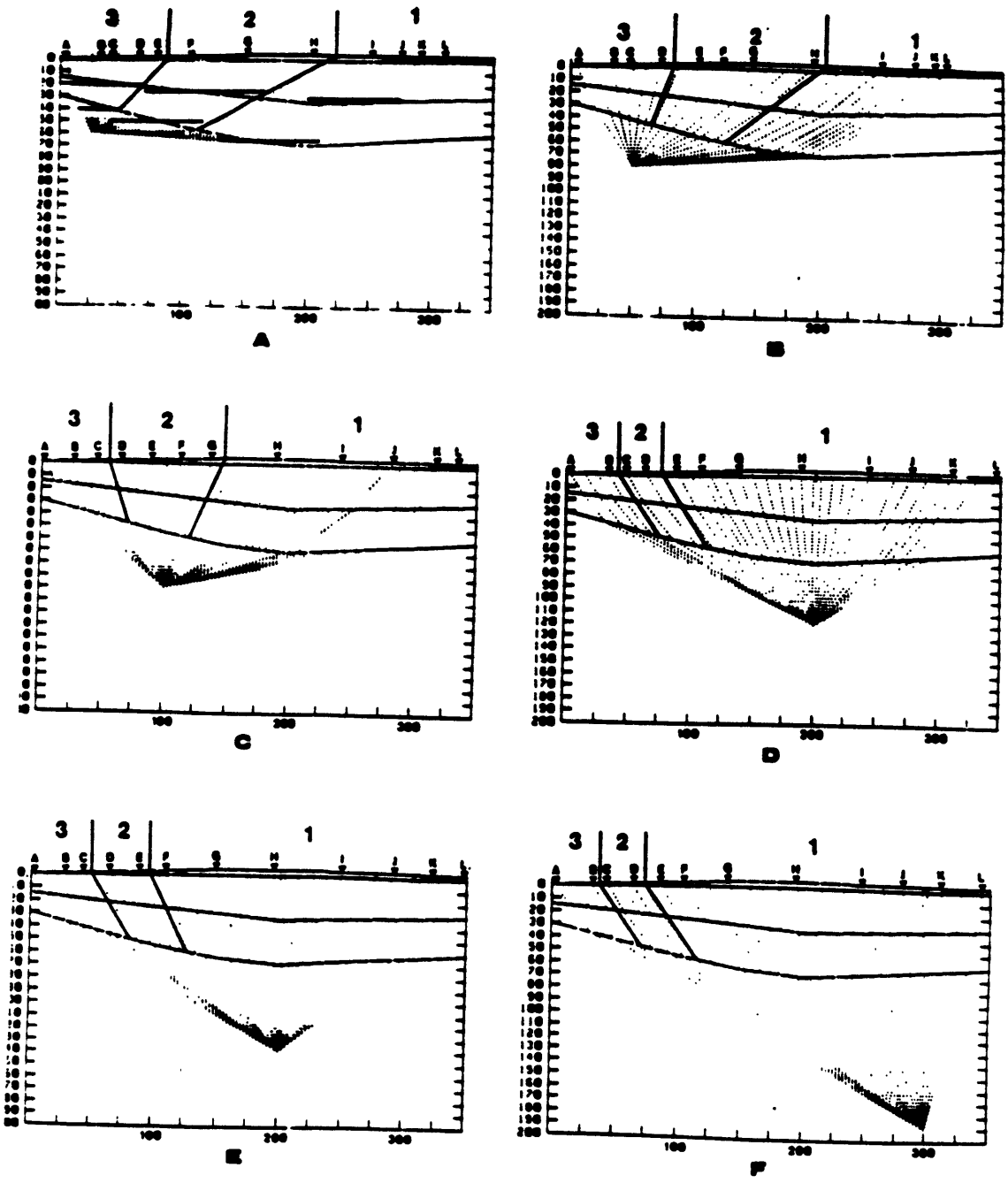

Model 1		Model 2		Model 3	
km/s	km	km/s	km	km/s	km
6.0	0.0	6.0	0.0	6.0	0.0
6.8	30.0	6.8	25.0	6.8	20.0
8.2	65.0	8.2	55.0	8.2	40.0

Figure 10.

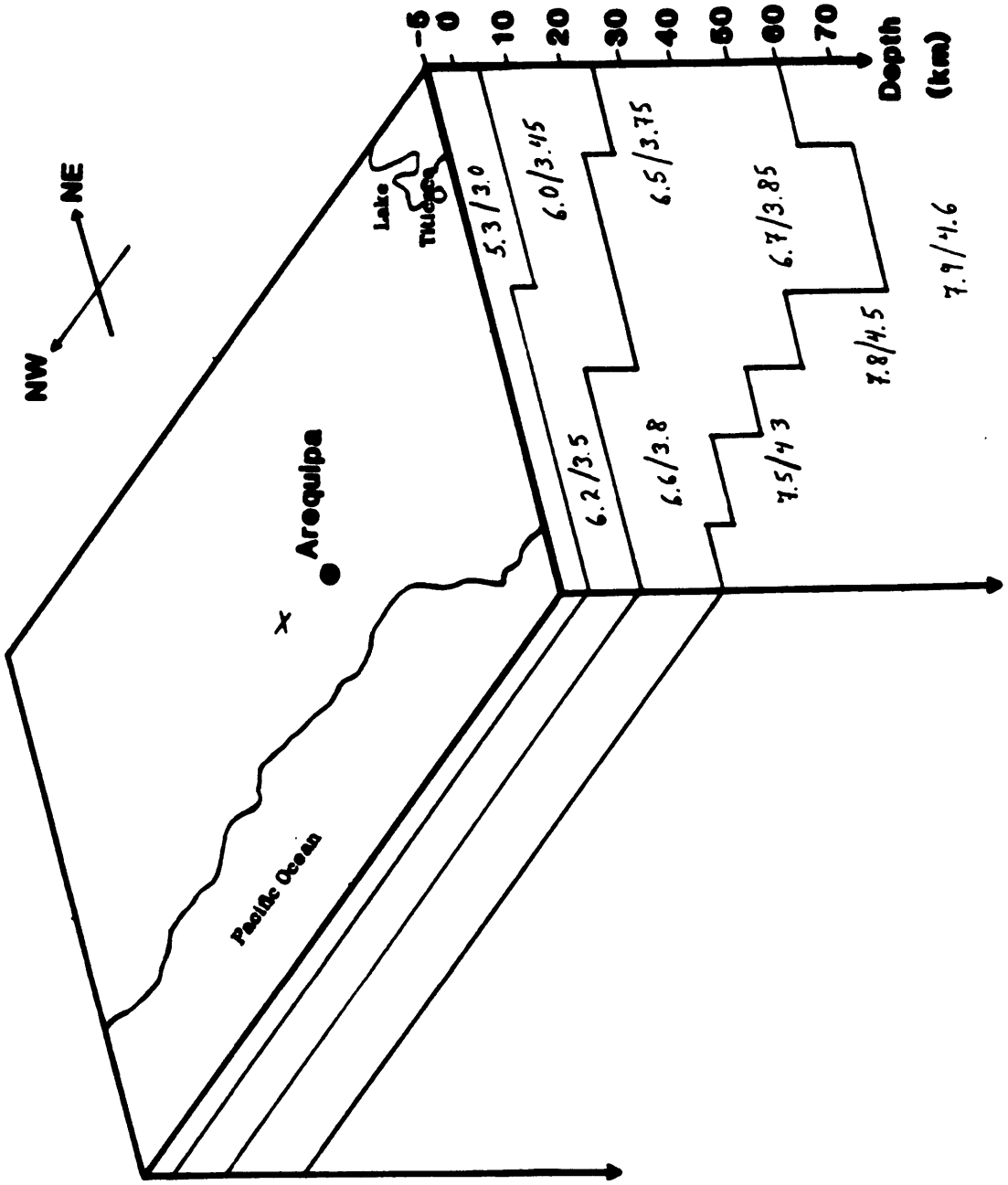
-5
0
10
20
30
40
50
60
70
Depth
(km)
NW
NE
Lake
Titicaca
Arequipa
Pacific Ocean
5.3/3.0
6.0/3.45
6.5/3.75
6.7/3.85
7.9/4.6
6.2/3.5
6.6/3.8
7.5/4.3
7.8/4.5

Figure 11.

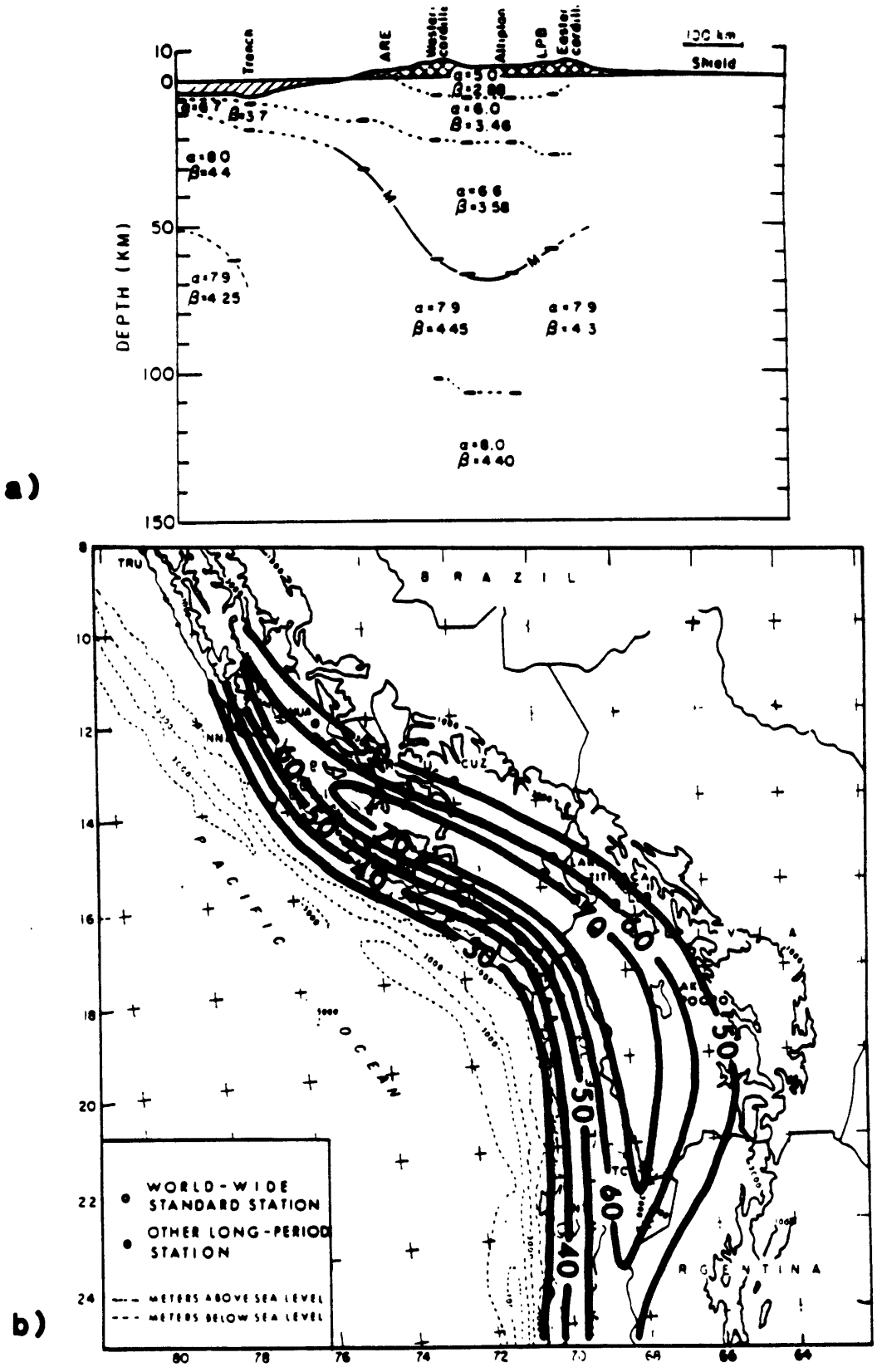
a)
Trench
ARE
Western cordill.
Altiplan
LPB
Eastern cordill.
100 km
Shield
DEPTH (KM)
10
0
50
100
150
α=8.0 β=4.4
α=6.6 β=3.58
α=7.9 β=4.25
α=7.9 β=4.45
α=7.9 β=4.3
α=8.0 β=4.40
b)
BRAZIL
PACIFIC OCEAN
ARGENTINA
WORLD-WIDE STANDARD STATION
OTHER LONG-PERIOD STATION
METERS ABOVE SEA LEVEL
METERS BELOW SEA LEVEL
80
78
76
74
72
70
68
66
64

Figure 12.

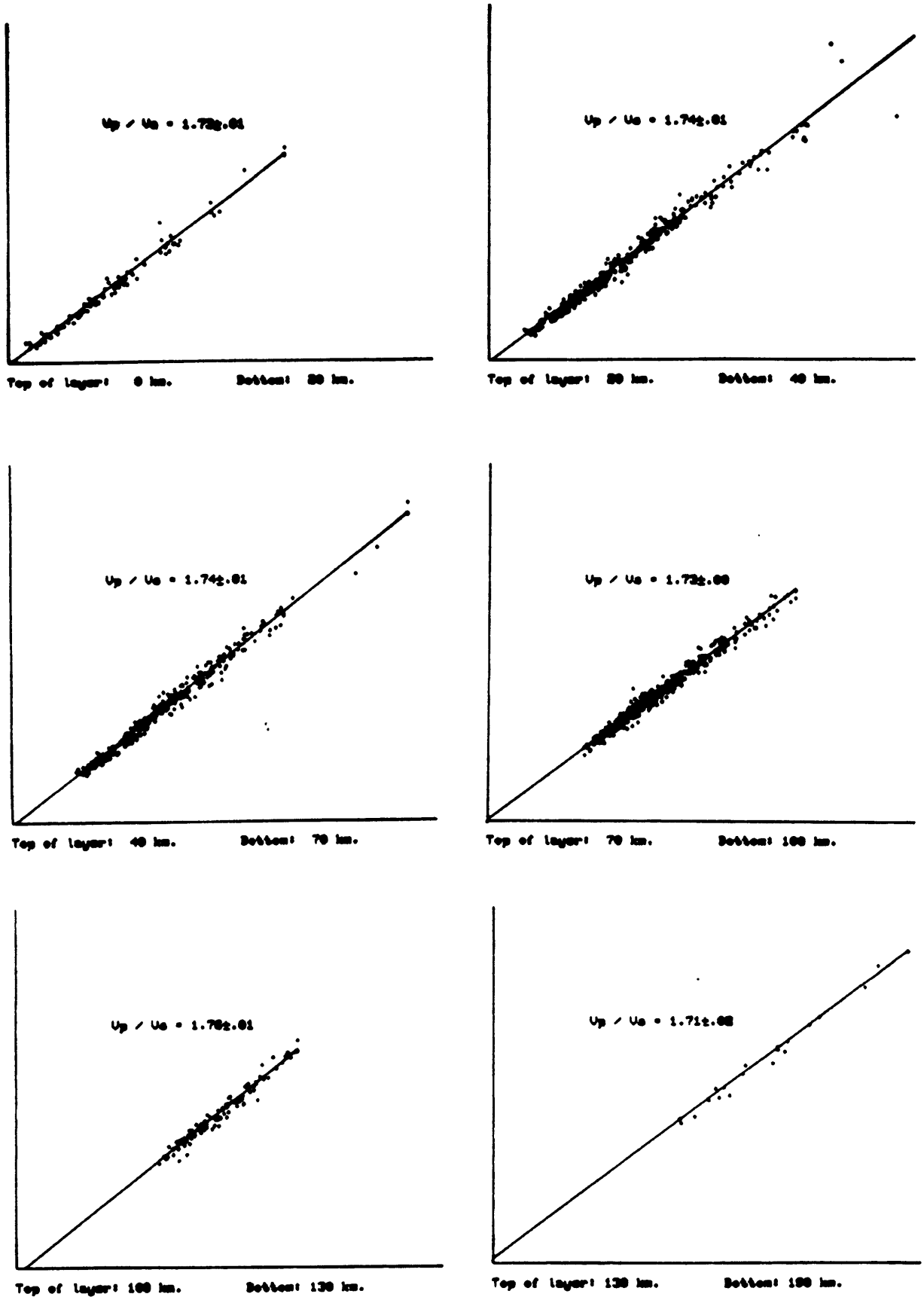
Up / Us = 1.72±.01
Top of layer: 0 km. Bottom: 20 km.
Up / Us = 1.74±.01
Top of layer: 20 km. Bottom: 40 km.
Up / Us = 1.74±.01
Top of layer: 40 km. Bottom: 70 km.
Up / Us = 1.73±.00
Top of layer: 70 km. Bottom: 100 km.
Up / Us = 1.70±.01
Top of layer: 100 km. Bottom: 130 km.
Up / Us = 1.71±.00
Top of layer: 130 km. Bottom: 180 km.

Figure 13.

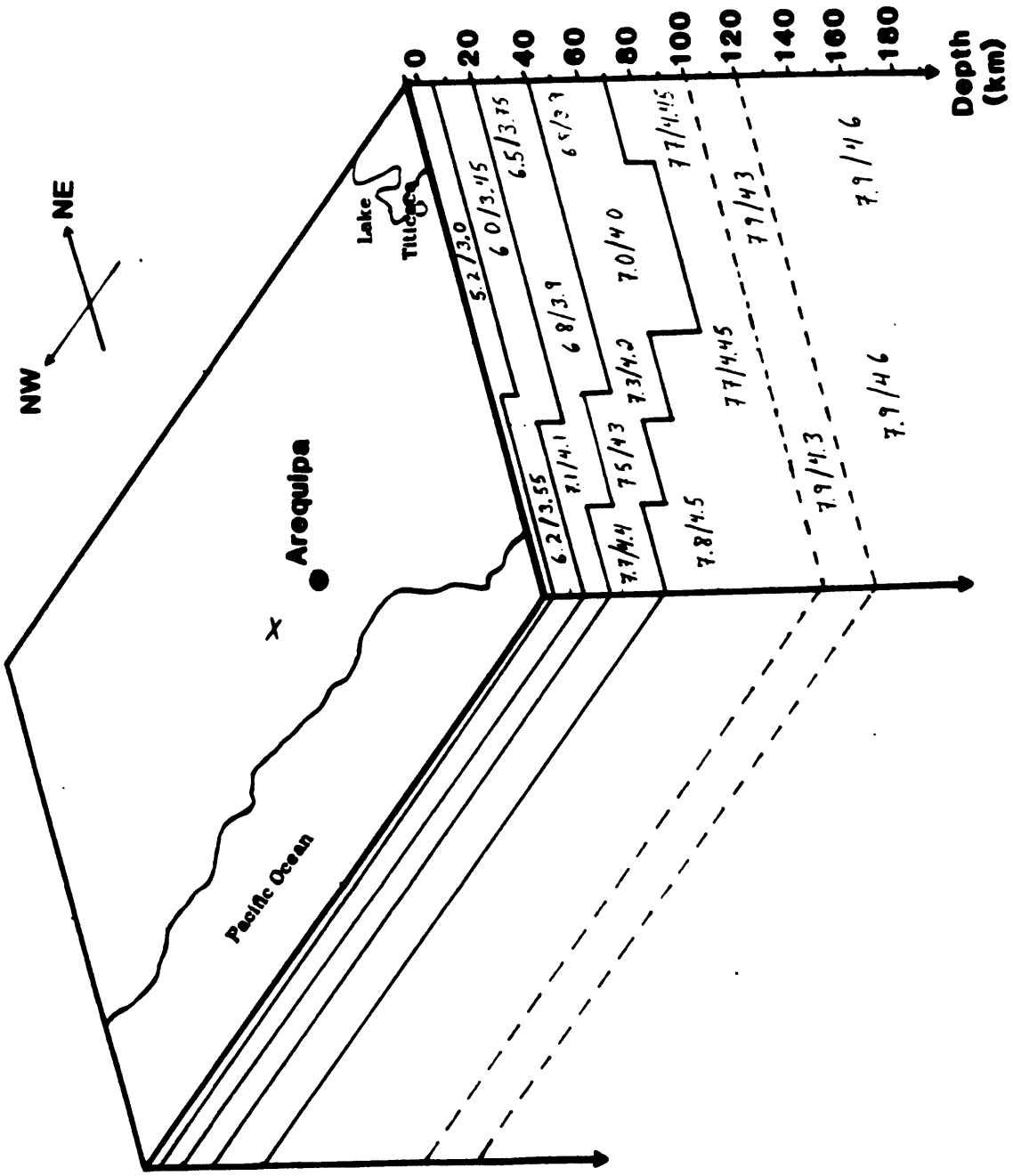
NW
NE
Lake
Titicaca
Arequipa
Pacific Ocean
0
20
40
60
80
100
120
140
160
180
Depth
(km)
5.2/3.0
6.0/3.15
6.5/3.75
6.8/3.9
7.0/4.0
7.3/4.2
7.5/4.3
7.7/4.4
7.8/4.5
7.7/4.45
7.9/4.3
7.9/4.6
7.7/4.45
7.9/4.3
7.9/4.6
6.2/3.55
7.1/4.1

Figure 14.

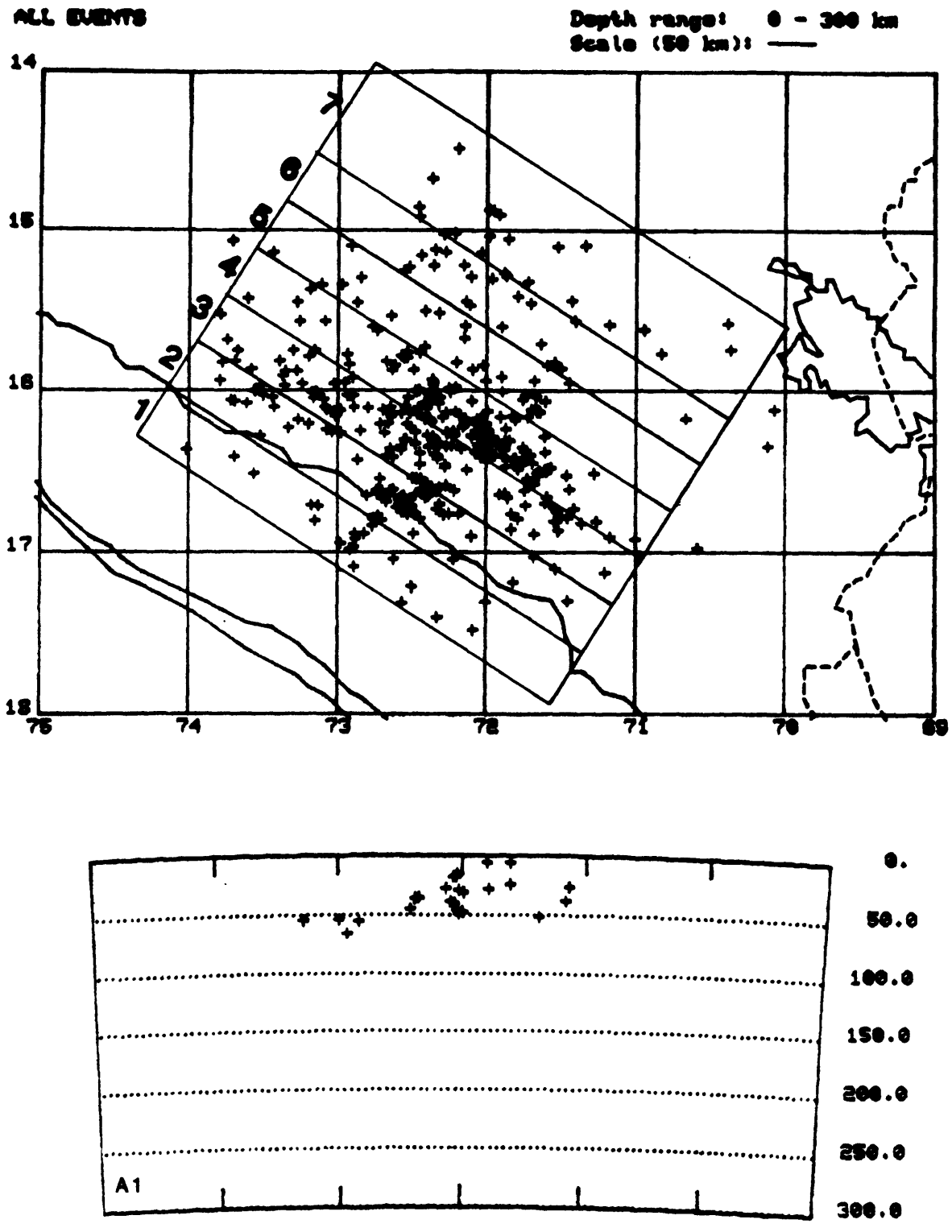
ALL EVENTS
Depth range: 0 - 300 km
Scale (50 km):
14
15
16
17
18
76
74
73
72
71
70
69
1
2
3
4
5
6
7
A1
0.
50.0
100.0
150.0
200.0
250.0
300.0

Figure 15.

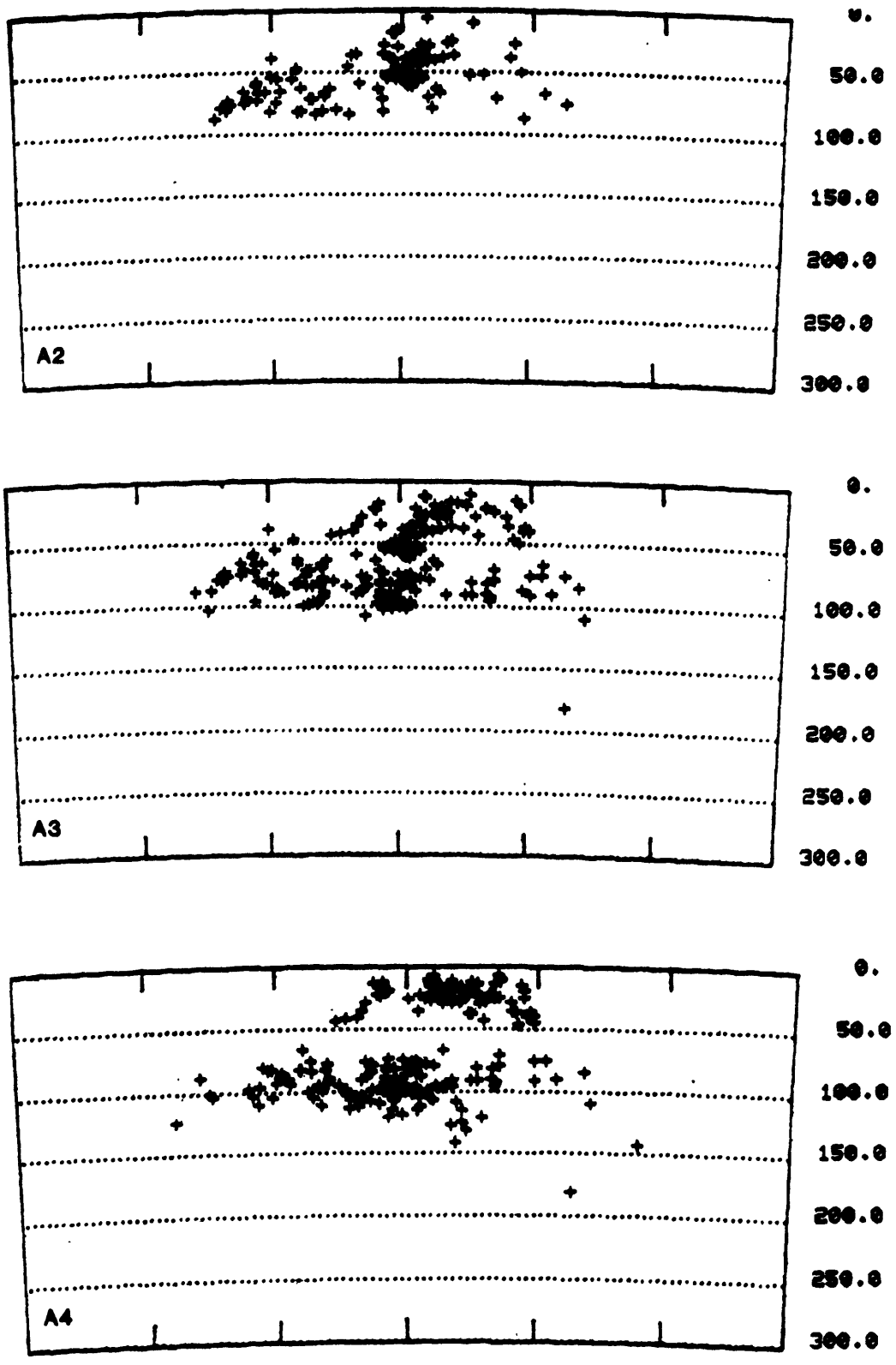

Figure 15(cont.).

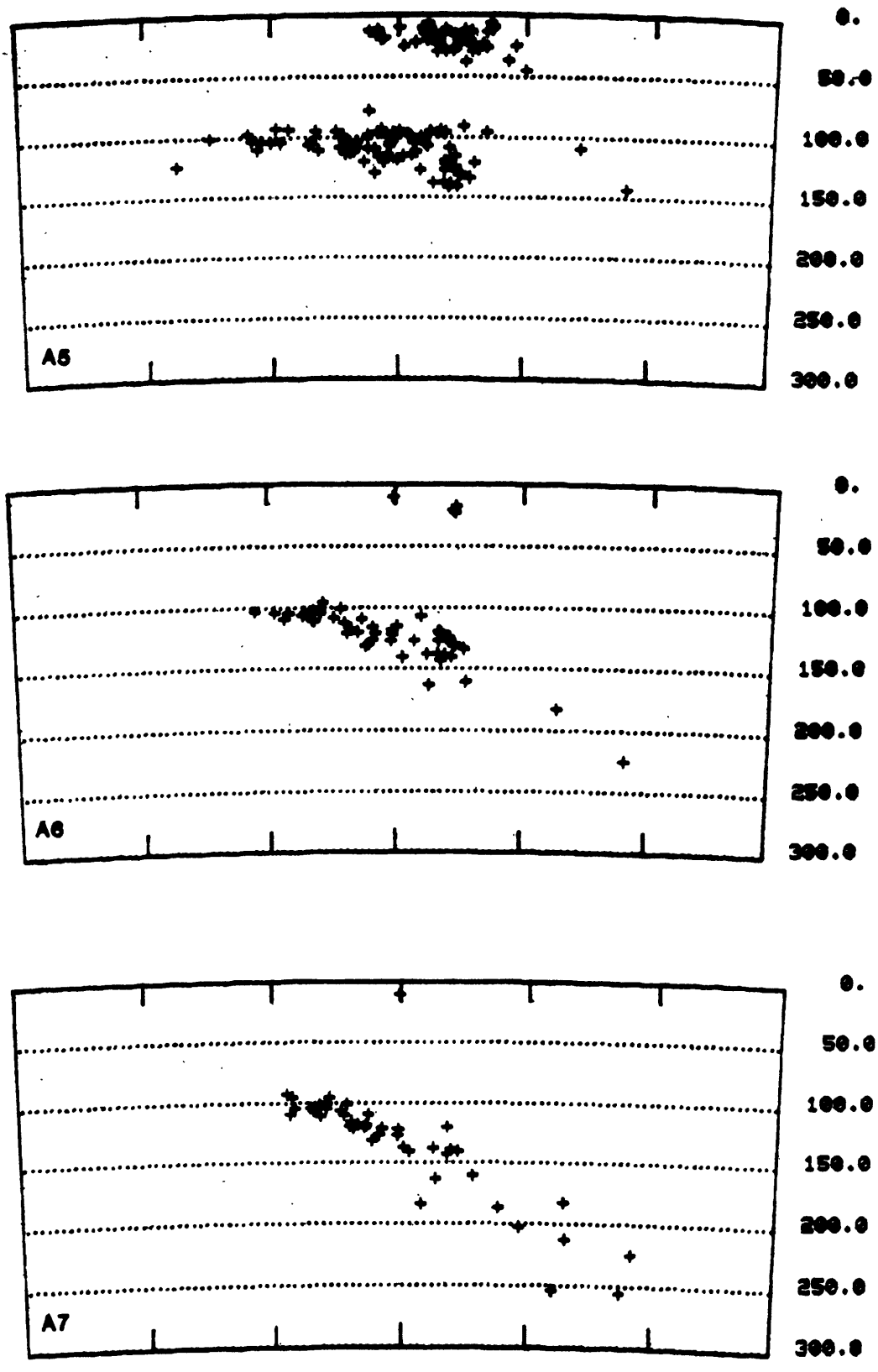
0.
50.0
100.0
150.0
200.0
250.0
300.0
A5
0.
50.0
100.0
150.0
200.0
250.0
300.0
A6
0.
50.0
100.0
150.0
200.0
250.0
300.0
A7

Figure 16.

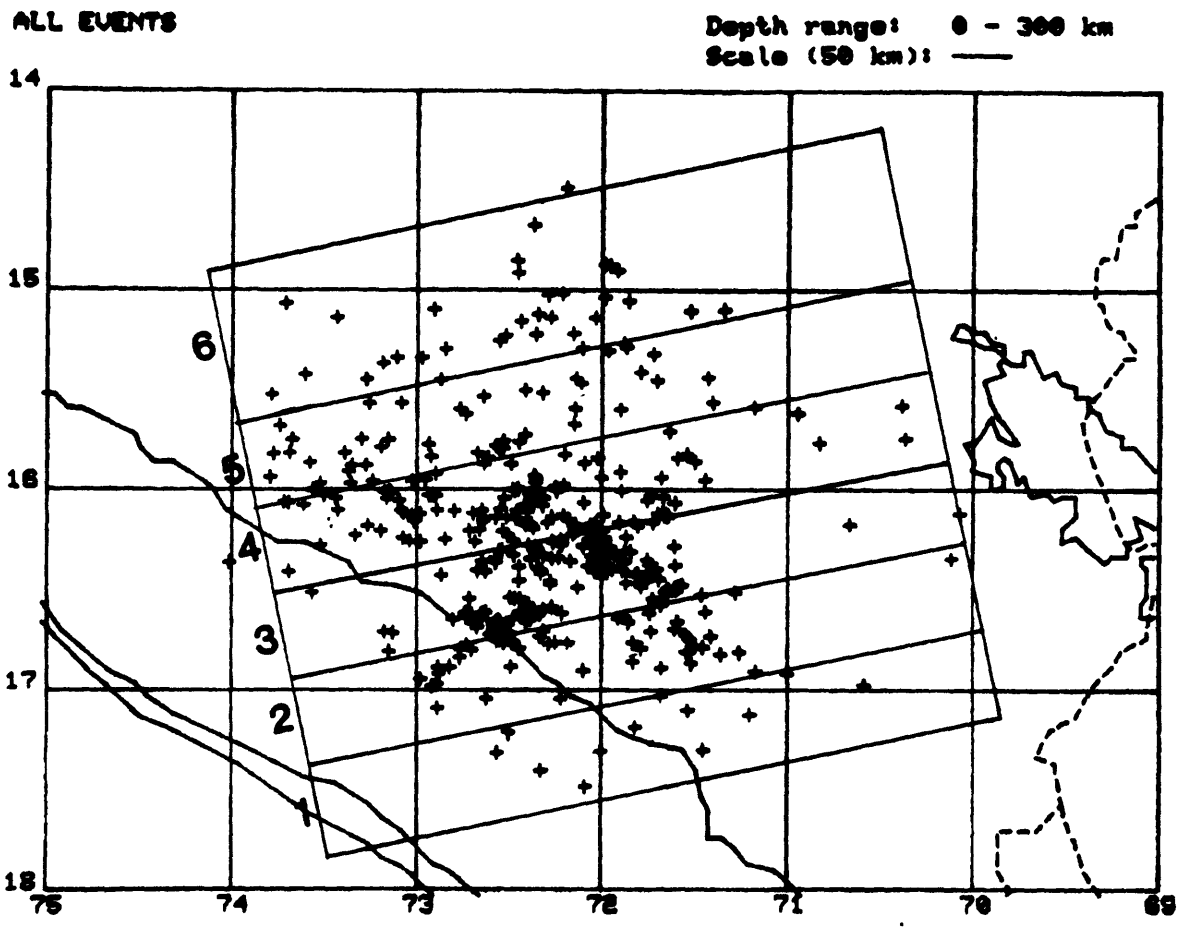

Figure 15(cont.).

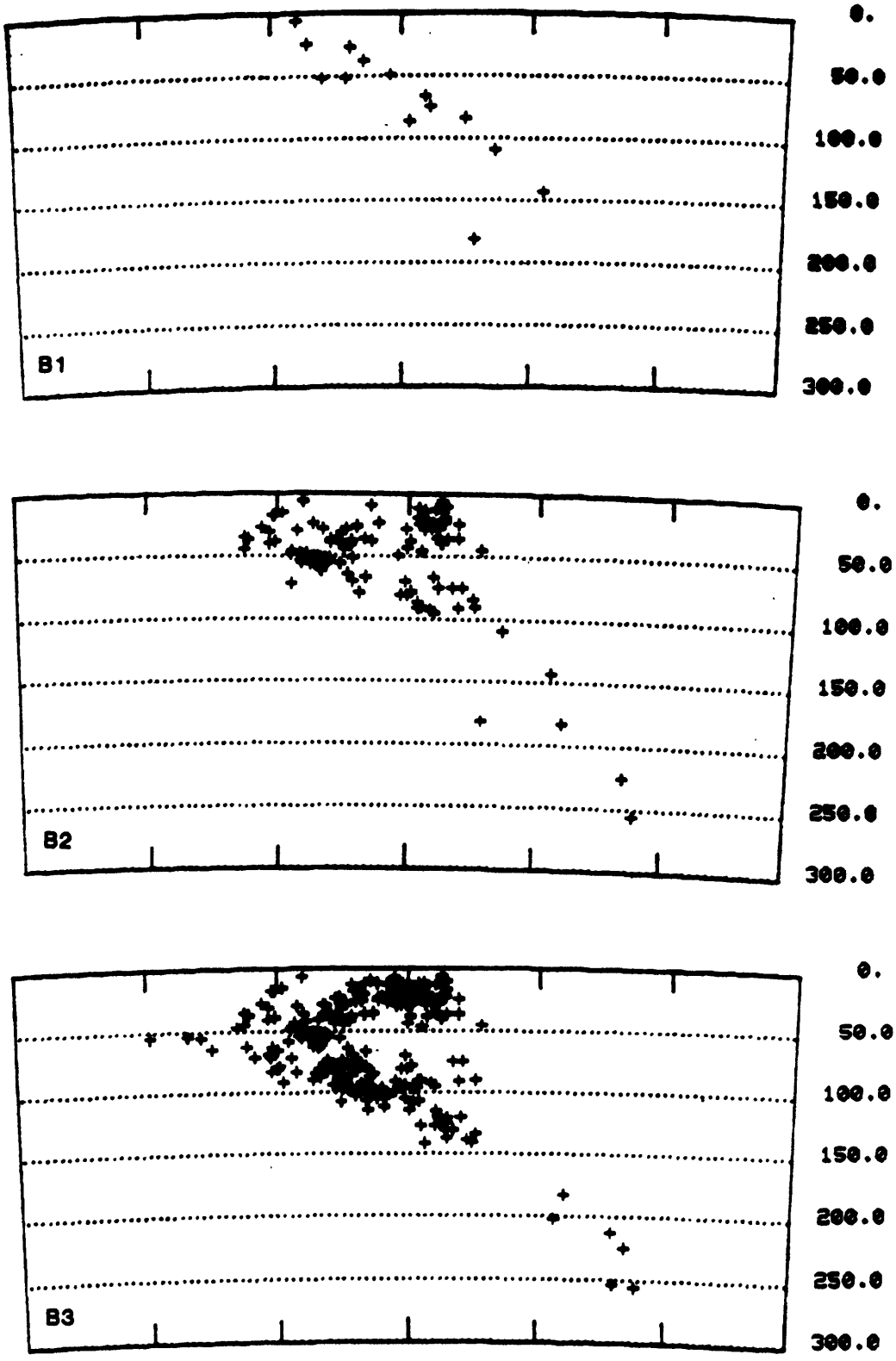

Figure 16(cont.).

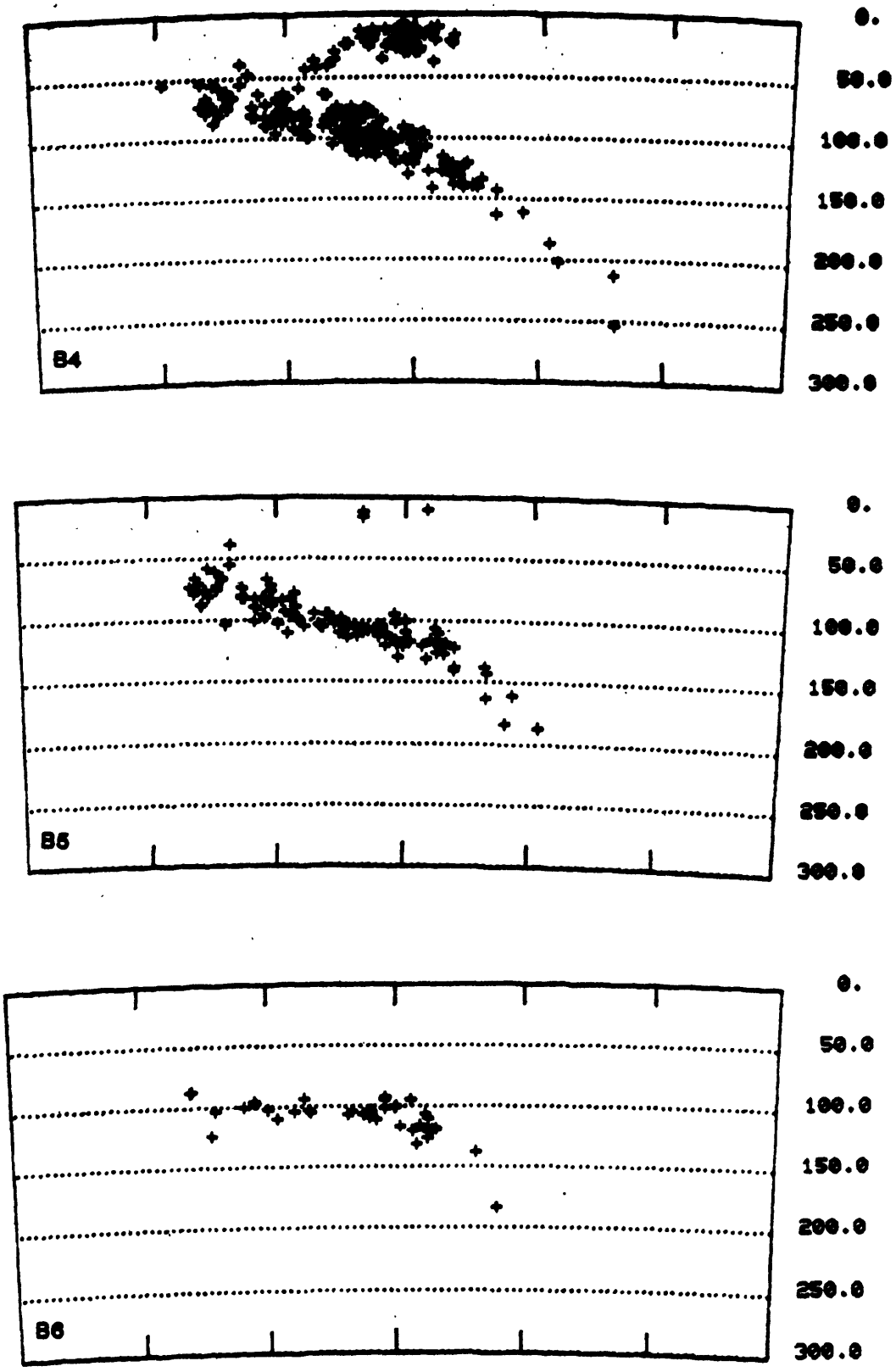

Figure 16(cont.).

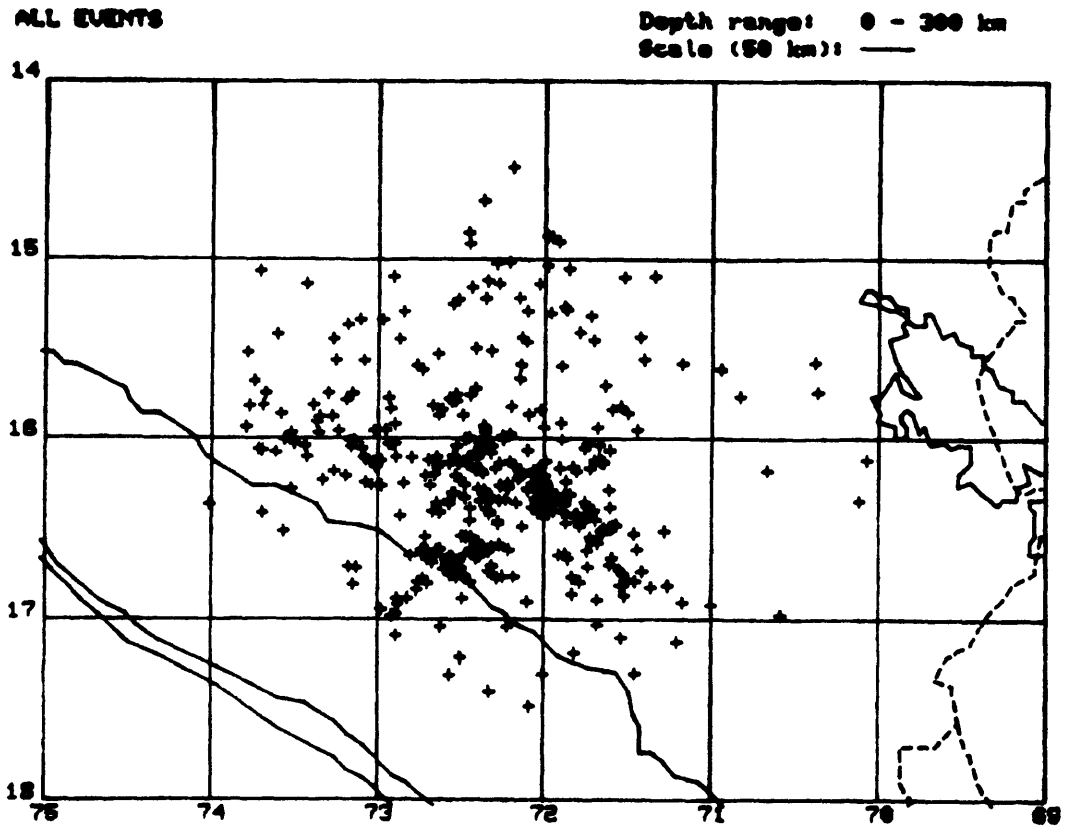
ALL EVENTS
Depth range: 0 - 300 km
Scale (50 km):
14
15
16
17
18
75
74
73
72
71
70
69

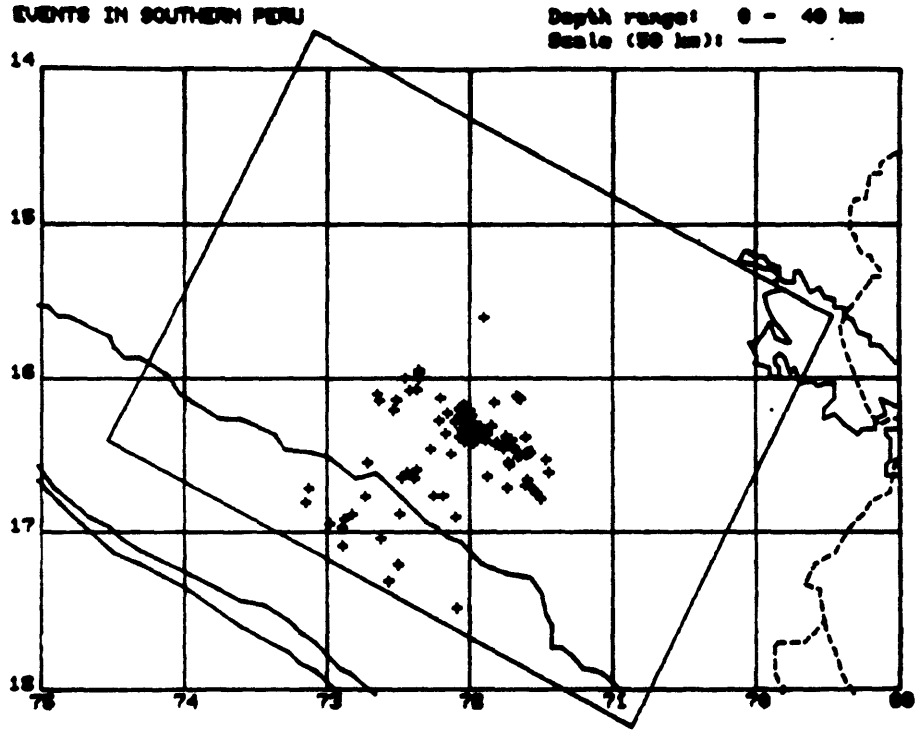
EVENTS IN SOUTHERN PERU
Depth range: 0 - 40 km
Scale (50 km):
14
15
16
17
18
75
74
73
72
71
70
69

Figure 17.

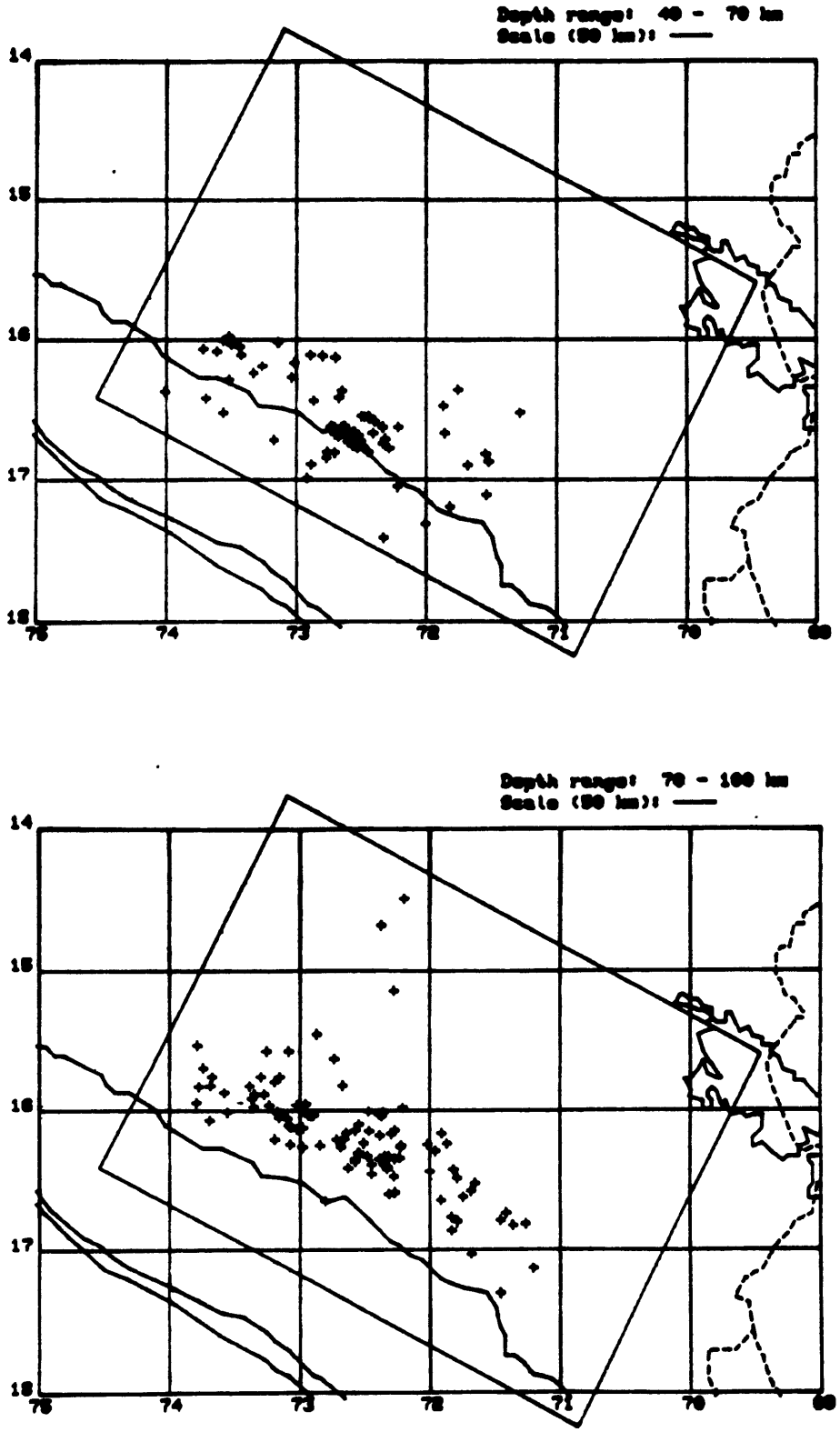

Figure 17(cont.).

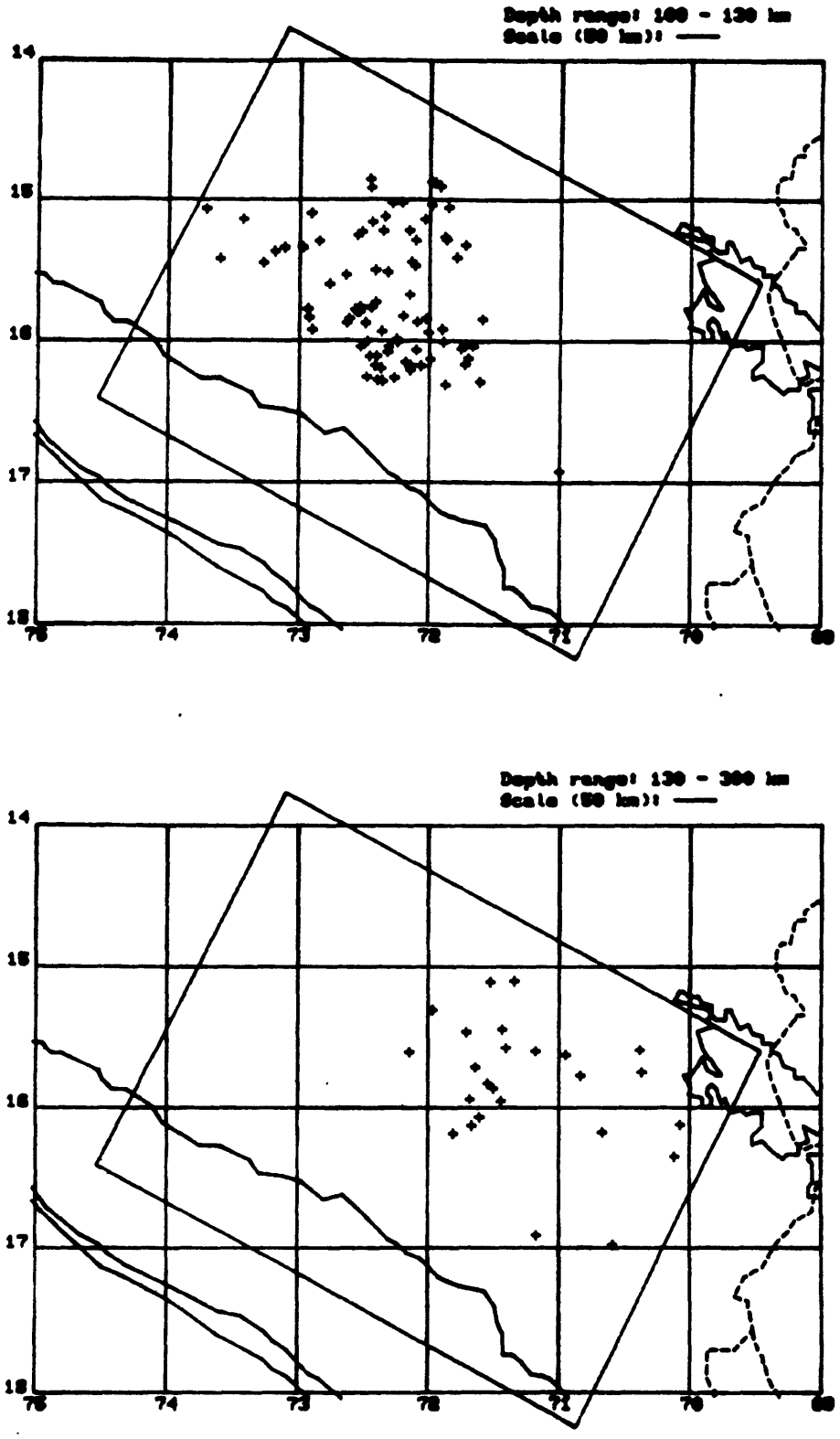

Figure 17(cont.).

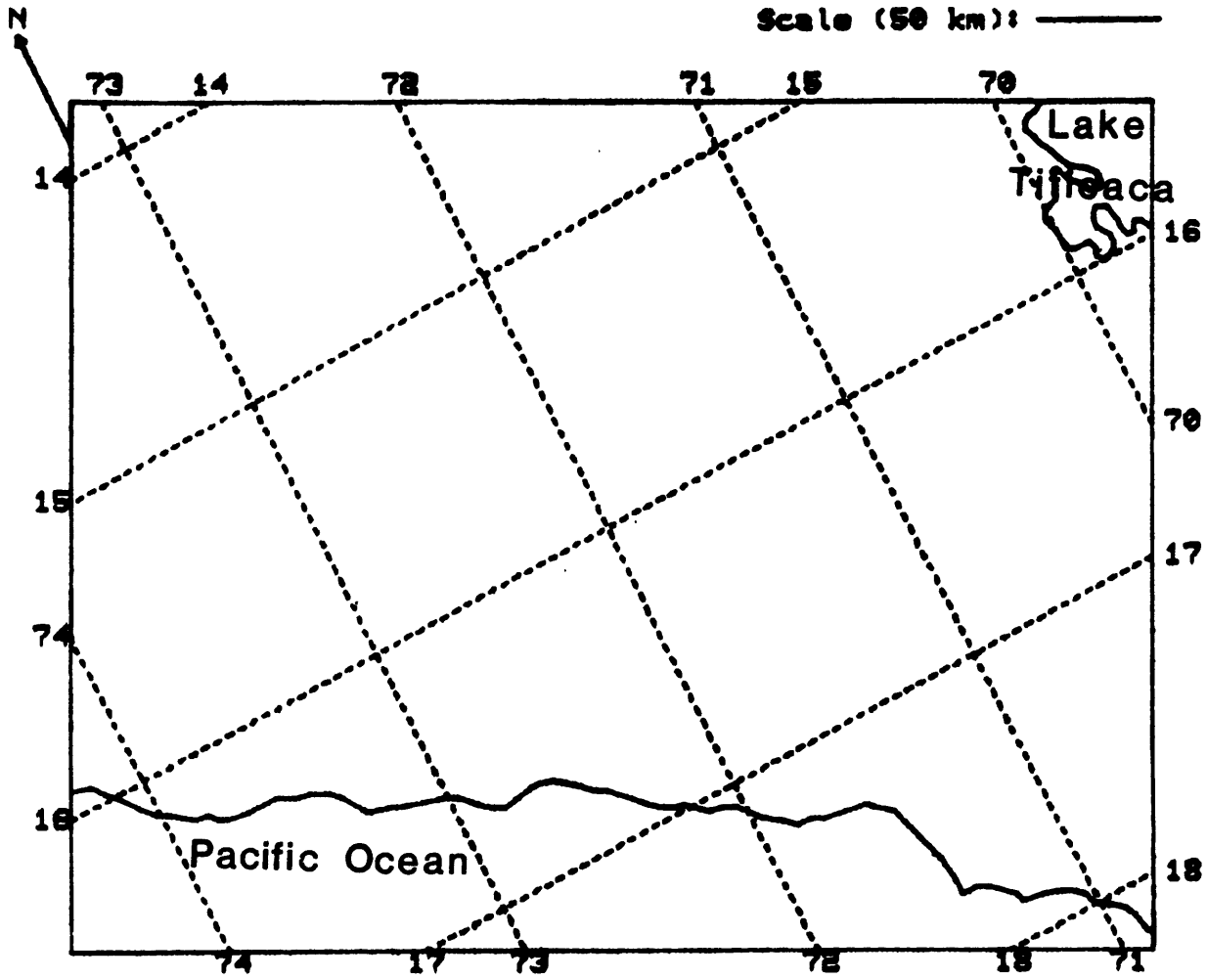
N
Scale (50 km):
73
14
72
71
15
70
Lake
Titicaca
14
16
15
70
17
74
16
Pacific Ocean
18
74
17
73
72
18
71

Figure 18.

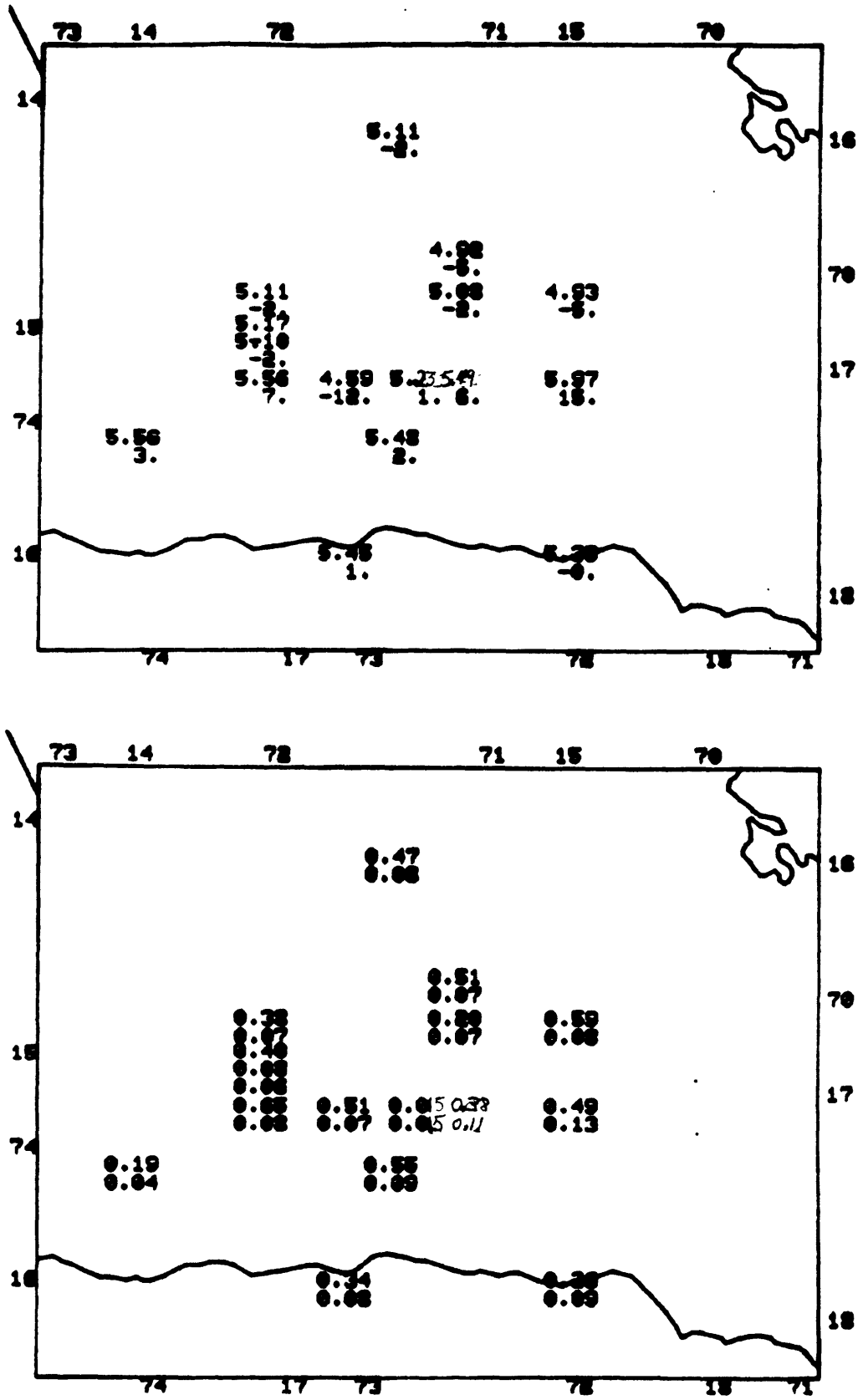

Figure 19. 1; -5 to 5 km; P

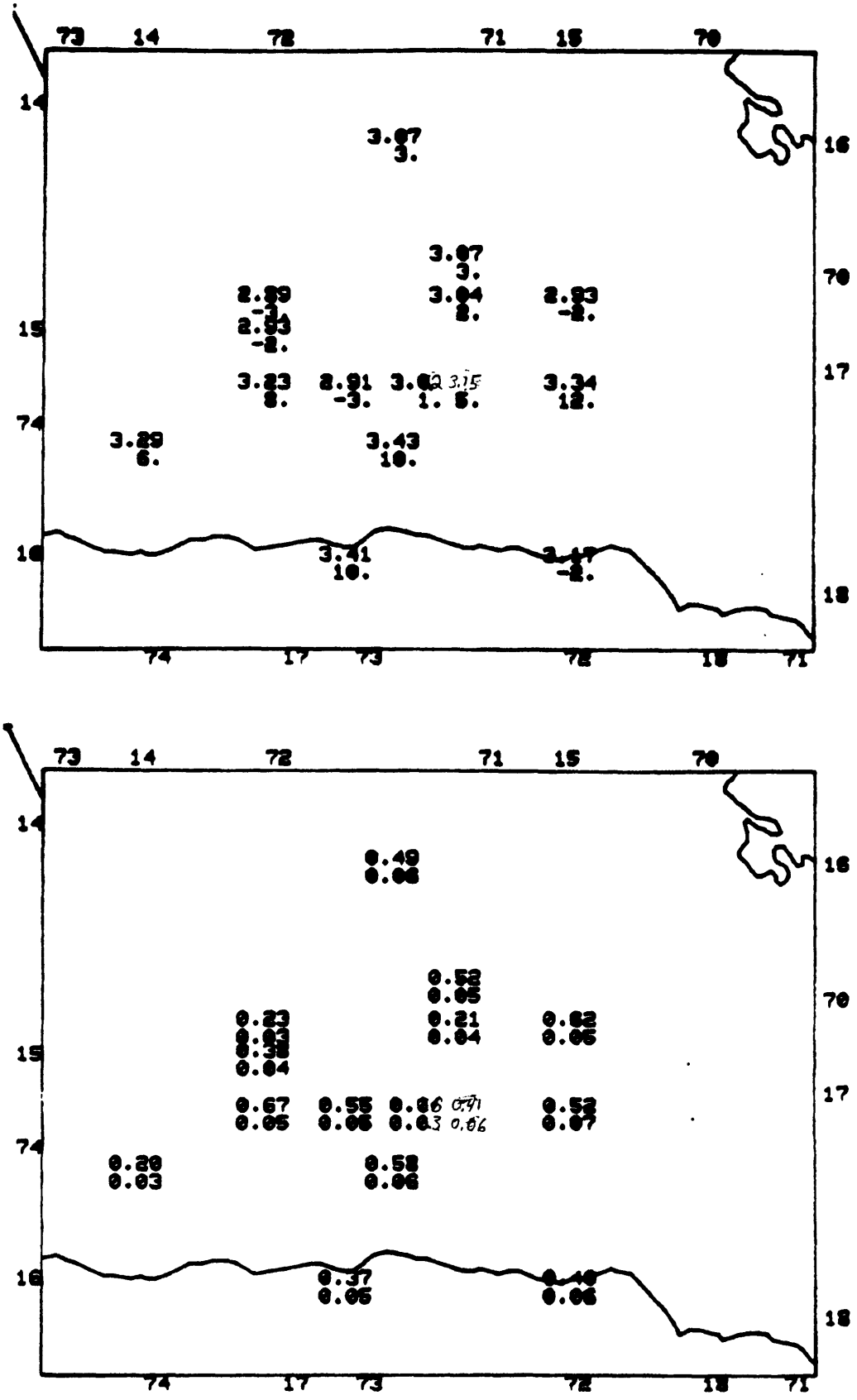

Figure 20. 1; -5 to 5 km; S

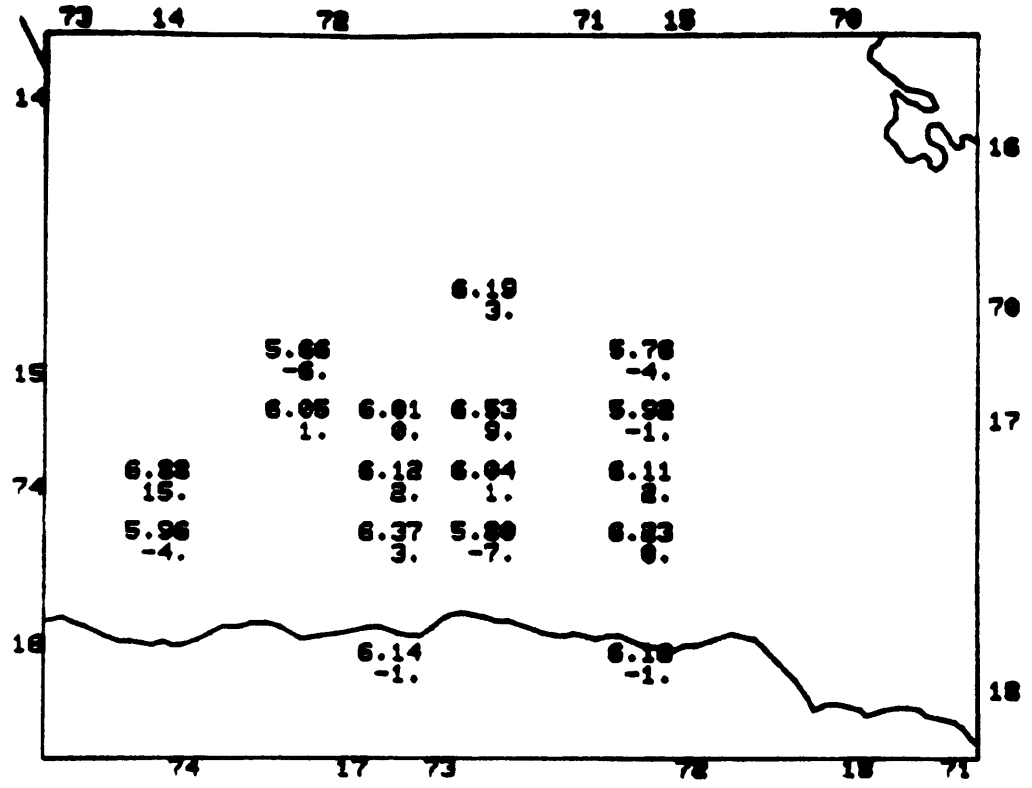

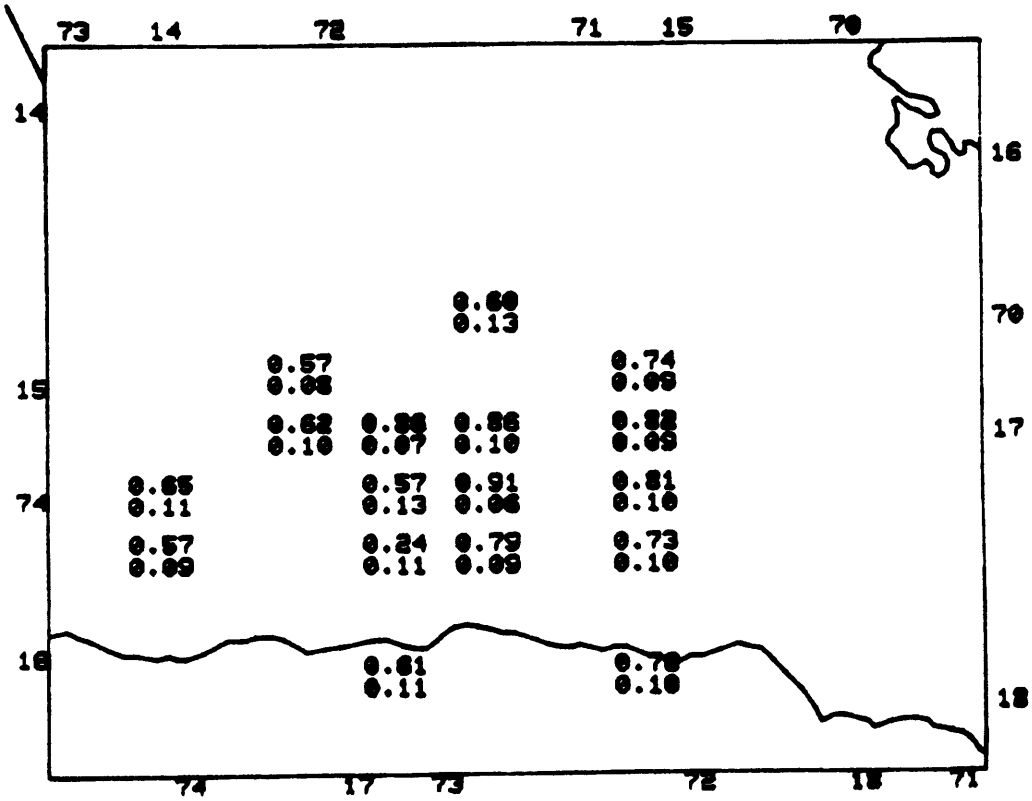

Figure 21. 1; 5 to 20 km; P

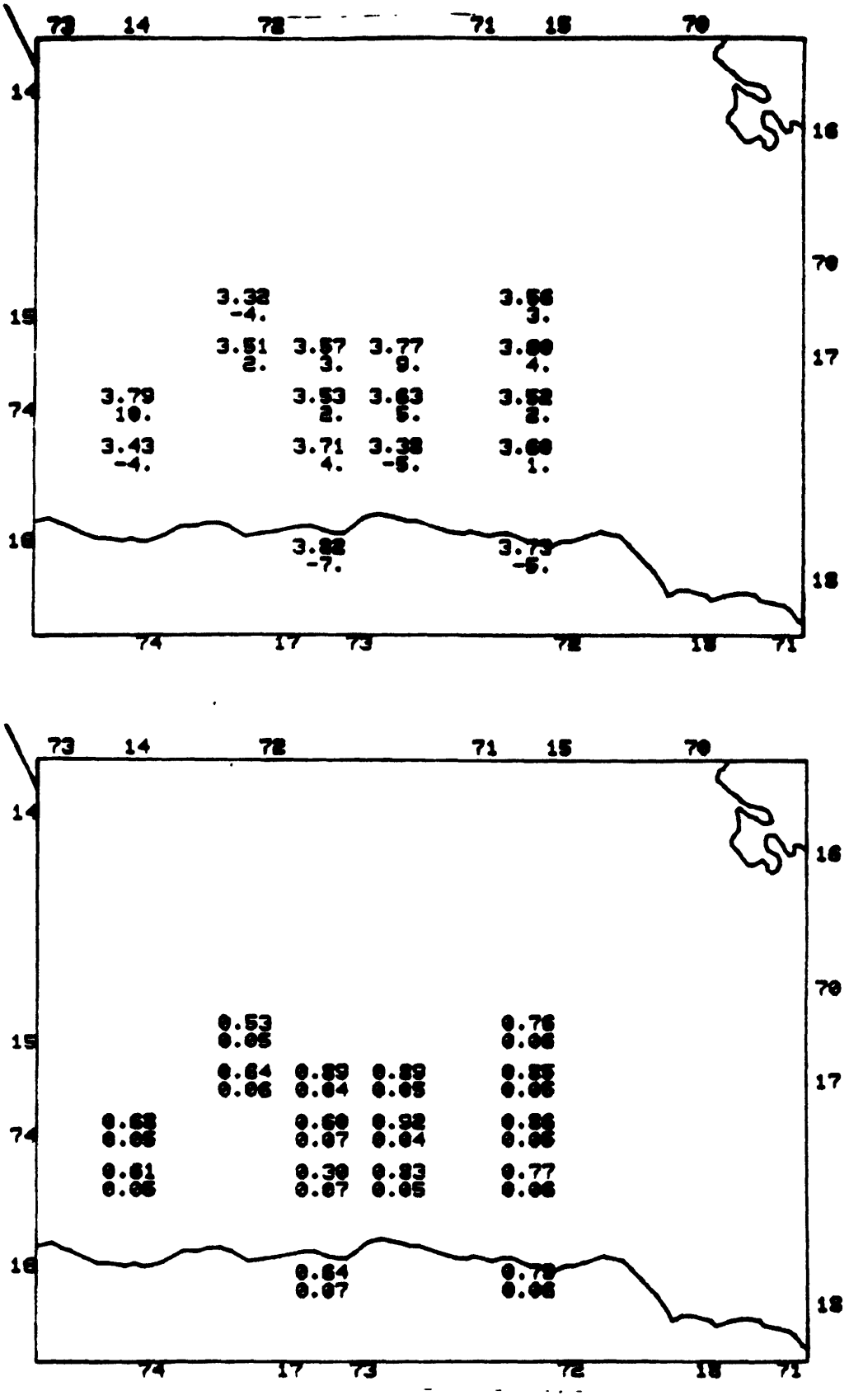

Figure 22. 1; 5 to 20 km; S

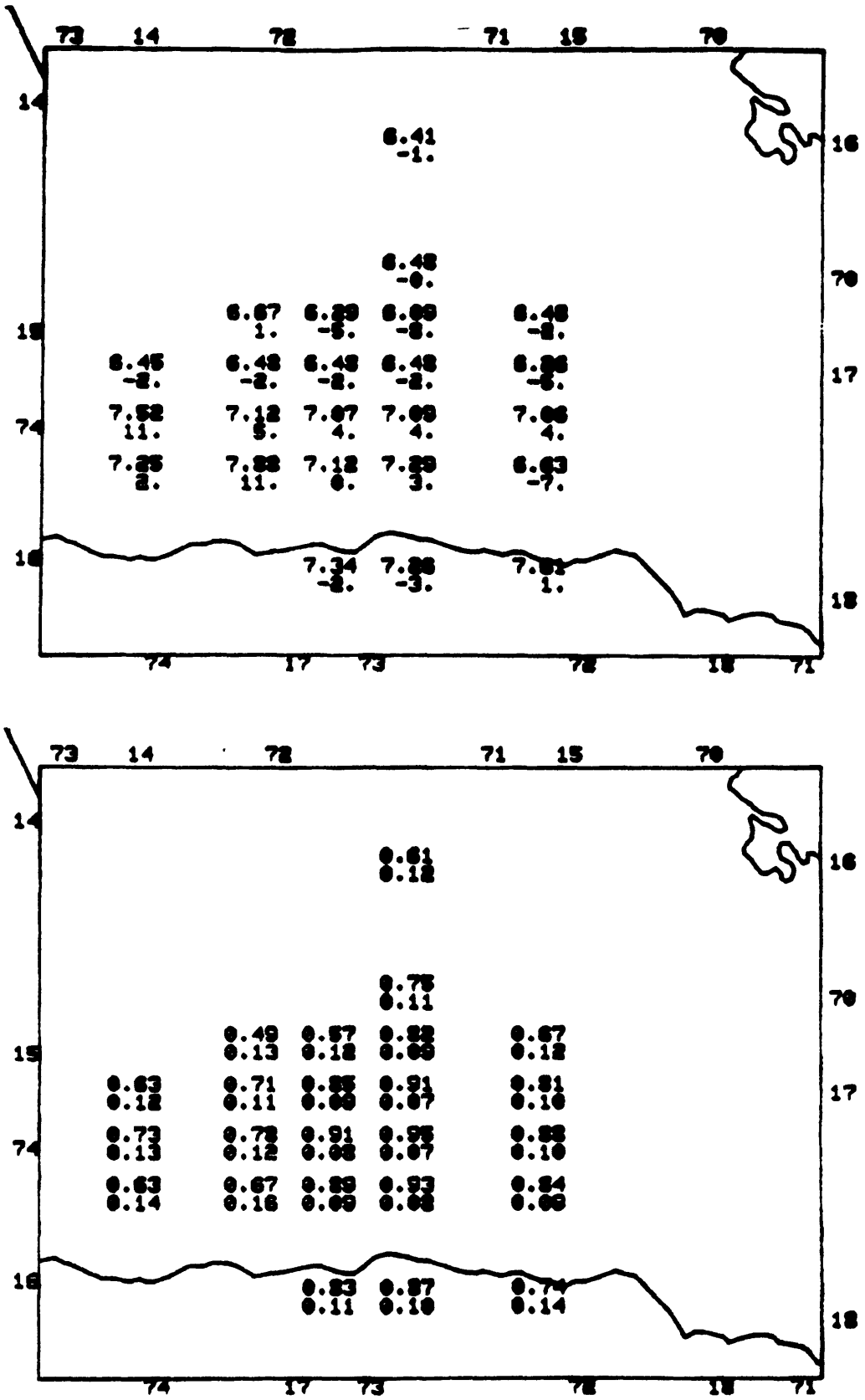

Figure 23. 1; 20 to 40 km; P

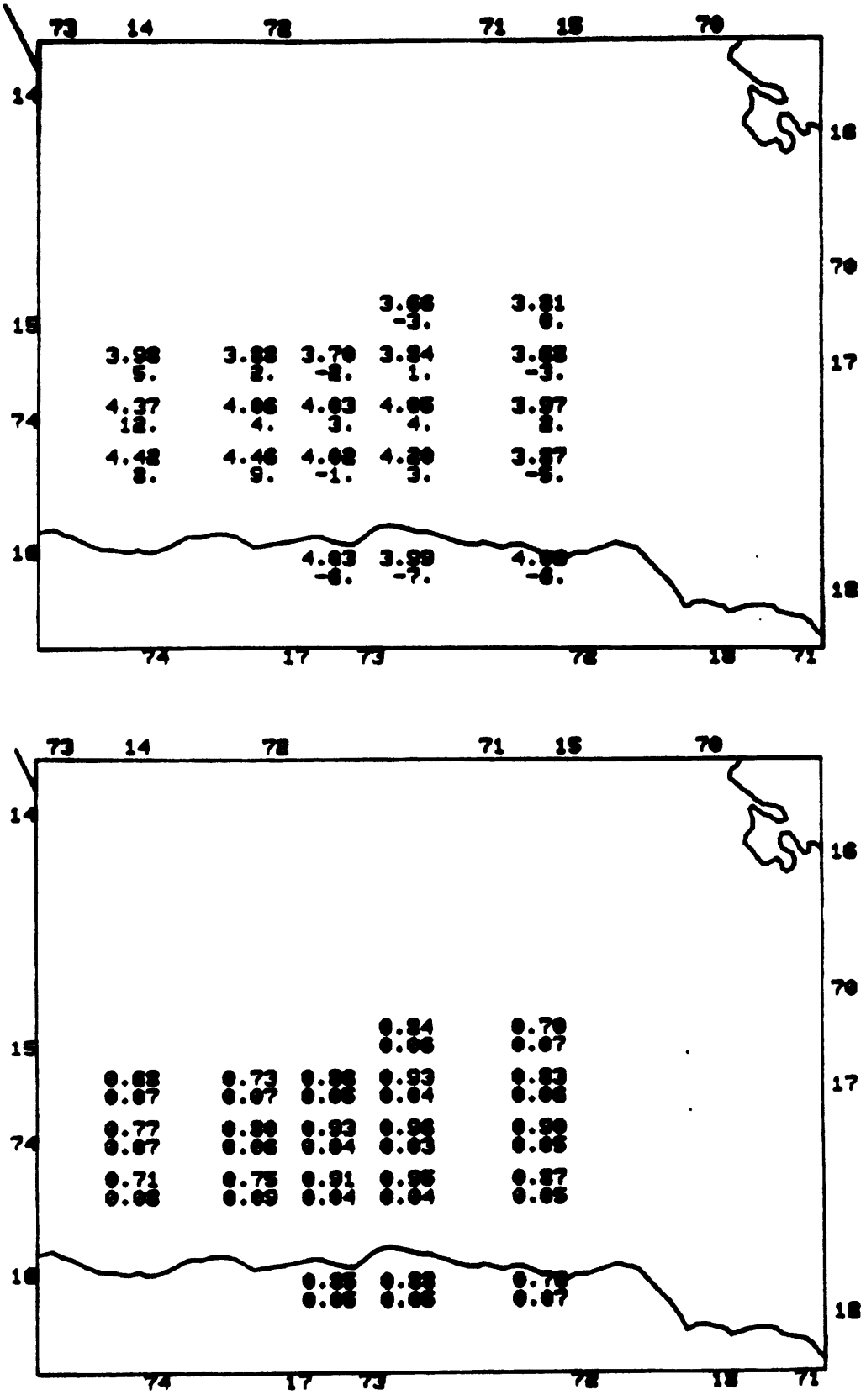

Figure 24. 1; 20 to 40 km; S

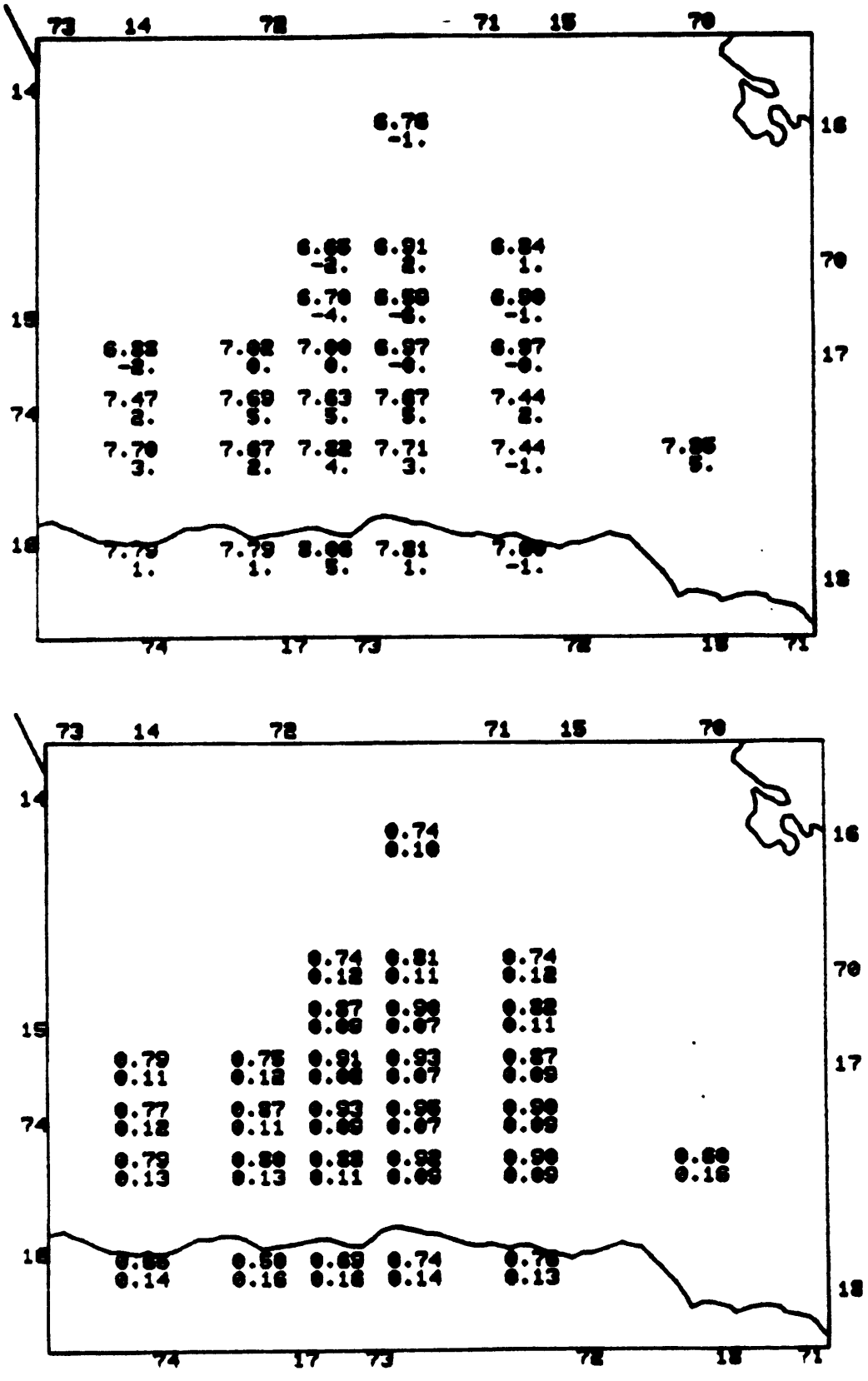

Figure 25. 1; 40 to 70 km; P

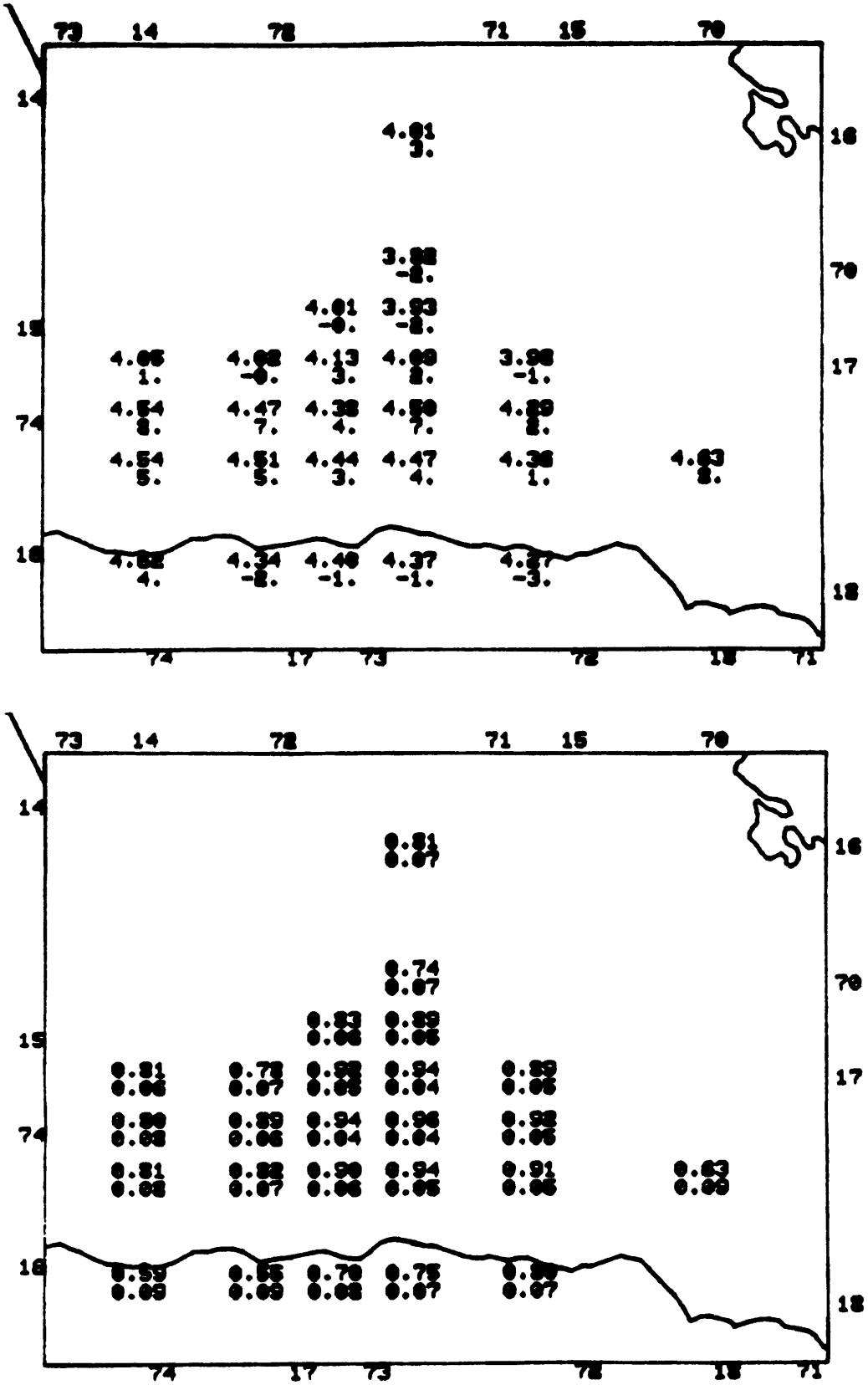

Figure 26. 1; 40 to 70 km; S

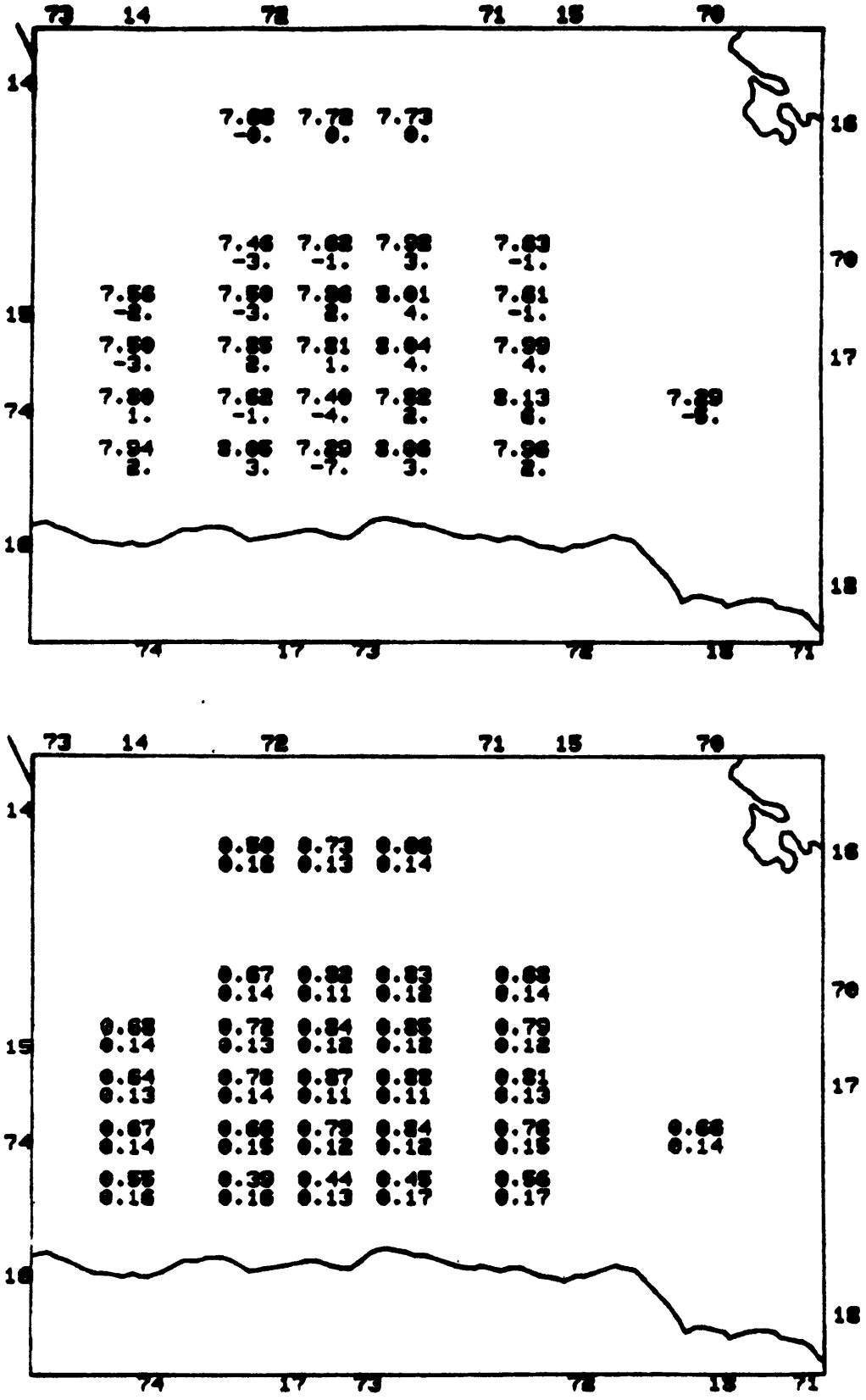

Figure 27. 1; 70 to 100 km; P

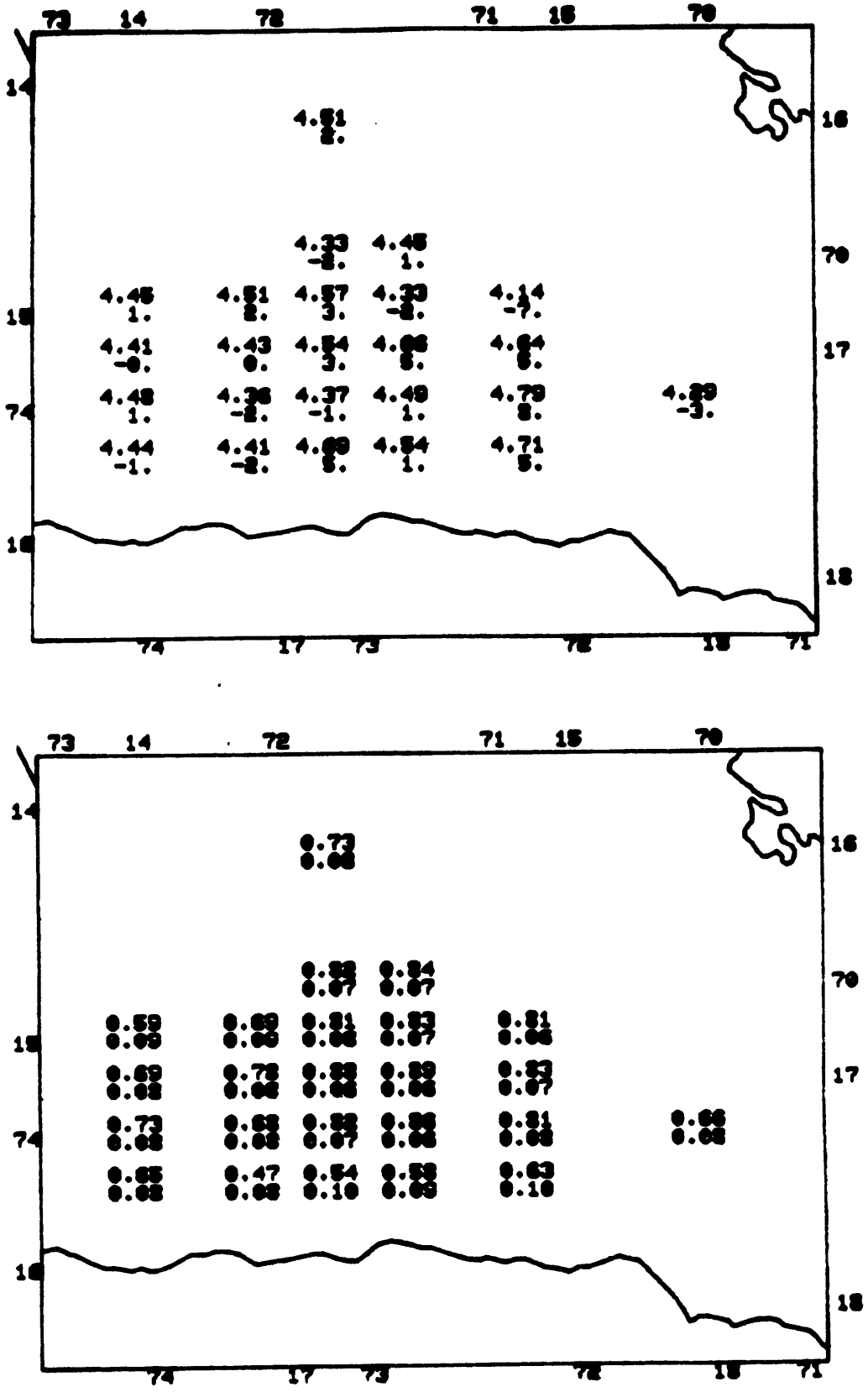

Figure 28. 1; 70 to 100 km; S

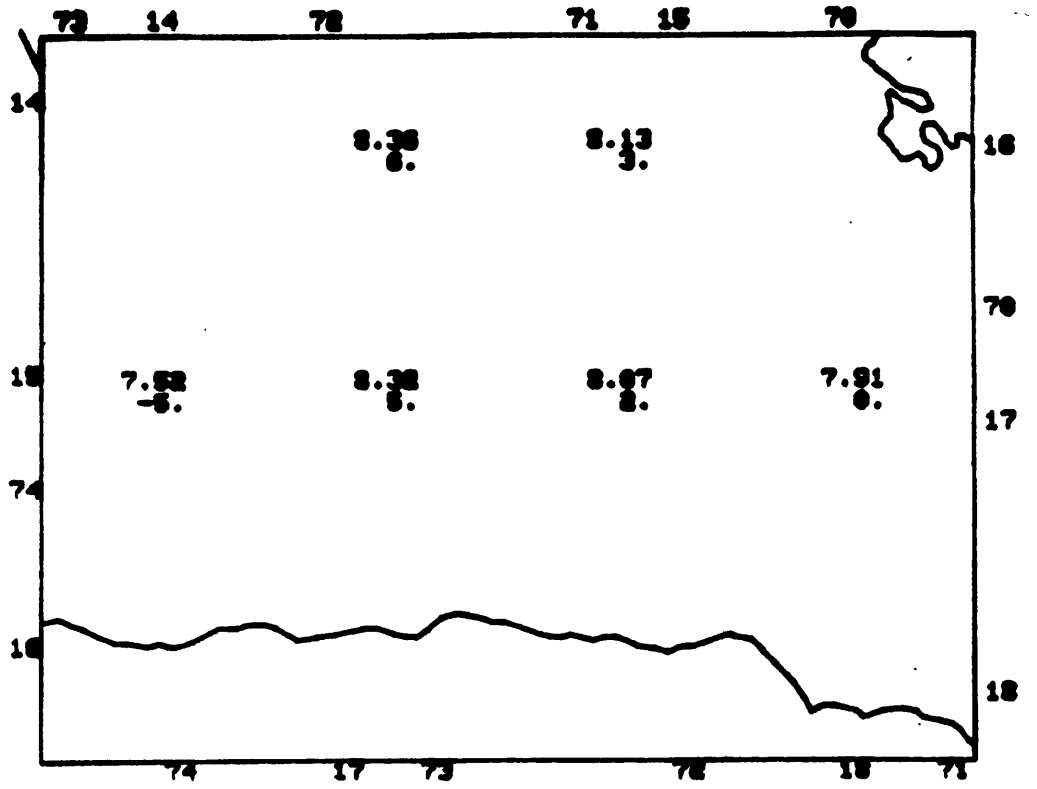

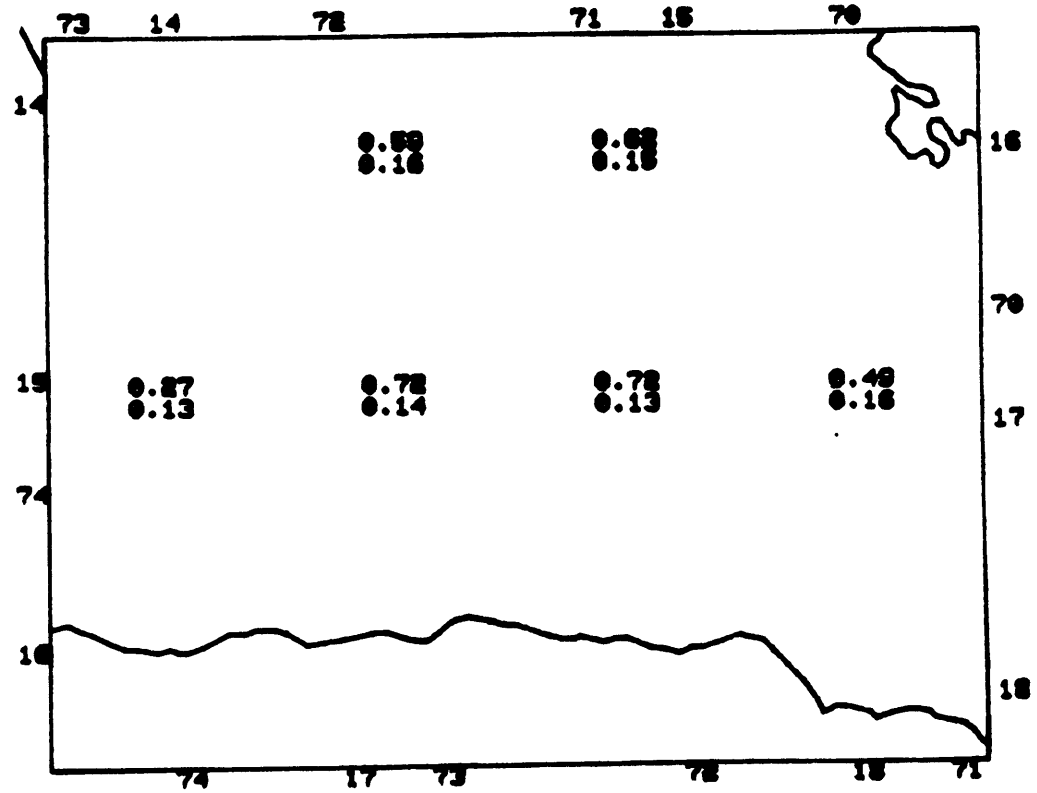

Figure 29. 1; 100 to 130 km; P

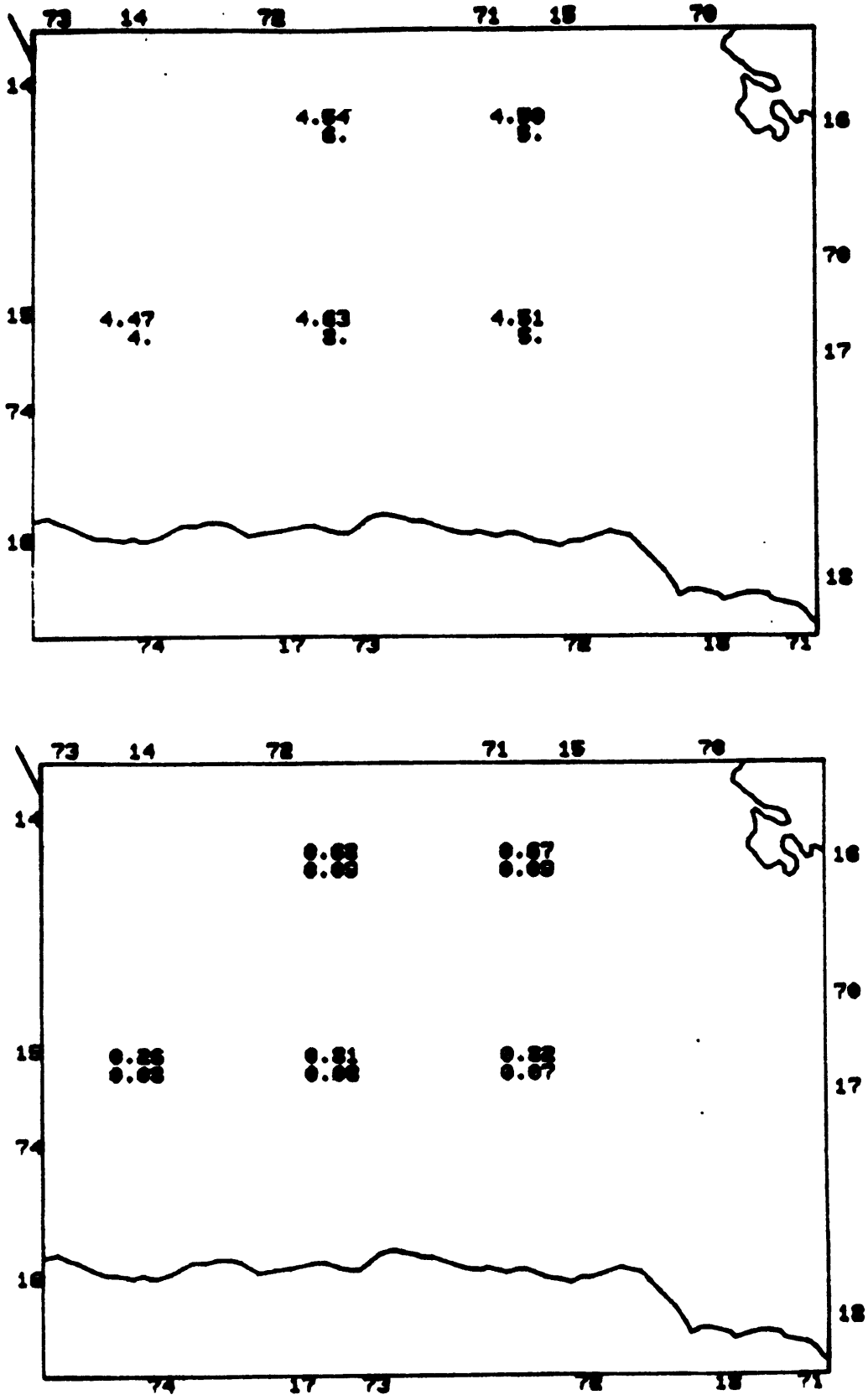

Figure 30. 1; 100 to 130 km; S

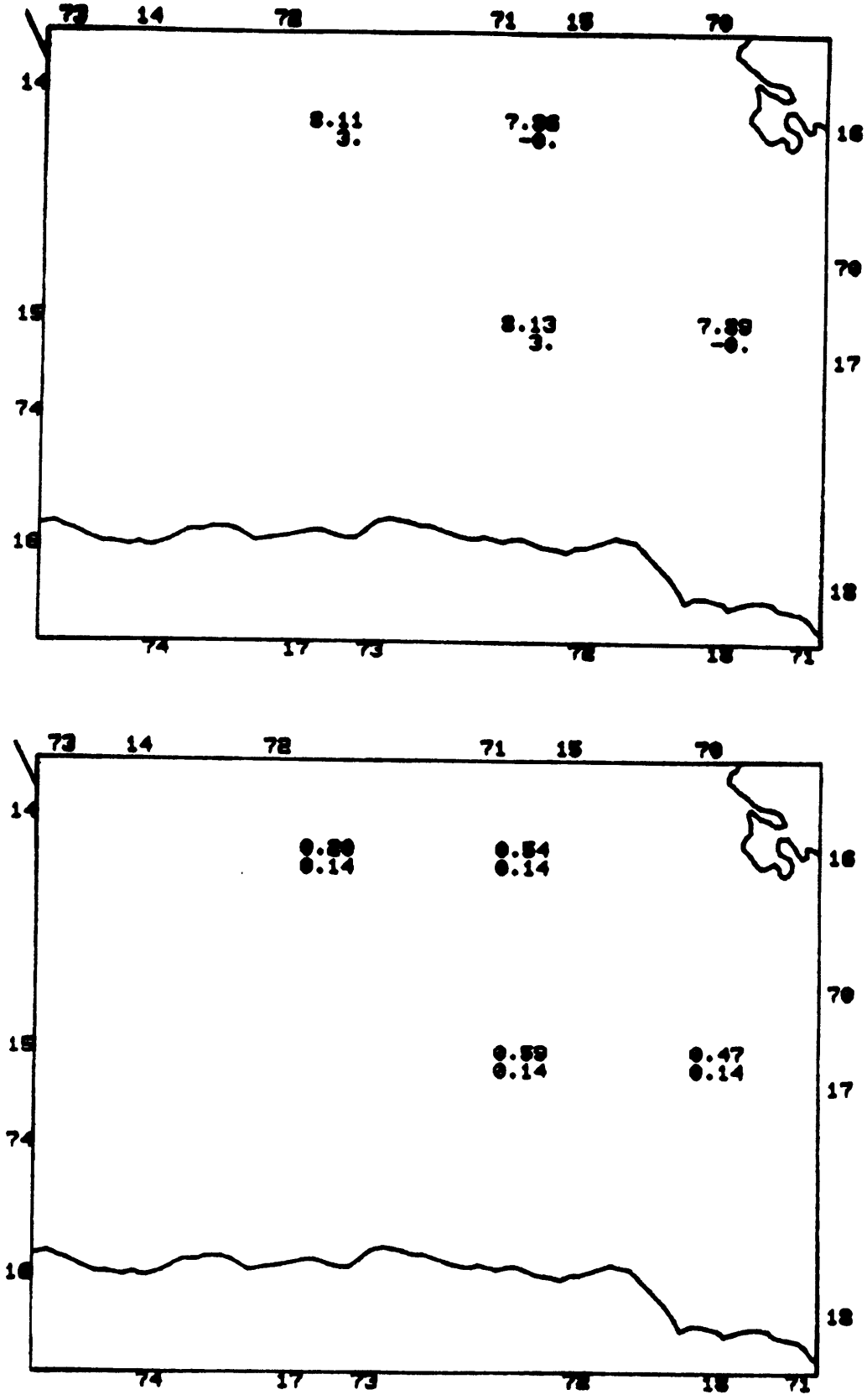

Figure 31. 1; 130 to 160 km; P

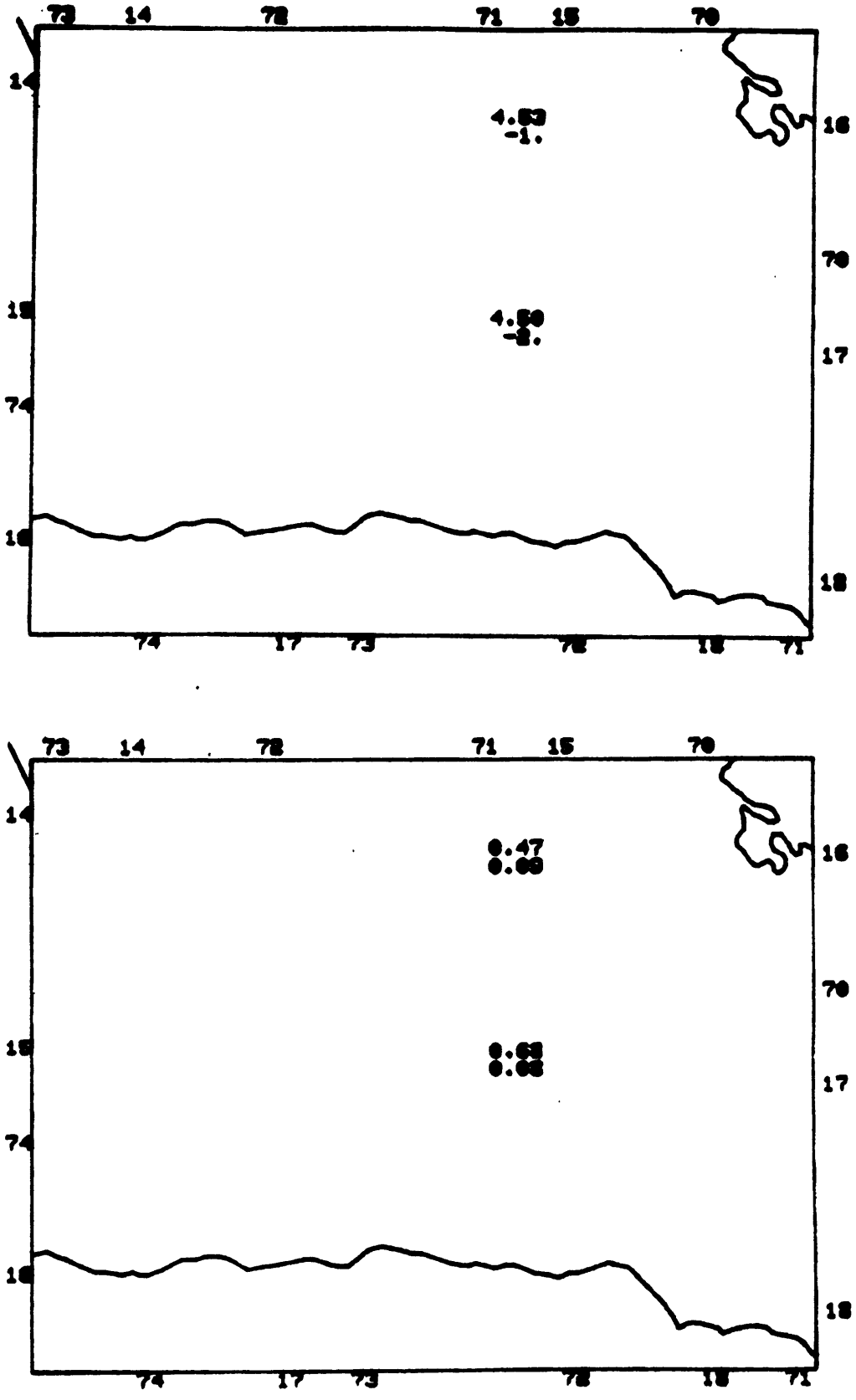

Figure 32. 1; 130 to 160 km; S

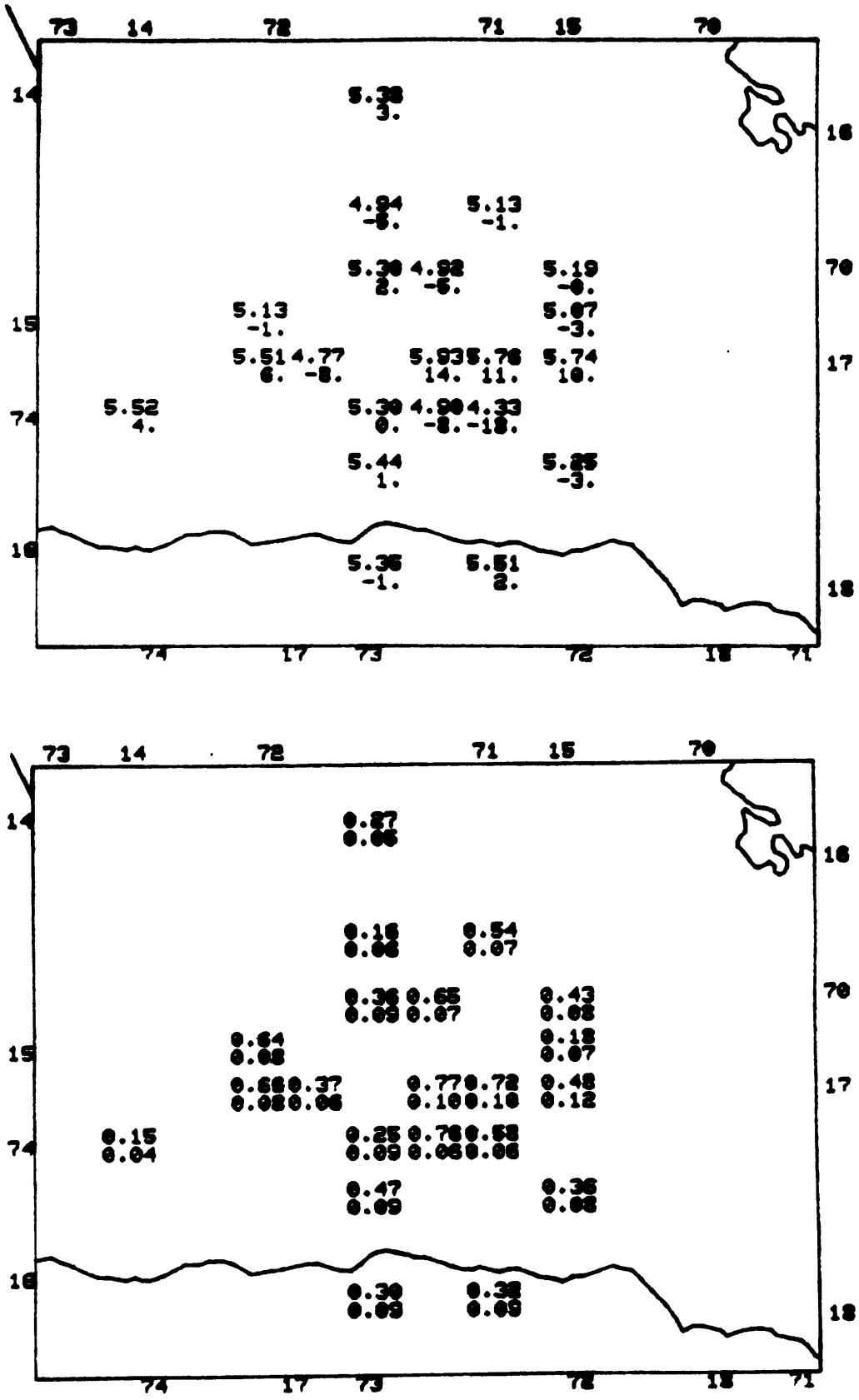

Figure 33. 2; -5 to 5 km; P

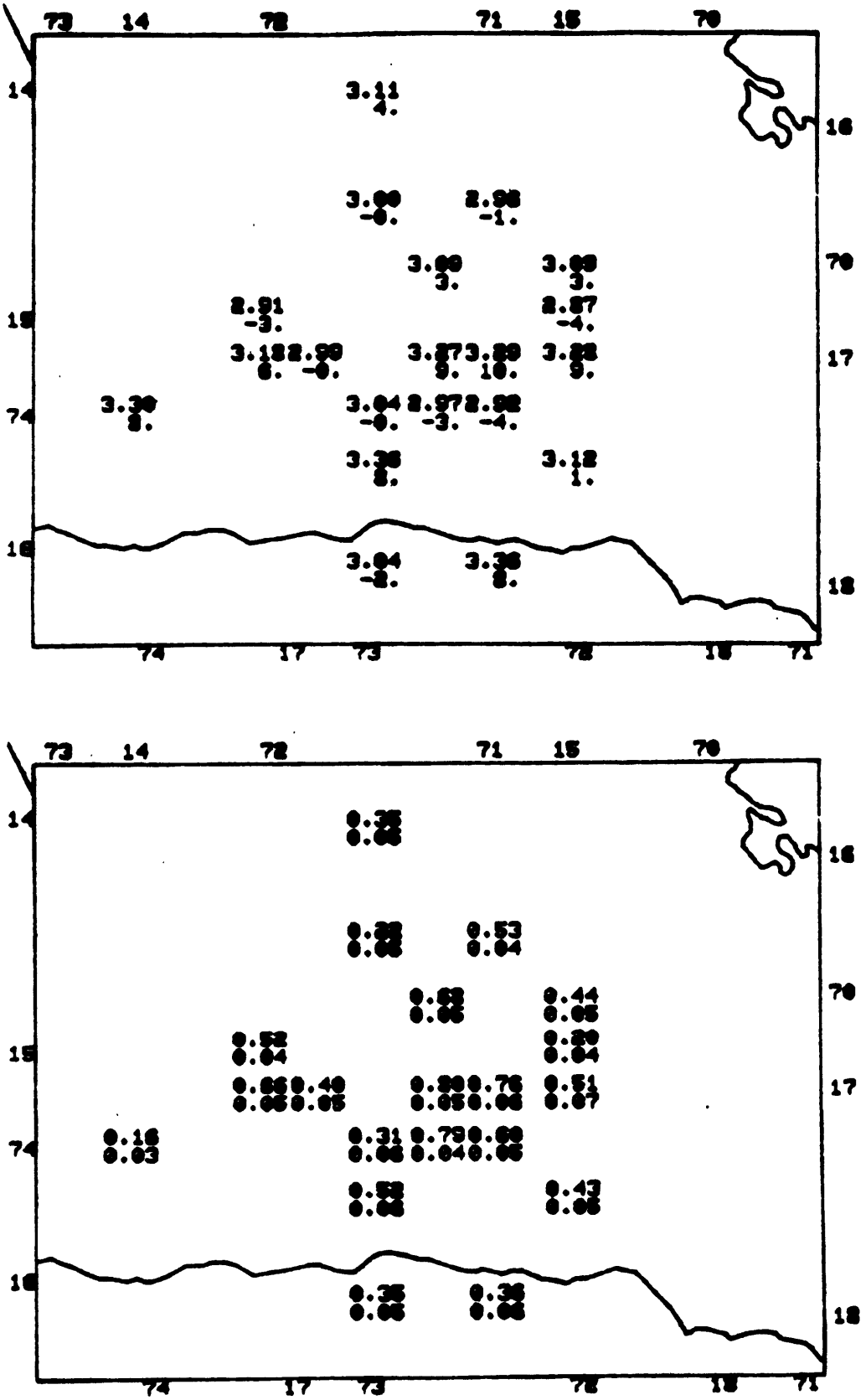

Figure 34. 2; -5 to 5 km; S

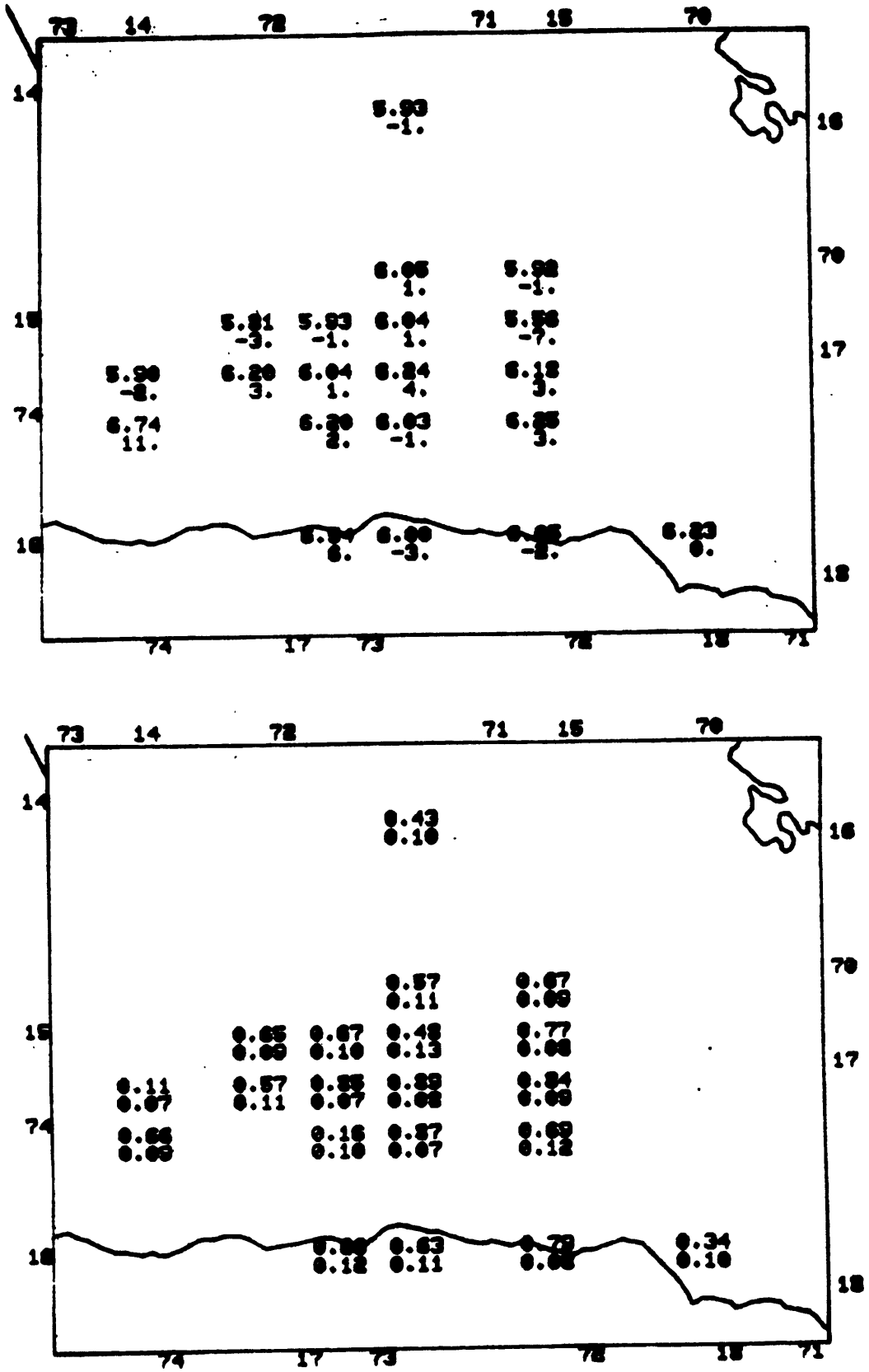

Figure 35. 2; 5 to 20 km; P

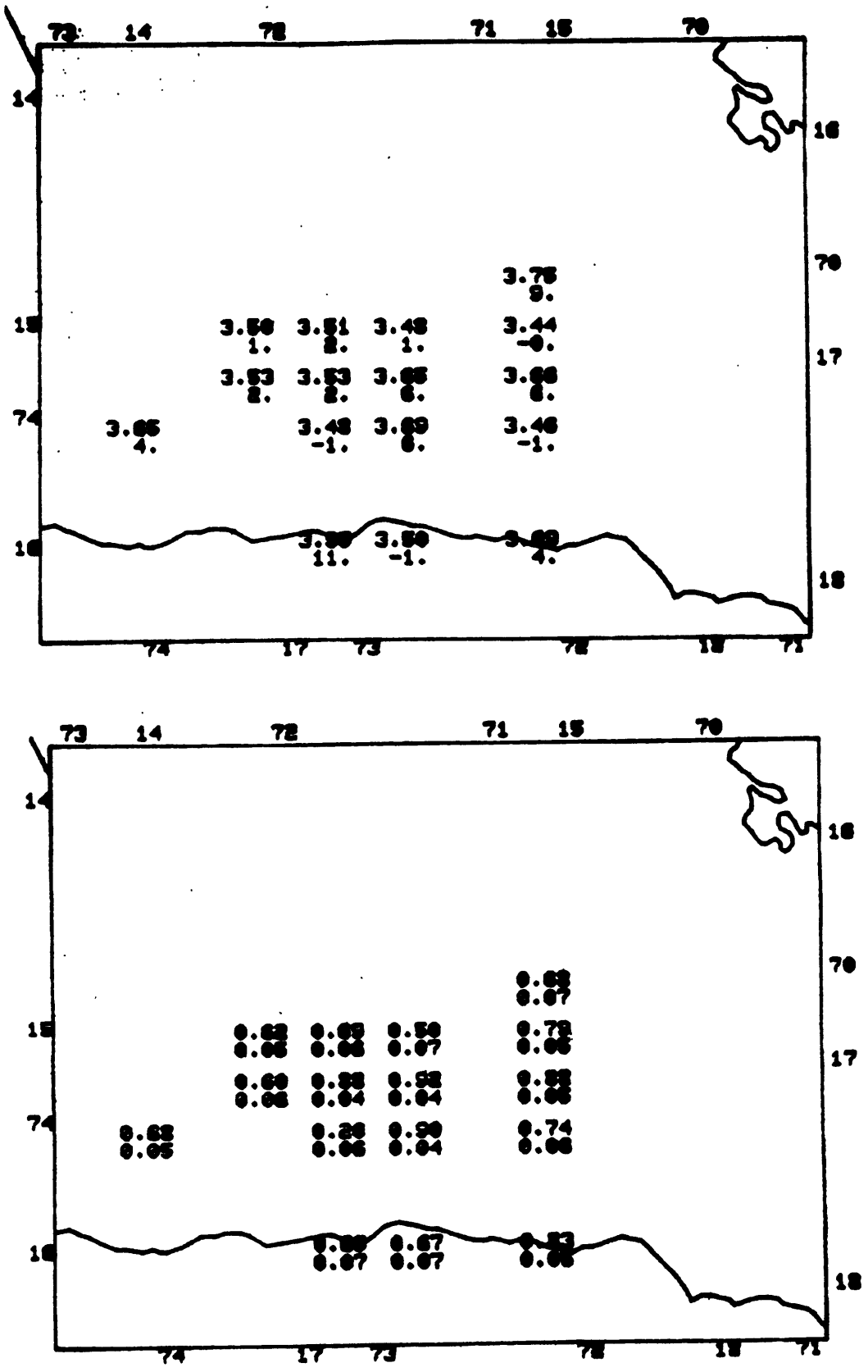

Figure 36. 2; 5 to 20 km; S

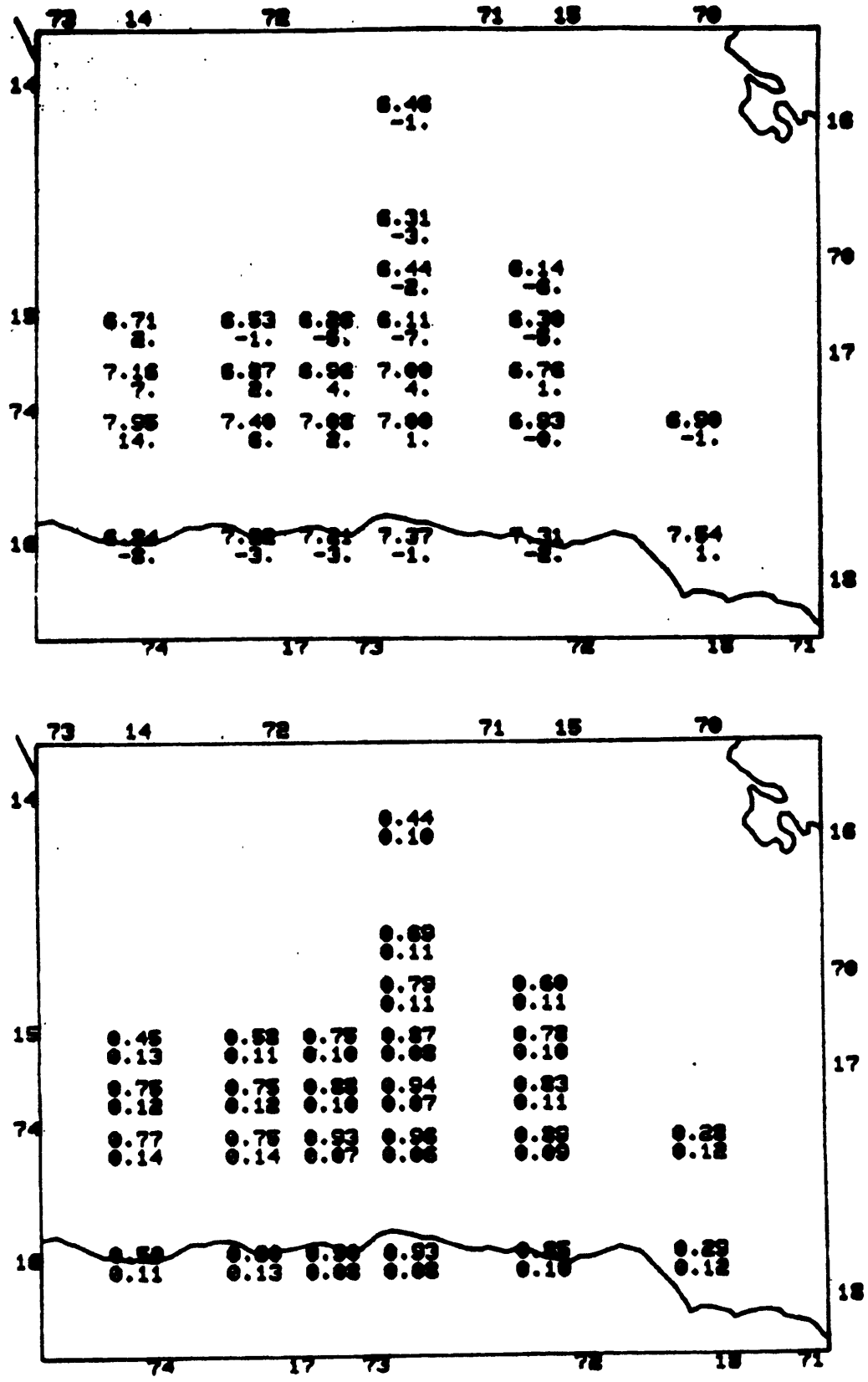

Figure 37. 2; 20 to 40 km; P

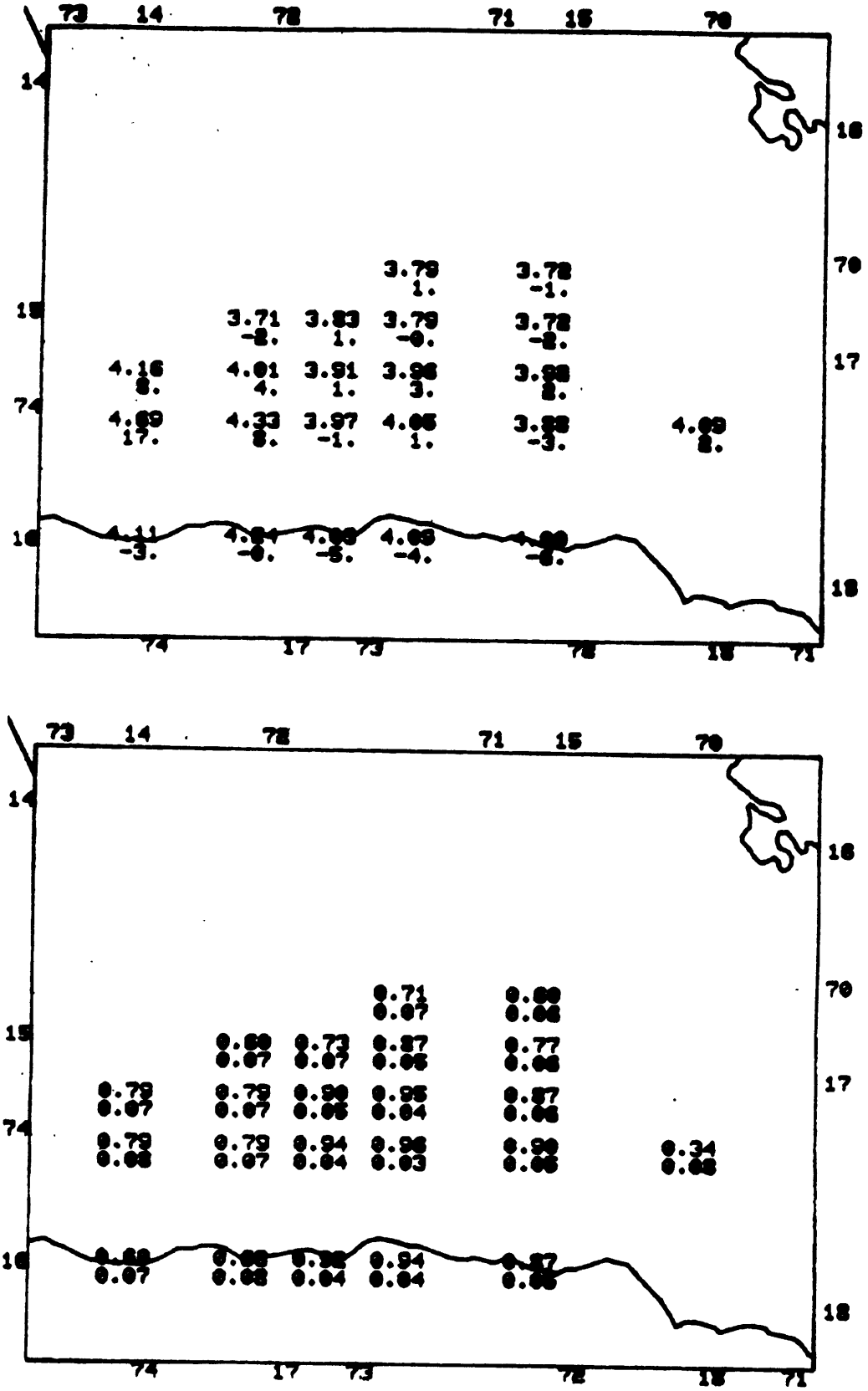

Figure 38. 2; 20 to 40 km; S

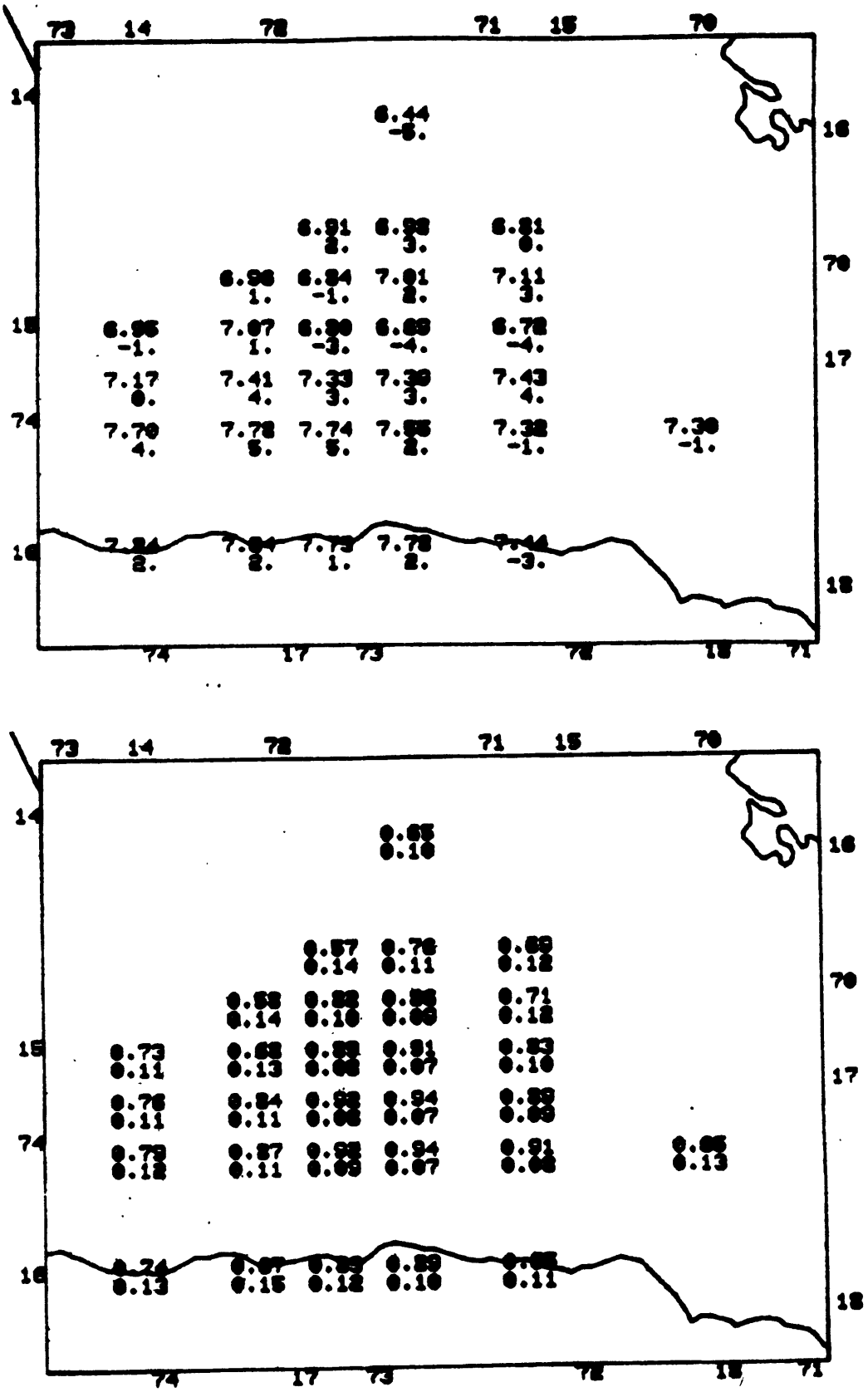

Figure 39. 2; 40 to 70 km; P

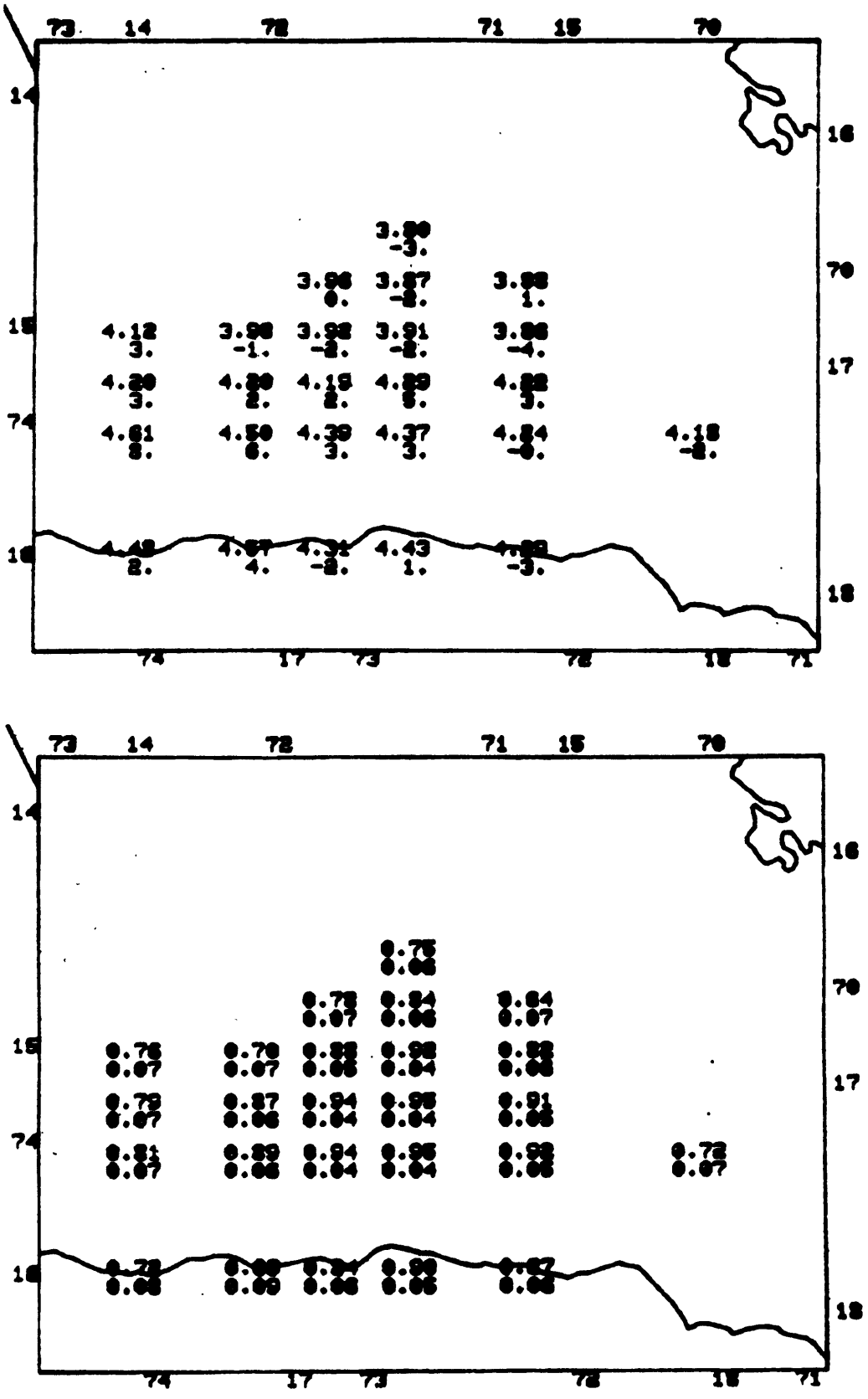

Figure 40. 2; 40 to 70 km; S

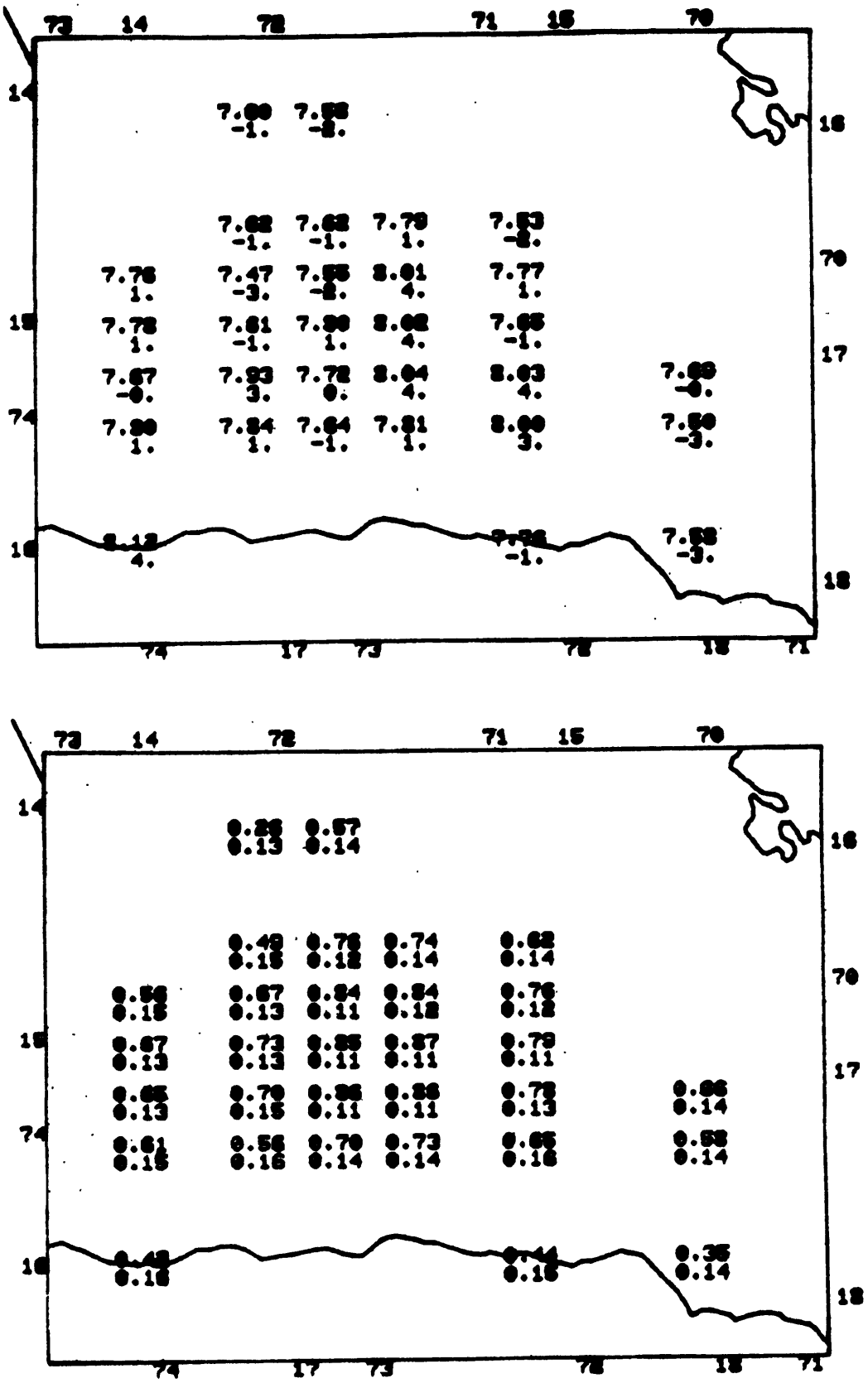

Figure 41. 2; 70 to 100 km; P

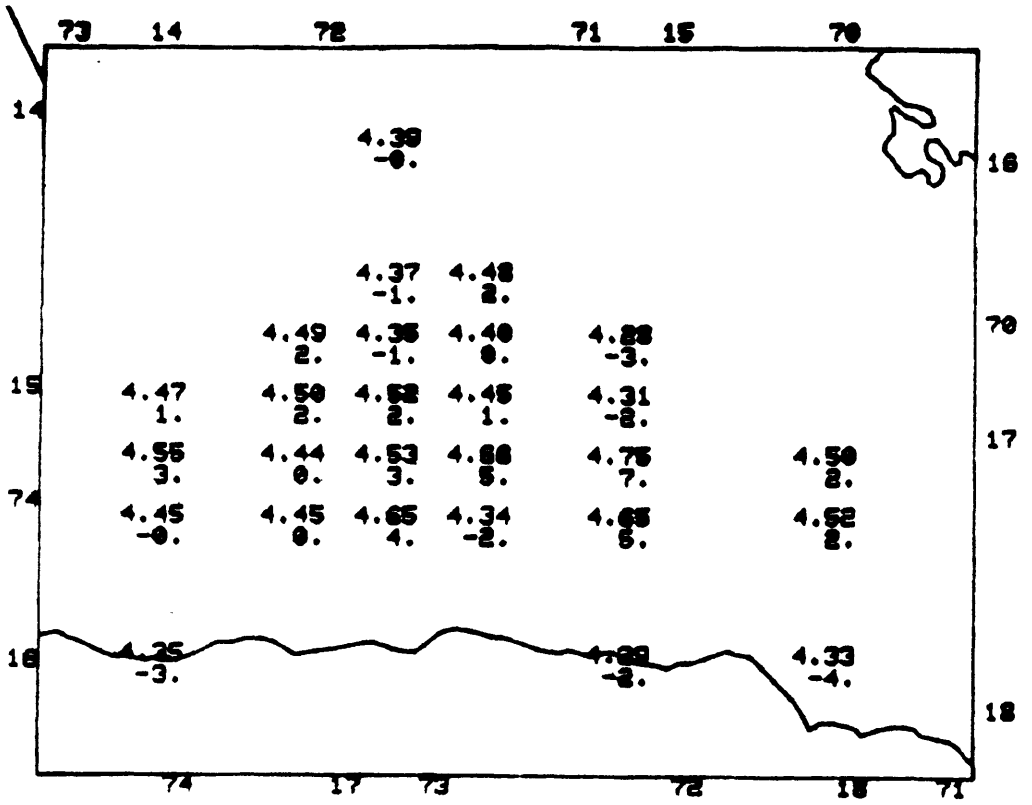

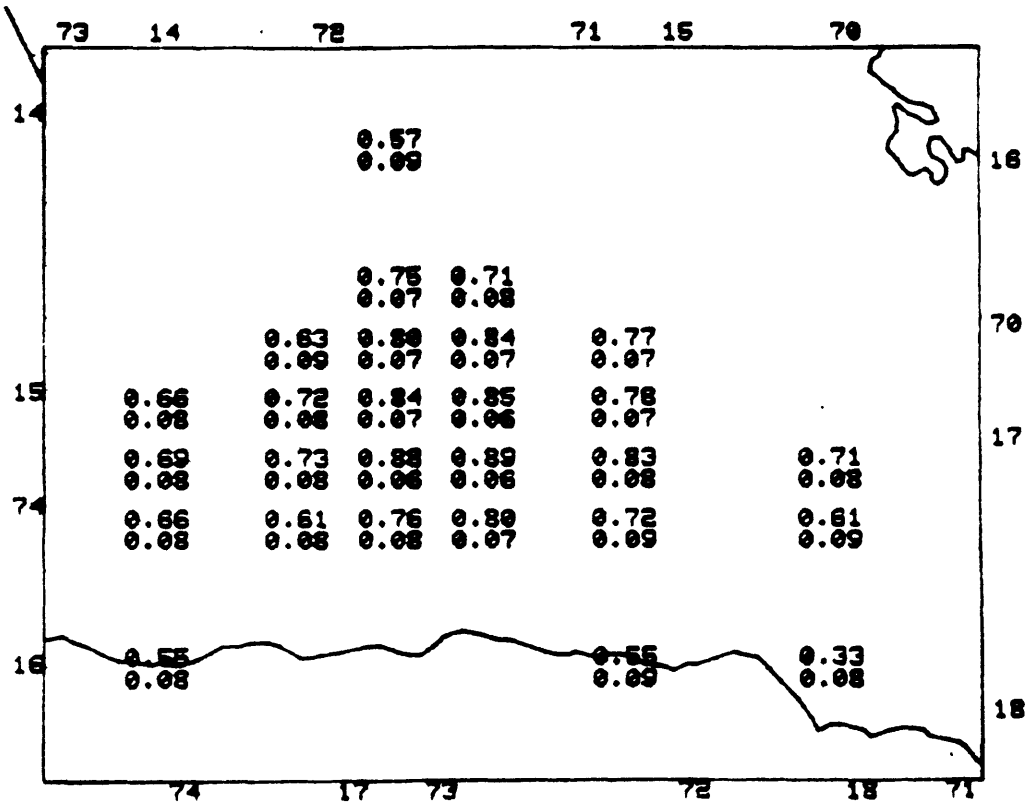

Figure 42 2; 70 to 100 km; S

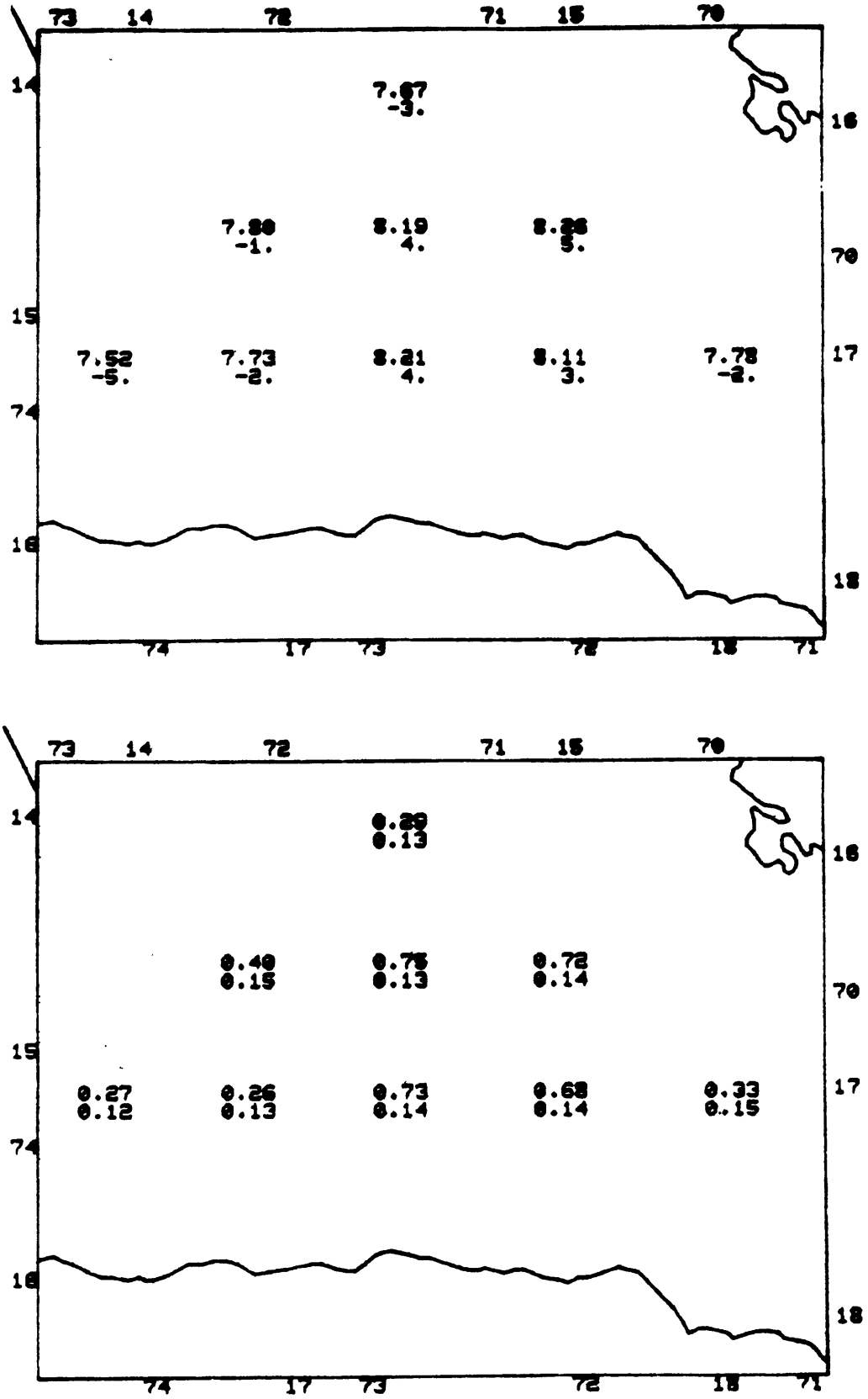

Figure 43. 2; 100 to 130 km, P

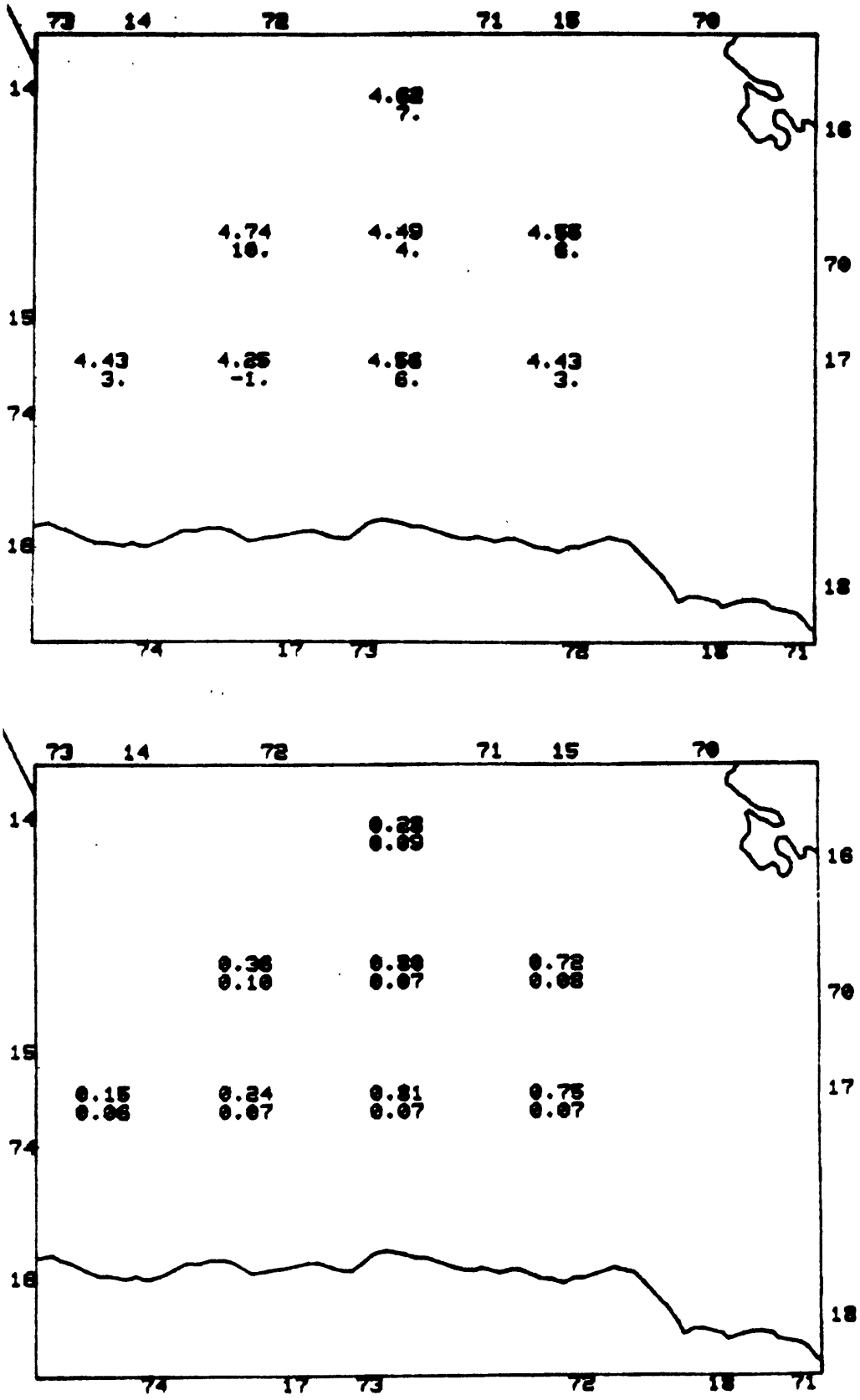

Figure 44. 2; 100 to 130 km; S

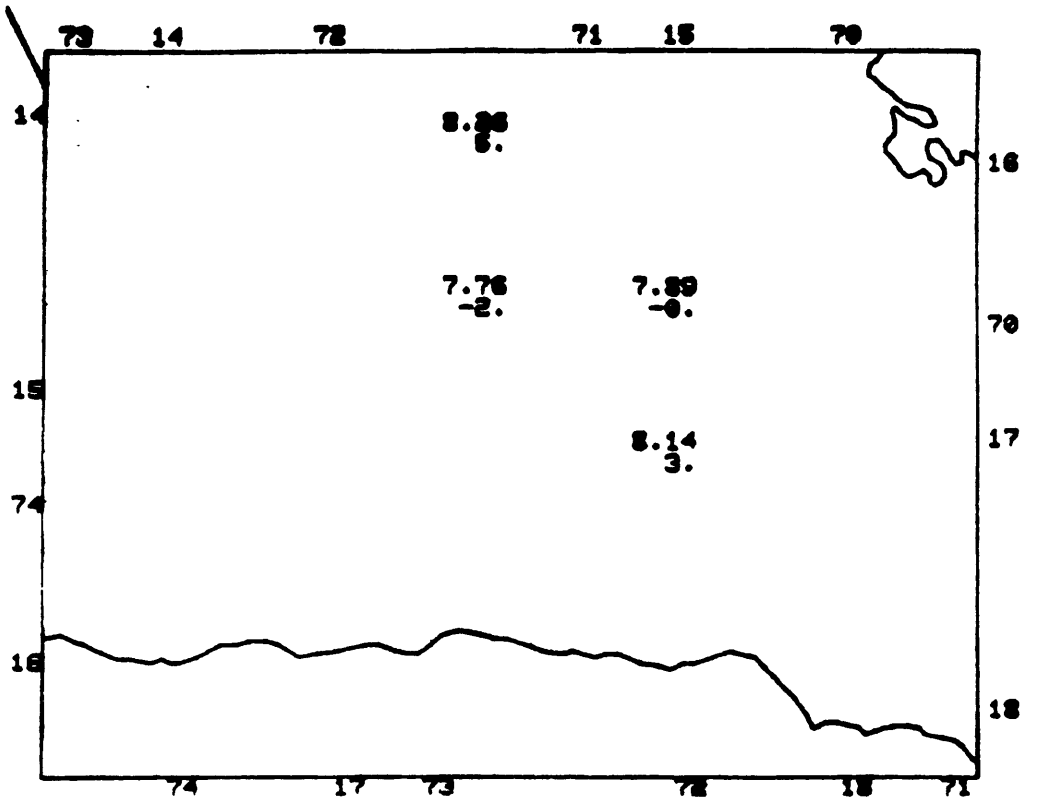

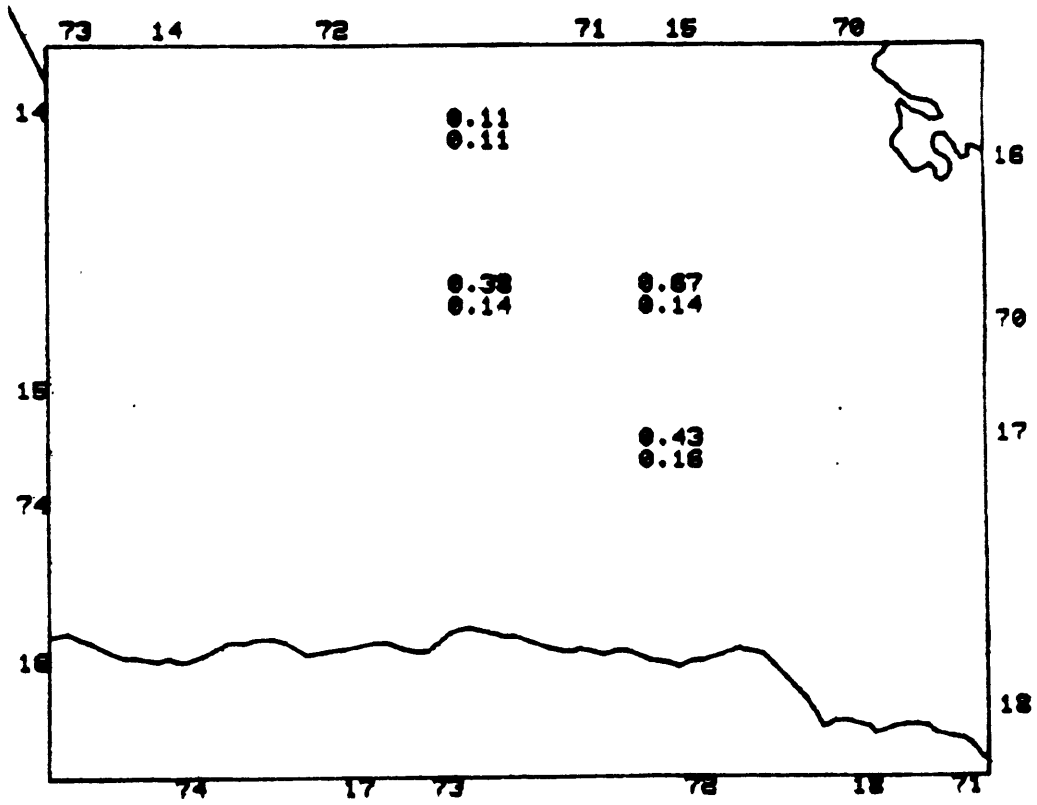

Figure 45. 2: 130 to 160 km; P

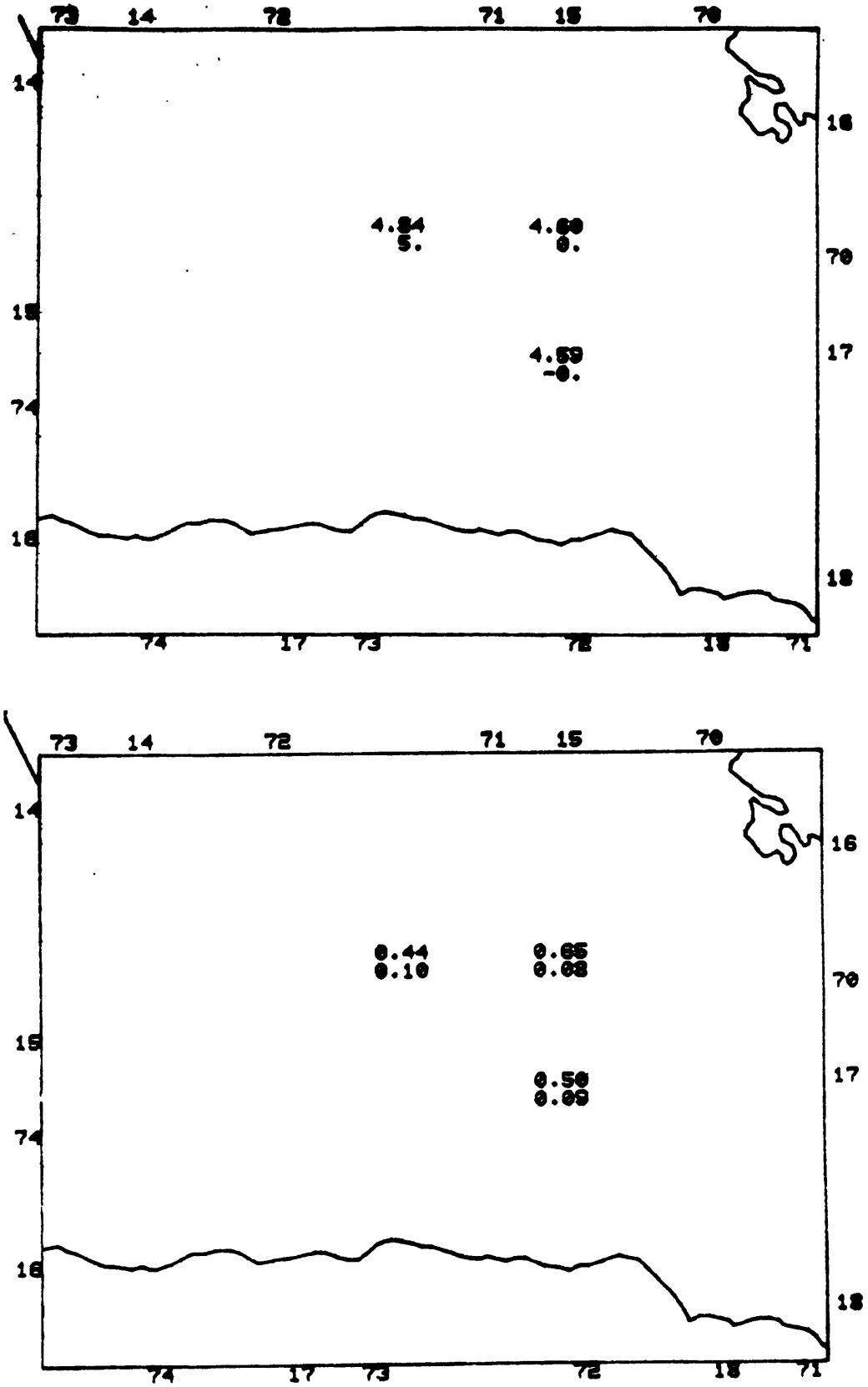

Figure 46 2; 130 to 160 km; S

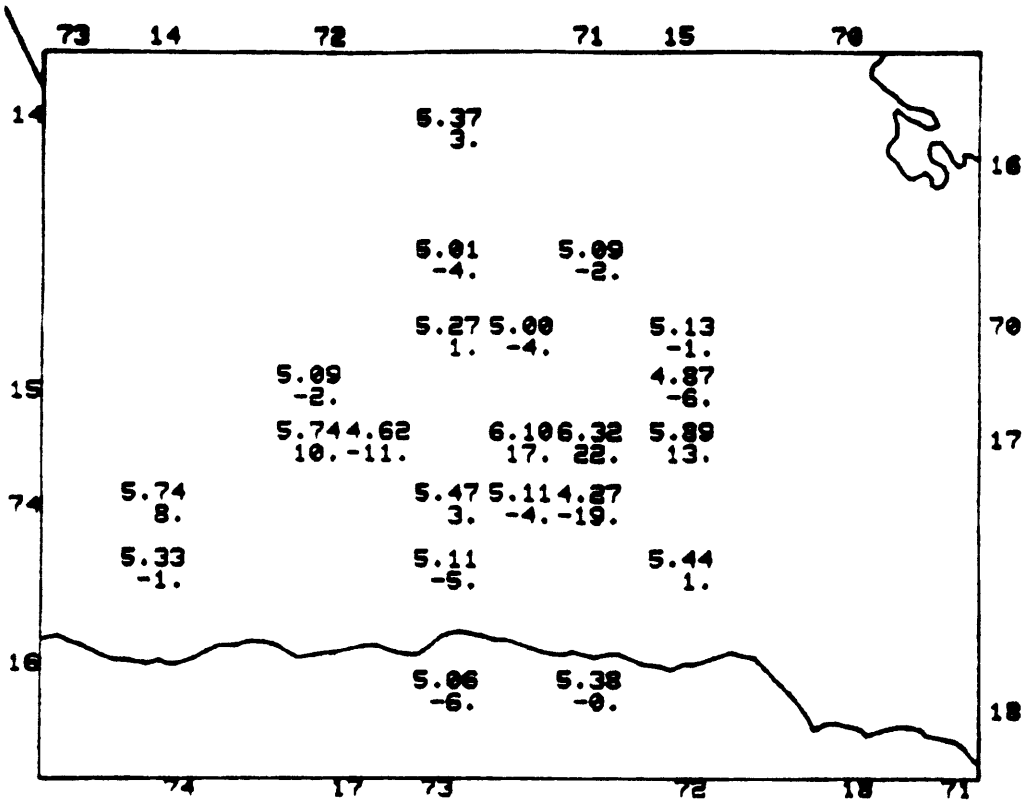

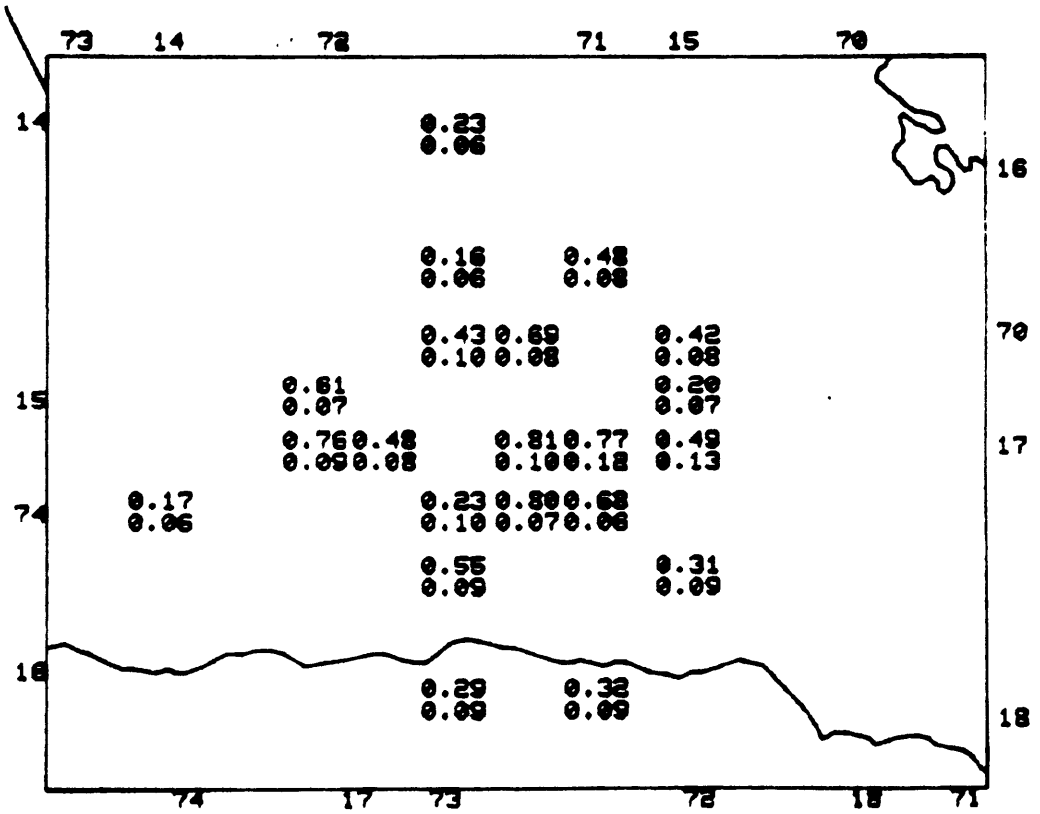

Figure 47. 3; -5 to 5 km; P

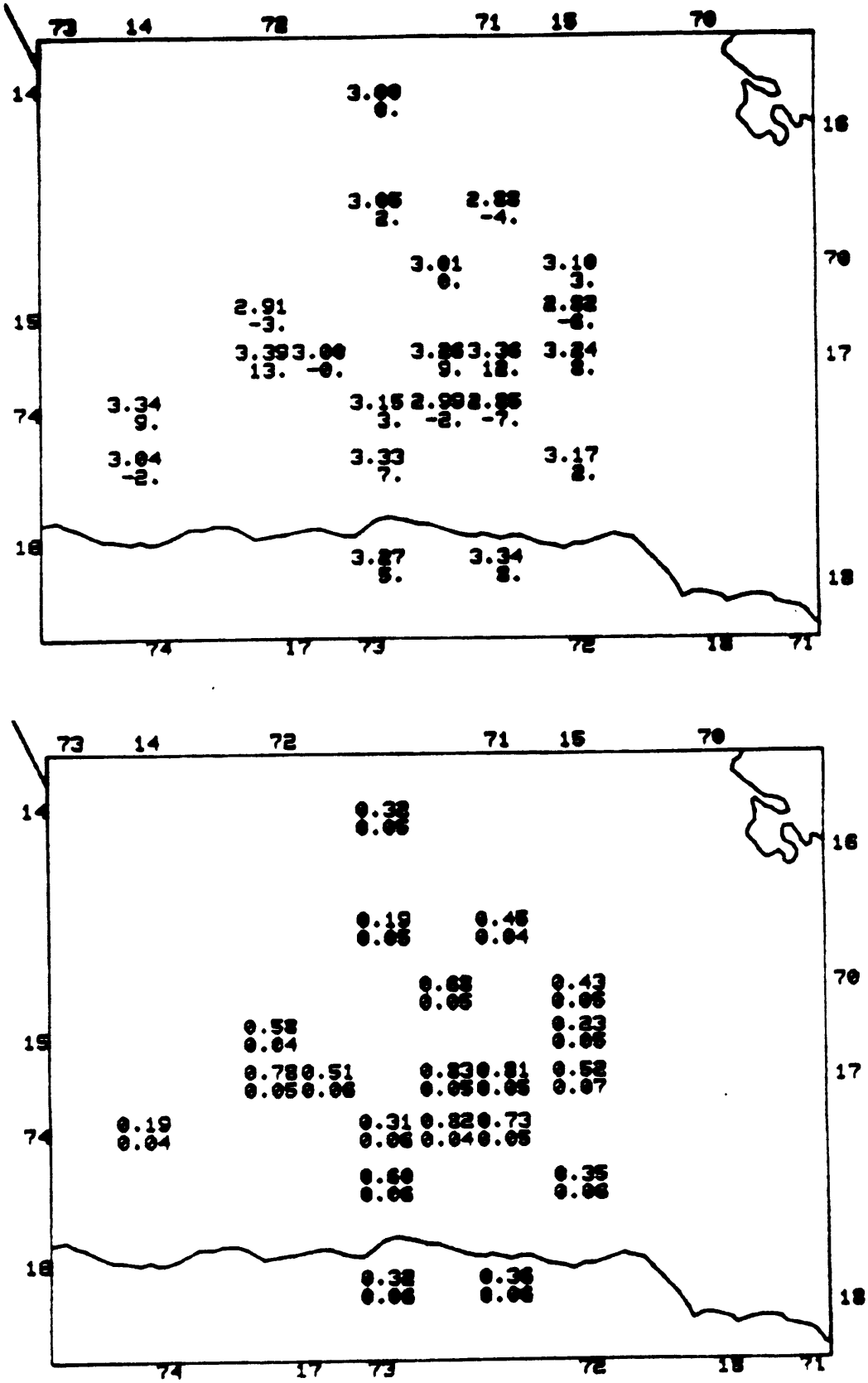

Figure 48. 3, -5 to 5 km, S

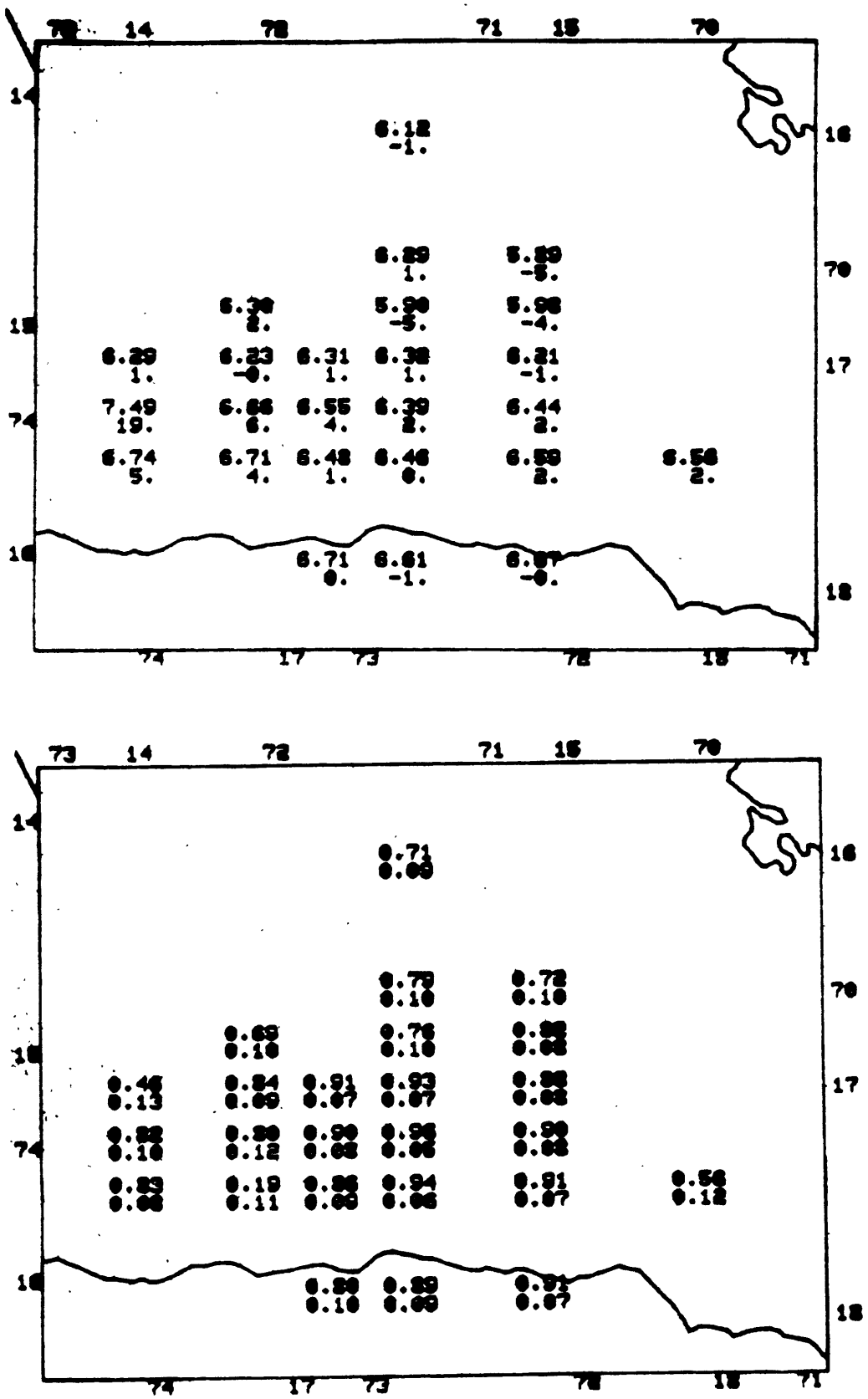

Figure 49. 3; 5 to 30 km, P

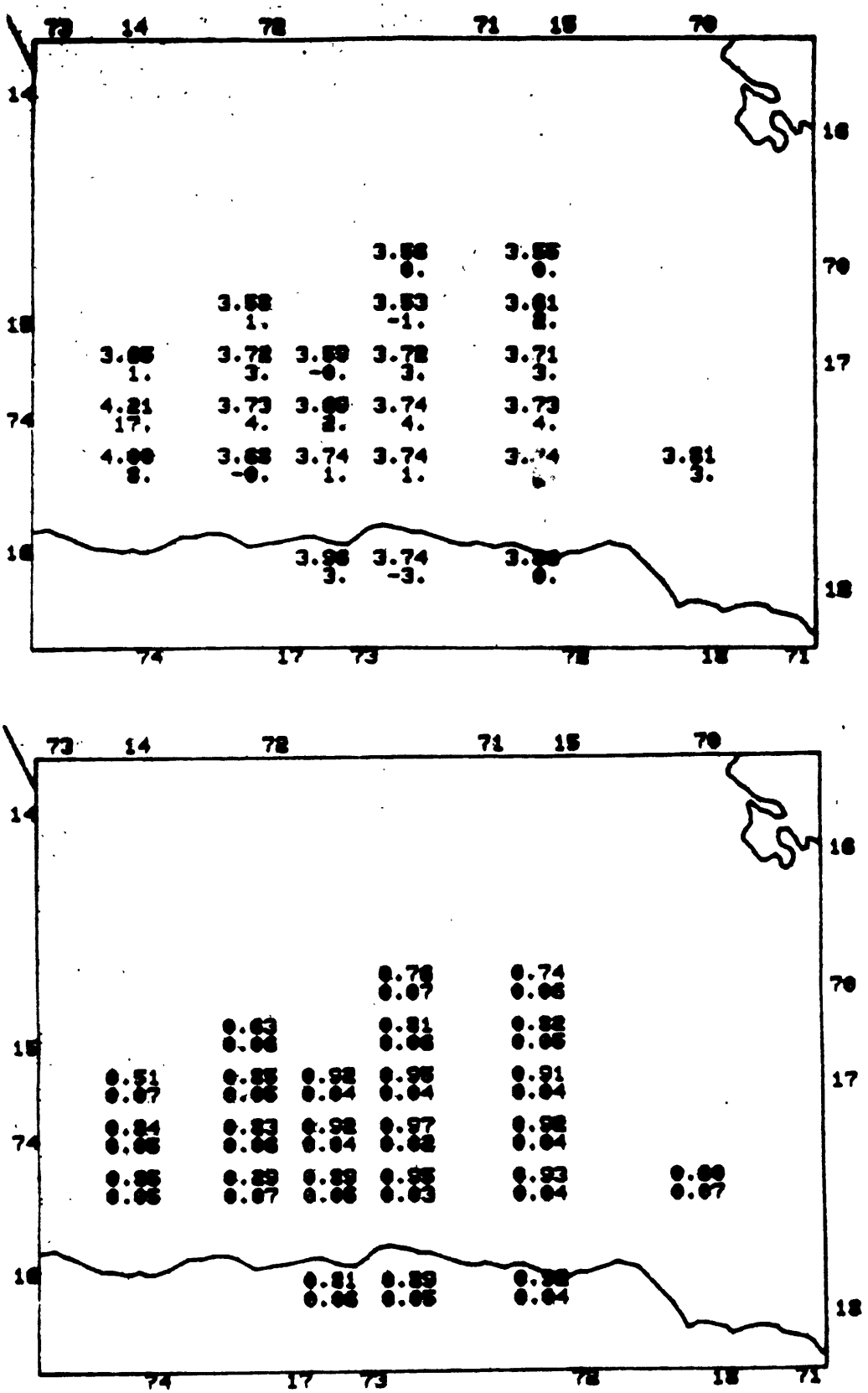

Figure 50. 3; 5 to 30 km; S

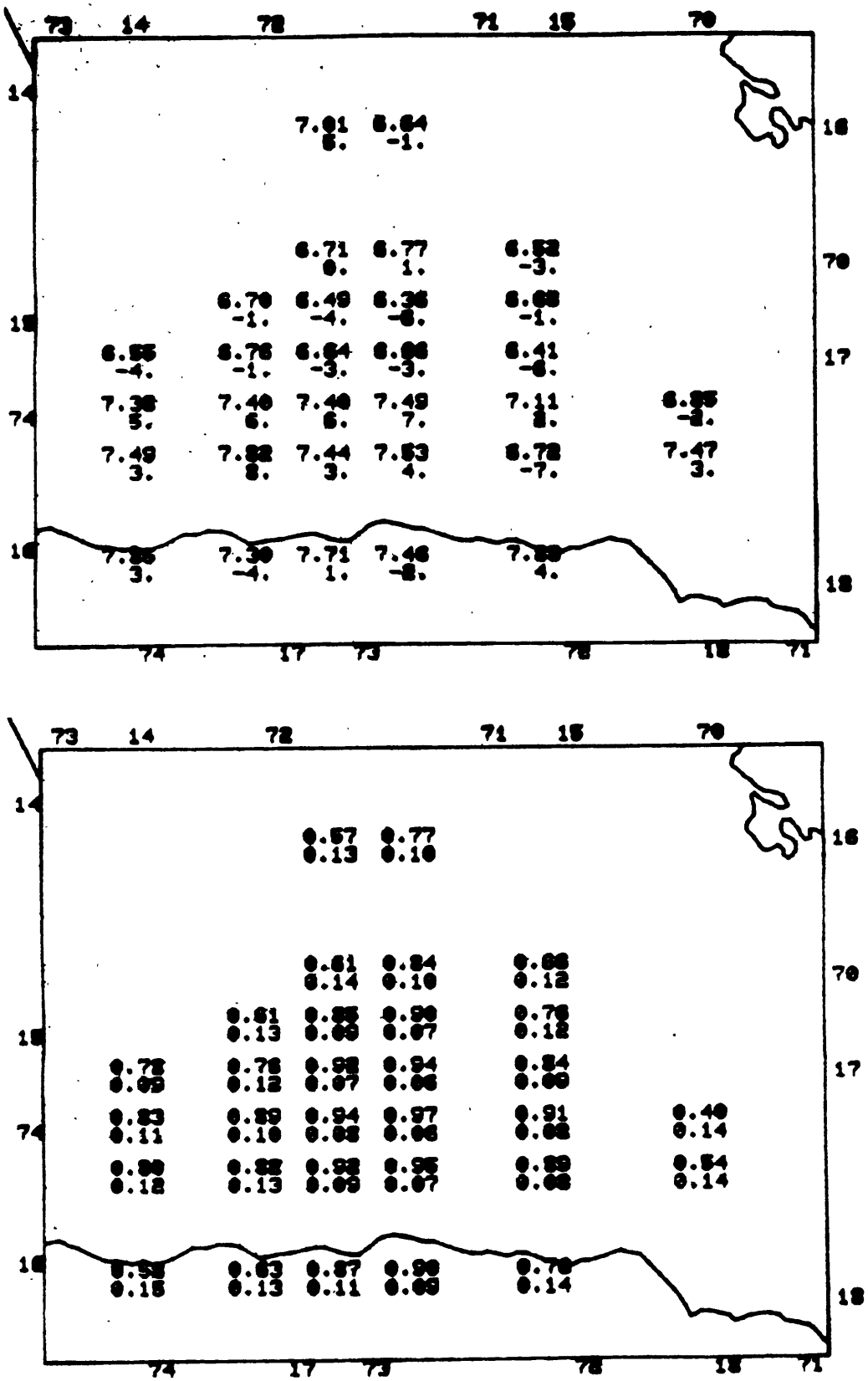

Figure 51. 3; 30 to 60 km; P

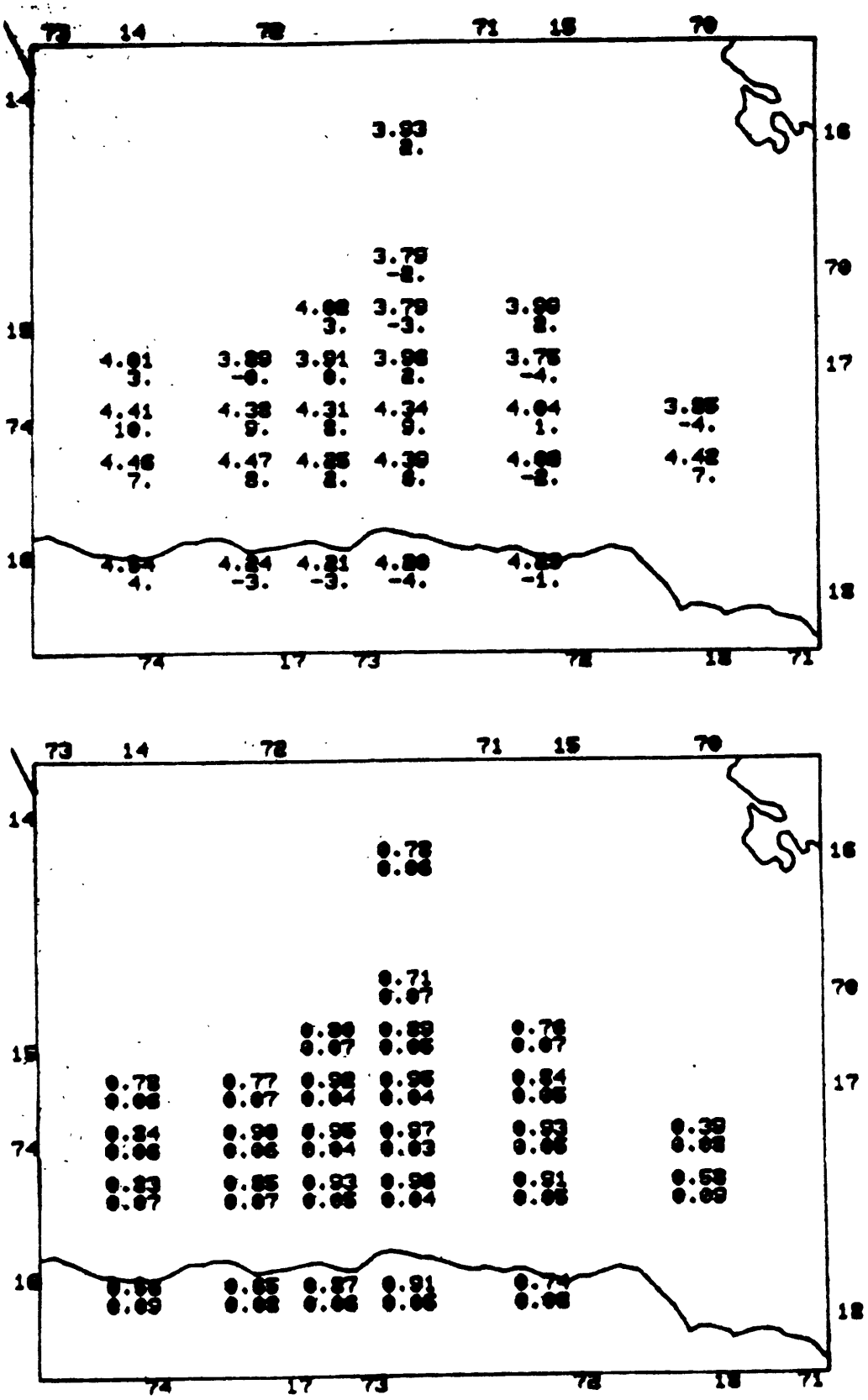

Figure 52 3; 30 to 60 km; S

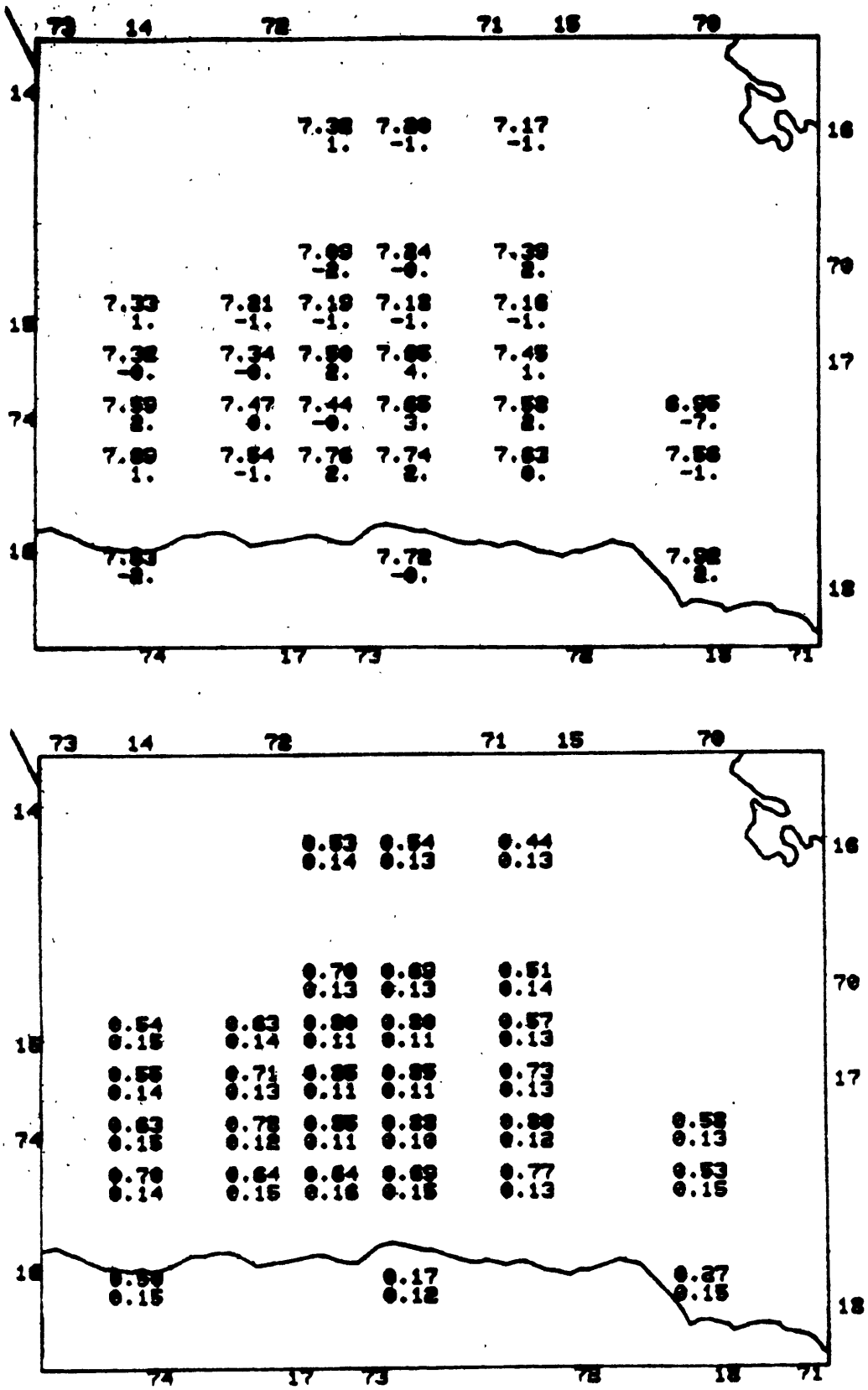

Figure 53 3; 60 to 80 km, P

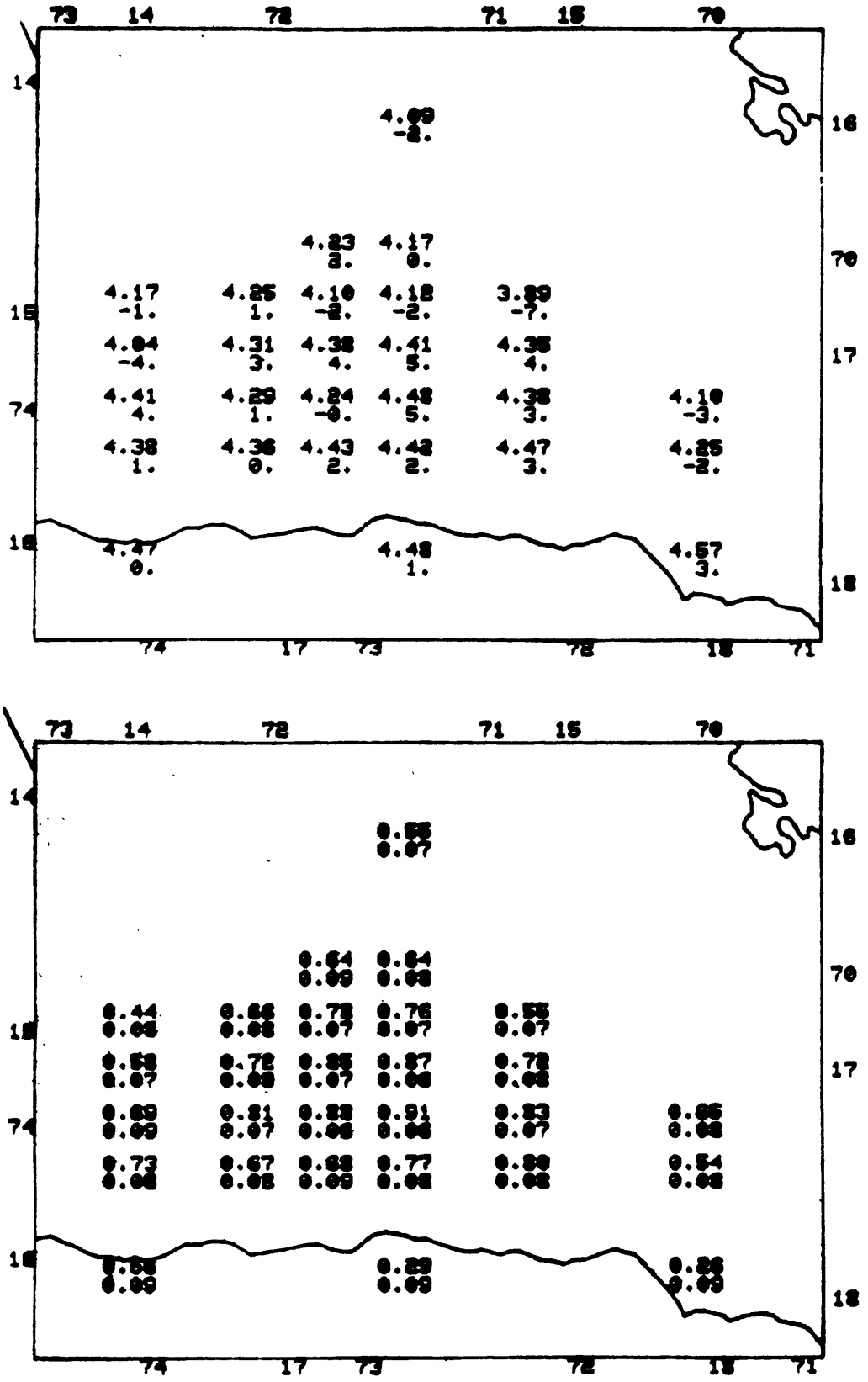

Figure 54. 3; 60 to 80 km; S

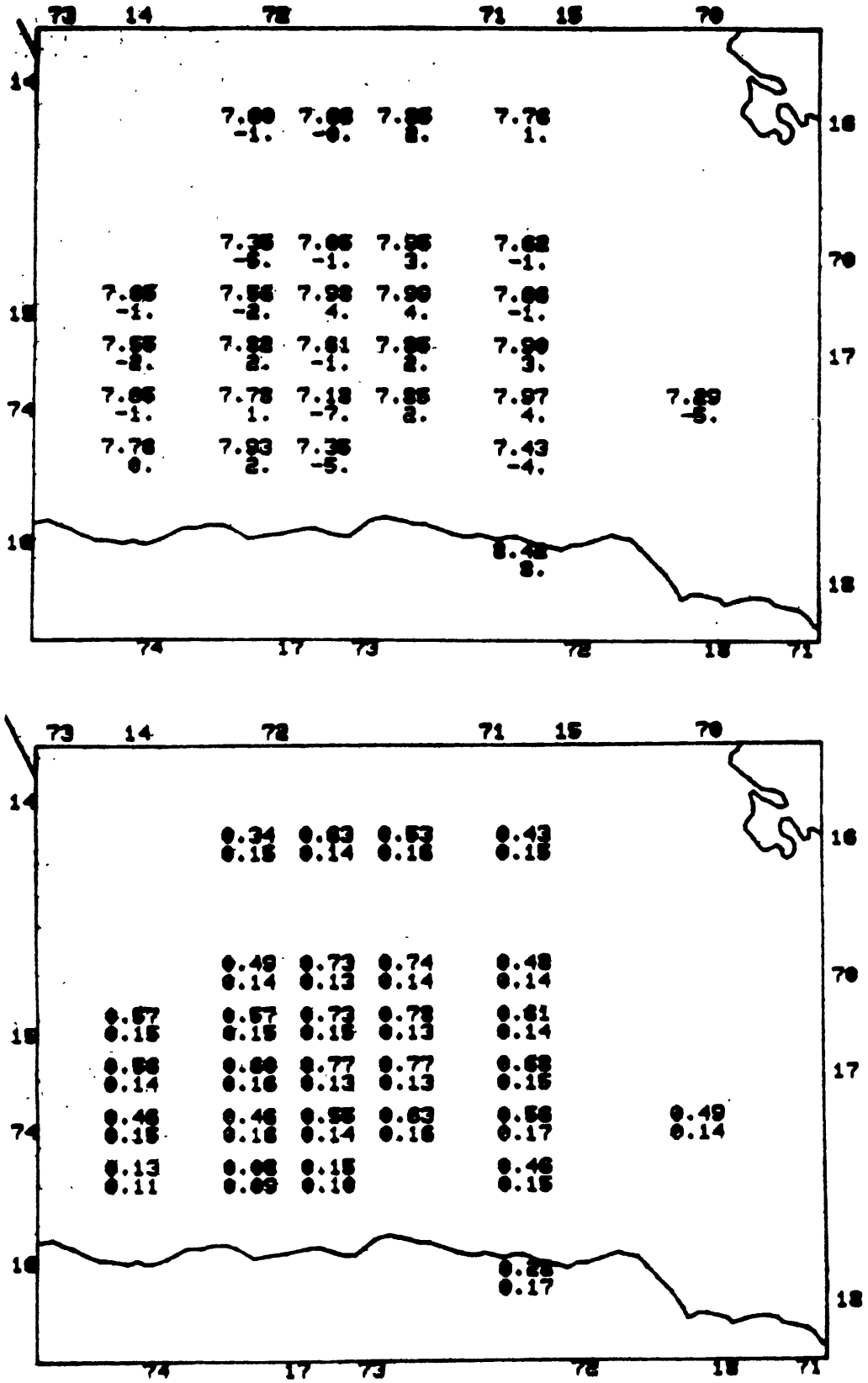

Figure 55. 3; 80 to 100 km; P

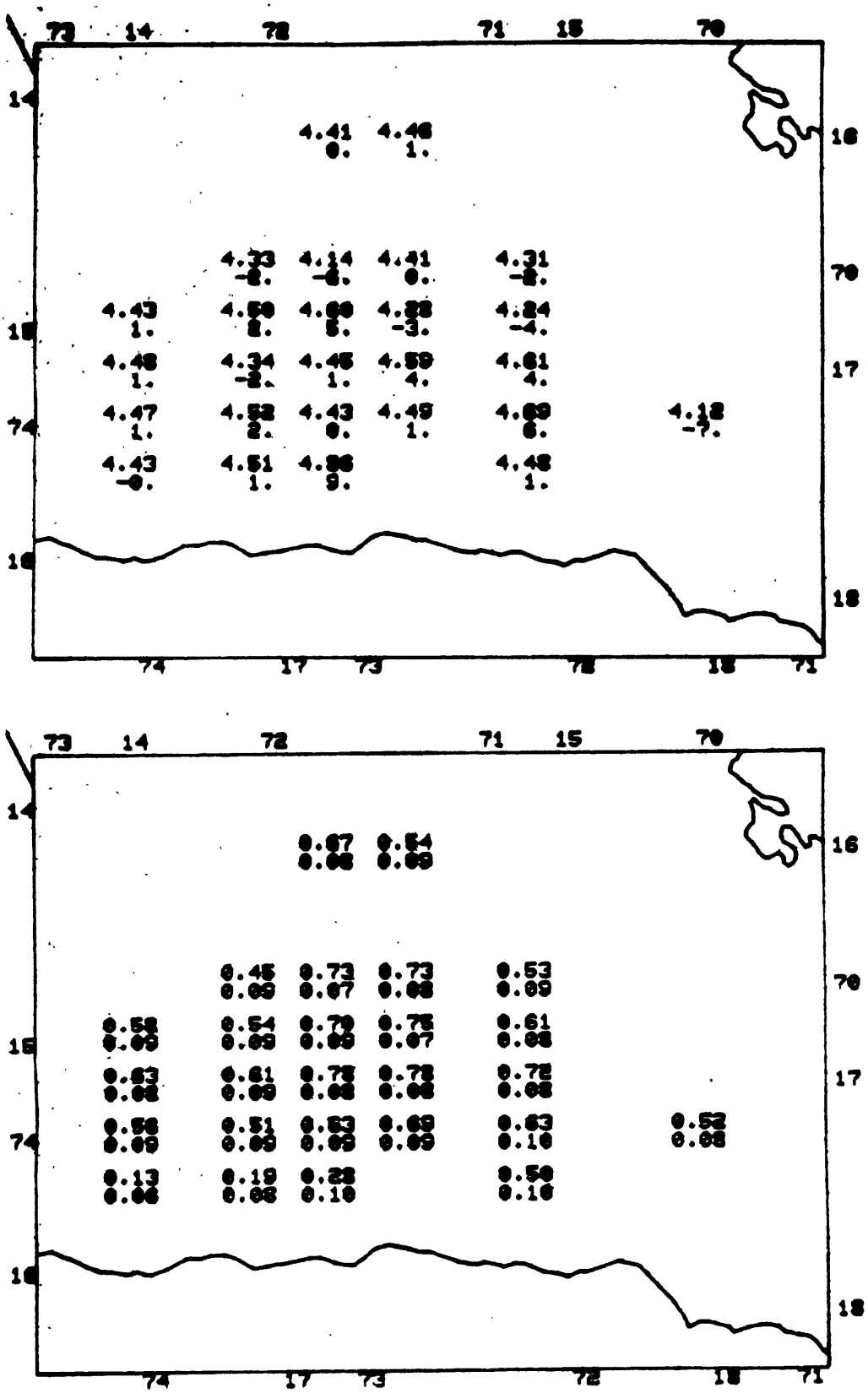

Figure 56. 3; 80 to 100 km; S

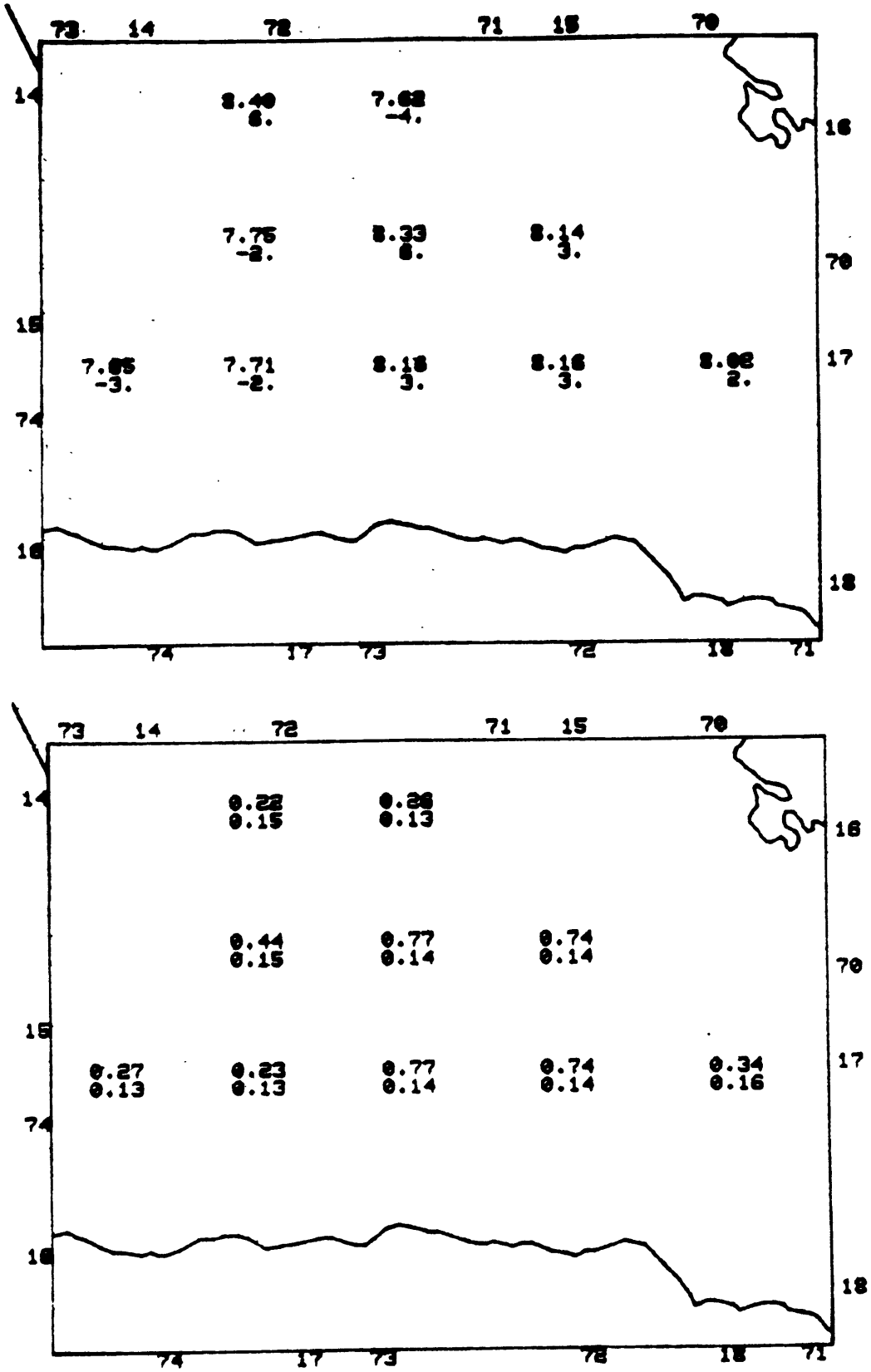

Figure 57. 3; 100 to 130 km; P

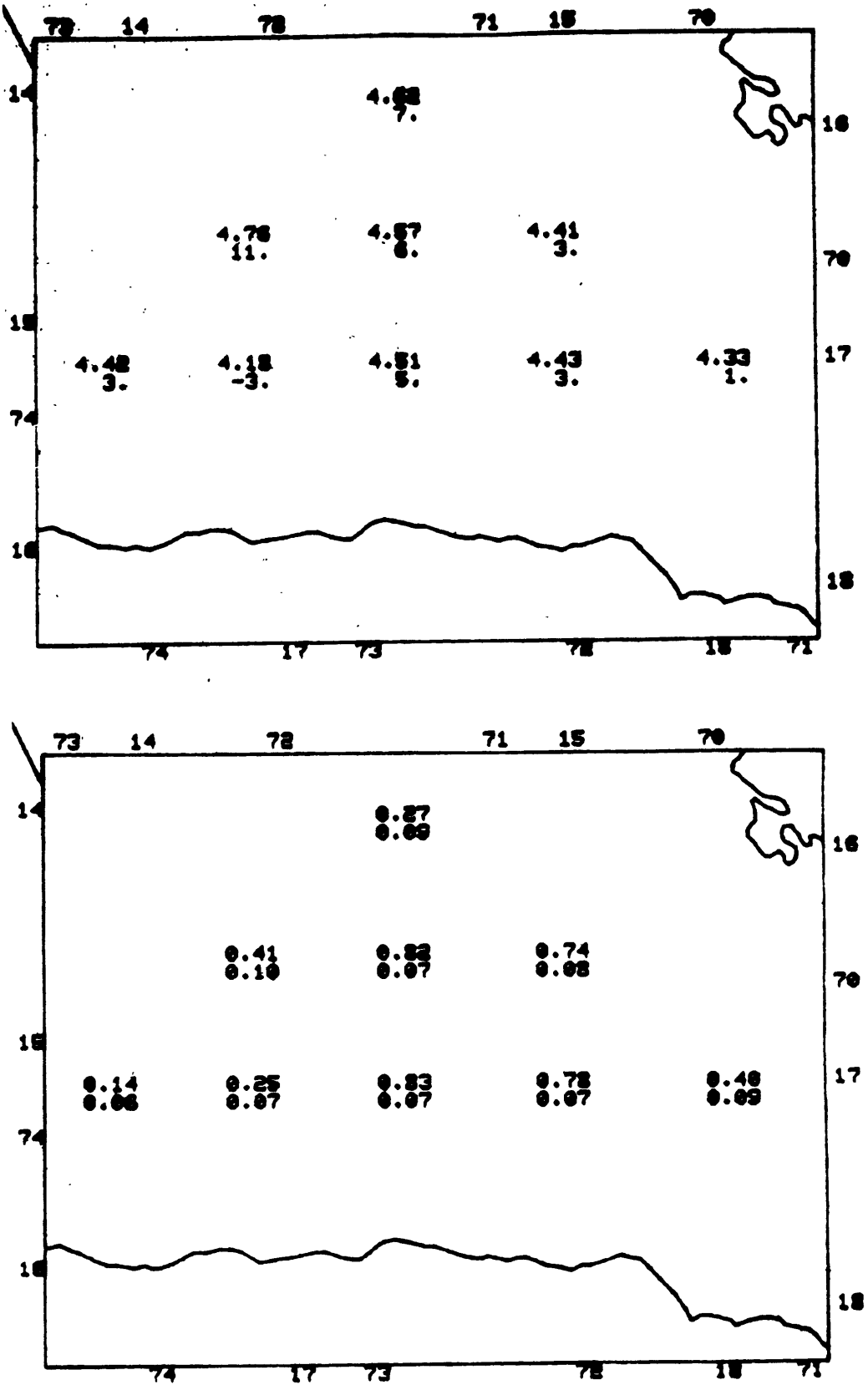

Figure 58. 3; 100 to 130 km; S

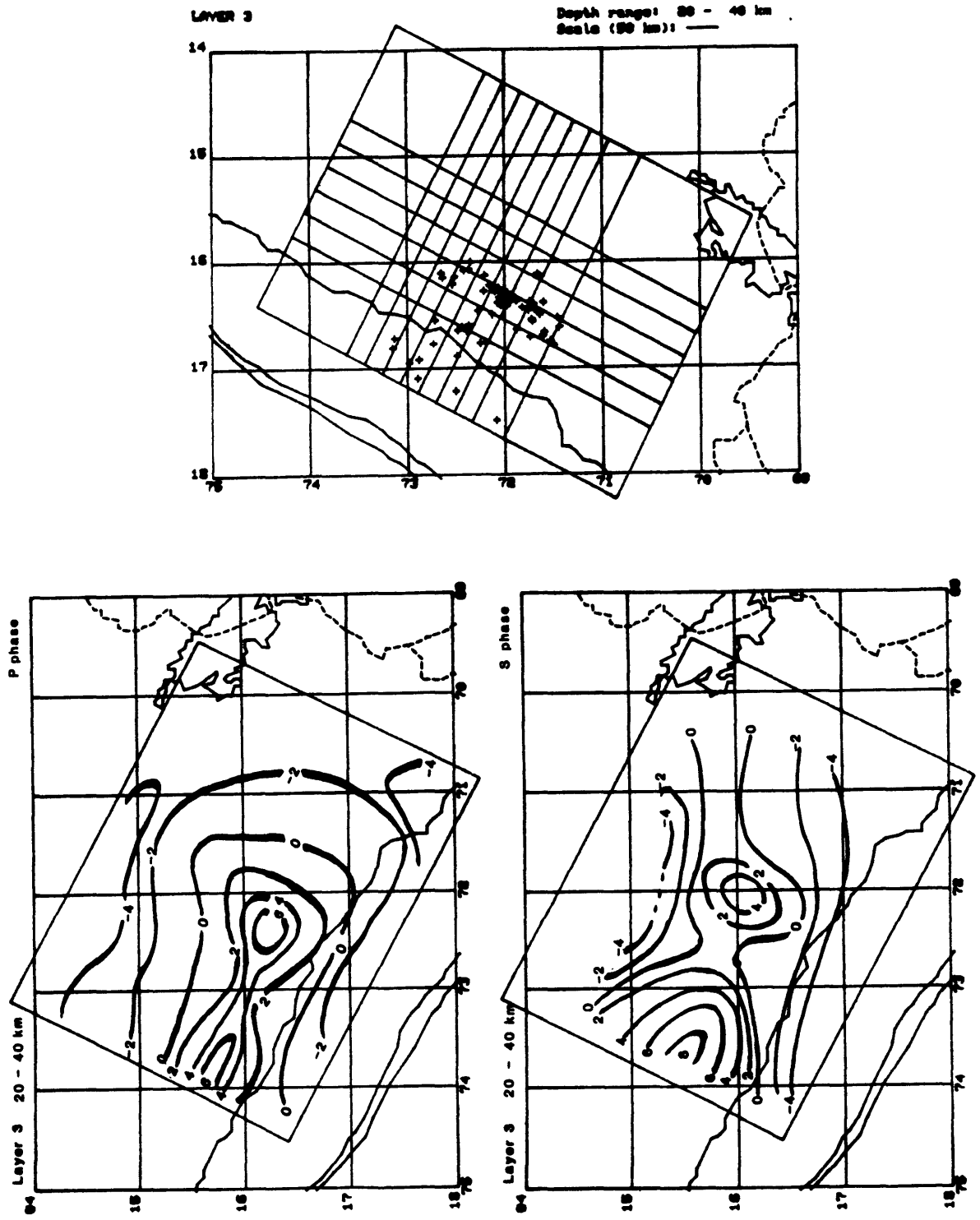
LAYER 3
Depth range: 20 - 40 km
Scale (50 km):
P phase
S phase
Layer 3 20 - 40 km

Figure 59.

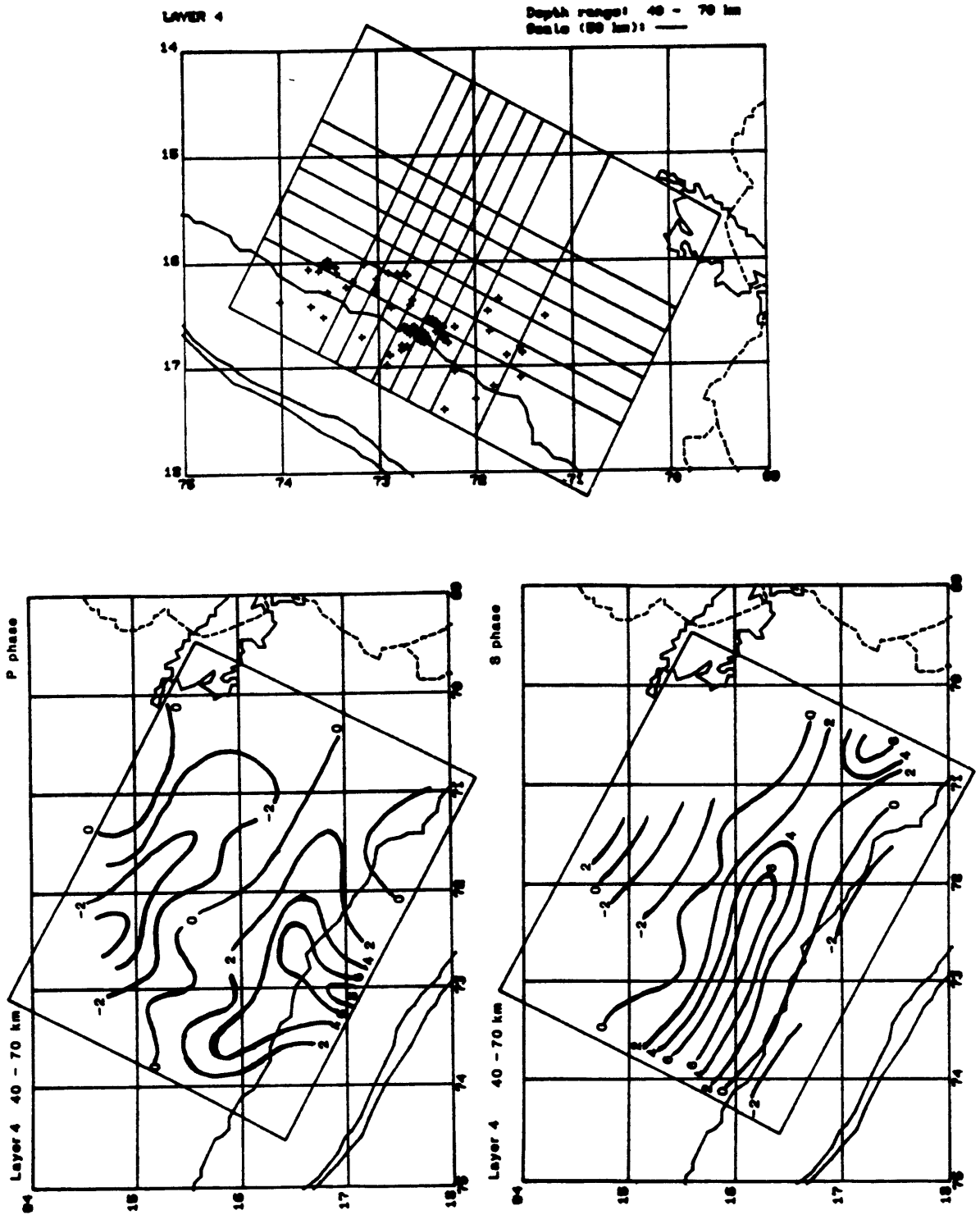
LAYER 4
Depth range: 40 - 70 km
Scale (50 km):
P phase
S phase
Layer 4 40 - 70 km

Figure 60.

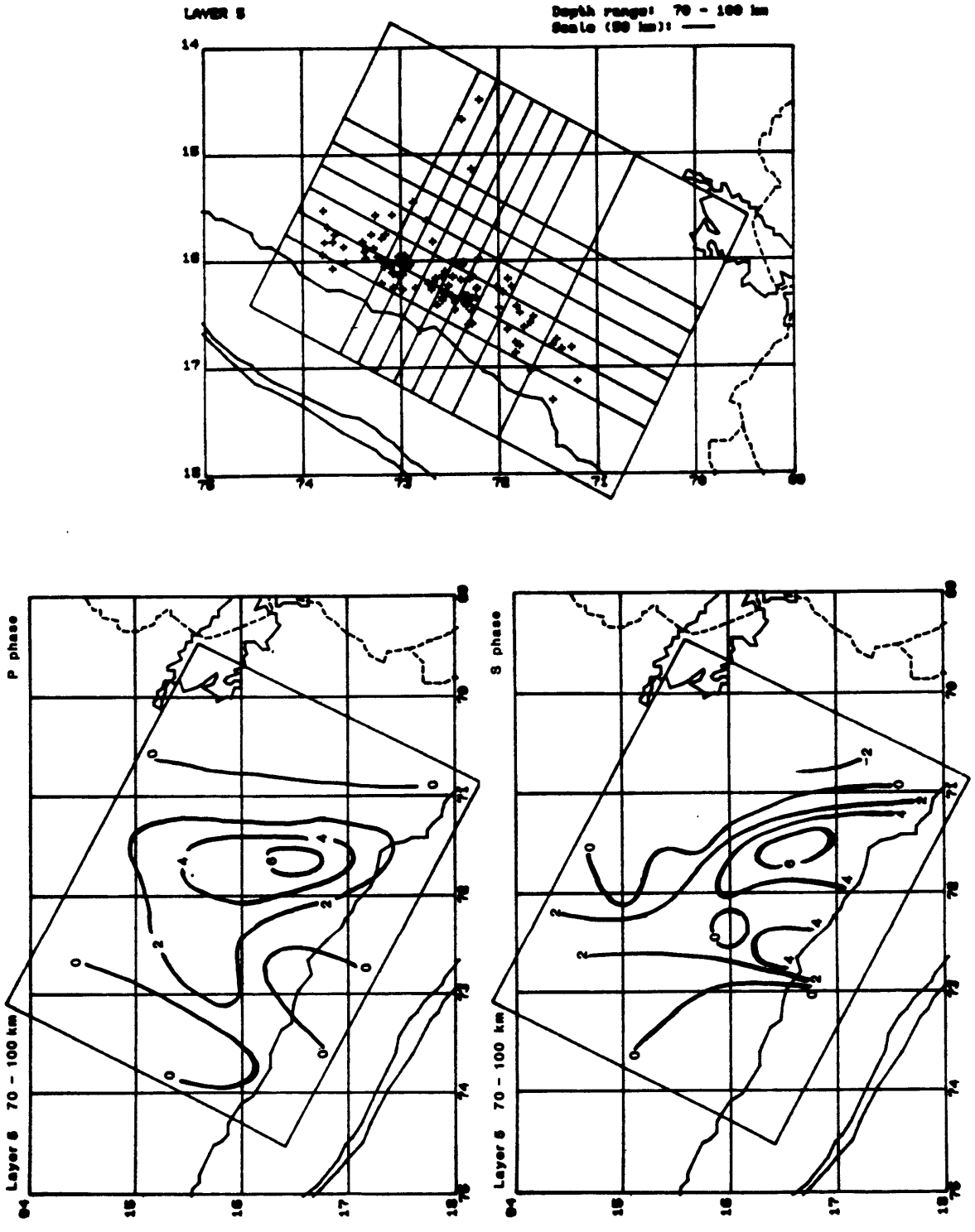

Figure 61.

APPENDIX A

This appendix contains a list of the 396 events used in the velocity inversion. These locations were determined in the second relocation run and are considered reliable. The following information is presented for each earthquake:

(1) Number used as a reference during this study.

(2) Date (year, month, day).

(3) Origin time (hour, minute, second).

(4) Latitude, longitude, and depth.

(5) Magnitude determined by Grange (1983) using the duration of the coda T in seconds and the formula $M_L = -1.1 + 2\log\left[T\right] + 0.007Z + 0.0035D$ where D is the epicentral distance and Z the depth at which the earthquake occurred (modified from Lee et al., 1972).

(6) RMS - root mean square of the time residual.

(7) GAP - maximum azimuthal aperture without stations measured from the epicenter.

(8) DMIN - distance to the nearest station.

(9) Number of recorded phases.

number	date			time			latitude	longitude	depth (km)	magnitude	RMS	GAP (deg)	DMIN (km)	number phases
7	81	6	5	23	26	27.7	16.14 S	72.ØØ W	1Ø7.6	3.3	Ø.229	92	5.5	12
9	81	6	6	1	Ø	4.1	16.9Ø S	72.83 W	17.6	3.Ø	Ø.Ø79	268	38.8	12
1Ø	81	6	6	2	51	33.3	15.15 S	72.28 W	98.Ø		Ø.Ø14	263	63.2	8
11	81	6	6	3	3	48.6	16.24 S	72.17 W	24.3	2.3	Ø.134	13Ø	15.3	8
12	81	6	6	3	19	28.4	16.3Ø S	71.62 W	123.4	3.5	Ø.Ø73	253	17.9	11
19	81	6	6	7	22	37.3	16.21 S	72.38 W	1Ø4.4	3.3	Ø.1Ø7	118	36.8	11
32	81	6	6	15	37	33.Ø	15.54 S	73.8Ø W	9Ø.5	3.4	Ø.Ø11	313	43.9	8
37	81	6	6	17	59	43.7	16.27 S	73.Ø4 W	65.6	4.8	Ø.278	247	47.8	15
41	81	6	6	23	27	57.4	16.12 S	72.46 W	1ØØ.2	3.9	Ø.321	8Ø	24.2	24
46	81	6	7	2	26	39.8	16.67 S	72.56 W	57.4	2.6	Ø.Ø44	254	2Ø.4	1Ø
48	81	6	7	3	42	52.7	16.73 S	72.61 W	56.Ø	2.6	Ø.18Ø	2Ø1	21.9	17
5Ø	81	6	7	4	43	52.Ø	16.15 S	72.52 W	24.9	1.7	Ø.Ø11	168	21.4	8
54	81	6	7	7	5	49.8	15.88 S	72.5Ø W	1Ø5.9	3.1	Ø.25Ø	183	28.4	12
58	81	6	7	7	39	35.7	15.33 S	71.73 W	124.6	3.9	Ø.178	135	22.9	16
59	81	6	7	7	41	33.7	16.3Ø S	71.96 W	96.7	2.8	Ø.219	133	12.5	13
68	81	6	7	15	52	29.5	16.54 S	71.47 W	38.8		Ø.ØØ9	287	39.Ø	8
74	81	6	8	Ø	4	13.2	15.Ø5 S	71.99 W	118.5	4.Ø	Ø.153	23Ø	23.3	14
75	81	6	8	Ø	17	37.1	14.69 S	72.37 W	95.6		Ø.164	284	79.5	9
76	81	6	8	Ø	34	6.Ø	16.49 S	72.28 W	8Ø.Ø	2.9	Ø.239	144	25.7	16
77	81	6	8	Ø	51	31.1	15.98 S	73.36 W	76.7	3.4	Ø.172	217	24.9	14
87	81	6	8	5	36	1Ø.Ø	16.8Ø S	71.51 W	38.6	2.6	Ø.239	255	56.6	11
88	81	6	8	6	3Ø	45.4	16.78 S	72.26 W	28.5	2.7	Ø.Ø12	286	53.4	1Ø
89	81	6	8	6	56	13.4	16.15 S	73.Ø3 W	84.Ø	3.2	Ø.228	2ØØ	54.1	1Ø
9Ø	81	6	8	7	38	4Ø.3	16.56 S	72.45 W	4Ø.7	2.8	Ø.Ø14	269	24.4	9
91	81	6	8	7	39	48.5	16.78 S	72.73 W	32.4	3.2	Ø.222	215	56.1	18
94	81	6	8	8	39	47.6	16.3Ø S	72.11 W	15.6	2.1	Ø.136	166	3.Ø	8
1Ø1	81	6	8	11	44	4Ø.7	16.65 S	71.88 W	3Ø.9	4.4	Ø.244	14Ø	34.7	14
1Ø5	81	6	8	13	56	31.1	15.83 S	71.55 W	141.2	4.1	Ø.Ø57	11Ø	14.4	16
112	81	6	8	18	Ø	27.6	16.85 S	72.77 W	51.7	3.5	Ø.1Ø8	224	64.8	24
118	81	6	8	22	55	32.1	15.Ø3 S	72.3Ø W	1Ø4.6		Ø.ØØ8	238	55.1	9
125	81	6	9	5	6	43.9	15.62 S	72.77 W	1Ø7.7		Ø.Ø33	2Ø9	13.2	12
129	81	6	9	7	5Ø	42.1	15.31 S	72.85 W	1Ø7.4	4.6	Ø.236	2Ø8	23.8	26
132	81	6	9	9	42	5Ø.4	16.66 S	71.92 W	83.6	3.8	Ø.279	235	36.8	2Ø
148	81	6	1Ø	2	37	54.7	15.24 S	72.37 W	1Ø7.1		Ø.152	196	62.4	16
16Ø	81	6	1Ø	1Ø	24	45.8	16.59 S	71.69 W	95.Ø		Ø.Ø79	259	52.6	8
167	81	6	1Ø	19	4	16.Ø	16.5Ø S	71.8Ø W	93.4	3.Ø	Ø.Ø51	24Ø	37.2	8
171	81	6	1Ø	21	53	41.3	16.36 S	72.28 W	82.3	2.7	Ø.21Ø	153	2Ø.7	11
172	81	6	1Ø	22	11	39.5	15.Ø6 S	71.86 W	121.1	Ø.	Ø.162	25Ø	1Ø.6	9
175	81	6	11	5	1Ø	27.Ø	17.Ø6 S	72.63 W	8.7	2.4	Ø.Ø48	3Ø1	55.1	12
176	81	6	11	5	21	45.8	16.93 S	72.89 W	2Ø.2	2.5	Ø.Ø2Ø	271	44.3	13
199	81	6	11	19	27	5.9	16.Ø4 S	71.74 W	124.6		Ø.194	14Ø	34.5	13
2Ø1	81	6	11	2Ø	3	52.4	16.72 S	71.74 W	26.7	3.2	Ø.18Ø	131	33.5	18
2Ø3	81	6	11	21	5	16.6	16.34 S	71.97 W	18.Ø	2.8	Ø.147	177	12.5	1Ø
2Ø7	81	6	12	Ø	12	18.6	16.Ø5 S	72.32 W	117.Ø	3.2	Ø.151	167	33.5	1Ø
2Ø9	81	6	12	Ø	32	12.6	15.58 S	71.41 W	145.1	4.1	Ø.115	147	8.Ø	12
21Ø	81	6	12	1	8	9.Ø	16.66 S	72.4Ø W	33.2		Ø.146	284	36.3	8

number	date	time	latitude	longitude	depth (km)	magnitude	RMS	GAP (deg)	DMIN (km)	number phases
220	81 6 12	8 : 23 : 4.0	15.93 S	72.90 W	101.1	4.2	0.181	142	27.1	22
224	81 6 12	9 : 26 : 40.4	16.27 S	72.23 W	99.6		0.300	87	16.7	19
229	81 6 12	11 : 54 : 9.8	16.72 S	72.58 W	60.8	2.7	0.036	252	43.2	10
231	81 6 12	14 : 39 : 6.2	16.63 S	72.65 W	57.3	3.1	0.114	199	9.9	15
232	81 6 12	14 : 41 : 53.1	16.70 S	72.68 W	50.8	3.5	0.105	202	15.1	19
233	81 6 12	15 : 26 : 33.0	15.15 S	72.04 W	123.2	4.8	0.377	201	26.8	25
241	81 6 13	0 : 58 : 21.4	15.98 S	73.52 W	69.2	3.0	0.072	247	22.6	9
253	81 6 13	6 : 40 : 13.0	15.83 S	73.39 W	82.9	3.3	0.205	161	10.1	11
255	81 6 13	8 : 9 : 36.8	15.87 S	71.50 W	142.8	4.1	0.257	155	20.9	20
256	81 6 13	8 : 15 : 14.2	16.43 S	72.05 W	23.2	2.0	0.199	207	14.3	8
260	81 6 13	11 : 37 : 2.0	16.20 S	72.04 W	17.8	2.0	0.169	116	2.8	8
263	81 6 13	13 : 8 : 7.2	16.56 S	72.72 W	37.9	3.2	0.196	192	1.2	24
265	81 6 13	13 : 32 : 40.6	15.76 S	73.68 W	82.9	3.8	0.066	318	22.1	14
268	81 6 13	16 : 32 : 57.2	17.20 S	71.83 W	52.2	3.4	0.349	267	26.3	23
269	81 6 13	18 : 8 : 20.7	16.65 S	72.66 W	58.6	2.8	0.040	247	11.6	11
270	81 6 13	19 : 59 : 15.1	15.08 S	73.72 W	125.8	4.5	0.187	290	82.8	17
272	81 6 13	21 : 54 : 45.9	16.19 S	73.27 W	65.5	3.5	0.237	209	50.5	16
275	81 6 13	22 : 56 : 36.5	15.44 S	73.61 W	105.8	4.3	0.200	297	92.3	15
279	81 6 14	2 : 41 : 5.9	16.03 S	73.15 W	69.0	2.3	0.057	165	44.2	8
291	81 6 14	9 : 27 : 43.5	16.44 S	72.87 W	61.5	3.2	0.222	190	21.6	18
295	81 6 14	10 : 44 : 57.5	16.35 S	72.06 W	22.0	2.7	0.195	159	5.3	13
305	81 6 14	16 : 45 : 61.1	16.27 S	72.48 W	100.5	3.5	0.244	124	8.4	13
306	81 6 14	17 : 27 : 9.6	15.84 S	73.78 W	81.2	3.6	0.161	319	33.7	11
309	81 6 14	20 : 46 : 36.0	17.31 S	71.46 W	77.8	4.0	0.300	294	39.8	24
310	81 6 14	21 : 30 : 34.5	15.13 S	72.35 W	113.7		0.282	211	58.8	15
311	81 6 14	22 : 55 : 9.7	16.25 S	73.08 W	71.6	3.3	0.144	189	52.2	14
316	81 6 15	1 : 18 : 15.6	16.08 S	72.38 W	21.5	2.2	0.152	151	30.1	10
317	81 6 15	1 : 28 : 10.3	14.93 S	72.46 W	106.8	4.5	0.155	239	70.6	19
322	81 6 15	4 : 52 : 8.4	16.00 S	72.26 W	107.7	2.8	0.267	188	30.8	13
323	81 6 15	5 : 0 : 17.5	16.42 S	71.90 W	19.5	2.7	0.257	132	14.8	17
328	81 6 15	7 : 30 : 43.7	16.92 S	71.18 W	183.2		0.155	312	60.4	10
332	81 6 15	8 : 31 : 8.1	17.05 S	72.22 W	54.7	2.7	0.212	241	19.5	15
333	81 6 15	8 : 36 : 43.3	16.20 S	71.81 W	144.0		0.105	230	17.9	10
336	81 6 15	10 : 37 : 13.2	15.03 S	72.22 W	103.4	3.7	0.327	226	47.5	20
340	81 6 15	14 : 9 : 11.3	16.18 S	71.73 W	118.1	3.0	0.076	183	20.3	13
342	81 6 15	15 : 37 : 55.0	16.78 S	72.29 W	40.4	2.6	0.127	164	36.0	12
343	81 6 15	14 : 48 : 18.1	16.32 S	72.55 W	96.6	4.2	0.280	88	8.7	29
353	81 6 15	18 : 17 : 17.7	16.98 S	72.90 W	20.0	2.9	0.045	274	49.7	12
355	81 6 15	21 : 14 : 61.3	15.86 S	72.62 W	105.2	3.0	0.195	165	16.2	12
359	81 6 15	22 : 2 : 3.7	16.04 S	72.94 W	85.0	3.1	0.252	139	39.2	16
362	81 6 15	23 : 11 : 40.2	16.01 S	72.46 W	15.6	2.2	0.294	119	12.0	10
363	81 6 16	0 : 0 : 21.1	16.36 S	72.58 W	85.4	2.7	0.025	160	11.7	12
364	81 6 16	0 : 52 : 6.7	14.89 S	71.99 W	109.5	3.5	0.158	293	34.7	13
367	81 6 16	1 : 51 : 50.9	16.21 S	72.08 W	12.5	1.6	0.128	161	6.5	8
369	81 6 16	3 : 11 : 26.7	16.09 S	72.43 W	20.1	1.8	0.136	144	28.2	12
372	81 6 16	4 : 42 : 33.3	16.78 S	72.19 W	38.6	2.8	0.195	142	29.7	18

number	date			time			latitude	longitude	depth (km)	magnitude	RMS	GAP (deg)	DMIN (km)	number phases
373	81	6	16	4	46	28.8	16.27 S	72.27 W	104.8	3.4	0.167	71	20.4	25
374	81	6	16	4	49	16.6	16.17 S	72.30 W	97.1	2.6	0.175	135	25.7	12
375	81	6	16	4	58	55.1	15.97 S	73.24 W	92.0	3.1	0.319	170	31.9	15
376	81	6	16	5	20	59.3	15.61 S	71.91 W	13.1	1.9	0.213	251	8.7	8
379	81	6	16	8	47	44.4	16.02 S	72.36 W	22.4	2.3	0.151	160	17.6	14
380	81	6	16	8	52	32.0	16.32 S	71.85 W	18.6	2.1	0.066	141	8.6	14
381	81	6	16	9	48	52.5	15.76 S	73.30 W	85.1	2.8	0.180	186	18.2	12
382	81	6	16	10	37	32.1	16.80 S	71.46 W	77.7	2.9	0.053	258	32.6	8
383	81	6	16	10	54	14.3	16.81 S	71.80 W	81.6	3.0	0.148	142	26.4	18
384	81	6	16	11	11	18.1	16.24 S	72.03 W	16.0	1.9	0.118	122	7.1	8
387	81	6	16	12	47	56.9	16.19 S	72.39 W	84.9	2.6	0.070	114	33.3	10
388	81	6	16	13	35	23.7	17.32 S	72.57 W	8.4	3.6	0.136	260	65.7	25
389	81	6	16	14	26	9.4	17.11 S	71.54 W	69.2	2.8	0.017	298	17.6	8
391	81	6	16	16	1	27.8	16.12 S	72.41 W	105.2	3.2	0.102	139	25.2	10
394	81	6	16	16	28	32.2	16.42 S	72.68 W	66.0	3.4	0.264	116	16.5	24
401	81	6	16	22	35	38.0	16.15 S	71.65 W	19.8	2.6	0.148	210	26.2	8
402	81	6	16	23	4	7.8	16.01 S	72.48 W	100.9	2.7	0.066	115	12.9	13
404	81	6	16	23	49	52.2	16.14 S	72.21 W	27.7	2.1	0.090	153	19.6	10
406	81	6	17	8	33	60.0	16.37 S	74.02 W	57.3	4.0	0.328	303	87.5	22
407	81	6	17	7	48	9.8	16.28 S	72.69 W	87.8	4.2	0.476	118	24.5	34
409	81	6	17	8	53	15.4	16.81 S	73.16 W	37.6	2.9	0.189	272	54.8	16
412	81	6	17	11	28	53.7	16.75 S	72.56 W	58.3	3.2	0.153	200	26.9	24
416	81	6	17	16	39	59.8	16.42 S	72.64 W	84.4	3.2	0.094	223	19.9	14
417	81	6	17	16	41	35.5	16.25 S	72.00 W	16.7	2.1	0.144	140	9.2	8
418	81	6	17	16	42	22.5	16.72 S	73.18 W	47.3	2.8	0.082	272	52.6	16
420	81	6	17	17	30	31.1	16.22 S	72.54 W	25.6	2.3	0.092	132	15.6	10
422	81	6	17	17	41	10.2	15.70 S	73.75 W	90.0	3.6	0.241	307	31.0	16
424	81	6	17	18	26	25.4	15.74 S	72.42 W	110.1	3.6	0.218	137	18.7	25
428	81	6	17	5	42	8.3	16.76 S	72.57 W	53.3	3.5	0.244	202	26.7	30
431	81	6	17	20	34	49.0	16.89 S	72.89 W	40.8	2.8	0.312	235	41.2	20
433	81	6	18	0	1	48.7	16.11 S	72.90 W	45.7		0.407	142	43.5	19
436	81	6	18	1	37	23.1	15.95 S	73.80 W	75.6	3.8	0.157	302	39.7	16
437	81	6	18	1	47	9.9	15.17 S	72.45 W	109.2	3.6	0.283	208	70.4	22
441	81	6	18	5	0	19.5	16.53 S	73.57 W	57.7		0.072	274	82.7	12
443	81	6	18	5	14	43.6	16.92 S	72.11 W	12.2	2.7	0.070	152	12.1	14
444	81	6	18	5	24	11.7	15.89 S	72.64 W	101.1	3.2	0.293	91	17.1	19
447	81	6	18	7	4	56.9	16.99 S	72.92 W	42.7	3.3	0.120	244	52.2	23
450	81	6	18	8	15	41.6	16.16 S	72.64 W	31.5	3.3	0.193	157	26.9	24
451	81	6	18	8	20	1.2	16.35 S	72.24 W	90.1	3.4	0.190	80	17.6	23
453	81	6	18	8	54	13.2	16.04 S	72.90 W	91.4	2.7	0.104	186	36.9	10
455	81	6	18	9	37	56.5	16.32 S	72.56 W	82.8	3.6	0.248	89	9.5	27
462	81	6	18	13	25	56.3	15.79 S	72.94 W	102.5		0.085	130	23.3	10
468	81	6	18	16	39	39.7	15.80 S	72.54 W	105.8	4.1	0.198	122	12.7	26
471	81	6	18	18	20	42.8	15.92 S	73.37 W	84.7	3.0	0.189	189	18.8	8
474	81	6	18	18	42	16.1	16.67 S	71.86 W	46.0	3.0	0.154	136	36.5	19
477	81	6	18	20	37	54.6	15.81 S	72.56 W	105.4	3.5	0.181	119	13.5	18

number	date			time			latitude	longitude	depth (km)	magnitude	RMS	GAP (deg)	DMIN (km)	number phases
478	81	6	18	20	59	13.8	16.24 S	73.34 W	49.3	3.5	0.386	228	52.6	20
479	81	6	18	21	5	33.0	14.50 S	72.20 W	97.7	4.4	0.279	277	82.5	16
480	81	6	18	21	42	57.9	16.40 S	72.45 W	77.2	3.4	0.266	89	6.9	26
484	81	6	19	0	17	34.9	16.83 S	71.27 W	92.3	3.2	0.041	290	48.0	8
489	81	6	19	6	12	48.4	15.72 S	71.65 W	140.6	3.5	0.110	124	4.1	11
491	81	6	19	7	43	25.0	16.69 S	72.54 W	58.4	2.6	0.043	242	22.9	14
498	81	6	19	13	1	32.7	15.76 S	70.38 W	214.4	4.5	0.369	290	107.1	15
500	81	6	19	15	23	51.0	16.22 S	73.20 W	73.9	3.3	0.130	201	56.2	12
502	81	6	19	18	6	27.9	16.19 S	72.07 W	101.8		0.055	128	4.2	10
504	81	6	19	20	14	8.8	16.22 S	72.72 W	92.5	3.2	0.442	122	38.5	19
509	81	6	20	0	22	1.9	16.31 S	72.02 W	25.7	2.4	0.141	147	7.0	12
512	81	6	20	1	3	58.1	15.78 S	72.45 W	114.2	4.6	0.180	90	13.5	32
513	81	6	20	4	6	41.7	16.43 S	71.98 W	27.1	2.3	0.043	188	23.8	10
519	81	6	20	6	0	18.6	16.32 S	71.88 W	111.3	3.2	0.315	150	12.1	16
525	81	6	20	6	32	43.6	15.99 S	72.22 W	99.9	3.1	0.109	217	28.6	10
529	81	6	20	7	28	59.1	16.43 S	71.82 W	93.6	2.9	0.097	135	10.3	14
530	81	6	20	8	43	21.7	16.77 S	72.53 W	59.4	2.9	0.106	200	29.9	24
531	81	6	20	9	50	29.5	16.28 S	72.98 W	82.4		0.304	238	43.0	14
532	81	6	20	10	36	47.0	17.49 S	72.09 W	29.0	3.2	0.378	287	53.8	22
538	81	6	20	15	17	59.8	16.34 S	72.32 W	79.1	2.8	0.145	147	16.0	10
540	81	6	20	17	13	37.2	16.50 S	71.62 W	8.8		0.291	115	14.0	24
541	81	6	20	17	18	48.0	15.83 S	73.69 W	78.7	3.3	0.181	309	24.2	10
543	81	6	20	17	43	26.8	16.14 S	72.98 W	94.8	3.4	0.179	244	50.3	12
549	81	6	20	19	30	54.7	16.63 S	72.74 W	56.0	4.4	0.376	237	7.8	27
555	81	6	20	23	27	16.5	16.34 S	72.35 W	83.8	2.9	0.427	126	29.0	17
558	81	6	21	2	6	4.5	15.89 S	73.36 W	84.6	2.9	0.028	176	17.3	9
561	81	6	21	2	46	34.9	16.07 S	73.73 W	68.5	3.6	0.204	283	42.0	20
562	81	6	21	3	4	58.5	15.12 S	71.53 W	139.9	4.7	0.269	251	28.6	28
568	81	6	21	6	0	47.1	16.26 S	72.07 W	22.9		0.210	121	4.5	8
572	81	6	21	10	19	20.9	16.02 S	72.25 W	105.1	3.0	0.129	205	29.0	12
573	81	6	21	10	38	42.0	16.29 S	72.40 W	100.3	3.2	0.272	102	9.0	17
575	81	6	21	13	47	22.6	15.35 S	72.98 W	107.1	4.1	0.117	211	29.7	26
580	81	6	21	17	47	19.0	16.08 S	73.70 W	73.3	3.6	0.257	279	41.0	18
584	81	6	21	20	5	57.1	15.58 S	73.09 W	95.1	4.6	0.201	189	37.9	27
585	81	6	21	23	42	37.7	14.89 S	71.97 W	112.5	3.7	0.272	258	32.5	14
590	81	6	22	2	26	40.0	17.14 S	71.21 W	87.1	3.8	0.449	283	50.8	19
591	81	6	22	1	49	24.5	15.79 S	72.58 W	101.0	3.5	0.212	81	16.1	27
593	81	6	22	5	11	38.8	15.88 S	73.59 W	77.3	3.1	0.178	280	16.0	13
594	81	6	22	6	24	30.1	15.93 S	71.91 W	129.2	3.3	0.123	76	30.1	16
597	81	6	22	7	18	45.2	16.07 S	71.76 W	129.3	3.4	0.084	164	31.4	15
601	81	6	22	9	49	49.9	16.19 S	72.15 W	107.3	2.9	0.139	155	12.5	10
602	81	6	22	9	14	56.5	15.96 S	72.96 W	98.9	3.0	0.226	131	33.8	14
603	81	6	22	9	0	6.6	16.63 S	72.45 W	38.8	2.2	0.153	216	29.3	10
605	81	6	22	11	12	16.0	15.23 S	72.17 W	103.3		0.220	208	41.4	8
611	81	6	22	13	54	16.4	15.51 S	72.42 W	110.7	3.7	0.306	162	42.4	27
617	81	6	22	20	31	36.1	15.60 S	71.19 W	162.9	4.2	0.151	252	19.2	13

number	date	time	latitude	longitude	depth (km)	magnitude	RMS	GAP (deg)	DMIN (km)	number phases
622	81 6 23	0 : 12 : 23.3	15.85 S	71.60 W	122.9	3.6	0.155	96	12.3	17
632	81 6 23	4 : 37 : 18.8	16.43 S	71.82 W	14.3		0.069	251	9.8	8
635	81 6 23	7 : 45 : 34.8	16.66 S	72.49 W	38.9	2.7	0.121	226	26.2	12
642	81 6 23	13 : 57 : 23.0	16.02 S	72.48 W	81.4	3.0	0.092	186	35.7	11
645	81 6 23	14 : 15 : 37.7	16.73 S	72.51 W	58.0	2.4	0.046	247	28.0	10
646	81 6 23	16 : 48 : 46.0	16.81 S	72.45 W	41.4		0.244	209	38.6	19
650	81 6 23	20 : 25 : 6.9	15.48 S	72.12 W	112.0		0.284	146	51.8	22
652	81 6 23	17 : 29 : 8.7	16.05 S	73.51 W	68.6	3.5	0.121	242	29.1	17
655	81 6 23	20 : 32 : 17.6	16.60 S	72.38 W	30.8	3.1	0.403	156	30.9	24
658	81 6 23	23 : 58 : 44.6	16.17 S	71.91 W	99.8	2.8	0.070	122	13.2	11
660	81 6 24	1 : 50 : 47.3	16.13 S	70.08 W	257.4	5.7	0.156	299	137.8	28
662	81 6 24	1 : 15 : 55.9	16.77 S	72.49 W	56.3	2.7	0.066	206	32.6	12
666	81 6 24	3 : 25 : 53.6	16.26 S	72.85 W	86.6	3.3	0.383	152	36.5	24
670	81 6 24	5 : 33 : 46.5	16.69 S	72.58 W	58.0	3.1	0.401	244	19.9	19
673	81 6 24	6 : 0 : 60.5	16.83 S	71.55 W	42.3	2.5	0.186	218	24.6	13
674	81 6 24	7 : 45 : 16.8	16.05 S	72.38 W	96.0	2.6	0.093	259	33.9	10
675	81 6 24	6 : 57 : 23.5	16.44 S	71.82 W	22.1	2.2	0.121	216	11.3	12
678	81 6 24	9 : 15 : 9.2	16.71 S	71.61 W	37.8	2.4	0.083	214	34.2	11
679	81 6 24	9 : 47 : 47.5	16.63 S	72.73 W	58.3	2.7	0.154	263	7.2	11
680	81 6 24	10 : 8 : 15.2	16.74 S	72.34 W	66.5	3.1	0.201	162	42.5	23
681	81 6 24	10 : 22 : 54.8	16.47 S	72.45 W	84.0	2.8	0.166	122	13.9	20
682	81 6 24	11 : 6 : 15.8	16.37 S	72.65 W	66.6	2.7	0.044	156	19.6	11
683	81 6 24	11 : 15 : 42.1	16.61 S	72.32 W	72.5	3.3	0.315	131	34.0	28
684	81 6 24	11 : 35 : 42.3	15.59 S	70.40 W	255.8		0.179	292	102.7	17
685	81 6 24	11 : 16 : 31.0	16.30 S	71.98 W	22.9	2.5	0.117	187	10.5	10
687	81 6 24	12 : 41 : 57.8	16.14 S	71.71 W	127.0	3.9	0.272	76	25.1	23
689	81 6 24	14 : 12 : 45.8	16.41 S	71.98 W	27.1	2.1	0.072	130	10.5	8
691	81 6 24	15 : 27 : 1.9	16.12 S	73.43 W	58.1	3.2	0.104	229	36.9	12
692	81 6 24	15 : 28 : 24.9	16.47 S	72.28 W	27.6	2.7	0.148	124	25.0	18
694	81 6 24	15 : 36 : 39.8	16.51 S	72.14 W	26.2	2.0	0.030	210	22.3	8
695	81 6 24	16 : 6 : 38.7	15.30 S	71.87 W	123.6	4.4	0.201	144	20.0	27
697	81 6 24	17 : 57 : 58.9	16.89 S	72.50 W	30.9	2.9	0.049	265	43.0	14
702	81 6 24	20 : 27 : 21.5	16.37 S	71.88 W	29.7	2.0	0.102	120	11.6	10
705	81 6 24	22 : 9 : 40.0	16.13 S	71.68 W	23.7	2.3	0.056	125	27.0	8
706	81 6 24	22 : 15 : 23.8	16.14 S	71.66 W	25.5	2.5	0.042	133	26.4	8
710	81 6 24	23 : 57 : 55.5	15.78 S	70.84 W	204.4		0.191	267	64.3	18
711	81 6 24	23 : 9 : 31.7	16.16 S	72.47 W	95.2	3.0	0.219	93	20.3	18
713	81 6 25	0 : 12 : 26.1	16.26 S	72.23 W	87.7	2.8	0.035	173	16.2	12
717	81 6 25	1 : 5 : 33.8	17.32 S	72.02 W	40.5	3.2	0.266	270	34.4	25
718	81 6 25	2 : 26 : 2.9	16.17 S	73.02 W	68.9	2.6	0.205	203	55.8	12
723	81 6 25	7 : 51 : 29.5	16.03 S	72.40 W	98.8	3.3	0.219	160	34.7	15
728	81 6 25	15 : 38 : 46.0	15.83 S	72.68 W	97.9	3.3	0.271	118	10.2	19
730	81 6 25	14 : 7 : 52.2	15.95 S	72.37 W	112.0	3.8	0.187	114	12.5	24
731	81 6 25	13 : 6 : 53.5	16.71 S	72.32 W	43.1	2.7	0.144	231	44.3	8
734	81 6 25	17 : 3 : 28.9	15.98 S	72.36 W	14.4	2.1	0.212	176	14.6	12
735	81 6 25	17 : 8 : 47.6	15.96 S	72.37 W	18.4	2.1	0.234	184	13.2	14

number	date	time	latitude	longitude	depth (km)	magnitude	RMS	GAP (deg)	DMIN (km)	number phases
736	81 6 25	17 : 2Ø : 51.9	16.Ø9 S	73.62 W	6Ø.4		Ø.354	266	37.1	17
737	81 6 25	18 : 2Ø : 28.9	15.97 S	73.Ø3 W	86.4	3.2	Ø.291	14Ø	4Ø.1	16
74Ø	81 6 25	2Ø : 14 : 12.3	16.41 S	71.95 W	18.4	2.5	Ø.Ø52	94	9.5	15
748	81 6 25	22 : 26 : 26.9	16.Ø3 S	73.16 W	84.5	2.7	Ø.196	168	43.2	12
75Ø	81 6 25	23 : 29 : 14.7	15.61 S	72.15 W	131.7	4.1	Ø.223	186	47.3	24
754	81 6 26	Ø : 2 : 24.5	16.37 S	71.77 W	4Ø.1	2.4	Ø.Ø78	221	1.5	12
755	81 6 26	Ø : 13 : 2.1	16.13 S	73.Ø8 W	86.2	2.9	Ø.238	171	56.Ø	16
763	81 6 26	5 : 8 : 25.6	15.53 S	72.33 W	115.1	3.3	Ø.19Ø	212	44.Ø	17
764	81 6 26	5 : 4 : 16.1	15.11 S	71.35 W	185.8	4.5	Ø.121	3Ø6	79.2	1Ø
772	81 6 26	1Ø : 13 : 3.4	16.47 S	71.76 W	31.5	2.7	Ø.376	177	12.4	19
773	81 6 26	11 : 13 : 19.9	16.7Ø S	72.56 W	57.5	2.6	Ø.Ø25	248	22.4	1Ø
774	81 6 26	12 : 46 : 56.7	16.29 S	72.22 W	38.Ø	1.9	Ø.174	14Ø	15.Ø	12
775	81 6 26	14 : 34 : 22.7	16.63 S	72.65 W	56.Ø	2.5	Ø.Ø98	244	9.6	11
778	81 6 26	16 : 35 : 37.7	16.74 S	71.56 W	16.9	3.Ø	Ø.297	23Ø	32.7	16
779	81 6 26	17 : 23 : 13.1	16.51 S	71.61 W	11.2		Ø.23Ø	119	13.2	21
782	81 6 26	19 : 23 : 8.6	16.19 S	7Ø.68 W	184.9	4.4	Ø.133	3Ø8	75.3	14
784	81 6 26	21 : 19 : 48.5	16.Ø4 S	72.92 W	8Ø.2	3.2	Ø.392	136	37.9	17
786	81 6 26	21 : 5Ø : 7.3	15.24 S	72.53 W	1Ø6.8	3.7	Ø.2Ø3	224	37.1	19
787	81 6 26	21 : 44 : 47.9	16.33 S	71.94 W	14.6	1.9	Ø.Ø2Ø	129	15.8	8
788	81 6 26	22 : 39 : 4Ø.9	16.Ø5 S	71.68 W	126.9	4.1	Ø.333	93	32.8	27
792	81 6 26	23 : 4Ø : 49.4	16.67 S	72.56 W	59.7	2.3	Ø.Ø31	237	19.9	12
793	81 6 27	Ø : 5 : 62.4	17.41 S	72.33 W	54.Ø	2.9	Ø.35Ø	278	54.1	16
795	81 6 27	Ø : 55 : 2.1	16.71 S	72.57 W	63.6	3.4	Ø.Ø79	2Ø7	22.Ø	2Ø
796	81 6 27	2 : 12 : 57.2	16.42 S	72.33 W	77.9	2.9	Ø.3Ø5	115	17.4	24
799	81 6 27	3 : 45 : 1Ø.1	16.43 S	72.33 W	79.3	3.5	Ø.368	117	17.9	3Ø
8ØØ	81 6 27	3 : 26 : 12.3	16.34 S	72.Ø1 W	26.Ø	1.6	Ø.136	114	8.8	1Ø
8Ø2	81 6 27	7 : 46 : 43.6	16.37 S	72.18 W	14.7	1.4	Ø.2Ø9	189	12.8	8
8Ø3	81 6 27	6 : 53 : 59.1	16.Ø7 S	73.1Ø W	78.3	3.5	Ø.337	165	5Ø.4	22
8Ø8	81 6 27	1Ø : 19 : 31.Ø	16.63 S	71.75 W	92.7	3.Ø	Ø.298	173	24.3	18
814	81 6 27	11 : 24 : 12.6	16.63 S	72.22 W	69.6	2.7	Ø.Ø77	213	34.3	1Ø
817	81 6 27	14 : 6 : 26.8	15.45 S	72.14 W	123.1	3.8	Ø.298	151	51.3	23
818	81 6 27	13 : 23 : 1Ø.3	14.91 S	71.93 W	122.1	4.7	Ø.255	258	28.4	26
82Ø	81 6 27	12 : 3Ø : 42.5	16.69 S	72.53 W	54.3	2.6	Ø.117	235	24.3	12
824	81 6 27	22 : 3 : 28.2	16.54 S	71.66 W	98.2	2.8	Ø.Ø54	213	23.6	1Ø
827	81 6 28	1 : 13 : 21.6	16.88 S	71.53 W	42.3	2.6	Ø.256	214	21.7	18
828	81 6 28	2 : 31 : 32.1	16.36 S	72.39 W	88.8	2.6	Ø.19Ø	147	8.7	12
83Ø	81 6 28	2 : 32 : 1.6	16.81 S	72.71 W	5Ø.2	2.9	Ø.23Ø	25Ø	27.3	21
832	81 6 28	2 : 43 : 1Ø.1	15.15 S	73.44 W	1Ø2.9	4.2	Ø.Ø61	266	7Ø.4	13
835	81 6 28	2 : 49 : 13.7	16.2Ø S	72.Ø6 W	14.4	2.1	Ø.213	96	4.1	16
836	81 6 28	3 : 8 : 18.9	16.56 S	71.73 W	24.4	2.4	Ø.Ø73	138	22.6	2Ø
838	81 6 28	3 : 41 : 33.1	16.18 S	72.Ø4 W	17.4	1.5	Ø.126	154	1.1	8
839	81 6 28	3 : 43 : 56.6	16.66 S	72.69 W	55.1	2.7	Ø.Ø85	275	11.Ø	14
84Ø	81 6 28	3 : 52 : 48.8	16.Ø6 S	73.44 W	4Ø.8	3.Ø	Ø.1Ø1	227	3Ø.2	18
841	81 6 28	4 : 1Ø : 3.9	16.21 S	72.Ø4 W	16.7	1.4	Ø.1ØØ	121	3.9	8
842	81 6 28	4 : 2Ø : 5.3	15.95 S	72.Ø1 W	117.Ø	3.7	Ø.298	65	24.8	3Ø
843	81 6 28	4 : 18 : 38.4	16.62 S	72.63 W	53.4	2.5	Ø.1Ø3	227	1Ø.6	16

number	date	time	latitude	longitude	depth (km)	magnitude	RMS	GAP (deg)	DMIN (km)	number phases
849	81 6 28	6 : 2Ø : 35.7	16.73 S	72.53 W	6Ø.2	2.3	Ø.ØØ25	266	26.4	12
853	81 6 28	9 : 3Ø : 18.3	15.3Ø S	72.11 W	119.9	3.7	Ø.448	169	38.7	22
859	81 6 28	1Ø : 51 : 3.Ø	16.56 S	72.48 W	46.Ø	2.2	Ø.ØØ3Ø	13Ø	23.9	8
86Ø	81 6 28	11 : 41 : 34.Ø	15.11 S	72.91 W	1Ø5.8	3.8	Ø.2Ø6	232	46.8	26
864	81 6 28	14 : 47 : 59.Ø	16.57 S	71.72 W	23.6		Ø.172	186	23.7	18
866	81 6 28	17 : 56 : 49.2	15.43 S	71.8Ø W	129.4	3.9	Ø.296	111	32.3	2Ø
868	81 6 28	16 : 43 : 2Ø.Ø	16.96 S	72.98 W	3Ø.2	3.5	Ø.172	244	52.3	28
874	81 6 28	21 : 2 : 36.1	16.55 S	72.5Ø W	4Ø.9	2.4	Ø.147	192	22.7	12
875	81 6 28	21 : 29 : 21.1	16.17 S	72.65 W	78.9	2.8	Ø.132	155	26.8	13
878	81 6 28	23 : 4Ø : 3.5	16.22 S	72.Ø1 W	15.Ø	1.3	Ø.ØØ79	154	5.5	8
882	81 6 29	1 : 51 : 5.7	16.15 S	72.58 W	8Ø.4	2.7	Ø.ØØ61	159	24.Ø	14
884	81 6 29	1 : 57 : 5Ø.8	16.68 S	72.71 W	52.5	3.4	Ø.193	2Ø3	12.7	3Ø
887	81 6 29	2 : 47 : 56.4	16.Ø9 S	72.33 W	1Ø9.8	2.7	Ø.Ø33	155	31.5	1Ø
89Ø	81 6 29	3 : 31 : 36.2	17.22 S	72.51 W	26.6	3.Ø	Ø.215	251	54.4	27
894	81 6 29	6 : 27 : 5.5	15.89 S	73.28 W	91.3	2.7	Ø.Ø53	158	24.Ø	8
897	81 6 29	7 : 16 : 34.1	16.39 S	71.98 W	3Ø.9	2.2	Ø.Ø87	1ØØ	12.2	14
9Ø2	81 6 29	9 : 24 : 25.7	16.34 S	72.Ø2 W	31.6	1.9	Ø.157	119	17.6	8
9Ø5	81 6 29	1Ø : 48 : 3Ø.Ø	15.95 S	71.69 W	139.9	3.9	Ø.258	71	21.8	23
9Ø7	81 6 29	1Ø : 57 : 59.4	16.67 S	71.6Ø W	3Ø.7	2.3	Ø.138	219	38.5	12
91Ø	81 6 29	12 : 47 : Ø.9	15.58 S	73.26 W	98.4	3.8	Ø.167	2Ø6	32.2	22
911	81 6 29	12 : 38 : 59.3	16.59 S	72.4Ø W	46.7	2.6	Ø.293	153	28.6	17
913	81 6 29	13 : 22 : 52.5	16.63 S	72.34 W	43.5	2.2	Ø.177	21Ø	35.1	1Ø
921	81 6 29	18 : 8 : 18.7	16.39 S	71.61 W	25.4	2.5	Ø.128	247	17.7	8
929	81 6 3Ø	2 : 58 : 17.6	15.85 S	72.93 W	1ØØ.6	3.8	Ø.338	113	24.1	27
93Ø	81 6 3Ø	2 : 43 : Ø.1	16.21 S	72.67 W	9Ø.2	2.8	Ø.467	112	25.4	16
931	81 6 3Ø	1 : 58 : 15.4	16.83 S	71.37 W	77.5	3.1	Ø.147	277	38.Ø	14
933	81 6 3Ø	3 : 25 : 13.Ø	16.51 S	71.65 W	27.9	2.5	Ø.116	15Ø	21.8	2Ø
934	81 6 3Ø	4 : 1 : 45.5	16.Ø3 S	73.18 W	84.6	4.2	Ø.3Ø2	17Ø	41.Ø	27
939	81 6 3Ø	7 : 2 : 49.8	16.25 S	72.Ø3 W	97.6	3.Ø	Ø.244	119	7.9	16
941	81 6 3Ø	6 : 27 : Ø.6	16.19 S	72.42 W	1Ø1.4	3.6	Ø.278	75	17.8	25
942	81 6 3Ø	5 : 46 : 37.9	16.63 S	71.45 W	26.8		Ø.Ø89	278	45.8	1Ø
944	81 6 3Ø	8 : 18 : 21.4	15.54 S	72.65 W	112.9	3.1	Ø.186	243	24.8	13
947	81 6 3Ø	1Ø : 12 : 34.4	16.Ø6 S	72.53 W	11Ø.5	3.5	Ø.399	87	32.2	21
948	81 6 3Ø	9 : 39 : 6.7	16.3Ø S	72.36 W	1Ø2.9	3.5	Ø.451	94	12.3	23
966	81 6 3Ø	22 : 3 : 29.2	15.28 S	71.89 W	129.Ø	3.6	Ø.32Ø	17Ø	18.9	15
968	81 6 3Ø	23 : 31 : 53.2	16.Ø6 S	73.16 W	84.3	3.4	Ø.241	173	45.1	2Ø
977	81 7 1	5 : 41 : 4.7	16.38 S	72.Ø4 W	27.6	2.Ø	Ø.Ø41	139	16.8	8
983	81 7 1	1Ø : 1 : 15.Ø	14.86 S	72.46 W	112.1	4.2	Ø.233	245	76.8	2Ø
992	81 7 1	2Ø : 55 : 16.6	16.46 S	71.7Ø W	3Ø.3	2.1	Ø.Ø69	294	13.8	8
994	81 7 1	23 : 53 : 21.2	16.Ø8 S	72.11 W	1Ø2.Ø	3.Ø	Ø.15Ø	179	13.1	13
997	81 7 2	1 : 11 : 12.1	16.15 S	72.28 W	97.4	2.9	Ø.Ø59	168	26.1	12
998	81 7 2	Ø : 57 : 59.3	15.88 S	72.1Ø W	121.1	3.1	Ø.Ø99	183	34.Ø	12
1ØØ1	81 7 2	2 : 2Ø : 9.3	16.44 S	71.77 W	16.1	1.6	Ø.1Ø4	258	1Ø.Ø	8
1ØØ4	81 7 2	3 : 19 : 4Ø.5	16.48 S	71.88 W	4Ø.5	2.4	Ø.113	219	5.7	11
1ØØ6	81 7 2	7 : 3 : 44.Ø	15.47 S	71.71 W	143.1	4.1	Ø.384	114	38.2	19
1ØØ7	81 7 2	6 : 19 : 12.9	16.38 S	72.58 W	76.5	3.1	Ø.218	89	12.1	22

number	date			time			latitude		longitude		depth (km)	magnitude	RMS	GAP (deg)	DMIN (km)	number phases
1ØØ9	81	7	2	4	49	48.5	16.45	S	72.Ø1	W	93.9	3.Ø	Ø.213	76	1Ø.Ø	18
1Ø11	81	7	2	1Ø	4Ø	43.8	16.34	S	72.48	W	92.3	2.9	Ø.291	94	1.2	17
1Ø12	81	7	2	1Ø	24	45.8	15.26	S	72.56	W	1Ø9.Ø	4.1	Ø.44Ø	2ØØ	33.1	22
1Ø13	81	7	2	9	21	21.1	17.Ø4	S	71.69	W	89.8	3.9	Ø.329	246	3.7	24
1Ø16	81	7	2	1Ø	49	2Ø.4	16.14	S	72.7Ø	W	42.4	2.4	Ø.Ø64	174	33.4	14
1Ø26	81	7	2	17	19	29.6	16.49	S	71.58	W	12.4		Ø.291	123	9.7	2Ø
1Ø27	81	7	2	19	54	35.2	16.25	S	71.87	W	99.Ø	3.Ø	Ø.221	196	15.6	15
1Ø3Ø	81	7	2	2Ø	11	43.4	16.44	S	71.76	W	26.3	2.1	Ø.Ø59	263	1Ø.1	8
1Ø31	81	7	2	22	24	57.1	16.12	S	72.81	W	44.2	2.6	Ø.2Ø3	196	41.2	16
1Ø32	81	7	3	Ø	5	44.Ø	16.14	S	71.67	W	133.2	4.3	Ø.374	77	26.2	28
1Ø33	81	7	2	22	36	58.Ø	16.Ø2	S	73.56	W	74.8	3.3	Ø.231	255	27.3	17
1Ø39	81	7	3	6	44	55.3	16.67	S	72.57	W	61.9	2.5	Ø.146	232	18.5	16
1Ø41	81	7	3	9	6	21.1	16.Ø4	S	71.74	W	121.7	3.7	Ø.147	266	34.5	12
1Ø42	81	7	3	8	28	51.Ø	15.86	S	72.Ø3	W	117.5	4.1	Ø.348	8Ø	35.3	27
1Ø46	81	7	3	1Ø	16	39.2	15.84	S	72.21	W	123.Ø	3.6	Ø.392	87	29.3	23
1Ø47	81	7	3	9	57	3Ø.6	16.29	S	72.11	W	29.5	1.9	Ø.157	154	3.Ø	1Ø
1Ø49	81	7	3	11	48	36.7	15.63	S	7Ø.95	W	188.6	4.5	Ø.1Ø9	265	43.8	16
1Ø51	81	7	3	14	26	9.7	16.42	S	71.71	W	27.Ø	2.Ø	Ø.Ø36	294	9.6	8
1Ø53	81	7	3	17	18	3Ø.1	16.64	S	72.71	W	55.Ø	3.Ø	Ø.Ø81	246	8.Ø	16
1Ø59	81	7	3	19	17	27.6	16.73	S	73.14	W	38.6	3.3	Ø.4Ø1	236	49.Ø	26
1Ø6Ø	81	7	3	19	57	2.2	16.39	S	72.Ø8	W	27.1	2.8	Ø.188	77	1Ø.Ø	2Ø
1Ø64	81	7	3	22	6	17.2	16.6Ø	S	72.28	W	82.2	3.7	Ø.249	122	35.2	26
1Ø65	81	7	3	21	5Ø	16.1	16.17	S	71.83	W	13.8		Ø.238	93	21.7	23
1Ø67	81	7	3	23	49	2.6	16.25	S	72.51	W	91.3	3.2	Ø.376	85	11.6	16
1Ø71	81	7	4	1	58	56.3	16.81	S	72.77	W	48.8	2.8	Ø.134	3Ø8	27.4	13
1Ø72	81	7	4	2	24	4.9	15.77	S	73.16	W	9Ø.Ø	3.5	Ø.355	149	33.9	16
1Ø73	81	7	4	2	17	37.8	16.39	S	71.75	W	22.9	1.9	Ø.Ø86	291	22.5	8
1Ø74	81	7	4	3	14	38.1	16.33	S	71.93	W	32.2	2.1	Ø.Ø92	211	16.Ø	8
1Ø78	81	7	4	4	8	Ø.4	16.53	S	71.29	W	47.7		Ø.Ø48	283	52.4	8
1Ø89	81	7	4	8	43	33.5	15.77	S	72.54	W	116.3	3.1	Ø.Ø96	226	16.Ø	9
1Ø9Ø	81	7	4	8	4Ø	42.8	16.Ø8	S	71.61	W	133.Ø	3.5	Ø.147	157	25.8	15
1Ø91	81	7	4	8	24	23.7	15.46	S	73.28	W	1ØØ.1	4.1	Ø.113	227	41.2	24
1Ø93	81	7	4	7	2Ø	34.5	16.68	S	72.59	W	59.8	2.9	Ø.Ø34	263	18.3	12
1Ø96	81	7	4	11	51	38.3	16.99	S	7Ø.6Ø	W	145.1	4.3	Ø.214	295	114.5	16
1Ø97	81	7	4	1Ø	36	43.7	16.71	S	72.59	W	56.1	2.7	Ø.1Ø8	267	2Ø.8	16
1Ø99	81	7	4	14	54	12.7	16.41	S	72.35	W	8Ø.5	3.7	Ø.286	113	14.7	25
11Ø3	81	7	4	16	39	42.6	16.36	S	7Ø.13	W	226.6	4.9	Ø.Ø79	299	137.1	12
11Ø4	81	7	4	16	11	27.3	15.31	S	71.97	W	134.Ø	4.Ø	Ø.Ø72	263	59.8	14
11Ø5	81	7	4	15	5	23.5	16.75	S	72.51	W	54.8	2.7	Ø.Ø16	271	3Ø.3	12
11Ø8	81	7	4	18	47	2Ø.9	16.66	S	72.81	W	74.4	3.Ø	Ø.Ø71	251	14.9	16
111Ø	81	7	4	19	4Ø	17.6	16.52	S	71.66	W	15.6	2.8	Ø.1Ø2	111	19.3	18
1119	81	7	4	21	35	33.2	15.38	S	73.19	W	1Ø5.5		Ø.168	251	49.1	11
1125	81	7	5	1	41	5Ø.5	16.93	S	71.Ø1	W	111.7		Ø.297	284	7Ø.9	2Ø
1127	81	7	5	Ø	54	42.2	16.11	S	72.65	W	37.6	2.7	Ø.113	16Ø	3Ø.5	15
1128	81	7	5	2	33	25.7	16.78	S	71.84	W	83.8	3.Ø	Ø.163	188	33.9	16
1129	81	7	5	2	7	38.3	17.1Ø	S	72.89	W	33.5	4.4	Ø.235	251	62.5	19

number	date			time			latitude		longitude		depth (km)	magnitude	RMS	GAP (deg)	DMIN (km)	number phases
1135	81	7	5	4	34	46.3	16.11	S	73.09	W	74.1	3.2	0.281	171	54.7	21
1137	81	7	5	6	18	30.3	16.22	S	72.15	W	114.3	2.9	0.106	120	11.9	12
1138	81	7	5	5	49	42.7	15.80	S	73.20	W	88.0	4.7	0.312	142	29.3	27
1139	81	7	5	5	35	22.5	16.02	S	71.90	W	109.4	3.0	0.274	163	22.7	13
1145	81	7	5	8	31	13.1	16.03	S	72.36	W	99.0		0.226	104	18.5	10
1148	81	7	5	7	59	43.6	16.73	S	72.55	W	64.5	2.6	0.264	253	25.5	16
1151	81	7	5	10	35	24.0	16.26	S	72.05	W	17.0	1.2	0.097	111	6.1	8
1154	81	7	5	11	13	43.7	16.67	S	72.41	W	58.3	2.4	0.132	228	34.2	9
1158	81	7	5	14	50	37.2	16.26	S	72.06	W	9.4	1.6	0.006	115	5.0	8
1161	81	7	5	17	18	39.6	16.17	S	72.19	W	100.5	3.1	0.252	140	16.4	16
1162	81	7	5	16	43	37.7	16.71	S	72.56	W	54.5	3.5	0.392	193	22.8	27
1165	81	7	5	20	47	29.7	16.38	S	71.89	W	31.1	1.9	0.053	196	12.5	8
1170	81	7	5	22	27	34.9	16.76	S	71.54	W	21.6	3.1	0.301	194	31.6	18
1171	81	7	6	4	7	12.3	15.35	S	73.12	W	112.9	3.5	0.019	269	61.3	12
1173	81	7	6	0	21	55.4	16.11	S	72.55	W	86.4	2.6	0.021	135	27.0	10
1178	81	7	6	6	41	41.3	16.90	S	71.69	W	48.8	2.6	0.357	152	12.3	19
1179	81	7	6	7	37	45.8	15.46	S	72.88	W	96.7	3.8	0.174	212	14.4	18
1181	81	7	6	8	16	31.9	15.45	S	71.44	W	165.2	5.3	0.370	226	13.4	28
1184	81	7	6	10	55	58.9	15.69	S	72.16	W	118.9	3.8	0.350	150	40.9	23
1186	81	7	6	12	23	5.6	16.42	S	73.70	W	56.6		0.213	280	74.8	15
1188	81	7	6	12	47	60.1	15.64	S	72.74	W	97.8	3.9	0.286	96	12.9	23
1189	81	7	6	12	32	40.6	16.87	S	71.84	W	73.3	3.0	0.301	105	23.7	20
1192	81	7	6	14	36	25.5	16.74	S	72.55	W	58.1	3.6	0.139	199	26.6	18
1197	81	7	6	17	18	41.9	16.50	S	71.60	W	13.0		0.372	119	11.9	30
1210	81	7	7	3	55	22.3	16.29	S	73.53	W	67.5		0.039	257	56.7	8
1211	81	7	7	5	45	49.8	16.02	S	73.57	W	63.6		0.137	259	27.6	10
1218	81	7	7	16	19	55.4	15.97	S	71.45	W	136.0	3.6	0.012	186	13.5	8
1231	81	7	8	18	15	47.8	16.74	S	71.42	W	93.4	4.0	0.065	236	32.2	8

HYPIT OUTPUT - 1st INVERSION RUN

origin of cartesian coordinates				depth	strike
-16	Ø.	-72	Ø.	Ø.	62.5Ø

short distance conversions
one min lat 1.8443 km
one min lon 1.7839 km

ztr	wfac	wsum	swtfac	vthet	iwgt	iasn
Ø.	1.ØØØØ	1.ØØØØ	8.ØØ	5Ø.ØØØ	Ø	Ø

nl	neqs	ires	nkr	nmin	kfirst
9	396	1	Ø	3Ø	Ø

layer	depth	pvel	svel	p/s
1	-5.ØØ	5.3Ø	3.ØØ	1.77
2	5.ØØ	6.1Ø	3.5Ø	1.74
3	2Ø.ØØ	6.8Ø	3.9Ø	1.74
4	4Ø.ØØ	7.2Ø	4.1Ø	1.76
5	7Ø.ØØ	7.7Ø	4.4Ø	1.75
6	1ØØ.ØØ	7.9Ø	4.3Ø	1.84
7	13Ø.ØØ	7.9Ø	4.6Ø	1.72
8	16Ø.ØØ	7.9Ø	4.6Ø	1.72
9	19Ø.ØØ	7.9Ø	4.6Ø	1.72

	stn	wt	latitude	longitude	elev	pdelay	sdelay	flr	psed	ssed	dx	dy	dz
1	are	1.Ø	-16 27.73	-71 29.48	2452	Ø.	Ø.	Ø.	5.3Ø	3.ØØ	-2Ø.28	71.79	-2.45
2	aye	1.Ø	-17 Ø.8Ø	-71 4Ø.31	24Ø	Ø.	Ø.	Ø.	5.3Ø	3.ØØ	-83.33	82.77	-Ø.24
3	cab	1.Ø	-15 39.62	-71 56.66	3770	Ø.	Ø.	Ø.	5.3Ø	3.ØØ	36.1Ø	-12.Ø6	-3.77
4	cal	1.Ø	-16 3.74	-71 22.21	3950	Ø.	Ø.	Ø.	5.3Ø	3.ØØ	25.ØØ	62.96	-3.95
5	cay	1.Ø	-16 21.25	-71 46.45	17ØØ	Ø.	Ø.	Ø.	5.3Ø	3.ØØ	-23.62	39.5Ø	-1.7Ø
6	cho	1.Ø	-15 8.ØØ	-71 47.71	45ØØ	Ø.	Ø.	Ø.	5.3Ø	3.ØØ	95.23	-24.75	-4.5Ø
7	crv	1.Ø	-15 47.Ø7	-73 28.38	178Ø	Ø.	Ø.	Ø.	5.3Ø	3.ØØ	-51.72	-151.ØØ	-1.78
8	llu	1.Ø	-16 1Ø.65	-72 2.11	18ØØ	Ø.	Ø.	Ø.	5.3Ø	3.ØØ	-19.16	5.73	-1.8Ø
9	mol	1.Ø	-17 Ø.52	-72 2.88	5Ø	Ø.	Ø.	Ø.	5.3Ø	3.ØØ	-1Ø1.36	47.Ø1	-Ø.Ø5
1Ø	org	1.Ø	-15 53.94	-72 28.39	88Ø	Ø.	Ø.	Ø.	5.3Ø	3.ØØ	-13.48	-5Ø.11	-Ø.88
11	pat	1.Ø	-15 45.47	-71 39.44	49ØØ	Ø.	Ø.	Ø.	5.3Ø	3.ØØ	4Ø.73	2Ø.2Ø	-4.9Ø
12	rat	1.Ø	-15 45.33	-72 43.62	4ØØØ	Ø.	Ø.	Ø.	5.3Ø	3.ØØ	-11.97	-81.6Ø	-4.ØØ
13	siq	1.Ø	-15 29.89	-72 45.Ø6	455Ø	Ø.	Ø.	Ø.	5.3Ø	3.ØØ	12.Ø5	-97.12	-4.55
14	sis	1.Ø	-16 18.13	-72 4.85	1475	Ø.	Ø.	Ø.	5.3Ø	3.ØØ	-33.65	7.78	-1.48
15	sgp	1.Ø	-16 33.87	-72 42.75	14Ø	Ø.	Ø.	Ø.	5.3Ø	3.ØØ	-9Ø.52	-38.61	-Ø.14
16	tor	1.Ø	-16 2Ø.46	-72 28.25	35Ø	Ø.	Ø.	Ø.	5.3Ø	3.ØØ	-56.7Ø	-27.2Ø	-Ø.35
17	yan	1.Ø	-15 32.Ø9	-71 21.Ø3	4Ø5Ø	Ø.	Ø.	Ø.	5.3Ø	3.ØØ	77.83	38.Ø4	-4.Ø5
18	pin	1.Ø	-15 38.ØØ	-71 49.69	37ØØ	Ø.	Ø.	Ø.	5.3Ø	3.ØØ	44.5Ø	-2.39	-3.7Ø
19	can	1.Ø	-16 29.62	-71 55.79	12ØØ	Ø.	Ø.	Ø.	5.3Ø	3.ØØ	-45.ØØ	31.87	-1.2Ø
2Ø	con	1.Ø	-15 36.4Ø	-71 57.72	336Ø	Ø.	Ø.	Ø.	5.3Ø	3.ØØ	4Ø.49	-16.48	-3.36

layer	NS ints	EW ints	P scale	S scale
1	9	13	1.ØØ	1.ØØ
2	8	11	1.ØØ	1.ØØ
3	8	11	1.ØØ	1.ØØ
4	8	1Ø	1.ØØ	1.ØØ
5	8	1Ø	1.ØØ	1.ØØ
6	4	5	1.ØØ	1.ØØ
7	4	5	1.ØØ	1.ØØ

```
   8          4          5        1.00       1.00
   9          4          5        1.00       1.00

1      NS vectors
  -165.00  -75.00  -40.00  -10.00     0.      10.00   35.00   55.00  165.00
       EW vectors
  -220.00 -110.00  -75.00  -55.00  -35.00  -27.50  -10.00     0.      10.00   25.00   55.00  110.00  220.00

2      NS vectors
  -165.00  -82.50  -55.00  -27.50     0.      27.50   55.00  165.00
       EW vectors
  -220.00 -110.00  -88.00  -66.00  -44.00  -22.00     0.      22.00   44.00   82.50  220.00

3      NS vectors
  -165.00  -82.50  -55.00  -27.50     0.      27.50   55.00  165.00
       EW vectors
  -220.00 -110.00  -88.00  -66.00  -44.00  -22.00     0.      22.00   44.00   82.50  220.00

4      NS vectors
  -165.00  -82.50  -55.00  -27.50     0.      27.50   55.00  165.00
       EW vectors
  -220.00 -110.00  -88.00  -66.00  -44.00  -22.00     0.      27.50   82.50  220.00

5      NS vectors
  -165.00  -82.50  -55.00  -27.50     0.      27.50   55.00  165.00
       EW vectors
  -220.00 -110.00  -88.00  -66.00  -44.00  -22.00     0.      27.50   82.50  220.00

6      NS vectors
  -165.00  -55.00   55.00  165.00
       EW vectors
  -220.00 -110.00     0.    110.00  220.00

7      NS vectors
  -165.00  -55.00   55.00  165.00
       EW vectors
  -220.00 -110.00     0.    110.00  220.00

8      NS vectors
  -165.00  -55.00   55.00  165.00
       EW vectors
  -220.00 -110.00     0.    110.00  220.00

9      NS vectors
  -165.00  -55.00   55.00  165.00
       EW vectors
  -220.00 -110.00     0.    110.00  220.00

 neqs = 396   nvar =   820   kvar =   336610

scale factors
 layer    p scale    s scale
   1        1.000      1.000
   2        1.000      1.000
            1.000      1.000
```

4	1.000	1.000
5	1.000	1.000
6	1.000	1.000
7	1.000	1.000
8	1.000	1.000
9	1.000	1.000

number of p arrivals	3365
p weight	1.0000
number of s arrivals	2845
s weight	0.5000
total number of arrivals	6210

p observation matrix

layer 1

0	217	0	0	0	0	0	0
0	0	298	32	89	131	0	0
0	0	65	0	0	0	0	0
300	0	158	2	0	0	0	0
40	128	0	0	0	0	0	23
0	330	0	0	0	10	22	94
0	0	31	0	0	2	6	0
0	8	707	0	0	0	1	0
0	1	111	0	0	66	147	0
106	137	309	0	0	10	2	115
150	3	45	0	1	97	0	0
0	0	0	0	0	0	0	0

layer 2

0	71	198	5	5	0	0
0	0	13	97	129	1	0
0	0	70	345	49	0	0
62	44	69	220	3	0	2
313	341	171	98	2	8	77
29	89	270	169	12	39	27
17	36	581	448	53	122	30
78	21	363	289	49	74	115
117	113	121	100	96	27	9
4	17	0	0	0	0	0

layer 3

11	99	174	43	7	0	0
27	67	87	73	32	8	0
59	99	123	176	56	6	1
88	177	235	162	34	6	19
193	290	324	158	36	29	65
150	308	440	241	62	55	45
119	200	460	268	104	88	51
111	136	327	205	92	69	44

s observation matrix

0	197	0	0	0	0	0	0
0	0	263	21	60	66	0	0
0	0	62	0	0	0	0	0
287	0	143	2	0	0	0	0
38	123	0	0	0	0	0	12
0	313	0	0	0	6	10	50
0	0	31	0	0	1	4	0
0	6	645	0	0	0	1	0
0	0	99	0	0	54	91	0
100	126	268	0	0	8	2	68
124	3	35	0	1	57	0	0
0	0	0	0	0	0	0	0

0	70	178	5	3	0	0
0	0	13	83	66	0	0
0	0	66	292	16	0	0
59	43	64	200	2	0	0
295	329	156	93	1	2	46
27	84	245	156	9	19	11
16	32	525	401	39	71	16
73	18	334	246	35	55	68
101	95	113	85	57	18	6
4	16	0	0	0	0	0

11	98	155	37	4	0	0
26	67	89	66	13	0	0
56	93	108	131	22	0	0
81	162	211	129	20	4	10
170	273	295	138	24	13	38
136	286	395	213	41	21	21
107	189	431	218	64	40	27
101	110	296	155	53	41	22

71	173	196	87	55	27	8
3	22	23	4	2	1	0

61	139	175	74	34	21	5
3	21	20	2	0	0	0

layer 4

71	146	134	60	25	2	0
33	146	160	61	27	13	5
41	196	184	90	51	28	16
63	180	245	166	88	39	29
233	253	298	195	117	56	53
260	293	331	209	117	71	60
75	167	210	203	114	71	48
61	167	163	99	54	37	25
14	42	27	12	5	4	0

67	136	117	48	15	1	0
31	135	146	51	20	2	0
38	180	169	72	25	11	6
57	159	222	125	48	17	14
204	224	270	164	76	21	29
237	267	300	177	71	32	31
66	154	192	167	57	35	26
53	150	145	75	29	21	8
14	38	25	8	2	1	0

layer 5

19	97	79	78	61	21	2
0	90	105	98	75	41	38
0	62	118	127	78	75	76
2	52	137	184	110	86	75
8	105	219	190	126	87	70
0	99	236	174	118	78	43
0	53	109	162	94	52	36
14	62	91	77	61	37	26
25	23	48	12	7	4	3

17	85	69	62	42	14	1
0	84	94	70	48	25	19
0	61	106	92	45	52	36
2	46	123	143	74	52	42
8	100	193	154	78	55	46
0	92	208	135	77	46	25
0	48	94	132	59	25	22
12	57	81	65	41	22	10
23	19	43	11	3	1	1

layer 6

0	98	0
0	595	225
0	297	65
0	30	1

0	72	0
0	458	143
0	217	35
0	21	0

layer 7

0	0	0
0	21	36
0	138	93
0	36	7

0	0	0
0	11	20
0	105	51
0	25	2

layer 8

0	0	0
0	0	1
0	19	69
0	34	16

0	0	0
0	0	0
0	17	41
0	26	8

layer 9

```
 Ø   Ø   Ø
 Ø   Ø   Ø
 Ø   1  22
 Ø  18  45
```

```
 Ø   Ø   Ø
 Ø   Ø   Ø
 Ø   1  12
 Ø  14  27
```

a total number of 587 blocks were hit
172578 elements of g are used

a total number of 402 blocks are kept for inversion
81003 elements of g are used

g diagonals for p velocity model

layer 1

```
 Ø.    3.3Ø  Ø.    Ø.    Ø.    Ø.    Ø.    Ø.
 Ø.    Ø.    8.7Ø  Ø.21  1.67  1.87  Ø.    Ø.
 Ø.    Ø.    Ø.35  Ø.    Ø.    Ø.    Ø.    Ø.
2.57   Ø.    2.22  Ø.    Ø.    Ø.    Ø.    Ø.
Ø.Ø3   Ø.93  Ø.    Ø.    Ø.    Ø.    Ø.    Ø.
 Ø.    2.59  Ø.    Ø.    Ø.    Ø.    Ø.    2.91
 Ø.    Ø.    Ø.Ø3  Ø.    Ø.    Ø.    Ø.    Ø.
 Ø.    Ø.   1Ø.51  Ø.    Ø.    Ø.    Ø.    Ø.
 Ø.    Ø.    Ø.6Ø  Ø.    Ø.    Ø.63  4.39  Ø.
1.Ø1   2.14  6.Ø1   Ø.    Ø.    Ø.    Ø.    4.53
1.4Ø   Ø.    1.15  Ø.    Ø.    3.64  Ø.    Ø.
 Ø.    Ø.    Ø.    Ø.    Ø.    Ø.    Ø.    Ø.
```

g diagonals for s velocity model

```
 Ø.    4.73  Ø.    Ø.    Ø.    Ø.    Ø.    Ø.
 Ø.    Ø.   1Ø.56  Ø.    1.62  Ø.72  Ø.    Ø.
 Ø.    Ø.    Ø.51  Ø.    Ø.    Ø.    Ø.    Ø.
3.34   Ø.    2.85  Ø.    Ø.    Ø.    Ø.    Ø.
Ø.Ø4   1.19  Ø.    Ø.    Ø.    Ø.    Ø.    Ø.
 Ø.    3.35  Ø.    Ø.    Ø.    Ø.    Ø.    2.33
 Ø.    Ø.    Ø.Ø5  Ø.    Ø.    Ø.    Ø.    Ø.
 Ø.    Ø.   11.98  Ø.    Ø.    Ø.    Ø.    Ø.
 Ø.    Ø.    Ø.69  Ø.    Ø.    Ø.79  3.43  Ø.
1.43   2.67  7.93  Ø.    Ø.    Ø.    Ø.    4.Ø3
1.8Ø   Ø.    1.35  Ø.    Ø.    3.38  Ø.    Ø.
 Ø.    Ø.    Ø.    Ø.    Ø.    Ø.    Ø.    Ø.
```

layer 2

```
 Ø.    4.33 1Ø.61  Ø.    Ø.    Ø.    Ø.
 Ø.    Ø.    Ø.    2.94  3.18  Ø.    Ø.
 Ø.    Ø.    1.77 12.55  Ø.99  Ø.    Ø.
2.36   Ø.33  1.Ø6 11.14  Ø.    Ø.    Ø.
8.58  11.29  7.77  1.88  Ø.    Ø.    5.91
 Ø.    3.56 12.49  7.14  Ø.    1.Ø9  Ø.
 Ø.    Ø.46 18.13 1Ø.58  3.98  4.98  Ø.26
4.79   Ø.   15.68 1Ø.19  3.18  2.17  6.46
4.41   6.99  4.67  4.39  6.Ø1  Ø.    Ø.
 Ø.    Ø.    Ø.    Ø.    Ø.    Ø.    Ø.
```

```
 Ø.    6.87 14.49  Ø.    Ø.    Ø.    Ø.
 Ø.    Ø.    Ø.    3.28  2.Ø3  Ø.    Ø.
 Ø.    Ø.    2.Ø7 13.82  Ø.    Ø.    Ø.
2.76   Ø.48  1.2Ø 14.8Ø  Ø.    Ø.    Ø.
11.13 14.22  9.29  3.11  Ø.    Ø.    5.Ø1
 Ø.    4.63 17.15  9.95  Ø.    Ø.    Ø.
 Ø.    Ø.6Ø 22.Ø2 13.22  4.73  2.85  Ø.
7.37   Ø.   21.ØØ 12.11  3.76  2.16  5.13
5.13   9.45  6.Ø7  5.73  5.58  Ø.    Ø.
 Ø.    Ø.    Ø.    Ø.    Ø.    Ø.    Ø.
```

layer 3

```
 Ø.    4.2Ø 11.57  1.86  Ø.    Ø.    Ø.
 Ø.    3.22  3.33  3.29  Ø.92  Ø.    Ø.
2.65   2.65  4.94  6.51  3.7Ø  Ø.    Ø.
4.19   9.56 11.55  6.16  Ø.97  Ø.    Ø.
7.16  13.Ø5 16.9Ø  5.4Ø  2.Ø5  Ø.    3.12
5.ØØ  12.34 17.55 1Ø.83  3.22  2.67  2.18
5.74  1Ø.Ø5 14.52 14.89  5.96  4.ØØ  3.18
3.87   5.12  9.37  9.64  4.Ø7  4.2Ø  1.64
3.Ø9   9.49  5.8Ø  3.53  1.78  Ø.    Ø.
 Ø.    Ø.    Ø.    Ø.    Ø.    Ø.    Ø.
```

```
 Ø.    6.46 15.25  2.45  Ø.    Ø.    Ø.
 Ø.    5.18  4.2Ø  3.88  Ø.    Ø.    Ø.
3.42   3.34  5.54  6.44  Ø.    Ø.    Ø.
5.1Ø  11.69 15.ØØ  5.99  Ø.    Ø.    Ø.
7.Ø5  16.ØØ 21.43  7.22  Ø.    Ø.    2.54
6.Ø1  14.33 22.64 13.Ø7  3.21  Ø.    Ø.
6.61  12.85 2Ø.69 16.63  6.Ø2  2.61  Ø.
5.Ø4   6.44 11.74 1Ø.54  2.87  2.93  Ø.
3.55  13.12  7.1Ø  4.27  1.74  Ø.    Ø.
 Ø.    Ø.    Ø.    Ø.    Ø.    Ø.    Ø.
```

layer 4

1.81	4.17	5.34	4.60	Ø.	Ø.	Ø.
Ø.87	3.92	8.81	2.53	Ø.	Ø.	Ø.
1.33	6.42	8.46	4.62	2.74	Ø.	Ø.
2.33	5.72	10.92	9.94	5.63	1.96	Ø.
4.02	10.44	16.28	11.56	8.52	3.73	2.91
3.46	9.93	17.08	12.23	8.80	3.77	4.52
1.65	8.26	12.46	15.04	9.32	4.25	2.74
2.19	7.91	9.74	7.20	4.28	2.92	Ø.
Ø.	1.27	Ø.	Ø.	Ø.	Ø.	Ø.

1.46	4.58	6.39	5.04	Ø.	Ø.	Ø.
1.12	4.80	11.20	2.79	Ø.	Ø.	Ø.
1.34	8.42	11.12	4.95	Ø.	Ø.	Ø.
3.45	7.05	14.63	10.20	3.33	Ø.	Ø.
5.13	12.00	19.86	12.00	7.77	Ø.	Ø.
4.21	12.71	20.68	13.84	6.87	1.81	3.69
2.09	11.57	16.74	16.47	6.54	2.82	Ø.
2.74	8.95	10.90	7.77	Ø.	Ø.	Ø.
Ø.	1.48	Ø.	Ø.	Ø.	Ø.	Ø.

layer 5

Ø.	1.05	2.07	2.10	1.80	Ø.	Ø.
Ø.	Ø.57	1.51	2.59	1.92	1.34	Ø.70
Ø.	Ø.53	2.28	4.25	3.32	2.28	1.41
Ø.	Ø.63	3.11	5.94	3.89	3.89	2.38
Ø.	Ø.88	5.07	5.92	5.23	3.90	2.57
Ø.	Ø.66	4.97	6.36	4.58	3.94	1.75
Ø.	Ø.38	2.82	6.69	4.21	2.95	1.97
Ø.	Ø.96	2.68	4.53	4.25	2.14	Ø.
Ø.	Ø.	1.42	Ø.	Ø.	Ø.	Ø.

Ø.	1.65	2.82	2.12	1.11	Ø.	Ø.
Ø.	Ø.84	1.81	2.89	1.73	Ø.	Ø.
Ø.	Ø.80	2.88	4.24	2.62	1.72	1.19
Ø.	1.02	4.19	6.12	2.99	3.42	2.06
Ø.	1.63	5.95	6.68	4.30	3.12	2.43
Ø.	1.28	5.98	6.43	3.48	3.84	Ø.
Ø.	Ø.61	3.67	6.42	3.50	Ø.	Ø.
Ø.	1.28	3.55	5.68	3.29	Ø.	Ø.
Ø.	Ø.	1.56	Ø.	Ø.	Ø.	Ø.

layer 6

Ø.	Ø.27	Ø.
Ø.	4.27	1.70
Ø.	5.80	2.54
Ø.	Ø.85	Ø.

Ø.	Ø.27	Ø.
Ø.	6.28	2.43
Ø.	6.85	2.47
Ø.	Ø.	Ø.

layer 7

Ø.	Ø.	Ø.
Ø.	Ø.	Ø.22
Ø.	2.51	1.47
Ø.	1.05	Ø.

Ø.	Ø.	Ø.
Ø.	Ø.	Ø.
Ø.	2.81	Ø.95
Ø.	Ø.	Ø.

layer 8

Ø.	Ø.	Ø.
Ø.	Ø.	Ø.
Ø.	Ø.	Ø.67
Ø.	Ø.78	Ø.

Ø.	Ø.	Ø.
Ø.	Ø.	Ø.
Ø.	Ø.	Ø.59
Ø.	Ø.	Ø.

layer 9

Ø.	Ø.	Ø.
Ø.	Ø.	Ø.
Ø.	Ø.	Ø.
Ø.	Ø.	Ø.71

Ø.	Ø.	Ø.
Ø.	Ø.	Ø.
Ø.	Ø.	Ø.
Ø.	Ø.	Ø.

nvar, irnk, ier, are 402 402 Ø

residual norm 1010.05798
standard variance Ø.17391

original variance	Ø.17391
residual variance	Ø.Ø7247
mod residual norm	994.Ø3403
mod standard variance	Ø.Ø3475
mod original variance	Ø.Ø3547
mod residual variance	Ø.Ø9599
percentage improvement	58.33ØØ1
mod percentage improvement	59.23454

velocities for p velocity model

layer 1

Ø.	5.56	Ø.	Ø.	Ø.	Ø.	Ø.	Ø.
Ø.	Ø.	5.56	5.1Ø	5.17	5.11	Ø.	Ø.
Ø	Ø.	5.5Ø	Ø.	Ø.	Ø.	Ø.	Ø.
5.45	Ø.	4.59	Ø.	Ø.	Ø.	Ø.	Ø.
5.32	5.36	Ø.	Ø.	Ø.	Ø.	Ø.	Ø.
Ø.	5.48	Ø.	Ø.	Ø.	Ø.	Ø.	5.11
Ø.	Ø.	5.23	Ø.	Ø.	Ø.	Ø.	Ø.
Ø.	Ø.	5.29	Ø.	Ø.	Ø.	Ø.	Ø.
Ø.	Ø.	5.49	Ø.	Ø.	5.Ø8	4.92	Ø.
5.51	4.26	5.96	Ø.	Ø.	Ø.	Ø.	4.98
5.39	Ø.	5.97	Ø.	Ø.	4.93	Ø.	Ø.
Ø.	Ø.	Ø.	Ø.	Ø.	Ø.	Ø.	Ø.

velocities for s velocity model

Ø.	3.29	Ø.	Ø.	Ø.	Ø.	Ø.	Ø.
Ø.	Ø.	3.23	Ø.	2.93	2.89	Ø.	Ø.
Ø.	Ø.	3.Ø2	Ø.	Ø.	Ø.	Ø.	Ø.
3.41	Ø.	2.91	Ø.	Ø.	Ø.	Ø.	Ø.
3.Ø7	3.Ø9	Ø.	Ø.	Ø.	Ø.	Ø.	Ø.
Ø.	3.43	Ø.	Ø.	Ø.	Ø.	Ø.	3.Ø7
Ø.	Ø.	3.Ø2	Ø.	Ø.	Ø.	Ø.	Ø.
Ø.	Ø.	3.Ø7	Ø.	Ø.	Ø.	Ø.	Ø.
Ø.	Ø.	3.15	Ø.	Ø.	3.Ø4	3.Ø7	Ø.
3.33	2.93	3.35	Ø.	Ø.	Ø.	Ø.	2.95
3.17	Ø.	3.34	Ø.	Ø.	2.93	Ø.	Ø.
Ø.	Ø.	Ø.	Ø.	Ø.	Ø.	Ø.	Ø.

layer 2

Ø.	5.96	6.Ø8	Ø.	Ø.	Ø.	Ø.
Ø.	Ø.	Ø.	6.Ø5	5.66	Ø.	Ø.
Ø.	Ø.	5.9Ø	5.92	5.96	Ø.	Ø.
6.14	6.37	6.12	6.Ø1	Ø.	Ø.	Ø.
5.84	6.13	6.28	5.82	Ø.	Ø.	5.88
Ø.	5.8Ø	6.Ø4	6.53	Ø.	6.19	Ø.
Ø	6.29	5.89	6.49	5.75	6.Ø1	6.Ø5

Ø.	3.43	3.79	Ø.	Ø.	Ø.	Ø.
Ø.	Ø.	Ø.	3.51	3.32	Ø.	Ø.
Ø.	Ø.	3.47	3.54	Ø.	Ø.	Ø.
3.82	3.71	3.53	3.57	Ø.	Ø.	Ø.
3.61	3.76	3.73	3.59	Ø.	Ø.	3.29
Ø.	3.38	3.63	3.77	Ø.	Ø.	Ø.
Ø.	3.46	3.52	3.73	3.54	3.33	Ø.

6.33	Ø.	6.11	6.21	5.85	5.83	5.94
6.16	6.23	6.11	5.92	5.76	Ø.	Ø.
Ø.	Ø.	Ø.	Ø.	Ø.	Ø.	Ø.

3.85	Ø.	3.54	3.55	3.46	3.37	3.43
3.73	3.6Ø	3.52	3.6Ø	3.56	Ø.	Ø.
Ø.	Ø.	Ø.	Ø.	Ø.	Ø.	Ø.

layer 3

Ø.	7.25	7.52	6.45	Ø.	Ø.	Ø.
Ø.	7.88	7.12	6.48	6.67	Ø.	Ø.
7.37	7.48	6.83	6.28	6.38	Ø.	Ø.
7.34	7.12	7.Ø7	6.48	6.29	Ø.	Ø.
7.22	7.36	7.23	6.77	6.12	Ø.	6.8Ø
7.26	7.29	7.Ø9	6.48	6.Ø9	6.48	6.41
7.46	7.Ø4	6.61	6.53	6.12	6.52	6.43
7.2Ø	7.Ø1	6.72	6.43	6.37	6.4Ø	6.72
7.61	6.63	7.Ø6	6.26	6.48	Ø.	Ø.
Ø.	Ø.	Ø.	Ø.	Ø.	Ø.	Ø.

Ø.	4.42	4.37	3.98	Ø.	Ø.	Ø.
Ø.	4.46	4.Ø6	3.88	Ø.	Ø.	Ø.
4.ØØ	4.13	3.94	3.62	Ø.	Ø.	Ø.
4.Ø3	4.Ø2	4.Ø3	3.7Ø	Ø.	Ø.	Ø.
3.93	4.21	4.1Ø	3.82	Ø.	Ø.	3.62
3.99	4.2Ø	4.Ø5	3.84	3.66	Ø.	Ø.
4.13	4.Ø5	3.9Ø	3.8Ø	3.61	3.7Ø	Ø.
4.1Ø	4.18	3.87	3.9Ø	3.97	3.67	Ø.
4.Ø6	3.87	3.97	3.68	3.81	Ø.	Ø.
Ø.	Ø.	Ø.	Ø.	Ø.	Ø.	Ø.

layer 4

7.79	7.7Ø	7.47	6.88	Ø.	Ø.	Ø.
7.79	7.67	7.69	7.Ø2	Ø.	Ø.	Ø.
7.77	7.86	7.48	6.74	6.58	Ø.	Ø.
8.Ø6	7.82	7.63	7.ØØ	6.7Ø	6.65	Ø.
8.38	7.86	7.88	6.85	6.74	6.73	6.85
7.81	7.71	7.67	6.97	6.59	6.91	6.76
7.73	7.86	7.57	6.75	6.75	6.9Ø	6.92
7.6Ø	7.44	7.44	6.97	6.9Ø	6.84	Ø.
Ø.	7.85	Ø.	Ø.	Ø.	Ø.	Ø.

4.62	4.54	4.54	4.Ø5	Ø.	Ø.	Ø.
4.34	4.51	4.47	4.Ø2	Ø.	Ø.	Ø.
4.45	4.53	4.52	4.18	Ø.	Ø.	Ø.
4.4Ø	4.44	4.38	4.13	4.Ø1	Ø.	Ø.
4.5Ø	4.61	4.53	4.Ø2	3.89	Ø.	Ø.
4.37	4.47	4.5Ø	4.Ø9	3.93	3.82	4.Ø1
4.29	4.47	4.33	4.Ø1	3.87	4.Ø8	Ø.
4.27	4.36	4.29	3.98	Ø.	Ø.	Ø.
Ø.	4.63	Ø.	Ø.	Ø.	Ø.	Ø.

layer 5

Ø.	7.94	7.8Ø	7.5Ø	7.56	Ø.	Ø.
Ø.	8.Ø5	7.62	7.85	7.5Ø	7.46	7.68
Ø.	7.94	7.8Ø	8.16	8.Ø2	7.98	7.82
Ø.	7.29	7.4Ø	7.81	7.86	7.62	7.72
Ø.	7.78	7.61	7.97	7.75	7.78	7.85
Ø.	8.Ø6	7.82	8.Ø4	8.Ø1	7.92	7.73
Ø.	7.83	7.97	8.25	7.81	7.89	7.48
Ø.	7.9Ø	8.13	7.99	7.61	7.63	Ø.
Ø.	Ø.	7.29	Ø.	Ø.	Ø.	Ø.

Ø.	4.44	4.48	4.41	4.45	Ø.	Ø.
Ø.	4.41	4.36	4.43	4.51	Ø.	Ø.
Ø.	4.72	4.52	4.71	4.49	4.65	4.52
Ø.	4.69	4.37	4.54	4.57	4.33	4.51
Ø.	4.78	4.52	4.62	4.56	4.44	4.26
Ø.	4.54	4.49	4.66	4.33	4.45	Ø.
Ø.	4.64	4.71	4.81	4.31	Ø.	Ø.
Ø.	4.71	4.79	4.64	4.14	Ø.	Ø.
Ø.	Ø.	4.29	Ø.	Ø.	Ø.	Ø.

layer 6

Ø.	7.52	Ø.
Ø.	8.32	8.36
Ø.	8.Ø7	8.13
Ø.	7.91	Ø.

Ø.	4.47	Ø.
Ø.	4.63	4.54
Ø.	4.51	4.5Ø
Ø.	Ø.	Ø.

layer 7

Ø.	Ø.	Ø.
Ø.	Ø.	8.11
Ø.	8.13	7.86
Ø.	7.89	Ø.

Ø.	Ø.	Ø.
Ø.	Ø.	Ø.
Ø.	4.5Ø	4.53
Ø.	Ø.	Ø.

layer 8

Ø.	Ø.	Ø.
Ø	Ø.	Ø.
Ø.	Ø.	8.21
Ø	7.2Ø	Ø.

Ø.	Ø.	Ø.
Ø.	Ø.	Ø.
Ø.	Ø.	4.56
Ø.	Ø.	Ø.

layer 9

Ø.	Ø.	Ø.						Ø.	Ø.	Ø.					
Ø.	Ø.	Ø.						Ø.	Ø.	Ø.					
Ø.	Ø.	Ø.						Ø.	Ø.	Ø.					
Ø	Ø.	7.9Ø						Ø.	Ø.	Ø.					

%fraction change for p velocity model

%fraction change for s velocity model

layer 1

Ø	-7.9Ø	Ø.	Ø.	Ø.	Ø.	Ø.	Ø.	Ø.	5.96	Ø.	Ø.	Ø.	Ø.	Ø.	Ø.
Ø	Ø.	7.ØØ	-1.84	-Ø.65	-1.79	Ø.	Ø.	Ø.	Ø.	8.25	Ø.	-1.82	-3.41	Ø.	Ø.
Ø	Ø.	5.81	Ø.	Ø.	Ø.	Ø.	Ø.	Ø.	Ø.	1.Ø6	Ø.	Ø.	Ø.	Ø.	Ø.
1.Ø1	Ø.	-11.67	Ø.	Ø.	Ø.	Ø.	Ø.	9.93	Ø.	-2.51	Ø.	Ø.	Ø.	Ø.	Ø.
-1.37	-Ø.76	Ø.	Ø.	Ø.	Ø.	Ø.	Ø.	-1.17	-Ø.34	Ø.	Ø.	Ø.	Ø.	Ø.	Ø.
Ø.	1.56	Ø.	Ø.	Ø.	Ø.	Ø.	-1.74	Ø.	1Ø.46	Ø.	Ø.	Ø.	Ø.	Ø.	2.6Ø
Ø.	Ø.	Ø.52	Ø.	Ø.	Ø.	Ø.	Ø.	Ø.	Ø.	1.11	Ø.	Ø.	Ø.	Ø.	Ø.
Ø.	Ø.	1.73	Ø.	Ø.	Ø.	Ø.	Ø.	Ø.	Ø.	2.7Ø	Ø.	Ø.	Ø.	Ø.	Ø.
Ø.	Ø.	5.59	Ø.	Ø.	-2.38	-5.34	Ø.	Ø.	Ø.	5.43	Ø.	Ø.	1.79	2.64	Ø.
2.Ø5	-2.2Ø	14.16	Ø.	Ø.	Ø.	Ø.	-4.29	7.39	-5.48	12.25	Ø.	Ø.	Ø.	Ø.	-1.15
-Ø.24	Ø.	14.Ø1	Ø.	Ø.	-5.28	Ø.	Ø.	2.28	Ø.	11.9Ø	Ø.	Ø.	-1.95	Ø.	Ø.
Ø.	Ø.	Ø.	Ø.	Ø.	Ø.	Ø.	Ø.	Ø.	Ø.	Ø.	Ø.	Ø.	Ø.	Ø.	Ø.

layer 2

Ø.	-3.9Ø	14.7Ø	Ø.	Ø.	Ø.	Ø.	Ø.	-3.54	9.83	Ø.	Ø.	Ø.	Ø.	
Ø.	Ø.	Ø.	Ø.8Ø	-5.62	Ø.	Ø.	Ø.	Ø.	Ø.	Ø.	1.88	-3.81	Ø.	Ø.
Ø.	Ø.	-1.62	-1.27	-Ø.72	Ø.	Ø.	Ø.	Ø.	Ø.	Ø.63	2.58	Ø.	Ø.	Ø.
-Ø.98	2.8Ø	2.Ø1	Ø.19	Ø.	Ø.	Ø.	7.23	4.2Ø	2.31	3.38	Ø.	Ø.	Ø.	
-2.32	-1.1Ø	4.73	-2.94	Ø.	Ø.	-1.95	1.37	5.63	8.19	4.12	Ø.	Ø.	-4.64	

Ø.	-6.51	Ø.72	8.85	Ø.	3.2Ø	Ø.
Ø.	1.35	-1.64	8.2Ø	-4.21	Ø.Ø9	Ø.89
1.Ø4	Ø.	1.88	3.43	-2.44	-2.8Ø	-1.Ø2
-2.66	Ø.47	1.84	-1.4Ø	-4.Ø4	Ø.	Ø.
Ø.	Ø.	Ø.	Ø.	Ø.	Ø.	Ø.

Ø.	-5.Ø9	5.Ø9	9.17	Ø.	Ø.	Ø.
Ø.	-2.77	1.95	8.17	2.61	-3.57	Ø.
8.16	Ø.	2.52	2.88	Ø.37	-2.35	-Ø.52
4.72	1.22	1.94	4.42	3.12	Ø.	Ø.
Ø.	Ø.	Ø.	Ø.	Ø.	Ø.	Ø.

layer 3

Ø.	2.14	1Ø.61	-2.25	Ø.	Ø.	Ø.
Ø.	11.Ø1	4.64	-1.81	Ø.99	Ø.	Ø.
-1.69	5.39	Ø.19	-4.82	-3.34	Ø.	Ø.
-2.Ø8	4.2Ø	4.Ø1	-1.89	-4.63	Ø.	Ø.
-2.69	5.69	6.35	2.55	-7.26	Ø.	4.64
-3.25	2.69	4.28	-1.7Ø	-7.71	-Ø.36	-1.41
-Ø.54	-Ø.84	-2.87	-1.Ø4	-7.35	Ø.31	-1.12
-4.Ø4	-1.23	-1.11	-2.5Ø	-3.53	-1.55	3.41
1.41	-5.67	3.82	-5.Ø9	-1.79	Ø.	Ø.
Ø.	Ø.	Ø.	Ø.	Ø.	Ø.	Ø.

Ø.	8.38	11.83	4.97	Ø.	Ø.	Ø.
Ø.	9.31	3.89	2.22	Ø.	Ø.	Ø.
-7.1Ø	1.23	Ø.81	-4.44	Ø.	Ø.	Ø.
-6.42	-1.36	3.Ø4	-2.47	Ø.	Ø.	Ø.
-8.84	3.Ø6	4.95	Ø.73	Ø.	Ø.	-3.21
-7.34	2.97	3.56	1.19	-3.4Ø	Ø.	Ø.
-4.1Ø	-Ø.83	-Ø.22	Ø.15	-4.73	-Ø.83	Ø.
-4.95	2.32	-Ø.94	2.7Ø	4.75	-1.87	Ø.
-5.78	-5.2Ø	1.51	-2.95	Ø.45	Ø.	Ø.
Ø.	Ø.	Ø.	Ø.	Ø.	Ø.	Ø.

layer 4

1.17	2.7Ø	2.34	-1.7Ø	Ø.	Ø.	Ø.
1.14	2.32	5.31	Ø.31	Ø.	Ø.	Ø.
Ø.92	4.75	2.45	-3.72	-6.Ø3	Ø.	Ø.
4.69	4.31	4.59	Ø.Ø3	-4.29	-2.16	Ø.
8.84	4.79	7.92	-2.16	-3.69	-Ø.98	Ø.76
1.47	2.8Ø	5.Ø4	-Ø.41	-5.85	1.6Ø	-Ø.52
Ø.36	4.83	3.67	-3.63	-3.62	1.48	1.71
-1.28	-Ø.79	1.93	-Ø.43	-1.46	Ø.52	Ø.
Ø.	1.6Ø	Ø.	Ø.	Ø.	Ø.	Ø.

4.44	5.25	8.3Ø	Ø.56	Ø.	Ø.	Ø.
-1.94	4.59	6.61	-Ø.1Ø	Ø.	Ø.	Ø.
Ø.54	5.15	7.63	3.79	Ø.	Ø.	Ø.
-Ø.51	2.93	4.32	2.65	-Ø.33	Ø.	Ø.
1.8Ø	6.84	7.89	-Ø.Ø8	-3.31	Ø.	Ø.
-1.25	3.77	7.35	1.56	-2.27	-2.32	2.55
-3.Ø5	3.64	3.26	-Ø.25	-3.69	4.35	Ø.
-3.42	1.11	2.3Ø	-1.17	Ø.	Ø.	Ø.
Ø.	7.52	Ø.	Ø.	Ø.	Ø.	Ø.

layer 5

Ø	1.86	1.36	-2.53	-1.87	Ø.	Ø.	Ø.	-1.Ø3	1.25	-Ø.24	Ø.52	Ø.	Ø.
Ø.	2.23	-Ø.97	1.89	-2.57	-3.15	-Ø.27	Ø.	-1.54	-1.57	Ø.2Ø	1.92	Ø.	Ø.
Ø.	1.81	1.23	5.97	4.16	3.67	1.53	Ø.	5.29	2.12	6.41	1.5Ø	5.17	2.19
Ø.	-6.56	-3.87	1.37	2.Ø4	-1.Ø3	Ø.22	Ø.	4.67	-1.14	2.67	3.23	-2.19	2.ØØ
Ø.	-Ø.32	-1.21	3.56	Ø.59	1.Ø6	1.99	Ø.	6.56	2.21	4.29	2.99	Ø.24	-3.63
Ø.	3.3Ø	1.56	4.48	4.Ø4	2.86	Ø.42	Ø.	1.22	1.36	5.23	-2.16	Ø.54	Ø.
Ø.	Ø.42	3.49	7.Ø9	1.43	2.52	-2.9Ø	Ø.	3.56	6.34	8.8Ø	-2.5Ø	Ø.	Ø.
Ø.	.99	5.6Ø	3.76	-1.21	-Ø.85	Ø.	Ø.	5.1Ø	8.13	4.92	-6.53	Ø.	Ø.
Ø.	Ø.	-5.33	Ø.	Ø.	Ø.	Ø.	Ø.	Ø.	-3.Ø5	Ø.	Ø.	Ø.	Ø.

layer 6

Ø.	-4.87	Ø.	Ø.	4.19	Ø.
Ø	5.3Ø	5.87	Ø.	7.81	5.77
Ø.	2.18	2.95	Ø.	4.99	4.75
Ø.	Ø.11	Ø.	Ø.	Ø.	Ø.

layer 7

Ø.	Ø.	Ø.	Ø.	Ø.	Ø.
Ø.	Ø.	2.72	Ø.	Ø.	Ø.
Ø.	2.86	-Ø.46	Ø.	-2.Ø2	-1.26
Ø.	-Ø.Ø8	Ø.	Ø.	Ø.	Ø.

layer 8

Ø.	Ø.	Ø.	Ø.	Ø.	Ø.
Ø.	Ø.	Ø.	Ø.	Ø.	Ø.
Ø	Ø.	3.88	Ø.	Ø.	-Ø.61

Ø.	[illegible].85	Ø.						Ø.	Ø.	Ø.					

layer 9

Ø.	Ø.	Ø.						Ø.	Ø.	Ø.					
Ø.	Ø.	Ø.						Ø.	Ø.	Ø.					
Ø.	Ø.	Ø.						Ø.	Ø.	Ø.					
Ø.	[illegible].	-Ø.Ø2						Ø.	Ø.	Ø.					

free = 1 kmin = 1 kmax = 402

sum of diagonal elements of resolution matrix for 402 elements = 289.592

resolution for p velocity model

layer 1

Ø.	Ø.19	Ø.	Ø.	Ø.	Ø.	Ø.	Ø.	Ø.	Ø.2Ø	Ø.	Ø.	Ø.	Ø.	Ø.	Ø.
Ø.	Ø.	Ø.65	Ø.13	Ø.4Ø	Ø.38	Ø.	Ø.	Ø.	Ø.	Ø.67	Ø.	Ø.38	Ø.23	Ø.	Ø.
Ø.	.	Ø.14	Ø.	Ø.	Ø.	Ø.	Ø.	Ø.	Ø.	Ø.15	Ø.	Ø.	Ø.	Ø.	Ø.
Ø.34	Ø.	Ø.51	Ø.	Ø.	Ø.	Ø.	Ø.	Ø.37	Ø.	Ø.55	Ø.	Ø.	Ø.	Ø.	Ø.
Ø.Ø4	[illegible].38	Ø.	Ø.	Ø.	Ø.	Ø.	Ø.	Ø.Ø6	Ø.42	Ø.	Ø.	Ø.	Ø.	Ø.	Ø.
Ø.	Ø.55	Ø.	Ø.	Ø.	Ø.	Ø.	Ø.47	Ø.	Ø.58	Ø.	Ø.	Ø.	Ø.	Ø.	Ø.49
Ø.	Ø.	Ø.Ø5	Ø.	Ø.	Ø.	Ø.	Ø.	Ø.	Ø.	Ø.Ø6	Ø.	Ø.	Ø.	Ø.	Ø.
Ø.	[illegible].	Ø.72	Ø.	Ø.	Ø.	Ø.	Ø.	Ø.	Ø.	Ø.73	Ø.	Ø.	Ø.	Ø.	Ø.
Ø.	[illegible].	Ø.38	Ø.	Ø.	Ø.2Ø	Ø.51	Ø.	Ø.	Ø.	Ø.41	Ø.	Ø.	Ø.21	Ø.52	Ø.
Ø.3Ø	[illegible].65	Ø.73	Ø.	Ø.	Ø.	Ø.	Ø.51	Ø.34	Ø.7Ø	Ø.77	Ø.	Ø.	Ø.	Ø.	Ø.51
Ø.36	Ø.	Ø.49	Ø.	Ø.	Ø.59	Ø.	Ø.	Ø.4Ø	Ø.	Ø.52	Ø.	Ø.	Ø.62	Ø.	Ø.
Ø.	Ø.	Ø.	Ø.	Ø.	Ø.	Ø.	Ø.	Ø.	Ø.	Ø.	Ø.	Ø.	Ø.	Ø.	Ø.

layer 2

[illegible]	[illegible].57	Ø.65	Ø.	Ø.	Ø.	Ø.		Ø.	Ø.61	Ø.68	Ø.	Ø.	Ø.	Ø.	
[illegible]	[illegible]	Ø.	[illegible].62	Ø.57	[illegible].	Ø.		Ø.	Ø.	Ø.	Ø.64	Ø.53	Ø.	Ø.	

Ø.	Ø.	Ø.57	Ø.74	Ø.47	Ø.	Ø.
Ø.61	Ø.24	Ø.57	Ø.86	Ø.	Ø.	Ø.
Ø.75	Ø.87	Ø.83	Ø.67	Ø.	Ø.	Ø.7Ø
Ø.	Ø.79	Ø.91	Ø.86	Ø.	Ø.6Ø	Ø.
Ø.	Ø.43	Ø.92	Ø.88	Ø.74	Ø.63	Ø.21
Ø.74	Ø.	Ø.91	Ø.87	Ø.77	Ø.62	Ø.56
Ø.76	Ø.73	Ø.81	Ø.82	Ø.74	Ø.	Ø.
Ø.	Ø.	Ø.	Ø.	Ø.	Ø.	Ø.

Ø.	Ø.	Ø.6Ø	Ø.76	Ø.	Ø.	Ø.
Ø.64	Ø.3Ø	Ø.6Ø	Ø.89	Ø.	Ø.	Ø.
Ø.79	Ø.9Ø	Ø.86	Ø.76	Ø.	Ø.	Ø.69
Ø.	Ø.83	Ø.92	Ø.89	Ø.	Ø.	Ø.
Ø.	Ø.5Ø	Ø.94	Ø.92	Ø.75	Ø.59	Ø.
Ø.79	Ø.	Ø.93	Ø.9Ø	Ø.78	Ø.61	Ø.62
Ø.79	Ø.77	Ø.86	Ø.85	Ø.76	Ø.	Ø.
Ø.	Ø.	Ø.	Ø.	Ø.	Ø.	Ø.

layer 3

Ø.	Ø.63	Ø.73	Ø.63	Ø.	Ø.	Ø.
Ø.	Ø.67	Ø.78	Ø.71	Ø.49	Ø.	Ø.
Ø.72	Ø.73	Ø.34	Ø.82	Ø.73	Ø.	Ø.
Ø.83	Ø.89	Ø.91	Ø.85	Ø.57	Ø.	Ø.
Ø.88	Ø.92	Ø.94	Ø.86	Ø.7Ø	Ø.	Ø.56
Ø.87	Ø.93	Ø.95	Ø.91	Ø.82	Ø.75	Ø.61
Ø.88	Ø.93	Ø.94	Ø.93	Ø.87	Ø.8Ø	Ø.65
Ø.83	Ø.88	Ø.93	Ø.91	Ø.81	Ø.78	Ø.57
Ø.74	Ø.84	Ø.88	Ø.81	Ø.67	Ø.	Ø.
Ø.	Ø.	Ø.	Ø.	Ø.	Ø.	Ø.

Ø.	Ø.71	Ø.77	Ø.68	Ø.	Ø.	Ø.
Ø.	Ø.75	Ø.8Ø	Ø.73	Ø.	Ø.	Ø.
Ø.75	Ø.77	Ø.86	Ø.84	Ø.	Ø.	Ø.
Ø.85	Ø.91	Ø.93	Ø.86	Ø.	Ø.	Ø.
Ø.88	Ø.93	Ø.95	Ø.88	Ø.	Ø.	Ø.62
Ø.88	Ø.95	Ø.96	Ø.93	Ø.84	Ø.	Ø.
Ø.89	Ø.94	Ø.96	Ø.94	Ø.87	Ø.75	Ø.
Ø.85	Ø.9Ø	Ø.94	Ø.92	Ø.77	Ø.74	Ø.
Ø.76	Ø.87	Ø.9Ø	Ø.83	Ø.7Ø	Ø.	Ø.
Ø.	Ø.	Ø.	Ø.	Ø.	Ø.	Ø.

layer 4

Ø.65	Ø.79	Ø.77	Ø.79	Ø.	Ø.	Ø.
Ø.5Ø	Ø.8Ø	Ø.87	Ø.75	Ø.	Ø.	Ø.
Ø.64	Ø.84	Ø.89	Ø.85	Ø.76	Ø.	Ø.
Ø.69	Ø.88	Ø.93	Ø.91	Ø.87	Ø.74	Ø.
Ø.77	Ø.91	Ø.95	Ø.93	Ø.9Ø	Ø.82	Ø.75
Ø.74	Ø.92	Ø.95	Ø.93	Ø.9Ø	Ø.81	Ø.74

Ø.59	Ø.81	Ø.8Ø	Ø.81	Ø.	Ø.	Ø.
Ø.55	Ø.82	Ø.89	Ø.78	Ø.	Ø.	Ø.
Ø.64	Ø.86	Ø.91	Ø.86	Ø.	Ø.	Ø.
Ø.7Ø	Ø.9Ø	Ø.94	Ø.92	Ø.83	Ø.	Ø.
Ø.78	Ø.93	Ø.96	Ø.93	Ø.91	Ø.	Ø.
Ø.75	Ø.94	Ø.96	Ø.94	Ø.89	Ø.74	Ø.81

Ø.71	Ø.9Ø	Ø.94	Ø.93	Ø.9Ø	Ø.8Ø	Ø.7Ø	Ø.74	Ø.92	Ø.95	Ø.94	Ø.9Ø	Ø.77	Ø.
Ø.76	Ø.9Ø	Ø.9Ø	Ø.87	Ø.82	Ø.74	Ø.	Ø.8Ø	Ø.91	Ø.92	Ø.89	Ø.	Ø.	Ø.
Ø.	Ø.6Ø	Ø.	Ø.	Ø.	Ø.	Ø.	Ø.	Ø.63	Ø.	Ø.	Ø.	Ø.	Ø.

layer 5

Ø.	Ø.55	Ø.67	Ø.64	Ø.68	Ø.	Ø.	Ø.	Ø.65	Ø.73	Ø.69	Ø.59	Ø.	Ø.
Ø.	Ø.39	Ø.66	Ø.76	Ø.72	Ø.67	Ø.5Ø	Ø.	Ø.47	Ø.68	Ø.78	Ø.69	Ø.	Ø.
Ø.	Ø.44	Ø.73	Ø.83	Ø.81	Ø.76	Ø.63	Ø.	Ø.52	Ø.74	Ø.83	Ø.79	Ø.71	**Ø.59**
Ø.	Ø.44	Ø.79	Ø.87	Ø.84	Ø.82	Ø.73	Ø.	Ø.54	Ø.82	Ø.88	Ø.81	Ø.82	Ø.73
Ø.	Ø.51	Ø.85	Ø.88	Ø.86	Ø.82	Ø.72	Ø.	Ø.63	Ø.87	Ø.89	Ø.85	Ø.8Ø	Ø.75
Ø.	Ø.45	Ø.84	Ø.88	Ø.85	Ø.83	Ø.66	Ø.	Ø.58	Ø.86	Ø.89	Ø.83	Ø.84	Ø.
Ø.	Ø.37	Ø.78	Ø.86	Ø.83	Ø.77	Ø.66	Ø.	Ø.47	Ø.82	Ø.87	Ø.82	Ø.	Ø.
Ø.	Ø.56	Ø.76	Ø.81	Ø.79	Ø.68	Ø.	Ø.	Ø.63	Ø.81	Ø.83	Ø.81	Ø.	Ø.
Ø.	Ø.	Ø.66	Ø.	Ø.	Ø.	Ø.	Ø.	Ø.	Ø.66	Ø.	Ø.	Ø.	Ø.

layer 6

Ø.	Ø.27	Ø.	Ø.	Ø.26	Ø.
Ø.	Ø.72	Ø.59	Ø.	Ø.81	Ø.68
Ø.	Ø.72	Ø.62	Ø.	Ø.82	Ø.67
Ø.	Ø.49	Ø.	Ø.	Ø.	Ø.

layer 7

Ø.	Ø.	Ø.	Ø.	Ø.	Ø.
Ø.	Ø.	Ø.2Ø	Ø.	Ø.	Ø.
Ø.	Ø.59	Ø.54	Ø.	Ø.68	Ø.47
Ø.	Ø.47	Ø.	Ø.	Ø.	Ø.

layer 8

Ø.	Ø.	Ø.						Ø.	Ø.	Ø.					
Ø.	Ø.	Ø.						Ø.	Ø.	Ø.					
Ø.	Ø.	Ø.48						Ø.	Ø.	Ø.44					
Ø.	Ø.51	Ø.						Ø.	Ø.	Ø.					

layer 9

Ø.	Ø.	Ø.						Ø.	Ø.	Ø.					
Ø.	Ø.	Ø.						Ø.	Ø.	Ø.					
Ø.	Ø.	Ø.						Ø.	Ø.	Ø.					
Ø.	Ø.	Ø.54						Ø.	Ø.	Ø.					

standard error for p velocity model

standard error for s velocity model

layer 1

Ø.	Ø.Ø4	Ø.	Ø.	Ø.	Ø.	Ø.	Ø.	Ø.	Ø.Ø3	Ø.	Ø.	Ø.	Ø.	Ø.	Ø.
Ø.	Ø.	Ø.Ø8	Ø.Ø6	Ø.Ø8	Ø.Ø7	Ø.	Ø.	Ø.	Ø.	Ø.Ø5	Ø.	Ø.Ø4	Ø.Ø3	Ø.	Ø.
Ø.	Ø.	Ø.Ø7	Ø.	Ø.	Ø.	Ø.	Ø.	Ø.	Ø.	Ø.Ø4	Ø.	Ø.	Ø.	Ø.	Ø.
Ø.Ø8	Ø.	Ø.Ø7	Ø.	Ø.	Ø.	Ø.	Ø.	Ø.Ø5	Ø.	Ø.Ø5	Ø.	Ø.	Ø.	Ø.	Ø.
Ø.Ø4	Ø.1Ø	Ø.	Ø.	Ø.	Ø.	Ø.	Ø.	Ø.Ø3	Ø.Ø6	Ø.	Ø.	Ø.	Ø.	Ø.	Ø.
Ø.	Ø.Ø9	Ø.	Ø.	Ø.	Ø.	Ø.	Ø.Ø8	Ø.	Ø.Ø6	Ø.	Ø.	Ø.	Ø.	Ø.	Ø.Ø6
Ø.	Ø.	Ø.Ø5	Ø.	Ø.	Ø.	Ø.	Ø.	Ø.	Ø.	Ø.Ø3	Ø.	Ø.	Ø.	Ø.	Ø.
Ø.	Ø.	Ø.Ø8	Ø.	Ø.	Ø.	Ø.	Ø.	Ø.	Ø.	Ø.Ø5	Ø.	Ø.	Ø.	Ø.	Ø.
Ø.	Ø.	Ø.11	Ø.	Ø.	Ø.Ø7	Ø.Ø7	Ø.	Ø.	Ø.	Ø.Ø6	Ø.	Ø.	Ø.Ø4	Ø.Ø5	Ø.
Ø.Ø8	Ø.Ø6	Ø.11	Ø.	Ø.	Ø.	Ø.	Ø.Ø7	Ø.Ø6	Ø.Ø5	Ø.Ø6	Ø.	Ø.	Ø.	Ø.	Ø.Ø4
Ø.Ø9	Ø.	Ø.13	Ø.	Ø.	Ø.Ø8	Ø.	Ø.	Ø.Ø6	Ø.	Ø.Ø7	Ø.	Ø.	Ø.Ø5	Ø.	Ø.
Ø.	Ø.	Ø.	Ø.	Ø.	Ø.	Ø.	Ø.	Ø.	Ø.	Ø.	Ø.	Ø.	Ø.	Ø.	Ø.

layer 2

Ø.	Ø.Ø9	Ø.11	Ø.	Ø.	Ø.	Ø.
Ø.	Ø.	Ø.	Ø.1Ø	Ø.Ø8	Ø.	Ø.
Ø.	Ø.	Ø.11	Ø.Ø8	Ø.11	Ø.	Ø.
Ø.11	Ø.11	Ø.13	Ø.Ø7	Ø.	Ø.	Ø.
Ø.Ø7	Ø.Ø7	Ø.Ø9	Ø.1Ø	Ø.	Ø.	Ø.Ø9
Ø.	Ø.Ø9	Ø.Ø6	Ø.1Ø	Ø.	Ø.13	Ø.
Ø.	Ø.14	Ø.Ø6	Ø.Ø9	Ø.Ø9	Ø.Ø9	Ø.1Ø
Ø.1Ø	Ø.	Ø.Ø7	Ø.Ø8	Ø.Ø9	Ø.1Ø	Ø.Ø8
Ø.1Ø	Ø.1Ø	Ø.1Ø	Ø.Ø9	Ø.Ø9	Ø.	Ø.
Ø.	Ø.	Ø.	Ø.	Ø.	Ø.	Ø.

Ø.	Ø.Ø5	Ø.Ø5	Ø.	Ø.	Ø.	Ø.
Ø.	Ø.	Ø.	Ø.Ø6	Ø.Ø5	Ø.	Ø.
Ø.	Ø.	Ø.Ø6	Ø.Ø5	Ø.	Ø.	Ø.
Ø.Ø7	Ø.Ø7	Ø.Ø7	Ø.Ø4	Ø.	Ø.	Ø.
Ø.Ø5	Ø.Ø4	Ø.Ø5	Ø.Ø6	Ø.	Ø.	Ø.Ø5
Ø.	Ø.Ø5	Ø.Ø4	Ø.Ø5	Ø.	Ø.	Ø.
Ø.	Ø.Ø7	Ø.Ø3	Ø.Ø4	Ø.Ø6	Ø.Ø5	Ø.
Ø.Ø6	Ø.	Ø.Ø3	Ø.Ø4	Ø.Ø5	Ø.Ø6	Ø.Ø5
Ø.Ø6	Ø.Ø6	Ø.Ø5	Ø.Ø5	Ø.Ø6	Ø.	Ø.
Ø.	Ø.	Ø.	Ø.	Ø.	Ø.	Ø.

layer 3

Ø.	Ø.14	Ø.13	Ø.12	Ø.	Ø.	Ø.
Ø.	Ø.16	Ø.12	Ø.11	Ø.13	Ø.	Ø.
Ø.13	Ø.14	Ø.1Ø	Ø.Ø9	Ø.1Ø	Ø.	Ø.
Ø.11	Ø.Ø9	Ø.Ø8	Ø.Ø9	Ø.12	Ø.	Ø.
Ø.Ø9	Ø.Ø8	Ø.Ø8	Ø.1Ø	Ø.11	Ø.	Ø.13
Ø.1Ø	Ø.Ø8	Ø.Ø7	Ø.Ø7	Ø.Ø9	Ø.11	Ø.12
Ø.1Ø	Ø.Ø8	Ø.Ø6	Ø.Ø7	Ø.Ø8	Ø.1Ø	Ø.11
Ø.11	Ø.1Ø	Ø.Ø7	Ø.Ø7	Ø.1Ø	Ø.1Ø	Ø.13
Ø.14	Ø.Ø9	Ø.1Ø	Ø.1Ø	Ø.12	Ø.	Ø.
Ø.	Ø.	Ø.	Ø.	Ø.	Ø.	Ø.

Ø.	Ø.Ø8	Ø.Ø7	Ø.Ø7	Ø.	Ø.	Ø.
Ø.	Ø.Ø9	Ø.Ø6	Ø.Ø7	Ø.	Ø.	Ø.
Ø.Ø6	Ø.Ø7	Ø.Ø5	Ø.Ø5	Ø.	Ø.	Ø.
Ø.Ø5	Ø.Ø4	Ø.Ø4	Ø.Ø5	Ø.	Ø.	Ø.
Ø.Ø5	Ø.Ø4	Ø.Ø4	Ø.Ø5	Ø.	Ø.	Ø.Ø7
Ø.Ø5	Ø.Ø4	Ø.Ø3	Ø.Ø4	Ø.Ø6	Ø.	Ø.
Ø.Ø5	Ø.Ø4	Ø.Ø3	Ø.Ø4	Ø.Ø5	Ø.Ø7	Ø.
Ø.Ø6	Ø.Ø6	Ø.Ø4	Ø.Ø5	Ø.Ø7	Ø.Ø6	Ø.
Ø.Ø7	Ø.Ø5	Ø.Ø5	Ø.Ø6	Ø.Ø7	Ø.	Ø.
Ø.	Ø.	Ø.	Ø.	Ø.	Ø.	Ø.

layer 4

Ø.14	Ø.13	Ø.12	Ø.11	Ø.	Ø.	Ø.
Ø.16	Ø.13	Ø.11	Ø.12	Ø.	Ø.	Ø.
Ø.15	Ø.12	Ø.1Ø	Ø.1Ø	Ø.11	Ø.	Ø.
Ø.16	Ø.11	Ø.Ø9	Ø.Ø8	Ø.Ø9	Ø.12	Ø.

Ø.Ø9	Ø.Ø8	Ø.Ø8	Ø.Ø6	Ø.	Ø.	Ø.
Ø.Ø9	Ø.Ø7	Ø.Ø6	Ø.Ø7	Ø.	Ø.	Ø.
Ø.Ø9	Ø.Ø7	Ø.Ø6	Ø.Ø6	Ø.	Ø.	Ø.
Ø.Ø8	Ø.Ø6	Ø.Ø4	Ø.Ø5	Ø.Ø6	Ø.	Ø.

Ø.15	Ø.1Ø	Ø.Ø8	Ø.Ø7	Ø.Ø8	Ø.1Ø	Ø.12
Ø.14	Ø.Ø9	Ø.Ø7	Ø.Ø7	Ø.Ø7	Ø.11	Ø.1Ø
Ø.15	Ø.1Ø	Ø.Ø8	Ø.Ø7	Ø.Ø7	Ø.11	Ø.12
Ø.13	Ø.Ø9	Ø.Ø9	Ø.Ø9	Ø.11	Ø.12	Ø.
Ø.	Ø.16	Ø.	Ø.	Ø.	Ø.	Ø.

Ø.Ø8	Ø.Ø5	Ø.Ø4	Ø.Ø4	Ø.Ø5	Ø.	Ø.
Ø.Ø7	Ø.Ø5	Ø.Ø4	Ø.Ø4	Ø.Ø5	Ø.Ø7	Ø.Ø7
Ø.Ø8	Ø.Ø5	Ø.Ø4	Ø.Ø4	Ø.Ø5	Ø.Ø7	Ø.
Ø.Ø7	Ø.Ø5	Ø.Ø5	Ø.Ø5	Ø.	Ø.	Ø.
Ø.	Ø.Ø9	Ø.	Ø.	Ø.	Ø.	Ø.

layer 5

Ø.	Ø.16	Ø.14	Ø.13	Ø.14	Ø.	Ø.
Ø.	Ø.16	Ø.15	Ø.14	Ø.13	Ø.14	Ø.16
Ø.	Ø.16	Ø.14	Ø.13	Ø.13	Ø.15	Ø.15
Ø.	Ø.13	Ø.12	Ø.11	Ø.12	Ø.11	Ø.13
Ø.	Ø.16	Ø.11	Ø.11	Ø.11	Ø.12	Ø.14
Ø.	Ø.17	Ø.12	Ø.11	Ø.12	Ø.12	Ø.14
Ø.	Ø.16	Ø.14	Ø.12	Ø.12	Ø.14	Ø.14
Ø.	Ø.17	Ø.15	Ø.13	Ø.12	Ø.14	Ø.
Ø.	Ø.	Ø.14	Ø.	Ø.	Ø.	Ø.

Ø.	Ø.Ø8	Ø.Ø8	Ø.Ø8	Ø.Ø9	Ø.	Ø.
Ø.	Ø.Ø8	Ø.Ø8	Ø.Ø8	Ø.Ø9	Ø.	Ø.
Ø.	Ø.1Ø	Ø.Ø8	Ø.Ø8	Ø.Ø8	Ø.Ø9	Ø.Ø9
Ø.	Ø.1Ø	Ø.Ø7	Ø.Ø6	Ø.Ø8	Ø.Ø7	Ø.Ø8
Ø.	Ø.1Ø	Ø.Ø6	Ø.Ø6	Ø.Ø7	Ø.Ø7	Ø.Ø7
Ø.	Ø.Ø9	Ø.Ø6	Ø.Ø6	Ø.Ø7	Ø.Ø7	Ø.
Ø.	Ø.1Ø	Ø.Ø8	Ø.Ø7	Ø.Ø7	Ø.	Ø.
Ø.	Ø.1Ø	Ø.Ø8	Ø.Ø7	Ø.Ø6	Ø.	Ø.
Ø.	Ø.	Ø.Ø8	Ø.	Ø.	Ø.	Ø.

layer 6

Ø.	Ø.13	Ø.
Ø.	Ø.14	Ø.16
Ø.	Ø.13	Ø.15
Ø.	Ø.16	Ø.

Ø.	Ø.Ø8	Ø.
Ø.	Ø.Ø8	Ø.Ø9
Ø.	Ø.Ø7	Ø.Ø9
Ø.	Ø.	Ø.

layer 7

Ø.	Ø.	Ø.
Ø.	Ø.	Ø.14
Ø.	Ø.14	Ø.14
Ø.	Ø.14	Ø.

Ø.	Ø.	Ø.
Ø.	Ø.	Ø.
Ø.	Ø.Ø8	Ø.Ø9
Ø.	Ø.	Ø.

layer 8

Ø.	Ø.	Ø.	Ø.	Ø.	Ø.
Ø.	Ø.	Ø.	Ø.	Ø.	Ø.
Ø.	Ø.	Ø.17	Ø.	Ø.	Ø.Ø9
Ø.	Ø.18	Ø.	Ø.	Ø.	Ø.

layer 9

Ø.	Ø.	Ø.	Ø.	Ø.	Ø.
Ø.	Ø.	Ø.	Ø.	Ø.	Ø.
Ø.	Ø.	Ø.	Ø.	Ø.	Ø.
Ø.	Ø.	Ø.17	Ø.	Ø.	Ø.

HYPIT OUTPUT - 2nd INVERSION RUN

origin of cartesian coordinates				depth	strike
-16	Ø.	-72	Ø.	Ø.	62.5Ø

short distance conversions
one min lat 1.8443 km
one min lon 1.7839 km

ztr	wfac	wsum	swtfac	vthet	iwgt	iasn
Ø.	1.ØØØØ	1.ØØØØ	8.ØØ	5Ø.ØØØ	Ø	Ø

nl	neqs	ires	nkr	umin	kfirst
9	396	1	Ø	2Ø	Ø

layer	depth	pvel	svel	p/s
1	-5.ØØ	5.25	3.Ø5	1.72
2	5.ØØ	6.Ø5	3.45	1.75
3	2Ø.ØØ	6.75	3.9Ø	1.73
4	4Ø.ØØ	7.1Ø	4.Ø5	1.75
5	7Ø.ØØ	7.7Ø	4.45	1.73
6	1ØØ.ØØ	7.9Ø	4.3Ø	1.84
7	13Ø.ØØ	7.9Ø	4.6Ø	1.72
8	16Ø.ØØ	7.9Ø	4.6Ø	1.72
9	19Ø.ØØ	7.9Ø	4.6Ø	1.72

	stn	wt	latitude	longitude	elev	pdelay	sdelay	flr	psed	ssed	dx	dy	dz
1	are	1.Ø	-16 27.73	-71 29.48	2452	Ø.	Ø.	Ø.	5.25	3.Ø5	-2Ø.28	71.79	-2.45
2	aye	1.Ø	-17 Ø.8Ø	-71 4Ø.31	24Ø	Ø.	Ø.	Ø.	5.25	3.Ø5	-83.33	82.77	-Ø.24
3	cab	1.Ø	-15 39.62	-71 56.66	377Ø	Ø.	Ø.	Ø.	5.25	3.Ø5	36.1Ø	-12.Ø6	-3.77
4	cal	1.Ø	-16 3.74	-71 22.21	395Ø	Ø.	Ø.	Ø.	5.25	3.Ø5	25.ØØ	62.96	-3.95
5	cay	1.Ø	-16 21.25	-71 46.45	17ØØ	Ø.	Ø.	Ø.	5.25	3.Ø5	-23.62	39.5Ø	-1.7Ø
6	cho	1.Ø	-15 8.ØØ	-71 47.71	45ØØ	Ø.	Ø.	Ø.	5.25	3.Ø5	95.23	-24.75	-4.5Ø
7	crv	1.Ø	-15 47.Ø7	-73 28.38	178Ø	Ø.	Ø.	Ø.	5.25	3.Ø5	-51.72	-151.ØØ	-1.78
8	llu	1.Ø	-16 1Ø.65	-72 2.11	18ØØ	Ø.	Ø.	Ø.	5.25	3.Ø5	-19.16	5.73	-1.8Ø
9	mol	1.Ø	-17 Ø.52	-72 2.88	5Ø	Ø.	Ø.	Ø.	5.25	3.Ø5	-1Ø1.36	47.Ø1	-Ø.Ø5
10	ong	1.Ø	-15 53.94	-72 28.39	88Ø	Ø.	Ø.	Ø.	5.25	3.Ø5	-13.48	-5Ø.11	-Ø.88
11	pal	1.Ø	-15 45.47	-71 39.44	49ØØ	Ø.	Ø.	Ø.	5.25	3.Ø5	4Ø.73	2Ø.2Ø	-4.9Ø
12	ral	1.Ø	-15 45.33	-72 43.62	4ØØØ	Ø.	Ø.	Ø.	5.25	3.Ø5	-11.97	-81.6Ø	-4.ØØ
13	sij	1.Ø	-15 29.89	-72 45.Ø6	455Ø	Ø.	Ø.	Ø.	5.25	3.Ø5	12.Ø5	-97.12	-4.55
14	sis	1.Ø	-16 18.13	-72 4.85	1475	Ø.	Ø.	Ø.	5.25	3.Ø5	-33.65	7.78	-1.48
15	sqj	1.Ø	-16 33.87	-72 42.75	14Ø	Ø.	Ø.	Ø.	5.25	3.Ø5	-9Ø.52	-38.61	-Ø.14
16	tom	1.Ø	-16 2Ø.46	-72 28.25	35Ø	Ø.	Ø.	Ø.	5.25	3.Ø5	-56.7Ø	-27.2Ø	-Ø.35
17	yam	1.Ø	-15 32.Ø9	-71 21.Ø3	4Ø5Ø	Ø.	Ø.	Ø.	5.25	3.Ø5	77.83	38.Ø4	-4.Ø5
18	pch	1.Ø	-15 38.ØØ	-71 49.69	37ØØ	Ø.	Ø.	Ø.	5.25	3.Ø5	44.5Ø	-2.39	-3.7Ø
19	cal	1.Ø	-16 29.62	-71 55.79	12ØØ	Ø.	Ø.	Ø.	5.25	3.Ø5	-45.ØØ	31.87	-1.2Ø
20	cma	1.Ø	-15 36.4Ø	-71 57.72	336Ø	Ø.	Ø.	Ø.	5.25	3.Ø5	4Ø.49	-16.48	-3.36

layer	NS ints	EW ints	P scale	S scale
1	9	9	1.ØØ	1.ØØ
2	8	11	1.ØØ	1.ØØ
3	8	11	1.ØØ	1.ØØ
4	8	1Ø	1.ØØ	1.ØØ
5	8	1Ø	1.ØØ	1.ØØ
6	5	6	1.ØØ	1.ØØ
7	5	6	1.ØØ	1.ØØ

```
   8         3         4       1.ØØ       1.ØØ
   9         3         4       1.ØØ       1.ØØ

1      NS vectors
  -165.ØØ  -9Ø.ØØ  -55.ØØ  -3Ø.ØØ    Ø.     2Ø.ØØ   45.ØØ   9Ø.ØØ  165.ØØ
       EW vectors
  -22Ø.ØØ -11Ø.ØØ  -75.ØØ  -45.ØØ  -1Ø.ØØ   25.ØØ   55.ØØ  11Ø.ØØ  22Ø.ØØ

2      NS vectors
  -165.ØØ  -69.ØØ  -41.ØØ  -14.ØØ   14.ØØ   41.ØØ   69.ØØ  165.ØØ
       EW vectors
  -22Ø.ØØ -11Ø.ØØ  -88.ØØ  -66.ØØ  -44.ØØ  -22.ØØ    Ø.     22.ØØ   44.ØØ   82.5Ø  22Ø.ØØ

3      NS vectors
  -165.ØØ  -69.ØØ  -41.ØØ  -14.ØØ   14.ØØ   41.ØØ   69.ØØ  165.ØØ
       EW vectors
  -22Ø.ØØ -11Ø.ØØ  -88.ØØ  -66.ØØ  -44.ØØ  -22.ØØ    Ø.     22.ØØ   44.ØØ   82.5Ø  22Ø.ØØ

4      NS vectors
  -165.ØØ  -69.ØØ  -41.ØØ  -14.ØØ   14.ØØ   41.ØØ   69.ØØ  165.ØØ
       EW vectors
  -22Ø.ØØ -11Ø.ØØ  -88.ØØ  -66.ØØ  -44.ØØ  -22.ØØ    Ø.     27.5Ø   82.5Ø  22Ø.ØØ

5      NS vectors
  -165.ØØ  -69.ØØ  -41.ØØ  -14.ØØ   14.ØØ   41.ØØ   69.ØØ  165.ØØ
       EW vectors
  -22Ø.ØØ -11Ø.ØØ  -88.ØØ  -66.ØØ  -44.ØØ  -22.ØØ    Ø.     27.5Ø   82.5Ø  22Ø.ØØ

6      NS vectors
  -165.ØØ  -55.ØØ   15.ØØ   85.ØØ  165.ØØ
       EW vectors
  -22Ø.ØØ -14Ø.ØØ  -6Ø.ØØ   3Ø.ØØ  12Ø.ØØ  22Ø.ØØ

7      NS vectors
  -165.ØØ  -55.ØØ   15.ØØ   85.ØØ  165.ØØ
       EW vectors
  -22Ø.ØØ -14Ø.ØØ  -6Ø.ØØ   3Ø.ØØ  12Ø.ØØ  22Ø.ØØ

8      NS vectors
  -165.ØØ    Ø.    165.ØØ
       EW vectors
  -22Ø.ØØ  -7Ø.ØØ   7Ø.ØØ  22Ø.ØØ

9      NS vectors
  -165.ØØ    Ø.    165.ØØ
       EW vectors
  -22Ø.ØØ  -7Ø.ØØ   7Ø.ØØ  22Ø.ØØ


 neqs = 396   nvar =   764   kvar =   292232Ø

scale factors
 layer    p scale    s scale
   1        1.ØØØ      1.ØØØ
            1.ØØØ      1.ØØØ
            1.ØØØ      1.ØØØ
```

4	1.000	1.000
5	1.000	1.000
6	1.000	1.000
7	1.000	1.000
8	1.000	1.000
9	1.000	1.000

number of p arrivals	3365
p weight	1.0000
number of s arrivals	2845
s weight	0.5000
total number of arrivals	6210

p observation matrix

layer 1

0	16	217	0	0	0	0	0
0	0	0	298	131	0	0	0
0	0	0	219	0	0	0	0
300	551	107	11	0	22	39	94
0	0	341	385	0	155	3	0
106	0	145	306	1	10	115	0
0	150	0	45	36	97	0	0
0	0	0	0	0	0	0	0

layer 2

10	217	24	9	0	0	0
0	0	37	124	19	0	0
0	11	231	174	6	0	0
72	32	189	67	0	0	2
334	297	109	19	6	13	77
61	181	289	27	34	14	27
20	180	784	75	97	40	16
80	185	450	76	63	75	87
200	54	140	51	97	10	6
20	1	0	0	0	0	0

layer 3

33	204	91	22	0	0	0
66	97	77	54	15	1	0
113	93	154	121	23	1	1
138	242	215	86	9	8	15
323	363	258	48	30	35	53
281	360	424	91	48	38	31
193	299	451	148	89	64	26
150	188	341	106	79	54	23
161	18	159	52	49	7	5
20	2	8	5	2	0	0

s observation matrix

0	17	197	0	0	0	0	0
0	0	0	263	66	0	0	0
0	0	0	201	0	0	0	0
287	525	99	11	0	10	21	50
0	0	305	356	0	96	2	0
100	0	134	266	1	8	68	0
0	124	0	35	29	57	0	0
0	0	0	0	0	0	0	0

10	197	18	7	0	0	0
0	0	36	75	2	0	0
0	9	219	112	0	0	0
68	29	177	57	0	0	0
316	281	101	19	2	9	46
58	162	270	21	16	8	11
19	161	709	55	59	18	9
75	166	393	51	42	43	45
170	44	125	39	57	9	3
19	1	0	0	0	0	0

31	190	78	19	0	0	0
65	96	76	43	3	0	0
108	78	134	67	6	0	0
126	216	194	53	5	4	7
296	333	233	43	14	18	30
256	323	382	71	25	16	12
172	274	406	109	50	29	17
139	160	304	69	46	26	15
139	152	149	36	28	5	3
19	30	7	2	0	0	0

layer 4

137	138	98	41	8	1	Ø
91	186	11Ø	41	2Ø	11	2
1Ø5	224	118	7Ø	39	23	8
1Ø3	252	189	133	62	3Ø	17
3Ø?	33?	26Ø	147	86	44	28
347	294	284	143	89	59	35
158	196	235	155	85	46	26
135	186	137	73	53	27	12
19	46	17	7	5	1	Ø

128	129	8Ø	29	6	Ø	Ø
84	172	98	31	1Ø	2	Ø
96	2Ø8	1Ø7	44	15	8	4
94	231	166	86	28	1Ø	1Ø
27Ø	299	224	112	43	2Ø	17
313	274	258	1Ø2	43	25	17
144	184	2Ø6	1Ø5	39	21	16
122	164	117	46	32	12	6
18	42	16	4	2	Ø	Ø

layer 5

36	1Ø6	75	91	27	8	1
15	11Ø	91	86	47	25	3Ø
12	1Ø7	125	98	72	75	56
6	11Ø	16Ø	152	99	76	46
2Ø	188	232	146	111	74	46
12	184	213	14Ø	95	59	18
3Ø	71	141	131	71	34	18
36	76	84	78	47	21	14
36	4Ø	25	12	5	1	3

32	92	63	67	19	3	Ø
15	1Ø1	76	56	32	14	16
12	1Ø2	1Ø2	66	47	5Ø	28
6	1Ø1	133	115	63	43	28
2Ø	176	199	1ØØ	7Ø	5Ø	3Ø
12	167	179	99	6Ø	36	12
26	64	12Ø	1ØØ	36	18	11
34	7Ø	75	6Ø	3Ø	8	5
31	37	21	7	1	Ø	1

layer 6

Ø	48	2	Ø
Ø	135	166	17
Ø	414	292	67
Ø	126	1Ø4	7
Ø	23	4	Ø

Ø	34	Ø	Ø
Ø	1Ø8	111	7
Ø	338	183	41
Ø	1ØØ	6Ø	3
Ø	17	Ø	Ø

layer 7

Ø	Ø	Ø	Ø
Ø	Ø	Ø	Ø
Ø	11	89	23
Ø	49	1Ø3	9
Ø	14	16	Ø

Ø	Ø	Ø	Ø
Ø	Ø	Ø	Ø
Ø	12	57	14
Ø	4Ø	69	4
Ø	11	7	Ø

layer 8

Ø	Ø
Ø	47
Ø	73

Ø	Ø
Ø	29
4	46

layer 9

Ø	Ø
1	
Ø	56

Ø	Ø
Ø	Ø
Ø	34

a total number of 572 blocks were hit
163878 elements of g are used

a total number of 423 blocks are kept for inversion
89676 elements of g are used

g diagonals for p velocity model

layer 1

Ø.	Ø.	3.25	Ø.	Ø.	Ø.	Ø.	Ø.
Ø.	Ø.	Ø.	9.3Ø	5.Ø4	Ø.	Ø.	Ø.
Ø.	Ø.	Ø.	2.41	Ø.	Ø.	Ø.	Ø.
Ø.88	3.84	Ø.3Ø	Ø.	Ø.	Ø.67	Ø.35	2.13
Ø.	Ø.	6.28	7.79	Ø.	6.67	Ø.	Ø.
1.Ø1	Ø.	2.21	5.91	Ø.	Ø.	4.56	Ø.
Ø.	1.39	Ø.	1.14	Ø.33	2.66	Ø.	Ø.
Ø.	Ø.	Ø.	Ø.	Ø.	Ø.	Ø.	Ø.

layer 2

Ø.	14.89	Ø.23	Ø.	Ø.	Ø.	Ø.
Ø.	Ø.	1.72	5.34	Ø.	Ø.	Ø.
Ø.	Ø.	11.34	6.85	Ø.	Ø.	Ø.
2.78	Ø.14	1Ø.58	2.79	Ø.	Ø.	Ø.
14.41	14.68	3.Ø3	Ø.	Ø.	Ø.	4.71
1.28	7.8Ø	12.37	Ø.76	1.35	Ø.	1.23
Ø.44	5.54	22.Ø2	1.61	7.29	1.81	Ø.
5.16	4.2Ø	19.87	1.32	2.53	6.25	2.67
1Ø.69	1.71	6.47	3.64	4.55	Ø.	Ø.
Ø.8Ø	Ø.	Ø.	Ø.	Ø.	Ø.	Ø.

layer 3

1.36	1Ø.7Ø	5.48	Ø.75	Ø.	Ø.	Ø.
2.43	2.92	3.45	2.11	Ø.	Ø.	Ø.
4.82	2.77	7.5Ø	5.84	1.19	Ø.	Ø.
8.2Ø	14.24	6.7Ø	4.23	Ø.	Ø.	Ø.
14.37	14.Ø4	13.Ø2	2.48	2.Ø9	2.31	1.74
1Ø.64	17.18	15.99	6.21	3.Ø2	2.ØØ	1.58
9.34	14.6Ø	16.9Ø	9.63	4.35	3.84	1.75
7.13	5.77	11.44	6.17	4.31	2.21	Ø.75
7.9Ø	7.82	3.79	2.56	2.33	Ø.	Ø.
Ø.5Ø	Ø.39	Ø.	Ø.	Ø.	Ø.	Ø.

layer 4

2.99	5.22	4.76	4.Ø1	Ø.	Ø.	Ø.
2.Ø2	6.69	5.78	2.Ø1	Ø.99	Ø.	Ø.
3.51	8.84	6.15	3.81	2.38	1.65	Ø.
4.14	9.27	11.13	7.83	3.61	Ø.96	Ø.
8.35	12.89	13.24	9.83	5.61	3.27	1.82
8.13	15.33	15.64	9.98	6.Ø1	3.54	2.54
[illegible]	[illegible]	14.ØØ	10.53	6.3Ø	3.86	1.89

g diagonals for s velocity model

Ø.	Ø.	4.62	Ø.	Ø.	Ø.	Ø.
Ø.	Ø.	Ø.	1Ø.98	3.73	Ø.	Ø.
Ø.	Ø.	Ø.	3.Ø9	Ø.	Ø.	Ø.
1.1Ø	4.72	Ø.42	Ø.	Ø.	Ø.	Ø.32
Ø.	Ø.	7.65	9.87	Ø.	6.26	Ø.
1.44	Ø.	2.74	7.75	Ø.	Ø.	4.Ø3
Ø.	1.81	Ø.	1.34	Ø.46	2.Ø5	Ø.
Ø.	Ø.	Ø.	Ø.	Ø.	Ø.	Ø.

Ø.	21.66	Ø.	Ø.	Ø.	Ø.	Ø.
Ø.	Ø.	2.19	5.5Ø	Ø.	Ø.	Ø.
Ø.	Ø.	14.35	5.2Ø	Ø.	Ø.	Ø.
3.37	Ø.18	14.ØØ	3.17	Ø.	Ø.	Ø.
18.9Ø	17.94	4.39	Ø.	Ø.	Ø.	3.89
1.67	1Ø.93	16.76	Ø.88	Ø.	Ø.	Ø.
Ø.	6.65	25.8Ø	1.71	6.61	Ø.	Ø.
7.75	5.65	25.76	1.67	3.17	6.19	2.14
13.91	2.21	9.Ø7	4.78	3.3Ø	Ø.	Ø.
Ø.	Ø.	Ø.	Ø.	Ø.	Ø.	Ø.

2.Ø2	15.42	6.71	Ø.	Ø.	Ø.	Ø.
3.91	4.Ø6	4.19	2.1Ø	Ø.	Ø.	Ø.
5.91	3.Ø1	8.66	4.15	Ø.	Ø.	Ø.
9.79	18.Ø9	8.56	3.7Ø	Ø.	Ø.	Ø.
15.37	17.64	17.22	2.96	Ø.	Ø.	1.5Ø
11.78	2Ø.81	2Ø.96	6.Ø8	1.6Ø	Ø.	Ø.
1Ø.87	2Ø.28	2Ø.81	1Ø.72	3.72	1.94	Ø.
9.16	6.86	14.32	5.75	2.67	1.Ø2	Ø.
1Ø.84	8.12	5.33	2.7Ø	2.27	Ø.	Ø.
Ø.	Ø.53	Ø.	Ø.	Ø.	Ø.	Ø.

2.79	6.Ø6	5.63	4.14	Ø.	Ø.	Ø.
2.44	8.86	7.12	2.Ø2	Ø.	Ø.	Ø.
4.47	11.59	7.3Ø	3.31	Ø.	Ø.	Ø.
5.71	13.21	13.1Ø	6.22	2.6Ø	Ø.	Ø.
1Ø.36	15.39	15.35	1Ø.18	4.28	1.68	Ø.
11.11	18.64	18.75	9.96	4.21	2.59	Ø.
6.69	14.17	17.39	11.56	3.78	3.1Ø	Ø.

4.28	10.93	8.67	5.25	3.11	2.85	0.
0.	1.88	0.	0.	0.	0.	0.

layer 5

0.63	1.40	2.36	2.53	1.00	0.	0.
0.	1.06	2.08	2.47	1.94	0.73	0.26
0.	1.52	3.01	3.71	2.79	1.71	0.78
0.	1.88	5.32	4.54	4.25	2.78	1.11
0.06	2.68	5.91	6.00	4.25	2.99	1.26
0.	2.47	5.70	6.18	4.29	2.16	0.
0.05	1.38	4.86	5.87	4.00	2.14	0.
0.58	1.62	3.89	4.75	3.41	1.92	0.
0.36	1.16	1.77	0.	0.	0.	0.

layer 6

0.	0.28	0.	0.
0.	0.25	0.63	0.
0.	4.65	4.44	0.36
0.	3.71	3.84	0.
0.	0.39	0.	0.

layer 7

0.	0.	0.	0.
0.	0.	0.	0.
0.	0.	0.58	0.08
0.	0.67	2.30	0.
0.	0.	0.	0.

layer 8

0.	0.
0.	0.49
0.	0.48

layer 9

0.	0.
0.	0.
0.	0.29

nvar, irnk, ier, are 423 423 0

residual norm	1030.19531
standard variance	0.17738
original variance	0.17802
residual variance	0.07487
mod residual norm	988.58447
mod standard variance	0.23463
mod original variance	0.23521
mod residual variance	0.09319
percentage improvement	57.94295
mod percentage improvement	60.38184

5.07	12.89	9.56	4.44	2.32	0.	0.
0.	2.30	0.	0.	0.	0.	0.

1.04	1.96	2.93	2.27	0.	0.	0.
0.	1.48	2.31	2.24	1.81	0.	0.
0.	2.33	3.39	3.36	2.35	1.15	0.34
0.	2.80	6.45	3.98	3.35	2.39	0.98
0.10	3.88	6.60	5.86	2.93	3.02	1.06
0.	3.89	6.79	4.58	4.05	1.80	0.
0.11	1.93	5.98	5.37	2.70	0.	0.
0.88	2.18	5.30	4.49	2.84	0.	0.
0.34	1.44	2.30	0.	0.	0.	0.

0.	0.14	0.	0.
0.	0.23	0.74	0.
0.	6.85	5.54	0.35
0.	4.69	3.06	0.
0.	0.	0.	0.

0.	0.	0.	0.
0.	0.	0.	0.
0.	0.	0.72	0.
0.	1.07	1.92	0.
0.	0.	0.	0.

0.	0.
0.	0.56
0.	0.59

0.	0.
0.	0.
0.	0.66

velocities for p velocity model

layer 1

Ø.	Ø.	5.52	Ø.	Ø.	Ø.	Ø.	Ø.
Ø.	Ø.	Ø.	5.51	5.13	Ø.	Ø.	Ø.
Ø.	Ø.	Ø.	4.77	Ø.	Ø.	Ø.	Ø.
5.35	5.44	5.3Ø	Ø.	Ø.	5.3Ø	4.94	5.38
Ø.	Ø.	4.9Ø	5.93	Ø.	4.92	Ø.	Ø.
5.51	Ø.	4.33	5.76	Ø.	Ø.	5.13	Ø.
Ø.	5.25	Ø.	5.74	5.Ø7	5.19	Ø.	Ø.
Ø.	Ø.	Ø.	Ø.	Ø.	Ø.	Ø.	Ø.

layer 2

Ø.	6.74	5.9Ø	Ø.	Ø.	Ø.	Ø.
Ø.	Ø.	6.2Ø	5.81	Ø.	Ø.	Ø.
Ø.	Ø.	6.Ø5	5.83	Ø.	Ø.	Ø.
6.54	6.2Ø	6.Ø4	5.93	Ø.	Ø.	Ø.
6.Ø1	6.3Ø	5.8Ø	Ø.	Ø.	Ø.	6.Ø8
6.ØØ	6.Ø3	6.24	6.Ø4	6.Ø5	Ø.	5.93
6.41	6.21	6.13	5.94	6.Ø5	5.91	Ø.
6.3Ø	5.76	6.52	5.86	5.98	5.8Ø	6.24
6.Ø5	6.25	6.18	5.56	5.92	Ø.	Ø.
6.23	Ø.	Ø.	Ø.	Ø.	Ø.	Ø.

layer 3

6.84	7.95	7.16	6.71	Ø.	Ø.	Ø.
7.22	7.4Ø	6.87	6.53	Ø.	Ø.	Ø.
7.16	7.36	6.6Ø	6.2Ø	6.22	Ø.	Ø.

velocities for s velocity model

Ø.	Ø.	3.3Ø	Ø.	Ø.	Ø.	Ø.	Ø.
Ø.	Ø.	Ø.	3.18	2.91	Ø.	Ø.	Ø.
Ø.	Ø.	Ø.	2.99	Ø.	Ø.	Ø.	Ø.
3.Ø4	3.36	3.Ø4	Ø.	Ø.	Ø.	3.ØØ	3.11
Ø.	Ø.	2.97	3.27	Ø.	3.Ø9	Ø.	Ø.
3.36	Ø.	2.92	3.29	Ø.	Ø.	2.96	Ø.
Ø.	3.12	Ø.	3.28	2.87	3.Ø9	Ø.	Ø.
Ø.	Ø.	Ø.	Ø.	Ø.	Ø.	Ø.	Ø.

Ø.	3.65	Ø.	Ø.	Ø.	Ø.	Ø.
Ø.	Ø.	3.53	3.5Ø	Ø.	Ø.	Ø.
Ø.	Ø.	3.64	3.47	Ø.	Ø.	Ø.
3.95	3.48	3.53	3.51	Ø.	Ø.	Ø.
3.78	3.75	3.56	Ø.	Ø.	Ø.	3.32
3.5Ø	3.69	3.65	3.48	Ø.	Ø.	Ø.
Ø.	3.62	3.62	3.46	3.45	Ø.	Ø.
3.82	3.51	3.67	3.39	3.5Ø	3.4Ø	3.72
3.69	3.46	3.66	3.44	3.75	Ø.	Ø.
Ø.	Ø.	Ø.	Ø.	Ø.	Ø.	Ø.

4.11	4.69	4.16	Ø.	Ø.	Ø.	Ø.
4.24	4.33	4.Ø1	3.71	Ø.	Ø.	Ø.
4.ØØ	4.Ø4	3.73	3.78	Ø.	Ø.	Ø.

7.21	7.08	6.96	6.26	0.	0.	0.	4.03	3.97	3.91	3.83	0.	0.	0.
7.13	7.49	7.05	6.18	6.35	6.38	6.98	4.01	4.24	4.02	3.78	0.	0.	3.76
7.17	7.05	7.00	6.11	6.44	6.31	6.46	4.09	4.05	3.96	3.79	3.79	0.	0.
7.05	6.78	6.67	6.17	6.37	6.61	6.46	4.13	3.87	3.90	3.79	3.57	3.86	0.
7.33	7.09	6.67	6.17	6.39	6.65	6.52	4.18	3.92	3.91	3.85	3.78	3.68	0.
7.11	6.93	6.76	6.30	6.14	0.	0.	4.00	3.88	3.92	3.72	3.72	0.	0.
7.54	7.95	0.	0.	0.	0.	0.	0.	4.09	0.	0.	0.	0.	0.

layer 4

7.84	7.70	7.17	6.95	0.	0.	0.	4.48	4.61	4.20	4.12	0.	0.	0.
7.84	7.78	7.41	7.07	6.96	0.	0.	4.57	4.50	4.20	3.98	0.	0.	0.
7.51	7.74	7.75	6.81	6.74	6.61	0.	4.28	4.51	4.24	4.08	0.	0.	0.
7.73	7.74	7.33	6.80	6.84	6.91	0.	4.31	4.39	4.19	3.92	3.96	0.	0.
8.21	7.75	7.37	6.76	6.95	6.91	6.72	4.64	4.42	4.26	3.85	3.88	3.85	0.
7.78	7.55	7.39	6.69	7.01	6.98	6.44	4.43	4.37	4.29	3.91	3.87	3.80	0.
7.98	7.76	7.18	6.60	7.05	6.81	6.86	4.49	4.47	4.09	3.86	4.05	3.84	0.
7.44	7.32	7.43	6.72	7.11	6.81	0.	4.29	4.24	4.22	3.86	3.98	0.	0.
0.	7.30	0.	0.	0.	0.	0.	0.	4.18	0.	0.	0.	0.	0.

layer 5

8.12	7.80	7.67	7.78	7.76	0.	0.	4.35	4.45	4.55	4.47	0.	0.	0.
0.	7.84	7.93	7.61	7.47	7.62	7.60	0.	4.45	4.44	4.50	4.49	0.	0.
0.	7.88	7.93	7.91	7.91	7.75	7.75	0.	4.60	4.57	4.61	4.55	4.53	4.37
0.	7.64	7.72	7.80	7.55	7.62	7.58	0.	4.65	4.53	4.52	4.35	4.37	4.39
7.60	7.65	7.84	7.77	7.57	7.74	7.73	4.56	4.61	4.54	4.60	4.46	4.35	4.13
0.	7.81	8.04	8.02	8.01	7.79	0.	0.	4.34	4.66	4.45	4.40	4.48	0.
7.68	7.67	8.16	7.99	7.90	7.99	0.	4.65	4.43	4.83	4.53	4.30	0.	0.
7.76	7.85	8.03	7.65	7.77	7.53	0.	4.39	4.65	4.75	4.31	4.28	0.	0.

7.58	7.5Ø	7.69	Ø.	Ø.	Ø.	Ø.		4.33	4.52	4.5Ø	Ø.	Ø.	Ø.	Ø.

layer 6

Ø.	7.52	Ø.	Ø.					Ø.	4.43	Ø.	Ø.		
Ø.	7.73	7.8Ø	Ø.					Ø.	4.25	4.74	Ø.		
Ø.	8.21	8.19	7.67					Ø.	4.56	4.49	4.62		
Ø.	8.11	8.26	Ø.					Ø.	4.43	4.55	Ø.		
Ø.	7.78	Ø.	Ø.					Ø.	Ø.	Ø.	Ø.		

layer 7

Ø.	Ø.	Ø.	Ø.					Ø.	Ø.	Ø.	Ø.		
Ø.	Ø.	Ø.	Ø.					Ø.	Ø.	Ø.	Ø.		
Ø.	Ø.	7.76	8.26					Ø.	Ø.	4.84	Ø.		
Ø.	8.14	7.89	Ø.					Ø.	4.59	4.6Ø	Ø.		
Ø.	Ø.	Ø.	Ø.					Ø.	Ø.	Ø.	Ø.		

layer 8

Ø.	Ø.							Ø.	Ø.				
Ø.	7.93							Ø.	4.63				
Ø.	8.ØØ							Ø.	4.5Ø				

layer 9

Ø.	Ø.							Ø.	Ø.				
Ø.	Ø.							Ø.	Ø.				
Ø.	7.84							Ø.	4.64				

%fraction change for p velocity model

%fraction change for s velocity model

layer 1

0.	0.	4.09	0.	0.	0.	0.	0.
0.	0.	0.	6.02	-1.35	0.	0.	0.
0.	0.	0.	-8.31	0.	0.	0.	0.
-0.92	0.77	0.00	0.	0.	1.91	-5.09	3.46
0.	0.	-7.55	14.13	0.	-5.45	0.	0.
2.04	0.	-18.33	10.76	0.	0.	-1.43	0.
0.	-2.84	0.	10.30	-2.54	-0.24	0.	0.
0.	0.	0.	0.	0.	0.	0.	0.

0.	0.	8.26	0.	0.	0.	0.	0.
0.	0.	0.	5.86	-2.90	0.	0.	0.
0.	0.	0.	-0.49	0.	0.	0.	0.
-2.00	8.47	-0.44	0.	0.	0.	-0.01	3.50
0.	0.	-2.51	9.13	0.	2.88	0.	0.
8.33	0.	-4.23	9.74	0.	0.	-1.26	0.
0.	0.61	0.	9.34	-4.42	2.84	0.	0.
0.	0.	0.	0.	0.	0.	0.	0.

layer 2

0.	10.52	-1.68	0.	0.	0.	0.
0.	0.	3.35	-3.11	0.	0.	0.
0.	0.	0.77	-2.76	0.	0.	0.
5.54	1.68	0.72	-1.21	0.	0.	0.
-3.00	3.34	-3.28	0.	0.	0.	1.38
-3.27	-1.19	3.92	0.69	0.78	0.	-1.20
3.45	1.84	2.14	-1.00	0.77	-1.57	0.
1.65	-5.56	8.62	-2.26	-0.37	-3.26	4.08
-2.47	2.54	3.02	-7.37	-1.31	0.	0.
0.46	0.	0.	0.	0.	0.	0.

0.	4.27	0.	0.	0.	0.	0.
0.	0.	2.24	1.38	0.	0.	0.
0.	0.	5.47	0.61	0.	0.	0.
11.20	-0.66	2.19	1.71	0.	0.	0.
6.52	7.20	3.26	0.	0.	0.	-3.80
-1.48	5.53	5.93	0.86	0.	0.	0.
0.	3.29	4.99	0.15	0.00	0.	0.
7.62	0.33	6.52	-1.74	1.44	-1.37	7.83
3.89	-1.06	6.09	-0.27	8.71	0.	0.
0.	0.	0.	0.	0.	0.	0.

layer 3

-8.21	14.39	6.91	1.62	0.	0.	0.
-3.12	6.45	2.49	-1.12	0.	0.	0.
-3.84	5.95	-1.49	-6.03	-5.09	0.	0.
-3.23	1.93	3.94	-5.17	0.	0.	0.
-2.98	7.71	5.27	-6.43	-3.06	-1.90	7.31

-3.32	17.13	8.12	0.	0.	0.	0.
-0.20	8.20	4.07	-2.34	0.	0.	0.
-5.86	0.91	-3.13	-0.53	0.	0.	0.
-5.21	-0.70	1.46	0.78	0.	0.	0.
-5.67	5.95	4.40	-0.49	0.	0.	0.20

-1.12	Ø.73	4.46	-7.36	-1.63	-2.87	-Ø.6Ø
Ø.Ø2	-3.57	-Ø.44	-6.49	-2.75	1.72	-Ø.59
-Ø.84	-3.75	-Ø.46	-6.52	-2.49	2.24	Ø.37
-1.83	-Ø.23	Ø.91	-4.5Ø	-6.21	Ø.	Ø.
1.17	-Ø.69	Ø.	Ø.	Ø.	Ø.	Ø.

-3.88	1.31	2.8Ø	-Ø.28	1.15	Ø.	Ø.
-2.78	-3.26	1.25	-Ø.22	-4.88	3.Ø3	Ø.
-1.69	-1.93	1.53	1.25	Ø.88	-1.96	Ø.
-5.92	-3.Ø1	1.88	-2.22	-Ø.76	Ø.	Ø.
Ø.	2.15	Ø.	Ø.	Ø.	Ø.	Ø.

layer 4

2.46	4.Ø9	Ø.23	-Ø.78	Ø.	Ø.	Ø.
2.48	5.Ø9	3.62	Ø.98	Ø.82	Ø.	Ø.
-1.83	4.55	-1.39	-2.73	-2.35	-2.79	Ø.
1.Ø1	4.57	2.54	-2.87	-Ø.86	1.68	Ø.
7.32	4.76	3.Ø5	-3.49	Ø.67	1.66	-1.14
1.71	2.Ø5	3.37	-4.41	1.54	2.6Ø	-5.26
4.34	4.9Ø	Ø.35	-5.67	2.1Ø	Ø.14	Ø.87
-2.76	-1.14	3.96	-4.Ø1	3.Ø5	Ø.12	Ø.
Ø.	-1.36	Ø.	Ø.	Ø.	Ø.	Ø.

1.91	8.46	2.53	2.98	Ø.	Ø.	Ø.
3.79	5.97	2.49	-Ø.61	Ø.	Ø.	Ø.
-2.69	6.12	3.45	2.1Ø	Ø.	Ø.	Ø.
-2.13	3.33	2.25	-2.11	Ø.25	Ø.	Ø.
5.54	4.1Ø	3.8Ø	-3.82	-1.86	-1.28	Ø.
Ø.72	2.81	4.62	-2.22	-1.97	-2.59	Ø.
2.Ø9	5.Ø8	-Ø.32	-3.54	2.5Ø	-1.43	Ø.
-2.56	-Ø.13	2.87	-3.56	Ø.66	Ø.	Ø.
Ø.	-1.68	Ø.	Ø.	Ø.	Ø.	Ø.

layer 5

4.11	Ø.6Ø	-Ø.39	1.Ø8	Ø.74	Ø.	Ø.
Ø.	1.22	2.96	-1.12	-2.96	-1.Ø6	-1.36
Ø.	1.66	2.93	2.73	2.69	Ø.59	Ø.69
Ø.	-1.4Ø	Ø.3Ø	1.31	-1.96	-1.ØØ	-1.62
-2.62	-1.33	1.86	Ø.87	-1.65	Ø.5Ø	Ø.4Ø
Ø.	Ø.73	4.36	4.14	4.Ø5	1.21	Ø.
-1.58	-2.3Ø	5.91	3.28	2.56	3.78	Ø.
-Ø.5Ø	3.17	4.29	-Ø.63	Ø.92	-2.18	Ø.
-2.76	-3.28	-Ø.Ø7	Ø.	Ø.	Ø.	Ø.

-3.24	-Ø.Ø2	2.98	1.22	Ø.	Ø.	Ø.
Ø.	Ø.Ø8	Ø.45	1.78	1.96	Ø.	Ø.
Ø.	3.31	3.4Ø	4.23	3.48	3.Ø4	-Ø.66
Ø.	4.47	2.58	2.33	-1.19	-Ø.71	-Ø.16
1.44	3.57	2.74	3.96	1.37	-1.Ø3	-6.Ø3
Ø.	-2.41	5.37	Ø.73	Ø.Ø6	1.77	Ø.
3.35	-Ø.38	9.22	2.44	-2.28	Ø.	Ø.
-2.35	4.59	7.47	-2.43	-2.83	Ø.	Ø.
-3.77	1.5Ø	1.89	Ø.	Ø.	Ø.	Ø.

layer 6

Ø.	-4.86	Ø.	Ø.	Ø.	3.Ø8	Ø.	Ø.
Ø.	-2.16	-1.3Ø	Ø.	Ø.	-1.Ø8	1Ø.23	Ø.
Ø.	3.91	3.67	-2.96	Ø.	6.1Ø	4.3Ø	7.39
Ø.	2.7Ø	4.6Ø	Ø.	Ø.	3.Ø5	5.82	Ø.
Ø.	-1.56	Ø.	Ø.	Ø.	Ø.	Ø.	Ø.

layer 7

Ø.	Ø.	Ø.	Ø.	Ø.	Ø.	Ø.	Ø.
Ø.	Ø.	Ø.	Ø.	Ø.	Ø.	Ø.	Ø.
Ø.	Ø.	-1.77	4.55	Ø.	Ø.	5.19	Ø.
Ø.	2.98	-Ø.18	Ø.	Ø.	-Ø.3Ø	Ø.Ø2	Ø.
Ø.	Ø.	Ø.	Ø.	Ø.	Ø.	Ø.	Ø.

layer 8

Ø.	Ø.	Ø.	Ø.
Ø.	Ø.39	Ø.	Ø.57
Ø.	1.27	Ø.	-2.28

layer 9

Ø.	Ø.	Ø.	Ø.
Ø.	Ø.	Ø.	Ø.
Ø.	-Ø.73	Ø.	Ø.8Ø

fres = 1 kmin = 1 kmax = 423

sum of diagonal elements of resolution matrix for 423 elements = 295.965

resolution for p velocity model — resolution for s velocity model

layer 1

Ø.	Ø.	Ø.15	Ø.	Ø.	Ø.	Ø.	Ø.
Ø.	Ø.	Ø.	Ø.66	Ø.64	Ø.	Ø.	Ø.
Ø.	Ø.	Ø.	Ø.37	Ø.	Ø.	Ø.	Ø.
Ø.3Ø	Ø.47	Ø.25	Ø.	Ø.	Ø.36	Ø.16	Ø.27
Ø.	Ø.	Ø.76	Ø.77	Ø.	Ø.65	Ø.	Ø.
Ø.32	Ø.	Ø.58	Ø.72	Ø.	Ø.	Ø.54	Ø.
Ø	Ø.36	Ø.	Ø.48	Ø.18	Ø.43	Ø.	Ø.
Ø	Ø.	Ø.	Ø.	Ø.	Ø.	Ø.	Ø.

Ø.	Ø.	Ø.16	Ø.	Ø.	Ø.	Ø.	Ø.
Ø.	Ø.	Ø.	Ø.66	Ø.52	Ø.	Ø.	Ø.
Ø.	Ø.	Ø.	Ø.4Ø	Ø.	Ø.	Ø.	Ø.
Ø.35	Ø.52	Ø.31	Ø.	Ø.	Ø.	Ø.22	Ø.35
Ø.	Ø.	Ø.79	Ø.8Ø	Ø.	Ø.68	Ø.	Ø.
Ø.36	Ø.	Ø.6Ø	Ø.76	Ø.	Ø.	Ø.53	Ø.
Ø.	Ø.43	Ø.	Ø.51	Ø.2Ø	Ø.44	Ø.	Ø.
Ø.	Ø.	Ø.	Ø.	Ø.	Ø.	Ø.	Ø.

layer 2

Ø.	Ø.66	Ø.11	Ø.	Ø.	Ø.	Ø.
Ø.	.	Ø.57	Ø.65	Ø.	Ø.	Ø.
Ø.	Ø.	Ø.75	Ø.75	Ø.	Ø.	Ø.
Ø.66	Ø.16	Ø.85	Ø.67	Ø.	Ø.	Ø.
Ø.85	Ø.85	Ø.78	Ø.	Ø.	Ø.	Ø.59
Ø.63	Ø.87	Ø.89	Ø.48	Ø.57	Ø.	Ø.43
Ø.43	.87	Ø.91	Ø.65	Ø.73	Ø.6Ø	Ø.
Ø.76	Ø.7Ø	Ø.92	Ø.6Ø	Ø.67	Ø.71	Ø.46
Ø.79	.89	Ø.94	Ø.77	Ø.67	Ø.	Ø.
Ø.94	Ø.	Ø.	Ø.	Ø.	Ø.	Ø.

Ø.	Ø.68	Ø.	Ø.	Ø.	Ø.	Ø.
Ø.	Ø.	Ø.6Ø	Ø.62	Ø.	Ø.	Ø.
Ø.	Ø.	Ø.75	Ø.7Ø	Ø.	Ø.	Ø.
Ø.69	Ø.2Ø	Ø.88	Ø.69	Ø.	Ø.	Ø.
Ø.88	Ø.87	Ø.82	Ø.	Ø.	Ø.	Ø.66
Ø.67	Ø.9Ø	Ø.92	Ø.5Ø	Ø.	Ø.	Ø.
Ø.	Ø.89	Ø.94	Ø.68	Ø.74	Ø.	Ø.
Ø.8Ø	Ø.81	Ø.93	Ø.67	Ø.7Ø	Ø.68	Ø.56
Ø.83	Ø.74	Ø.88	Ø.79	Ø.68	Ø.	Ø.
Ø.	Ø.	Ø.	Ø.	Ø.	Ø.	Ø.

layer 3

Ø.6Ø	Ø.77	Ø.75	Ø.45	Ø.	Ø.	Ø.
Ø.6Ø	Ø.75	Ø.75	Ø.58	Ø.	Ø.	Ø.
Ø.81	Ø.79	Ø.88	Ø.78	Ø.56	Ø.	Ø.
Ø.9Ø	Ø.9Ø	Ø.98	Ø.75	Ø.	Ø.	Ø.
Ø.93	Ø.94	Ø.93	Ø.79	Ø.63	Ø.42	
Ø.94	Ø.9(	Ø.94	Ø.8	Ø.79	Ø.69	Ø.44

Ø.6Ø	Ø.79	Ø.79	Ø.	Ø.	Ø.	Ø.
Ø.68	Ø.79	Ø.79	Ø.6Ø	Ø.	Ø.	Ø.
Ø.83	Ø.81	Ø.9Ø	Ø.73	Ø.	Ø.	Ø.
Ø.92	Ø.94	Ø.9Ø	Ø.73	Ø.	Ø.	Ø.
Ø.93	Ø.95	Ø.94	Ø.78	Ø.	Ø.	Ø.5Ø
Ø.94	Ø.96	Ø.95	Ø.87	Ø.71	Ø.	Ø.

Ø.92	Ø.95	Ø.95	Ø.9Ø	Ø.82	Ø.73	Ø.54
Ø.9Ø	Ø.9Ø	Ø.93	Ø.88	Ø.79	Ø.63	Ø.39
Ø.85	Ø.89	Ø.83	Ø.78	Ø.6Ø	Ø.	Ø.
Ø.29	Ø.28	Ø.	Ø.	Ø.	Ø.	Ø.

Ø.93	Ø.96	Ø.96	Ø.9Ø	Ø.79	Ø.67	Ø.
Ø.91	Ø.91	Ø.94	Ø.87	Ø.72	Ø.53	Ø.
Ø.87	Ø.9Ø	Ø.87	Ø.77	Ø.6Ø	Ø.	Ø.
Ø.	Ø.34	Ø.	Ø.	Ø.	Ø.	Ø.

layer 4

Ø.74	Ø.79	Ø.76	Ø.73	Ø.	Ø.	Ø.
Ø.67	Ø.87	Ø.84	Ø.68	Ø.58	Ø.	Ø.
Ø.8Ø	Ø.89	Ø.88	Ø.8Ø	Ø.73	Ø.65	Ø.
Ø.83	Ø.92	Ø.92	Ø.89	Ø.82	Ø.57	Ø.
Ø.89	Ø.93	Ø.93	Ø.91	Ø.86	Ø.77	Ø.66
Ø.89	Ø.94	Ø.94	Ø.91	Ø.86	Ø.76	Ø.65
Ø.86	Ø.92	Ø.94	Ø.92	Ø.86	Ø.78	Ø.66
Ø.85	Ø.91	Ø.89	Ø.83	Ø.71	Ø.69	Ø.
Ø.	Ø.65	Ø.	Ø.	Ø.	Ø.	Ø.

Ø.72	Ø.81	Ø.79	Ø.76	Ø.	Ø.	Ø.
Ø.69	Ø.89	Ø.87	Ø.7Ø	Ø.	Ø.	Ø.
Ø.81	Ø.9Ø	Ø.9Ø	Ø.78	Ø.	Ø.	Ø.
Ø.84	Ø.94	Ø.94	Ø.88	Ø.78	Ø.	Ø.
Ø.9Ø	Ø.95	Ø.95	Ø.92	Ø.85	Ø.69	Ø.
Ø.9Ø	Ø.95	Ø.95	Ø.92	Ø.84	Ø.75	Ø.
Ø.89	Ø.94	Ø.95	Ø.92	Ø.82	Ø.76	Ø.
Ø.87	Ø.92	Ø.91	Ø.82	Ø.64	Ø.	Ø.
Ø.	Ø.72	Ø.	Ø.	Ø.	Ø.	Ø.

layer 5

Ø.42	Ø.61	Ø.65	Ø.67	Ø.56	Ø.	Ø.
Ø.	Ø.5Ø	Ø.7Ø	Ø.73	Ø.67	Ø.49	Ø.26
Ø.	Ø.65	Ø.78	Ø.82	Ø.77	Ø.69	Ø.48
Ø.	Ø.7Ø	Ø.86	Ø.85	Ø.84	Ø.76	Ø.57
Ø.1Ø	Ø.73	Ø.87	Ø.8Ø	Ø.83	Ø.78	Ø.58
Ø.	Ø.73	Ø.86	Ø.87	Ø.84	Ø.74	Ø.
Ø.Ø8	Ø.66	Ø.84	Ø.86	Ø.81	Ø.73	Ø.
Ø.44	Ø.65	Ø.78	Ø.79	Ø.76	Ø.62	Ø.
Ø.Ø	Ø.5Ø	Ø.66	Ø.	Ø.	Ø.	Ø.

Ø.55	Ø.66	Ø.69	Ø.66	Ø.	Ø.	Ø.
Ø.	Ø.61	Ø.73	Ø.72	Ø.63	Ø.	Ø.
Ø.	Ø.71	Ø.79	Ø.82	Ø.75	Ø.6Ø	Ø.3Ø
Ø.	Ø.76	Ø.88	Ø.84	Ø.8Ø	Ø.75	Ø.57
Ø.15	Ø.79	Ø.89	Ø.88	Ø.79	Ø.78	Ø.56
Ø.	Ø.8Ø	Ø.89	Ø.85	Ø.84	Ø.71	Ø.
Ø.16	Ø.72	Ø.87	Ø.85	Ø.76	Ø.	Ø.
Ø.55	Ø.72	Ø.83	Ø.78	Ø.77	Ø.	Ø.
Ø.33	Ø.61	Ø.71	Ø.	Ø.	Ø.	Ø.

layer 6

Ø.	Ø.27	Ø.	Ø.
Ø.	Ø.26	Ø.4Ø	Ø.
Ø.	Ø.73	Ø.75	Ø.29
Ø.	Ø.68	Ø.72	Ø.
Ø.	Ø.33	Ø.	Ø.

Ø.	Ø.15	Ø.	Ø.
Ø.	Ø.24	Ø.36	Ø.
Ø.	Ø.81	Ø.8Ø	Ø.28
Ø.	Ø.75	Ø.72	Ø.
Ø.	Ø.	Ø.	Ø.

layer 7

Ø.	Ø.	Ø.	Ø.
Ø.	Ø.	Ø.	Ø.
Ø.	Ø.	Ø.38	Ø.11
Ø.	Ø.43	Ø.67	Ø.
Ø.	Ø.	Ø.	Ø.

Ø.	Ø.	Ø.	Ø.
Ø.	Ø.	Ø.	Ø.
Ø.	Ø.	Ø.44	Ø.
Ø.	Ø.5Ø	Ø.65	Ø.
Ø.	Ø.	Ø.	Ø.

layer 8

Ø.	Ø.
Ø.	Ø.31
Ø.	Ø.29

Ø.	Ø.
Ø.	Ø.33
Ø.	Ø.34

layer 9

Ø.	Ø.
Ø.	Ø.
Ø.	Ø.19

Ø.	Ø.
Ø.	Ø.
Ø.	Ø.33

standard error for p velocity model

layer 1

Ø.	Ø.	Ø.Ø4	Ø.	Ø.	Ø.	Ø.	Ø.
Ø.	Ø.	Ø.	Ø.Ø8	Ø.Ø8	Ø.	Ø.	Ø.

standard error for s velocity model

Ø.	Ø.	Ø.Ø3	Ø.	Ø.	Ø.	Ø.	Ø.
Ø.	Ø.	Ø.	Ø.Ø5	Ø.Ø4	Ø.	Ø.	Ø.

Ø.	Ø.	Ø.	Ø.Ø6	Ø.	Ø.	Ø.	Ø.
Ø.Ø9	Ø.Ø9	Ø.Ø9	Ø.	Ø.	Ø.Ø9	Ø.Ø6	Ø.Ø5
Ø.	Ø.	Ø.Ø6	Ø.1Ø	Ø.	Ø.Ø7	Ø.	Ø.
Ø.Ø9	Ø.	Ø.Ø6	Ø.1Ø	Ø.	Ø.	Ø.Ø7	Ø.
Ø.	Ø.Ø8	Ø.	Ø.12	Ø.Ø7	Ø.Ø8	Ø.	Ø.
Ø.	Ø.	Ø.	Ø.	Ø.	Ø.	Ø.	Ø.

Ø.	Ø.	Ø.	Ø.Ø5	Ø.	Ø.	Ø.	Ø.
Ø.Ø5	Ø.Ø6	Ø.Ø6	Ø.	Ø.	Ø.	Ø.Ø5	Ø.Ø5
Ø.	Ø.	Ø.Ø4	Ø.Ø5	Ø.	Ø.Ø5	Ø.	Ø.
Ø.Ø6	Ø.	Ø.Ø5	Ø.Ø6	Ø.	Ø.	Ø.Ø4	Ø.
Ø.	Ø.Ø5	Ø.	Ø.Ø7	Ø.Ø4	Ø.Ø5	Ø.	Ø.
Ø.	Ø.	Ø.	Ø.	Ø.	Ø.	Ø.	Ø.

layer 2

Ø.	Ø.Ø9	Ø.Ø7	Ø.	Ø.	Ø.	Ø.
Ø.	Ø.	Ø.11	Ø.Ø9	Ø.	Ø.	Ø.
Ø.	Ø.	Ø.Ø8	Ø.Ø8	Ø.	Ø.	Ø.
Ø.12	Ø.1Ø	Ø.Ø7	Ø.1Ø	Ø.	Ø.	Ø.
Ø.Ø7	Ø.Ø7	Ø.Ø9	Ø.	Ø.	Ø.	Ø.Ø8
Ø.11	Ø.Ø7	Ø.Ø8	Ø.13	Ø.11	Ø.	Ø.1Ø
Ø.14	Ø.Ø9	Ø.Ø6	Ø.11	Ø.Ø9	Ø.11	Ø.
Ø.Ø9	Ø.Ø9	Ø.Ø7	Ø.11	Ø.1Ø	Ø.Ø8	Ø.Ø9
Ø.Ø8	Ø.12	Ø.Ø9	Ø.Ø8	Ø.Ø9	Ø.	Ø.
Ø.1Ø	Ø.	Ø.	Ø.	Ø.	Ø.	Ø.

Ø.	Ø.Ø5	Ø.	Ø.	Ø.	Ø.	Ø.
Ø.	Ø.	Ø.Ø6	Ø.Ø5	Ø.	Ø.	Ø.
Ø.	Ø.	Ø.Ø5	Ø.Ø5	Ø.	Ø.	Ø.
Ø.Ø7	Ø.Ø6	Ø.Ø4	Ø.Ø6	Ø.	Ø.	Ø.
Ø.Ø4	Ø.Ø4	Ø.Ø5	Ø.	Ø.	Ø.	Ø.Ø5
Ø.Ø7	Ø.Ø4	Ø.Ø4	Ø.Ø7	Ø.	Ø.	Ø.
Ø.	Ø.Ø5	Ø.Ø3	Ø.Ø7	Ø.Ø5	Ø.	Ø.
Ø.Ø6	Ø.Ø5	Ø.Ø4	Ø.Ø6	Ø.Ø6	Ø.Ø5	Ø.Ø6
Ø.Ø5	Ø.Ø6	Ø.Ø5	Ø.Ø5	Ø.Ø7	Ø.	Ø.
Ø.	Ø.	Ø.	Ø.	Ø.	Ø.	Ø.

layer 3

Ø.11	Ø.14	Ø.12	Ø.13	Ø.	Ø.	Ø.
Ø.13	Ø.14	Ø.12	Ø.11	Ø.	Ø.	Ø.
Ø.11	Ø.13	Ø.Ø8	Ø.Ø9	Ø.11	Ø.	Ø.
Ø.Ø8	Ø.Ø7	Ø.1Ø	Ø.1Ø	Ø.	Ø.	Ø.
Ø.Ø7	Ø.Ø8	Ø.Ø8	Ø.1Ø	Ø.11	Ø.11	Ø.12
Ø.Ø8	Ø.Ø6	Ø.Ø7	Ø.Ø8	Ø.11	Ø.11	Ø.1Ø
Ø.Ø8	Ø.Ø6	Ø.Ø6	Ø.Ø7	Ø.Ø9	Ø.11	Ø.12
Ø.Ø9	Ø.Ø8	Ø.Ø7	Ø.Ø8	Ø.1Ø	Ø.12	Ø.12

Ø.Ø7	Ø.Ø8	Ø.Ø7	Ø.	Ø.	Ø.	Ø.
Ø.Ø8	Ø.Ø7	Ø.Ø7	Ø.Ø7	Ø.	Ø.	Ø.
Ø.Ø6	Ø.Ø7	Ø.Ø4	Ø.Ø6	Ø.	Ø.	Ø.
Ø.Ø4	Ø.Ø4	Ø.Ø5	Ø.Ø7	Ø.	Ø.	Ø.
Ø.Ø4	Ø.Ø4	Ø.Ø4	Ø.Ø6	Ø.	Ø.	Ø.Ø7
Ø.Ø4	Ø.Ø3	Ø.Ø4	Ø.Ø5	Ø.Ø7	Ø.	Ø.
Ø.Ø4	Ø.Ø3	Ø.Ø3	Ø.Ø5	Ø.Ø6	Ø.Ø7	Ø.
Ø.Ø5	Ø.Ø5	Ø.Ø4	Ø.Ø5	Ø.Ø7	Ø.Ø7	Ø.

Ø.1Ø	Ø.ØØ9	Ø.11	Ø.1Ø	Ø.11	Ø.	Ø.
Ø.12	Ø.12	Ø.	Ø.	Ø.	Ø.	Ø.

Ø.Ø5	Ø.Ø5	Ø.Ø6	Ø.Ø6	Ø.Ø6	Ø.	Ø.
Ø.	Ø.Ø8	Ø.	Ø.	Ø.	Ø.	Ø.

layer 4

Ø.13	Ø.12	Ø.11	Ø.11	Ø.	Ø.	Ø.
Ø.15	Ø.11	Ø.11	Ø.13	Ø.14	Ø.	Ø.
Ø.12	Ø.1Ø	Ø.Ø9	Ø.1Ø	Ø.11	Ø.12	Ø.
Ø.12	Ø.Ø9	Ø.Ø8	Ø.Ø8	Ø.1Ø	Ø.14	Ø.
Ø.11	Ø.Ø8	Ø.Ø8	Ø.Ø7	Ø.Ø9	Ø.11	Ø.12
Ø.1Ø	Ø.Ø7	Ø.Ø7	Ø.Ø7	Ø.Ø9	Ø.11	Ø.1Ø
Ø.12	Ø.Ø9	Ø.Ø7	Ø.Ø6	Ø.Ø9	Ø.11	Ø.13
Ø.11	Ø.Ø8	Ø.Ø9	Ø.1Ø	Ø.12	Ø.12	Ø.
Ø.	Ø.13	Ø.	Ø.	Ø.	Ø.	Ø.

Ø.Ø8	Ø.Ø7	Ø.Ø7	Ø.Ø7	Ø.	Ø.	Ø.
Ø.Ø9	Ø.Ø6	Ø.Ø6	Ø.Ø7	Ø.	Ø.	Ø.
Ø.Ø7	Ø.Ø6	Ø.Ø5	Ø.Ø7	Ø.	Ø.	Ø.
Ø.Ø6	Ø.Ø4	Ø.Ø4	Ø.Ø5	Ø.Ø7	Ø.	Ø.
Ø.Ø6	Ø.Ø4	Ø.Ø4	Ø.Ø4	Ø.Ø6	Ø.Ø7	Ø.
Ø.Ø5	Ø.Ø4	Ø.Ø4	Ø.Ø4	Ø.Ø6	Ø.Ø6	Ø.
Ø.Ø6	Ø.Ø4	Ø.Ø4	Ø.Ø4	Ø.Ø6	Ø.Ø6	Ø.
Ø.Ø6	Ø.Ø5	Ø.Ø5	Ø.Ø6	Ø.Ø7	Ø.	Ø.
Ø.	Ø.Ø7	Ø.	Ø.	Ø.	Ø.	Ø.

layer 5

Ø.16	Ø.15	Ø.13	Ø.13	Ø.15	Ø.	Ø.
Ø.	Ø.16	Ø.15	Ø.13	Ø.13	Ø.15	Ø.13
Ø.	Ø.15	Ø.14	Ø.12	Ø.13	Ø.14	Ø.14
Ø.	Ø.14	Ø.11	Ø.11	Ø.11	Ø.12	Ø.14
Ø.Ø9	Ø.13	Ø.11	Ø.1Ø	Ø.11	Ø.13	Ø.15
Ø.	Ø.14	Ø.11	Ø.11	Ø.12	Ø.14	Ø.
Ø.Ø8	Ø.14	Ø.12	Ø.11	Ø.12	Ø.15	Ø.
Ø.15	Ø.16	Ø.13	Ø.11	Ø.12	Ø.14	Ø.
Ø.14	Ø.14	Ø.14	Ø.	Ø.	Ø.	Ø.

Ø.Ø8	Ø.Ø8	Ø.Ø8	Ø.Ø8	Ø.	Ø.	Ø.
Ø.	Ø.Ø8	Ø.Ø8	Ø.Ø8	Ø.Ø9	Ø.	Ø.
Ø.	Ø.Ø9	Ø.Ø8	Ø.Ø8	Ø.Ø8	Ø.Ø9	Ø.Ø8
Ø.	Ø.Ø8	Ø.Ø6	Ø.Ø7	Ø.Ø7	Ø.Ø7	Ø.Ø9
Ø.Ø7	Ø.Ø8	Ø.Ø6	Ø.Ø6	Ø.Ø7	Ø.Ø7	Ø.Ø8
Ø.	Ø.Ø7	Ø.Ø6	Ø.Ø6	Ø.Ø7	Ø.Ø8	Ø.
Ø.Ø7	Ø.Ø8	Ø.Ø7	Ø.Ø6	Ø.Ø7	Ø.	Ø.
Ø.Ø9	Ø.Ø9	Ø.Ø8	Ø.Ø7	Ø.Ø7	Ø.	Ø.
Ø.Ø8	Ø.Ø9	Ø.Ø8	Ø.	Ø.	Ø.	Ø.

layer 6

Ø.	Ø.12	Ø.	Ø.
Ø.	Ø.13	Ø.15	Ø.

Ø.	Ø.Ø6	Ø.	Ø.
Ø.	Ø.Ø7	Ø.1Ø	Ø.

Ø.	Ø.14	Ø.13	Ø.13
Ø.	Ø.14	Ø.14	Ø.
Ø.	Ø.15	Ø.	Ø.

Ø.	Ø.Ø7	Ø.Ø7	Ø.Ø9
Ø.	Ø.Ø7	Ø.Ø8	Ø.
Ø.	Ø.	Ø.	Ø.

layer 7

Ø.	Ø.	Ø.	Ø.
Ø.	Ø.	Ø.	Ø.
Ø.	Ø.	Ø.14	Ø.11
Ø.	Ø.16	Ø.14	Ø.
Ø.	Ø.	Ø.	Ø.

Ø.	Ø.	Ø.	Ø.
Ø.	Ø.	Ø.	Ø.
Ø.	Ø.	Ø.1Ø	Ø.
Ø.	Ø.Ø9	Ø.Ø8	Ø.
Ø.	Ø.	Ø.	Ø.

layer 8

Ø.	Ø.
Ø.	Ø.12
Ø.	Ø.12

Ø.	Ø.
Ø.	Ø.Ø8
Ø.	Ø.Ø7

layer 9

Ø.	Ø.
Ø.	Ø.
Ø.	Ø.1Ø

Ø.	Ø.
Ø.	Ø.
Ø.	Ø.Ø7

HYPIT OUTPUT - 3rd INVERSION RUN

origin of cartesian coordinates				depth	strike
-16	Ø.	-72	Ø.	Ø.	62.5Ø

short distance conversions
one min lat 1.8443 km
one min lon 1.7839 km

ztr	wfac	wsum	swtfac	vthet	iwgt	iasn
Ø.	1.ØØØØ	1.ØØØØ	8.ØØ	5Ø.ØØØ	Ø	Ø

nl	neqs	ires	nkr	nmin	kfirst
9	419	1	Ø	2Ø	Ø

layer	depth	pvel	svel	p/s
1	-5.ØØ	5.25	3.Ø5	1.72
2	5.ØØ	6.Ø5	3.45	1.75
3	3Ø.ØØ	6.75	3.9Ø	1.73
4	6Ø.ØØ	7.1Ø	4.Ø5	1.75
5	8Ø.ØØ	7.7Ø	4.45	1.73
6	1ØØ.ØØ	7.9Ø	4.3Ø	1.84
7	13Ø.ØØ	7.9Ø	4.6Ø	1.72
8	16Ø.ØØ	7.9Ø	4.6Ø	1.72
9	19Ø.ØØ	7.9Ø	4.6Ø	1.72

	stn	wt	latitude	longitude	elev	pdelay	sdelay	flr	psed	ssed	dx	dy	dz
1	are	1.Ø	-16 27.73	-71 29.48	2452	Ø.	Ø.	Ø.	5.25	3.Ø5	-2Ø.28	71.79	-2.45
2	aye	1.Ø	-17 Ø.8Ø	-71 4Ø.31	24Ø	Ø.	Ø.	Ø.	5.25	3.Ø5	-83.33	82.77	-Ø.24
3	cab	1.Ø	-15 39.62	-71 56.66	377Ø	Ø.	Ø.	Ø.	5.25	3.Ø5	36.1Ø	-12.Ø6	-3.77
4	cal	1.Ø	-16 3.74	-71 22.21	395Ø	Ø.	Ø.	Ø.	5.25	3.Ø5	25.ØØ	62.96	-3.95
5	cay	1.Ø	-16 21.25	-71 46.45	17ØØ	Ø.	Ø.	Ø.	5.25	3.Ø5	-23.62	39.5Ø	-1.7Ø
6	cho	1.Ø	-15 8.ØØ	-71 47.71	45ØØ	Ø.	Ø.	Ø.	5.25	3.Ø5	95.23	-24.75	-4.5Ø
7	crv	1.Ø	-15 47.Ø7	-73 28.38	178Ø	Ø.	Ø.	Ø.	5.25	3.Ø5	-51.72	-151.ØØ	-1.78
8	llu	1.Ø	-16 1Ø.65	-72 2.11	18ØØ	Ø.	Ø.	Ø.	5.25	3.Ø5	-19.16	5.73	-1.8Ø
9	mol	1.Ø	-17 Ø.52	-72 2.88	5Ø	Ø.	Ø.	Ø.	5.25	3.Ø5	-1Ø1.36	47.Ø1	-Ø.Ø5
1Ø	ong	1.Ø	-15 53.94	-72 28.39	88Ø	Ø.	Ø.	Ø.	5.25	3.Ø5	-13.48	-5Ø.11	-Ø.88
11	pat	1.Ø	-15 45.47	-71 39.44	49ØØ	Ø.	Ø.	Ø.	5.25	3.Ø5	4Ø.73	2Ø.2Ø	-4.9Ø
12	rat	1.Ø	-15 45.33	-72 43.62	4ØØØ	Ø.	Ø.	Ø.	5.25	3.Ø5	-11.97	-81.6Ø	-4.ØØ
13	siq	1.Ø	-15 29.89	-72 45.Ø6	455Ø	Ø.	Ø.	Ø.	5.25	3.Ø5	12.Ø5	-97.12	-4.55
14	sis	1.Ø	-16 18.13	-72 4.85	1475	Ø.	Ø.	Ø.	5.25	3.Ø5	-33.65	7.78	-1.48
15	sgp	1.Ø	-16 33.87	-72 42.75	14Ø	Ø.	Ø.	Ø.	5.25	3.Ø5	-9Ø.52	-38.61	-Ø.14
16	tor	1.Ø	-16 2Ø.46	-72 28.25	35Ø	Ø.	Ø.	Ø.	5.25	3.Ø5	-56.7Ø	-27.2Ø	-Ø.35
17	yan	1.Ø	-15 32.Ø9	-71 21.Ø3	4Ø5Ø	Ø.	Ø.	Ø.	5.25	3.Ø5	77.83	38.Ø4	-4.Ø5
18	pin	1.Ø	-15 38.ØØ	-71 49.69	37ØØ	Ø.	Ø.	Ø.	5.25	3.Ø5	44.5Ø	-2.39	-3.7Ø
19	can	1.Ø	-16 29.62	-71 55.79	12ØØ	Ø.	Ø.	Ø.	5.25	3.Ø5	-45.ØØ	31.87	-1.2Ø
2Ø	con	1.Ø	-15 36.4Ø	-71 57.72	336Ø	Ø.	Ø.	Ø.	5.25	3.Ø5	4Ø.49	-16.48	-3.36

layer	NS ints	EW ints	P scale	S scale
1	9	9	1.ØØ	1.ØØ
2	8	11	1.ØØ	1.ØØ
3	8	11	1.ØØ	1.ØØ
4	8	1Ø	1.ØØ	1.ØØ
5	8	1Ø	1.ØØ	1.ØØ
6	5	6	1.ØØ	1.ØØ
7	5	6	1.ØØ	1.ØØ

```
  8        3        4      1.00      1.00
  9        3        4      1.00      1.00

1      NS vectors
  -165.00  -90.00  -55.00  -30.00    0.      20.00   45.00   90.00  165.00
       EW vectors
  -220.00 -110.00  -75.00  -45.00  -10.00    25.00   55.00  110.00  220.00

2      NS vectors
  -165.00  -82.50  -55.00  -27.50    0.      27.50   55.00  165.00
       EW vectors
  -220.00 -110.00  -88.00  -66.00  -44.00   -22.00    0.      22.00   44.00   82.50  220.00

3      NS vectors
  -165.00  -82.50  -55.00  -27.50    0.      27.50   55.00  165.00
       EW vectors
  -220.00 -110.00  -88.00  -66.00  -44.00   -22.00    0.      22.00   44.00   82.50  220.00

4      NS vectors
  -165.00  -82.50  -55.00  -27.50    0.      27.50   55.00  165.00
       EW vectors
  -220.00 -110.00  -88.00  -66.00  -44.00   -22.00    0.      27.50   82.50  220.00

5      NS vectors
  -165.00  -82.50  -55.00  -27.50    0.      27.50   55.00  165.00
       EW vectors
  -220.00 -110.00  -88.00  -66.00  -44.00   -22.00    0.      27.50   82.50  220.00

6      NS vectors
  -165.00  -55.00   15.00   85.00  165.00
       EW vectors
  -220.00 -140.00  -60.00   30.00  120.00   220.00

7      NS vectors
  -165.00  -55.00   15.00   85.00  165.00
       EW vectors
  -220.00 -140.00  -60.00   30.00  120.00   220.00

8      NS vectors
  -165.00    0.    165.00
       EW vectors
  -220.00  -70.00   70.00  220.00

9      NS vectors
  -165.00    0.    165.00
       EW vectors
  -220.00  -70.00   70.00  220.00

neqn = 419   nvar =   764   kvar =   292230

scale factors
 [illegible]     p scale    s scale
                 [illegible]    1.000
                 [illegible]    [illegible]
                 [illegible]    [illegible]
```

4	1.000	1.000
5	1.000	1.000
6	1.000	1.000
7	1.000	1.000
8	1.000	1.000
9	1.000	1.000

number of p arrivals	3559
p weight	1.0000
number of s arrivals	3009
s weight	0.5000
total number of arrivals	6568

p observation matrix

layer 1

0	27	231	0	0	0	0	0
0	0	0	315	137	0	0	0
0	0	0	226	0	0	0	0
316	578	111	11	0	25	41	101
0	0	362	405	0	170	4	0
114	0	150	326	1	11	126	0
0	156	0	48	37	101	0	0
0	0	0	0	0	0	0	0

layer 2

10	100	214	24	7	0	0
9	44	42	113	136	6	0
44	19	133	384	69	4	0
78	118	161	275	14	2	13
378	400	312	149	12	22	83
107	208	426	247	38	61	38
87	144	733	560	88	153	44
96	89	449	356	88	98	126
122	159	202	124	110	36	13
7	23	8	4	2	0	0

layer 3

76	123	174	68	18	0	0
62	162	164	69	23	11	3
87	206	194	98	61	21	11
103	269	305	170	70	21	25
332	346	386	202	98	56	52
366	380	399	250	120	75	62
146	238	297	261	123	75	61
85	160	201	149	69	54	29
67	180	170	59	36	27	11
1	60	34	13	4	4	0

s observation matrix

0	25	209	0	0	0	0	0
0	0	0	278	72	0	0	0
0	0	0	208	0	0	0	0
303	547	98	10	0	12	22	55
0	0	324	375	0	104	2	0
107	0	138	282	2	10	77	0
0	131	0	37	28	58	0	0
0	0	0	0	0	0	0	0

10	97	194	22	5	0	0
12	45	40	97	73	0	0
42	20	118	324	27	0	0
77	110	152	240	10	1	6
350	382	281	139	8	10	50
94	192	395	228	25	27	19
83	135	672	491	59	88	26
85	66	411	296	58	67	77
106	126	192	106	67	25	9
8	22	8	2	1	0	0

69	116	155	56	13	0	0
58	145	148	56	13	2	0
81	190	168	79	26	6	5
90	241	273	126	33	8	12
288	314	338	167	65	20	28
328	346	359	206	73	31	30
127	215	263	204	71	36	32
71	135	177	106	35	27	14
60	163	149	45	26	18	6
12	59	31	9	2	1	0

layer 4

5Ø	1Ø8	82	5Ø	32	7	1
Ø	124	122	73	38	17	7
1	89	146	1Ø5	55	33	22
13	64	151	156	1ØØ	64	39
23	117	2Ø5	163	124	7Ø	49
54	119	247	167	1Ø2	54	46
14	87	148	139	81	43	37
15	84	117	72	5Ø	29	21
3Ø	37	43	9	4	4	1

47	98	75	43	22	3	Ø
Ø	114	11Ø	55	27	8	1
1	84	133	76	29	17	8
13	59	141	124	56	34	16
23	1Ø9	185	131	76	34	3Ø
54	11Ø	227	127	68	33	29
13	82	132	11Ø	47	23	2Ø
13	78	1Ø5	57	29	18	9
28	34	4Ø	6	1	1	Ø

layer 5

Ø	35	73	77	47	17	2
Ø	49	81	78	66	35	29
Ø	3Ø	62	98	62	69	7Ø
Ø	3Ø	65	151	85	71	67
Ø	61	163	15Ø	97	71	57
1	18	144	126	95	69	35
1	19	73	125	81	5Ø	33
22	46	71	68	69	42	28
13	19	37	12	6	5	3

Ø	31	63	61	34	13	1
Ø	44	67	52	43	25	15
Ø	3Ø	55	72	38	51	35
Ø	3Ø	61	126	56	47	4Ø
Ø	56	146	122	63	43	43
1	18	128	99	65	41	24
1	17	66	1Ø7	57	25	18
19	41	64	66	47	25	12
13	15	33	9	2	1	1

layer 6

Ø	5Ø	9	Ø
Ø	147	166	27
1	413	335	68
14	152	111	9
6	27	4	Ø

Ø	34	6	Ø
Ø	117	111	13
1	334	215	41
12	122	67	4
5	2Ø	Ø	Ø

layer 7

Ø	Ø	Ø	Ø
Ø	Ø	Ø	Ø
Ø	13	114	22
1	61	13Ø	9
11	17	14	Ø

Ø	Ø	Ø	Ø
Ø	Ø	Ø	Ø
Ø	13	77	14
2	51	93	4
9	13	7	Ø

layer 8

Ø	Ø
Ø	51
6	85

Ø	Ø
Ø	32
4	55

layer 9

Ø	Ø
[illegible]	1
[illegible]	68

Ø	Ø
Ø	Ø
Ø	43

a total number of 609 blocks were hit
19745 elements of g are used

a total number of 465 blocks are kept for inversion
18345 elements of g are used

g diagonals for p velocity model

layer 1

Ø.	Ø.Ø3	3.46	Ø.	Ø.	Ø.	Ø.	Ø.
Ø.	Ø.	Ø.	9.96	5.44	Ø.	Ø.	Ø.
Ø.	Ø.	Ø.	2.49	Ø.	Ø.	Ø.	Ø.
Ø.98	4.14	Ø.27	Ø.	Ø.	Ø.78	Ø.39	2.31
Ø.	Ø.	6.75	8.24	Ø.	7.31	Ø.	Ø.
1.Ø5	Ø.	2.24	6.23	Ø.	Ø.	4.89	Ø.
Ø.	1.36	Ø.	1.2Ø	Ø.24	2.77	Ø.	Ø.
Ø.	Ø.	Ø.	Ø.	Ø.	Ø.	Ø.	Ø.

layer 2

Ø.	16.44	25.43	Ø.76	Ø.	Ø.	Ø.	
Ø.	Ø.26	2.97	7.21	4.56	Ø.	Ø.	
Ø.51	Ø.	6.58	23.Ø2	3.36	Ø.	Ø.	
5.33	6.Ø4	8.91	16.28	Ø.	Ø.	Ø.	
14.16	22.93	22.92	5.18	Ø.	2.Ø9	11.98	
5.99	12.92	28.37	16.33	2.32	3.22	4.11	
2.5Ø	7.Ø6	32.84	22.16	9.57	3.99	2.33	
8.76	3.98	25.91	19.72	7.13	7.22	9.26	
1Ø.53	19.5Ø	9.99	7.61	8.48	2.78	Ø.	
Ø.	2.Ø9	Ø.	Ø.	Ø.	Ø.	Ø.	

layer 3

1.44	4.78	1Ø.68	5.84	Ø.	Ø.	Ø.	
2.39	6.Ø7	9.79	2.96	1.29	Ø.	Ø.	
3.56	9.64	7.92	5.54	4.88	1.59	Ø.	
5.96	1Ø.93	15.27	11.32	5.39	1.15	1.83	
9.51	18.Ø3	21.52	11.49	7.51	3.35	3.34	
8.73	18.Ø5	24.51	15.61	8.84	4.62	5.62	
7.53	11.84	15.27	19.5Ø	9.56	5.25	3.17	
3.77	8.Ø4	8.34	9.62	3.9Ø	4.37	2.Ø4	
2.55	7.71	9.61	3.98	2.74	2.Ø7	Ø.	
Ø.	1.77	Ø.47	Ø.	Ø.	Ø.	Ø.	

layer 4

Ø.81	2.31	1.66	1.48	1.Ø5	Ø.	Ø.
Ø.	1.54	3.43	2.46	1.58	Ø.	Ø.
Ø.	1.45	4.3Ø	3.46	1.75	Ø.98	Ø.72
Ø	1.27	4.9Ø	5.Ø6	3.5Ø	2.Ø6	1.Ø6
Ø.23	1.96	5.65	6.4Ø	5.9Ø	2.33	1.83
Ø.12	1.66	7.43	5.34	3.79	2.Ø3	1.37
Ø	1.57	4.46	5.2Ø	3.6Ø	1.91	1.64

g diagonals for s velocity model

Ø.	Ø.Ø5	4.91	Ø.	Ø.	Ø.	Ø.	Ø.
Ø.	Ø.	Ø.	11.72	4.23	Ø.	Ø.	Ø.
Ø.	Ø.	Ø.	3.2Ø	Ø.	Ø.	Ø.	Ø.
1.23	5.Ø4	Ø.38	Ø.	Ø.	Ø.	Ø.36	1.69
Ø.	Ø.	8.28	1Ø.47	Ø.	6.68	Ø.	Ø.
1.47	Ø.	2.83	8.11	Ø.	Ø.	4.4Ø	Ø.
Ø.	1.78	Ø.	1.4Ø	Ø.32	2.Ø9	Ø.	Ø.
Ø.	Ø.	Ø.	Ø.	Ø.	Ø.	Ø.	Ø.

Ø.	25.67	34.46	1.Ø6	Ø.	Ø.	Ø.
Ø.	Ø.47	3.84	8.41	2.72	Ø.	Ø.
Ø.76	Ø.45	7.89	23.36	1.2Ø	Ø.	Ø.
6.11	8.13	11.69	19.74	Ø.	Ø.	Ø.
17.22	29.38	27.56	7.94	Ø.	Ø.	1Ø.Ø2
5.94	16.39	37.81	21.1Ø	2.6Ø	2.15	Ø.
3.87	8.95	42.96	25.28	1Ø.42	6.32	1.44
13.12	3.64	33.76	22.Ø2	7.56	7.Ø8	7.5Ø
12.4Ø	26.95	11.43	9.8Ø	6.99	2.7Ø	Ø.
Ø.	2.65	Ø.	Ø.	Ø.	Ø.	Ø.

1.31	5.75	13.6Ø	6.85	Ø.	Ø.	Ø.
3.27	8.27	12.83	3.16	Ø.	Ø.	Ø.
4.22	12.31	9.86	5.73	2.89	Ø.	Ø.
7.55	12.49	19.94	11.23	3.51	Ø.	Ø.
1Ø.48	2Ø.69	27.79	12.61	6.91	1.54	2.96
1Ø.2Ø	22.53	29.72	18.47	7.14	1.78	4.5Ø
7.36	15.89	2Ø.6Ø	22.95	7.46	3.Ø6	3.39
4.Ø3	1Ø.84	1Ø.25	1Ø.1Ø	2.7Ø	3.68	Ø.
2.42	1Ø.ØØ	1Ø.61	4.48	2.83	Ø.	Ø.
Ø.	2.21	Ø.5Ø	Ø.	Ø.	Ø.	Ø.

1.Ø4	2.88	2.Ø6	1.6Ø	Ø.75	Ø.	Ø.
Ø.	1.87	4.Ø3	2.45	1.79	Ø.	Ø.
Ø.	2.21	5.54	3.93	1.26	Ø.	Ø.
Ø.	1.66	6.29	4.73	2.84	1.41	Ø.
Ø.4Ø	2.98	6.98	7.48	4.54	1.6Ø	1.94
Ø.25	2.98	9.47	5.9Ø	3.11	1.52	1.43
Ø.	2.53	5.71	5.56	2.61	1.45	1.33

Ø.	2.75	4.23	3.25	2.23	1.47	Ø.84
Ø.24	Ø.92	1.24	Ø.	Ø.	Ø.	Ø.

layer 5

Ø.	Ø.ØØ8	Ø.8Ø	1.37	1.16	Ø.	Ø.
Ø.	Ø.Ø6	Ø.6Ø	1.16	1.11	Ø.74	Ø.38
Ø.	Ø.Ø2	Ø.68	2.42	1.95	1.7Ø	1.Ø7
Ø.	Ø.12	Ø.9Ø	3.15	2.Ø1	2.41	1.64
Ø.	Ø.13	2.Ø5	3.29	2.66	2.22	1.47
Ø.	Ø.	1.58	3.1Ø	3.12	2.42	1.Ø2
Ø.	Ø.	1.Ø2	3.39	2.51	1.61	Ø.96
Ø.24	Ø.59	1.24	2.61	2.36	1.19	Ø.74
Ø.	Ø.	Ø.81	Ø.	Ø.	Ø.	Ø.

layer 6

Ø.	Ø.26	Ø.	Ø.
Ø.	Ø.21	Ø.76	Ø.19
Ø.	5.51	5.1Ø	Ø.34
Ø.	5.11	4.44	Ø.
Ø.	Ø.41	Ø.	Ø.

layer 7

Ø.	Ø.	Ø.	Ø.
Ø.	Ø.	Ø.	Ø.
Ø.	Ø.	Ø.67	Ø.Ø9
Ø.	Ø.85	2.61	Ø.
Ø.	Ø.	Ø.	Ø.

layer 8

Ø.	Ø.
Ø.	Ø.65
Ø.	Ø.59

layer 9

Ø.	Ø.
Ø.	Ø.
Ø.	Ø.34

nvar, irnk, ier, are 465 465 Ø

residual norm	1268.84448
standard variance	Ø.2Ø789
original variance	Ø.2Ø791
residual variance	Ø.ØØ232
mod residual norm	12Ø5.84875
mod standard variance	Ø.27132
mod original variance	Ø.27239
mod residual variance	Ø.Ø9925
percentage improvement	6Ø.4Ø7Ø7
mod percentage improvement	63.56284

Ø.	3.22	5.37	3.25	1.82	Ø.	Ø.
Ø.23	Ø.97	1.59	Ø.	Ø.	Ø.	Ø.

Ø.	Ø.Ø9	1.21	1.61	1.Ø5	Ø.	Ø.
Ø.	Ø.16	Ø.85	1.21	Ø.93	Ø.7Ø	Ø.
Ø.	Ø.Ø5	Ø.89	2.66	1.58	1.44	Ø.99
Ø.	Ø.27	1.26	3.35	1.67	2.2Ø	1.68
Ø.	Ø.31	2.61	3.72	2.26	1.56	1.37
Ø.	Ø.	2.Ø7	3.Ø7	2.49	2.35	1.Ø2
Ø.	Ø.	1.37	3.49	2.31	Ø.93	Ø.
Ø.	Ø.73	1.56	3.36	2.Ø5	Ø.89	Ø.
Ø.	Ø.	Ø.89	Ø.	Ø.	Ø.	Ø.

Ø.	Ø.13	Ø.	Ø.
Ø.	Ø.23	1.Ø1	Ø.
Ø.	8.1Ø	6.96	Ø.36
Ø.	5.94	3.8Ø	Ø.
Ø.	Ø.56	Ø.	Ø.

Ø.	Ø.	Ø.	Ø.
Ø.	Ø.	Ø.	Ø.
Ø.	Ø.	1.Ø1	Ø.
Ø.	1.37	2.1Ø	Ø.
Ø.	Ø.	Ø.	Ø.

Ø.	Ø.
Ø.	Ø.8Ø
Ø.	Ø.75

Ø.	Ø.
Ø.	Ø.
Ø.	Ø.78

velocities for p velocity model

layer 1

Ø.	5.33	5.74	Ø.	Ø.	Ø.	Ø.	Ø.
Ø.	Ø.	Ø.	5.74	5.Ø9	Ø.	Ø.	Ø.
Ø.	Ø.	Ø.	4.62	Ø.	Ø.	Ø.	Ø.
5.Ø6	5.11	5.47	Ø.	Ø.	5.27	5.Ø1	5.37
Ø.	Ø.	5.11	6.1Ø	Ø.	5.ØØ	Ø.	Ø.
5.38	Ø.	4.27	6.32	Ø.	Ø.	5.Ø9	Ø.
Ø.	5.44	Ø.	5.89	4.87	5.13	Ø.	Ø.
Ø.	Ø.	Ø.	Ø.	Ø.	Ø.	Ø.	Ø.

layer 2

Ø.	6.74	7.49	6.29	Ø.	Ø.	Ø.
Ø.	6.71	6.66	6.23	6.3Ø	Ø.	Ø.
6.8Ø	Ø.	6.35	6.14	6.2Ø	Ø.	Ø.
6.71	6.48	6.55	6.31	Ø.	Ø.	Ø.
6.56	6.68	6.7Ø	6.43	Ø.	6.Ø6	6.18
6.61	6.46	6.39	6.32	5.9Ø	6.29	6.12
6.51	6.51	6.42	6.3Ø	5.94	6.13	6.12
6.92	6.57	6.4Ø	6.22	6.11	5.95	6.23
6.67	6.59	6.44	6.21	5.98	5.89	Ø.
Ø.	6.56	Ø.	Ø.	Ø.	Ø.	Ø.

layer 3

7.85	7.49	7.38	6.55	Ø.	Ø.	Ø.
7.3Ø	7.82	7.4Ø	6.76	6.7Ø	Ø.	Ø.
7.19	7.74	7.28	6.35	6.34	6.27	Ø.

velocities for s velocity model

Ø.	3.Ø4	3.34	Ø.	Ø.	Ø.	Ø.	Ø.
Ø.	Ø.	Ø.	3.39	2.91	Ø.	Ø.	Ø.
Ø.	Ø.	Ø.	3.ØØ	Ø.	Ø.	Ø.	Ø.
3.27	3.33	3.15	Ø.	Ø.	Ø.	3.Ø5	3.ØØ
Ø.	Ø.	2.99	3.26	Ø.	3.Ø1	Ø.	Ø.
3.34	Ø.	2.85	3.36	Ø.	Ø.	2.88	Ø.
Ø.	3.17	Ø.	3.24	2.82	3.1Ø	Ø.	Ø.
Ø.	Ø.	Ø.	Ø.	Ø.	Ø.	Ø.	Ø.

Ø.	4.ØØ	4.21	3.65	Ø.	Ø.	Ø.
Ø.	3.68	3.73	3.72	3.58	Ø.	Ø.
3.71	3.76	3.67	3.52	3.41	Ø.	Ø.
3.96	3.74	3.69	3.59	Ø.	Ø.	Ø.
3.8Ø	3.9Ø	3.81	3.66	Ø.	Ø.	3.5Ø
3.74	3.74	3.74	3.72	3.53	3.56	Ø.
3.67	3.71	3.67	3.65	3.51	3.49	3.64
4.Ø7	3.89	3.67	3.65	3.71	3.56	3.47
3.86	3.74	3.73	3.71	3.61	3.55	Ø.
Ø.	3.81	Ø.	Ø.	Ø.	Ø.	Ø.

4.54	4.46	4.41	4.Ø1	Ø.	Ø.	Ø.
4.24	4.47	4.38	3.89	Ø.	Ø.	Ø.
4.13	4.35	4.38	3.94	4.ØØ	Ø.	Ø.

7.71	7.44	7.40	6.64	6.49	6.71	7.01
7.58	7.65	7.69	6.63	6.53	6.69	6.94
7.46	7.53	7.49	6.66	6.36	6.77	6.64
7.80	7.31	7.14	6.48	6.43	6.83	6.75
7.27	7.35	6.98	6.53	6.50	6.80	6.75
7.88	6.72	7.11	6.41	6.68	6.52	0.
0.	7.47	6.85	0.	0.	0.	0.

4.21	4.25	4.31	3.91	4.02	0.	0.
4.14	4.48	4.44	3.94	3.75	3.76	3.92
4.20	4.39	4.34	3.96	3.79	3.79	3.93
4.28	4.26	4.17	3.91	3.82	3.99	4.09
4.18	4.27	4.08	3.88	3.84	3.94	0.
4.29	4.08	4.04	3.75	3.99	0.	0.
0.	4.42	3.85	0.	0.	0.	0.

layer 4

7.63	7.69	7.59	7.32	7.33	0.	0.
0.	7.54	7.47	7.34	7.21	0.	0.
0.	7.75	7.70	7.72	7.15	7.46	7.33
0.	7.76	7.44	7.50	7.19	7.09	7.32
7.78	7.74	7.54	7.40	7.18	7.20	7.18
7.72	7.74	7.65	7.65	7.18	7.24	7.20
0.	7.63	7.71	7.55	7.28	7.30	7.48
0.	7.63	7.58	7.45	7.16	7.39	7.17
7.92	7.56	6.95	0.	0.	0.	0.

4.47	4.38	4.41	4.04	4.17	0.	0.
0.	4.36	4.29	4.31	4.25	0.	0.
0.	4.56	4.33	4.42	4.17	0.	0.
0.	4.43	4.24	4.38	4.10	4.23	0.
4.32	4.57	4.40	4.33	4.27	4.03	4.03
4.48	4.42	4.48	4.41	4.12	4.17	4.09
0.	4.43	4.38	4.38	4.11	4.09	4.19
0.	4.47	4.38	4.35	3.89	0.	0.
4.57	4.25	4.10	0.	0.	0.	0.

layer 5

0.	7.76	7.65	7.55	7.65	0.	0.
0.	7.93	7.78	7.82	7.56	7.35	7.60
0.	7.81	7.54	7.92	8.20	7.93	7.44
0.	7.35	7.18	7.61	7.98	7.65	7.68
0.	7.50	7.57	7.80	7.70	7.81	8.05
0.	0.	7.85	7.85	7.99	7.95	7.85
0.	0.	7.76	8.04	7.66	7.98	7.50
8.42	7.43	7.97	7.90	7.66	7.62	7.76

0.	4.43	4.47	4.48	4.43	0.	0.
0.	4.51	4.52	4.34	4.50	4.33	0.
0.	4.48	4.60	4.57	4.49	4.56	4.35
0.	4.86	4.43	4.45	4.60	4.14	4.41
0.	4.67	4.50	4.54	4.44	4.51	4.25
0.	0.	4.49	4.59	4.28	4.41	4.46
0.	0.	4.87	4.82	4.35	4.28	0.
0.	4.48	4.69	4.61	4.24	4.31	0.

Ø.	Ø.	7.29	Ø.	Ø.	Ø.	Ø.

Ø.	Ø.	4.12	Ø.	Ø.	Ø.	Ø.

layer 6

Ø.	7.65	Ø.	Ø.
Ø.	7.71	7.75	8.4Ø
Ø.	8.16	8.33	7.62
Ø.	8.16	8.14	Ø.
Ø.	8.Ø2	Ø.	Ø.

Ø.	4.42	Ø.	Ø.
Ø.	4.18	4.76	Ø.
Ø.	4.51	4.57	4.62
Ø.	4.43	4.41	Ø.
Ø.	4.33	Ø.	Ø.

layer 7

Ø.	Ø.	Ø.	Ø.
Ø.	Ø.	Ø.	Ø.
Ø.	Ø.	7.82	8.34
Ø.	8.13	7.89	Ø.
Ø.	Ø.	Ø.	Ø.

Ø.	Ø.	Ø.	Ø.
Ø.	Ø.	Ø.	Ø.
Ø.	Ø.	4.9Ø	Ø.
Ø.	4.62	4.52	Ø.
Ø.	Ø.	Ø.	Ø.

layer 8

Ø.	Ø.
Ø.	7.93
Ø.	8.Ø9

Ø.	Ø.
Ø.	4.57
Ø.	4.52

layer 9

Ø.	Ø.
Ø.	Ø.
Ø.	7.87

Ø.	Ø.
Ø.	Ø.
Ø.	4.71

%fraction change for p velocity model

%fraction change for s velocity model

layer 1

Ø.	-1.25	8.36	Ø.	Ø.	Ø.	Ø.	Ø.
Ø.	Ø.	Ø.	1Ø.34	-2.13	Ø.	Ø.	Ø.
Ø.	Ø.	Ø.	-11.14	Ø.	Ø.	Ø.	Ø.
-6.25	-5.4Ø	3.24	Ø.	Ø.	1.41	-3.72	3.18
Ø.	Ø.	-3.6Ø	17.27	Ø.	-3.91	Ø.	Ø.
-Ø.38	Ø.	-19.46	21.54	Ø.	Ø.	-2.Ø7	Ø.
Ø.	Ø.66	Ø.	13.33	-6.3Ø	-1.33	Ø.	Ø.
Ø.	Ø.	Ø.	Ø.	Ø.	Ø.	Ø.	Ø.

Ø.	-2.Ø7	9.36	Ø.	Ø.	Ø.	Ø.	Ø.
Ø.	Ø.	Ø.	12.93	-2.89	Ø.	Ø.	Ø.
Ø.	Ø.	Ø.	-Ø.Ø6	Ø.	Ø.	Ø.	Ø.
5.49	7.43	3.29	Ø.	Ø.	Ø.	1.51	Ø.13
Ø.	Ø.	-1.94	8.53	Ø.	Ø.34	Ø.	Ø.
7.7Ø	Ø.	-6.64	11.85	Ø.	Ø.	-3.83	Ø.
Ø.	2.33	Ø.	7.87	-6.14	3.33	Ø.	Ø.
Ø.	Ø.	Ø.	Ø.	Ø.	Ø.	Ø.	Ø.

layer 2

Ø.	4.51	18.93	Ø.67	Ø.	Ø.	Ø.
Ø.	4.Ø4	5.75	-Ø.29	1.68	Ø.	Ø.
1.46	Ø.	Ø.72	-1.68	-Ø.Ø1	Ø.	Ø.
Ø.13	Ø.51	3.89	Ø.95	Ø.	Ø.	Ø.
-2.Ø6	3.54	6.3Ø	2.83	Ø.	-2.18	-Ø.27
-1.41	Ø.Ø9	1.51	1.19	-4.89	1.46	-1.25
-2.81	Ø.9Ø	-1.2Ø	Ø.72	-4.24	-1.17	-1.31
3.3Ø	1.78	1.67	-Ø.5Ø	-1.52	-4.ØØ	Ø.43
-Ø.47	2.11	2.16	-Ø.64	-3.5Ø	-5.Ø6	Ø.
Ø.	1.64	Ø.	Ø.	Ø.	Ø.	Ø.

Ø.	8.15	17.ØØ	1.45	Ø.	Ø.	Ø.
Ø.	-Ø.44	3.68	3.22	Ø.79	Ø.	Ø.
-3.76	1.71	1.81	-2.Ø9	-3.84	Ø.	Ø.
2.87	Ø.97	2.46	-Ø.32	Ø.	Ø.	Ø.
-1.35	5.38	5.83	1.74	Ø.	Ø.	-1.34
-2.75	1.Ø1	3.88	3.45	-Ø.56	Ø.34	Ø.
-4.59	Ø.17	1.92	1.36	-1.Ø1	-1.81	2.4Ø
5.73	5.12	2.Ø2	1.28	4.59	Ø.22	-2.32
Ø.23	1.Ø7	3.53	3.13	1.8Ø	Ø.Ø1	Ø.
Ø.	3.Ø2	Ø.	Ø.	Ø.	Ø.	Ø.

layer 3

3.33	3.33	5.44	-4.31	Ø.	Ø.	Ø.
-4.ØØ	7.85	5.77	-1.27	-Ø.79	Ø.	Ø.
-1.42	6.71	3.93	-7.34	-6.Ø3	-6.45	Ø.
1.41	2.65	5.69	-3.ØØ	-3.79	Ø.Ø9	4.7Ø
-Ø.26	5.5Ø	9.82	-3.18	-3.27	-Ø.11	3.62

4.42	7.37	1Ø.32	2.9Ø	Ø.	Ø.	Ø.
-2.61	7.73	9.39	-Ø.18	Ø.	Ø.	Ø.
-5.16	4.87	9.46	1.Ø8	2.48	Ø.	Ø.
-3.21	2.36	7.65	Ø.3Ø	3.19	Ø.	Ø.
-4.82	7.92	11.Ø8	1.ØØ	-3.81	-2.28	1.93

-1.82	3.82	6.93	-2.77	-5.78	Ø.98	-Ø.84
2.66	Ø.82	2.ØØ	-5.39	-4.71	1.96	Ø.82
-4.35	1.4Ø	-Ø.27	-4.71	-3.74	1.55	Ø.72
3.64	-7.27	1.54	-6.47	-1.ØØ	-2.64	Ø.
Ø.	3.Ø8	-2.13	Ø.	Ø.	Ø.	Ø.

-3.54	5.67	8.53	1.51	-2.85	-1.64	2.Ø3
-1.59	2.55	4.32	Ø.28	-2.17	3.51	6.34
-3.91	2.89	2.Ø2	-Ø.4Ø	-1.41	2.31	Ø.
-1.41	-1.77	Ø.99	-3.78	2.38	Ø.	Ø.
Ø.	6.5Ø	-3.78	Ø.	Ø.	Ø.	Ø.

layer 4

-1.59	1.19	1.89	-Ø.35	1.16	Ø.	Ø.
Ø.	-Ø.73	Ø.21	-Ø.Ø8	-Ø.62	Ø.	Ø.
Ø.	2.Ø4	3.32	5.Ø1	-1.31	2.9Ø	1.13
Ø.	2.Ø9	-Ø.Ø7	2.Ø8	-Ø.81	-2.18	Ø.91
Ø.39	1.88	1.23	Ø.7Ø	-1.Ø3	-Ø.71	-Ø.9Ø
-Ø.45	1.79	2.64	4.1Ø	-Ø.99	-Ø.13	-Ø.73
Ø.	Ø.44	3.49	2.69	Ø.45	Ø.63	3.18
Ø.	Ø.36	1.69	1.41	-1.25	1.96	-1.Ø8
2.23	-Ø.53	-6.74	Ø.	Ø.	Ø.	Ø.

Ø.35	Ø.77	3.68	-3.78	-Ø.67	Ø.	Ø.
Ø.	Ø.24	Ø.89	2.6Ø	1.11	Ø.	Ø.
Ø.	4.76	1.98	5.27	-Ø.73	Ø.	Ø.
Ø.	1.84	-Ø.31	4.19	-2.27	1.92	Ø.
-2.88	4.99	3.63	3.19	1.7Ø	-2.77	-2.78
Ø.7Ø	1.72	5.34	4.97	-1.97	Ø.4Ø	-1.55
Ø.	1.89	3.Ø4	4.17	-2.25	-1.35	Ø.98
Ø.	2.68	3.ØØ	3.56	-7.42	Ø.	Ø.
2.64	-2.28	-3.43	Ø.	Ø.	Ø.	Ø.

layer 5

Ø.	Ø.14	-Ø.62	-1.94	-Ø.67	Ø.	Ø.
Ø.	2.28	1.Ø6	1.6Ø	-1.77	-4.59	-1.36
Ø.	Ø.84	-2.Ø4	2.88	6.47	3.Ø4	-3.41
Ø.	-5.17	-6.7Ø	-1.15	3.7Ø	-Ø.71	-Ø.23
Ø.	-3.2Ø	-1.62	1.24	Ø.Ø4	1.41	4.56
Ø.	Ø.	1.91	1.98	3.73	3.19	1.97
Ø.	Ø.	Ø.73	4.37	-Ø.5Ø	3.7Ø	-2.54
7.9Ø	-4.Ø9	3.5Ø	2.6Ø	-Ø.53	-1.Ø7	Ø.77
Ø.	Ø.	-5.37	Ø.	Ø.	Ø.	Ø.

Ø.	-Ø.45	1.23	1.42	Ø.67	Ø.	Ø.
Ø.	1.34	2.29	-1.79	2.2Ø	-1.67	Ø.
Ø.	Ø.73	4.Ø6	3.35	2.1Ø	3.74	-1.Ø5
Ø.	9.23	Ø.29	Ø.71	4.51	-5.95	Ø.27
Ø.	5.Ø3	1.81	2.62	Ø.97	2.49	-3.48
Ø.	Ø.	1.48	3.87	-2.68	Ø.31	1.43
Ø.	Ø.	1Ø.22	9.Ø2	-1.17	-2.83	Ø.
Ø.	Ø.67	6.Ø6	4.3Ø	-3.57	-1.94	Ø.
Ø.	Ø.	-6.68	Ø.	Ø.	Ø.	Ø.

layer 6

Ø.	-3.16	Ø.	Ø.	Ø.	2.71	Ø.	Ø.
Ø.	-2.41	-1.96	6.39	Ø.	-2.87	1Ø.7Ø	Ø.
Ø.	3.34	5.5Ø	-3.59	Ø.	4.91	6.19	7.36
Ø.	3.34	3.Ø1	Ø.	Ø.	3.Ø1	2.5Ø	Ø.
Ø.	1.51	Ø.	Ø.	Ø.	Ø.6Ø	Ø.	Ø.

layer 7

Ø.	Ø.	Ø.	Ø.	Ø.	Ø.	Ø.	Ø.
Ø.	Ø.	Ø.	Ø.	Ø.	Ø.	Ø.	Ø.
Ø.	Ø.	-Ø.97	5.62	Ø.	Ø.	6.49	Ø.
Ø.	2.89	-Ø.13	Ø.	Ø.	Ø.48	-1.72	Ø.
Ø.	Ø.	Ø.	Ø.	Ø.	Ø.	Ø.	Ø.

layer 8

Ø.	Ø.	Ø.	Ø.
Ø.	Ø.38	Ø.	-Ø.55
Ø.	2.4Ø	Ø.	-1.74

layer 9

Ø.	Ø.	Ø.	Ø.
Ø.	Ø.	Ø.	Ø.
Ø.	-Ø.33	Ø.	2.37

ires = 1 kmin = 1 kmax = 465

sum of diagonal elements of resolution matrix for 465 elements = 317.892

resolution for p velocity model

resolution for s velocity model

layer 1

Ø.	Ø.Ø3	Ø.17	Ø.	Ø.	Ø.	Ø.	Ø.
Ø.	Ø.	Ø.	Ø.76	Ø.61	Ø.	Ø.	Ø.
Ø.	Ø.	Ø.	Ø.48	Ø.	Ø.	Ø.	Ø.
Ø.29	Ø.55	Ø.23	Ø.	Ø.	Ø.43	Ø.16	Ø.23
Ø.	Ø.	Ø.8Ø	Ø.81	Ø.	Ø.69	Ø.	Ø.
Ø.32	Ø.	Ø.68	Ø.77	Ø.	Ø.	Ø.48	Ø.
Ø.	Ø.31	Ø.	Ø.49	Ø.2Ø	Ø.42	Ø.	Ø.
Ø.	Ø.	Ø.	Ø.	Ø.	Ø.	Ø.	Ø.

Ø.	Ø.Ø3	Ø.19	Ø.	Ø.	Ø.	Ø.	Ø.
Ø.	Ø.	Ø.	Ø.78	Ø.58	Ø.	Ø.	Ø.
Ø.	Ø.	Ø.	Ø.51	Ø.	Ø.	Ø.	Ø.
Ø.32	Ø.6Ø	Ø.31	Ø.	Ø.	Ø.	Ø.19	Ø.32
Ø.	Ø.	Ø.82	Ø.83	Ø.	Ø.68	Ø.	Ø.
Ø.36	Ø.	Ø.73	Ø.81	Ø.	Ø.	Ø.45	Ø.
Ø.	Ø.35	Ø.	Ø.52	Ø.23	Ø.43	Ø.	Ø.
Ø.	Ø.	Ø.	Ø.	Ø.	Ø.	Ø.	Ø.

layer 2

Ø.	Ø.83	Ø.82	Ø.46	Ø.	Ø.	Ø.
Ø.	Ø.19	Ø.8Ø	Ø.84	Ø.69	Ø.	Ø.
Ø.32	Ø.	Ø.86	Ø.91	Ø.71	Ø.	Ø.
Ø.8Ø	Ø.86	Ø.9Ø	Ø.91	Ø.	Ø.	Ø.
Ø.9Ø	Ø.93	Ø.95	Ø.84	Ø.	Ø.68	Ø.8Ø
Ø.89	Ø.94	Ø.96	Ø.93	Ø.76	Ø.79	Ø.71
Ø.77	Ø.91	Ø.97	Ø.94	Ø.86	Ø.86	Ø.6Ø
Ø.85	Ø.83	Ø.96	Ø.94	Ø.86	Ø.84	Ø.7Ø
Ø.91	Ø.91	Ø.9Ø	Ø.88	Ø.82	Ø.72	Ø.
Ø.	Ø.56	Ø.	Ø.	Ø.	Ø.	Ø.

Ø.	Ø.85	Ø.84	Ø.51	Ø.	Ø.	Ø.
Ø.	Ø.29	Ø.83	Ø.85	Ø.63	Ø.	Ø.
Ø.38	Ø.39	Ø.88	Ø.91	Ø.54	Ø.	Ø.
Ø.81	Ø.89	Ø.92	Ø.92	Ø.	Ø.	Ø.
Ø.92	Ø.94	Ø.96	Ø.88	Ø.	Ø.	Ø.81
Ø.89	Ø.95	Ø.97	Ø.95	Ø.81	Ø.76	Ø.
Ø.82	Ø.93	Ø.98	Ø.96	Ø.86	Ø.83	Ø.46
Ø.88	Ø.85	Ø.97	Ø.95	Ø.87	Ø.82	Ø.71
Ø.92	Ø.93	Ø.92	Ø.91	Ø.82	Ø.74	Ø.
Ø.	Ø.6Ø	Ø.	Ø.	Ø.	Ø.	Ø.

layer 3

Ø.58	Ø.8Ø	Ø.83	Ø.78	Ø.	Ø.	Ø.
Ø.63	Ø.82	Ø.89	Ø.76	Ø.61	Ø.	Ø.
Ø.78	Ø.87	Ø.9Ø	Ø.87	Ø.81	Ø.65	Ø.
Ø.87	Ø.92	Ø.94	Ø.92	Ø.85	Ø.61	Ø.57
Ø.89	Ø.95	Ø.96	Ø.93	Ø.89	Ø.79	Ø.67
Ø.9Ø	Ø.91	Ø.97	Ø.94	Ø.9Ø	Ø.84	Ø.77

Ø.56	Ø.83	Ø.84	Ø.78	Ø.	Ø.	Ø.
Ø.65	Ø.85	Ø.9Ø	Ø.77	Ø.	Ø.	Ø.
Ø.77	Ø.88	Ø.92	Ø.87	Ø.74	Ø.	Ø.
Ø.87	Ø.93	Ø.95	Ø.92	Ø.8Ø	Ø.	Ø.
Ø.9Ø	Ø.95	Ø.97	Ø.94	Ø.89	Ø.65	Ø.67
Ø.91	Ø.96	Ø.97	Ø.95	Ø.89	Ø.71	Ø.78

Ø.91	Ø.93	Ø.95	Ø.95	Ø.91	Ø.84	Ø.7Ø	Ø.9Ø	Ø.95	Ø.96	Ø.95	Ø.9Ø	Ø.76	Ø.72
Ø.83	Ø.9Ø	Ø.92	Ø.92	Ø.82	Ø.78	Ø.62	Ø.84	Ø.92	Ø.94	Ø.92	Ø.79	Ø.75	Ø.
Ø.76	Ø.89	Ø.91	Ø.84	Ø.76	Ø.66	Ø.	Ø.74	Ø.91	Ø.93	Ø.84	Ø.76	Ø.	Ø.
Ø.	Ø.54	Ø.4Ø	Ø.	Ø.	Ø.	Ø.	Ø.	Ø.58	Ø.39	Ø.	Ø.	Ø.	Ø.

layer 4

Ø.5Ø	Ø.7Ø	Ø.63	Ø.55	Ø.54	Ø.	Ø.	Ø.56	Ø.73	Ø.69	Ø.58	Ø.44	Ø.	Ø.
Ø.	Ø.64	Ø.78	Ø.71	Ø.63	Ø.	Ø.	Ø.	Ø.67	Ø.81	Ø.72	Ø.66	Ø.	Ø.
Ø.	Ø.64	Ø.82	Ø.78	Ø.67	Ø.56	Ø.47	Ø.	Ø.7Ø	Ø.85	Ø.8Ø	Ø.64	Ø.	Ø.
Ø.	Ø.64	Ø.85	Ø.85	Ø.8Ø	Ø.7Ø	Ø.53	Ø.	Ø.68	Ø.88	Ø.85	Ø.78	Ø.64	Ø.
Ø.25	Ø.71	Ø.86	Ø.87	Ø.84	Ø.72	Ø.59	Ø.37	Ø.78	Ø.89	Ø.88	Ø.82	Ø.64	Ø.6Ø
Ø.17	Ø.69	Ø.88	Ø.85	Ø.8Ø	Ø.69	Ø.54	Ø.29	Ø.77	Ø.91	Ø.87	Ø.76	Ø.64	Ø.55
Ø.	Ø.66	Ø.83	Ø.83	Ø.77	Ø.64	Ø.54	Ø.	Ø.75	Ø.87	Ø.85	Ø.73	Ø.58	Ø.59
Ø.	Ø.77	Ø.8Ø	Ø.73	Ø.57	Ø.51	Ø.44	Ø.	Ø.8Ø	Ø.83	Ø.72	Ø.55	Ø.	Ø.
Ø.27	Ø.53	Ø.58	Ø.	Ø.	Ø.	Ø.	Ø.26	Ø.54	Ø.65	Ø.	Ø.	Ø.	Ø.

layer 5

Ø.	Ø.13	Ø.46	Ø.56	Ø.57	Ø.	Ø.	Ø.	Ø.13	Ø.56	Ø.63	Ø.58	Ø.	Ø.
Ø.	Ø.Ø8	Ø.46	Ø.6Ø	Ø.57	Ø.49	Ø.34	Ø.	Ø.19	Ø.51	Ø.61	Ø.54	Ø.45	Ø.
Ø.	Ø.Ø4	Ø.45	Ø.72	Ø.71	Ø.67	Ø.52	Ø.	Ø.Ø8	Ø.5Ø	Ø.74	Ø.67	Ø.62	Ø.54
Ø.	Ø.15	Ø.55	Ø.77	Ø.73	Ø.73	Ø.63	Ø.	Ø.28	Ø.63	Ø.78	Ø.7Ø	Ø.73	Ø.67
Ø.	Ø.15	Ø.67	Ø.79	Ø.76	Ø.72	Ø.6Ø	Ø.	Ø.3Ø	Ø.73	Ø.81	Ø.73	Ø.64	Ø.61
Ø.	Ø.	Ø.63	Ø.77	Ø.78	Ø.74	Ø.53	Ø.	Ø.	Ø.69	Ø.78	Ø.75	Ø.73	Ø.54
Ø.	Ø.	Ø.55	Ø.76	Ø.73	Ø.61	Ø.47	Ø.	Ø.	Ø.64	Ø.77	Ø.71	Ø.52	Ø.
Ø.28	Ø.46	Ø.56	Ø.68	Ø.61	Ø.48	Ø.43	Ø.	Ø.5Ø	Ø.63	Ø.72	Ø.61	Ø.53	Ø.
Ø.	Ø.	Ø.49	Ø.	Ø.	Ø.	Ø.	Ø.	Ø.	Ø.52	Ø.	Ø.	Ø.	Ø.

layer 6

Ø.	Ø.27	Ø.	Ø.	Ø.	Ø.14	Ø.	Ø.
Ø.	Ø.23	Ø.44	Ø.22	Ø.	Ø.25	Ø.41	Ø.
Ø.	Ø.77	Ø.77	Ø.26	Ø.	Ø.83	Ø.82	Ø.27
Ø.	Ø.74	Ø.74	Ø.	Ø.	Ø.78	Ø.74	Ø.
Ø.	Ø.34	Ø.	Ø.	Ø.	Ø.4Ø	Ø.	Ø.

layer 7

Ø.	Ø.	Ø.	Ø.	Ø.	Ø.	Ø.	Ø.
Ø.	Ø.	Ø.	Ø.	Ø.	Ø.	Ø.	Ø.
Ø.	Ø.	Ø.4Ø	Ø.12	Ø.	Ø.	Ø.49	Ø.
Ø.	Ø.46	Ø.69	Ø.	Ø.	Ø.55	Ø.66	Ø.
Ø.	Ø.	Ø.	Ø.	Ø.	Ø.	Ø.	Ø.

layer 8

Ø.	Ø.	Ø.	Ø.
Ø.	Ø.34	Ø.	Ø.38
Ø.	Ø.31	Ø.	Ø.37

layer 9

Ø.	Ø.	Ø.	Ø.
Ø.	Ø.	Ø.	Ø.
Ø.	Ø.2Ø	Ø.	Ø.34

standard error for p velocity model

layer 1

Ø	Ø.Ø3	Ø.Ø6	Ø.	Ø.	Ø.	Ø.	Ø.
Ø	Ø.	Ø.	Ø.Ø9	Ø.Ø7	Ø.	Ø.	Ø.

standard error for s velocity model

Ø.	Ø.Ø2	Ø.Ø4	Ø.	Ø.	Ø.	Ø.	Ø.
Ø.	Ø.	Ø.	Ø.Ø5	Ø.Ø4	Ø.	Ø.	Ø.

Ø.	Ø.	Ø.	Ø.Ø8	Ø.	Ø.	Ø.	Ø.
Ø.Ø9	Ø.Ø9	Ø.1Ø	Ø.	Ø.	Ø.1Ø	Ø.Ø6	Ø.Ø6
Ø.	Ø.	Ø.Ø7	Ø.1Ø	Ø.	Ø.Ø8	Ø.	Ø.
Ø.Ø9	Ø.	Ø.Ø6	Ø.12	Ø.	Ø.	Ø.Ø8	Ø.
Ø.	Ø.Ø9	Ø.	Ø.13	Ø.Ø7	Ø.Ø8	Ø.	Ø.
Ø.	Ø.	Ø.	Ø.	Ø.	Ø.	Ø.	Ø.

Ø.	Ø.	Ø.	Ø.Ø6	Ø.	Ø.	Ø.	Ø.
Ø.Ø6	Ø.Ø6	Ø.Ø6	Ø.	Ø.	Ø.	Ø.Ø5	Ø.Ø5
Ø.	Ø.	Ø.Ø4	Ø.Ø5	Ø.	Ø.Ø5	Ø.	Ø.
Ø.Ø6	Ø.	Ø.Ø5	Ø.Ø5	Ø.	Ø.	Ø.Ø4	Ø.
Ø.	Ø.Ø6	Ø.	Ø.Ø7	Ø.Ø5	Ø.Ø5	Ø.	Ø.
Ø.	Ø.	Ø.	Ø.	Ø.	Ø.	Ø.	Ø.

layer 2

Ø.	Ø.Ø8	Ø.1Ø	Ø.13	Ø.	Ø.	Ø.
Ø.	Ø.11	Ø.12	Ø.Ø9	Ø.1Ø	Ø.	Ø.
Ø.13	Ø.	Ø.Ø9	Ø.Ø6	Ø.11	Ø.	Ø.
Ø.1Ø	Ø.Ø9	Ø.Ø8	Ø.Ø7	Ø.	Ø.	Ø.
Ø.Ø8	Ø.Ø7	Ø.Ø6	Ø.1Ø	Ø.	Ø.11	Ø.Ø7
Ø.Ø9	Ø.Ø6	Ø.Ø5	Ø.Ø7	Ø.1Ø	Ø.1Ø	Ø.Ø9
Ø.11	Ø.Ø8	Ø.Ø5	Ø.Ø6	Ø.Ø7	Ø.Ø8	Ø.11
Ø.Ø9	Ø.11	Ø.Ø5	Ø.Ø6	Ø.Ø8	Ø.Ø8	Ø.Ø9
Ø.Ø7	Ø.Ø7	Ø.Ø8	Ø.Ø8	Ø.Ø8	Ø.1Ø	Ø.
Ø.	Ø.12	Ø.	Ø.	Ø.	Ø.	Ø.

Ø.	Ø.Ø5	Ø.Ø5	Ø.Ø7	Ø.	Ø.	Ø.
Ø.	Ø.Ø7	Ø.Ø6	Ø.Ø5	Ø.Ø6	Ø.	Ø.
Ø.Ø7	Ø.Ø8	Ø.Ø5	Ø.Ø4	Ø.Ø7	Ø.	Ø.
Ø.Ø6	Ø.Ø5	Ø.Ø4	Ø.Ø4	Ø.	Ø.	Ø.
Ø.Ø4	Ø.Ø4	Ø.Ø3	Ø.Ø5	Ø.	Ø.	Ø.Ø4
Ø.Ø5	Ø.Ø3	Ø.Ø2	Ø.Ø4	Ø.Ø6	Ø.Ø7	Ø.
Ø.Ø6	Ø.Ø4	Ø.Ø2	Ø.Ø3	Ø.Ø5	Ø.Ø5	Ø.Ø7
Ø.Ø5	Ø.Ø6	Ø.Ø3	Ø.Ø3	Ø.Ø5	Ø.Ø5	Ø.Ø5
Ø.Ø4	Ø.Ø4	Ø.Ø4	Ø.Ø4	Ø.Ø5	Ø.Ø6	Ø.
Ø.	Ø.Ø7	Ø.	Ø.	Ø.	Ø.	Ø.

layer 3

Ø.15	Ø.12	Ø.11	Ø.Ø9	Ø.	Ø.	Ø.
Ø.13	Ø.13	Ø.1Ø	Ø.12	Ø.13	Ø.	Ø.
Ø.13	Ø.11	Ø.Ø9	Ø.Ø8	Ø.Ø9	Ø.11	Ø.
Ø.11	Ø.Ø9	Ø.Ø8	Ø.Ø7	Ø.Ø9	Ø.14	Ø.13
Ø.1Ø	Ø.Ø8	Ø.Ø7	Ø.Ø7	Ø.Ø8	Ø.11	Ø.12
Ø.Ø9	Ø.Ø7	Ø.Ø6	Ø.Ø6	Ø.Ø7	Ø.1Ø	Ø.1Ø
Ø.Ø8	Ø.	Ø.Ø7	Ø.Ø6	Ø.Ø7	Ø.1Ø	Ø.12
Ø.1Ø	Ø.	Ø.	Ø.Ø7	Ø.1Ø	Ø.11	Ø.13

Ø.Ø9	Ø.Ø7	Ø.Ø6	Ø.Ø6	Ø.	Ø.	Ø.
Ø.Ø8	Ø.Ø7	Ø.Ø6	Ø.Ø7	Ø.	Ø.	Ø.
Ø.Ø7	Ø.Ø6	Ø.Ø5	Ø.Ø6	Ø.Ø7	Ø.	Ø.
Ø.Ø6	Ø.Ø5	Ø.Ø4	Ø.Ø4	Ø.Ø7	Ø.	Ø.
Ø.Ø5	Ø.Ø4	Ø.Ø4	Ø.Ø4	Ø.Ø5	Ø.Ø7	Ø.Ø7
Ø.Ø5	Ø.Ø4	Ø.Ø3	Ø.Ø4	Ø.Ø5	Ø.Ø7	Ø.Ø6
Ø.Ø5	Ø.Ø4	Ø.Ø4	Ø.Ø3	Ø.Ø5	Ø.Ø7	Ø.Ø8
Ø.Ø6	Ø.Ø5	Ø.Ø4	Ø.Ø4	Ø.Ø7	Ø.Ø7	Ø.

Ø.[illegible]	[illegible].ØØ	Ø.ØØ	[illegible].ØØ	Ø.[illegible]	.12	Ø.		Ø.Ø8	Ø.Ø5	Ø.Ø5	Ø.Ø5	Ø.Ø7	Ø.	Ø.
[illegible]	[illegible].	Ø.[illegible]	[illegible].	Ø.	[illegible].	Ø.		Ø.	Ø.Ø9	Ø.Ø[illegible]	Ø.	Ø.	Ø.	Ø.

layer 4

Ø.15	[illegible].14	Ø.15	Ø.14	Ø.15	[illegible].	Ø.		Ø.Ø9	Ø.Ø8	Ø.Ø9	Ø.Ø7	Ø.Ø8	Ø.	Ø.
[illegible]	.15	Ø.12	Ø.13	Ø.14	[illegible].	Ø.		Ø.	Ø.Ø8	Ø.Ø7	Ø.Ø8	Ø.Ø8	Ø.	Ø.
Ø.	[illegible].1[illegible]	Ø.12	Ø.14	Ø.13	Ø.16	Ø.15		Ø.	Ø.Ø9	Ø.Ø7	Ø.Ø8	Ø.Ø8	Ø.	Ø.
Ø[illegible]	[illegible].16	Ø.[illegible]	Ø.11	Ø.11	[illegible].1[illegible]	Ø.14		Ø.	Ø.Ø9	Ø.Ø6	Ø.Ø7	Ø.Ø7	Ø.Ø9	Ø.
13	.1[illegible]	Ø.11	Ø.1Ø	Ø.1Ø	.13	Ø.13		Ø.Ø8	Ø.Ø8	Ø.Ø6	Ø.Ø6	Ø.Ø7	Ø.Ø8	Ø.Ø7
[illegible]	.1[illegible]	Ø.[illegible]Ø	[illegible].11	Ø.11	.13	Ø.13		Ø.Ø9	Ø.Ø8	Ø.Ø6	Ø.Ø6	Ø.Ø7	Ø.Ø8	Ø.Ø7
[illegible]	.1[illegible]	Ø.[illegible]2	[illegible].11	Ø.12	Ø.14	Ø.14		Ø.	Ø.Ø8	Ø.Ø6	Ø.Ø7	Ø.Ø7	Ø.Ø8	Ø.Ø8
Ø	.1	Ø.12	[illegible].13	Ø.13	Ø.14	Ø.13		Ø.	Ø.Ø8	Ø.Ø7	Ø.Ø8	Ø.Ø7	Ø.	Ø.
Ø.15	.1[illegible]	Ø.13	Ø.	Ø.	Ø.	Ø.		Ø.Ø9	Ø.Ø8	Ø.Ø8	Ø.	Ø.	Ø.	Ø.

layer 5

Ø.	[illegible].11	Ø.[illegible]5	Ø.1[illegible]	Ø.15	[illegible].	Ø.		Ø.	Ø.Ø6	Ø.Ø9	Ø.Ø8	Ø.Ø9	Ø.	Ø.
Ø.	[illegible].Ø9	Ø.[illegible]6	Ø.1[illegible]	Ø.[illegible]5	[illegible].14	Ø.15		Ø.	Ø.Ø8	Ø.Ø9	Ø.Ø9	Ø.Ø9	Ø.Ø9	Ø.
Ø.	[illegible].Ø[illegible]	Ø.15	Ø.1[illegible]	Ø.16	[illegible].15	Ø.13		Ø.	Ø.Ø5	Ø.1Ø	Ø.Ø8	Ø.Ø9	Ø.Ø9	Ø.Ø9
Ø.	[illegible].1[illegible]	Ø.14	Ø.13	Ø.15	[illegible].1[illegible]	Ø.14		Ø.	Ø.1Ø	Ø.Ø9	Ø.Ø8	Ø.Ø9	Ø.Ø7	Ø.Ø8
Ø.	[illegible].1Ø	Ø.14	Ø.13	Ø.13	Ø.14	Ø.16		Ø.	Ø.Ø9	Ø.Ø8	Ø.Ø8	Ø.Ø8	Ø.Ø9	Ø.Ø8
Ø.	Ø.	Ø.16	Ø.13	Ø.13	Ø.14	Ø.16		Ø.	Ø.	Ø.Ø9	Ø.Ø8	Ø.Ø7	Ø.Ø8	Ø.Ø9
Ø.	Ø.	Ø.16	Ø.14	Ø.13	Ø.16	Ø.14		Ø.	Ø.	Ø.11	Ø.Ø9	Ø.Ø8	Ø.Ø8	Ø.
Ø 17	[illegible].15	Ø.17	Ø.15	Ø.14	Ø.14	Ø.15		Ø.	Ø.1Ø	Ø.1Ø	Ø.Ø8	Ø.Ø8	Ø.Ø9	Ø.
Ø.	Ø.	Ø.14	Ø.	Ø.	Ø.	Ø.		Ø.	Ø.	Ø.Ø8	Ø.	Ø.	Ø.	Ø.

layer 6

[illegible].1[illegible]	Ø.	[illegible].		Ø.	Ø.Ø6	Ø.	Ø.
[illegible]	Ø.15	[illegible].15		Ø.	Ø.Ø7	Ø.1Ø	Ø.

Ø.	Ø.14	Ø.14	Ø.13
Ø.	Ø.14	Ø.14	Ø.
Ø.	Ø.16	Ø.	Ø.

layer 7

Ø.	Ø.	Ø.	Ø.
Ø.	Ø.	Ø.	Ø.
Ø.	Ø.	Ø.15	Ø.12
Ø.	Ø.17	Ø.14	Ø.
Ø.	Ø.	Ø.	Ø.

layer 8

Ø.	Ø.
Ø.	Ø.13
Ø.	Ø.13

layer 9

Ø.	Ø.
Ø.	Ø.
Ø.	Ø.11

Ø.	Ø.Ø7	Ø.Ø7	Ø.Ø9
Ø.	Ø.Ø7	Ø.Ø8	Ø.
Ø.	Ø.Ø9	Ø.	Ø.

Ø.	Ø.	Ø.	Ø.
Ø.	Ø.	Ø.	Ø.
Ø.	Ø.	Ø.1Ø	Ø.
Ø.	Ø.Ø9	Ø.Ø8	Ø.
Ø.	Ø.	Ø.	Ø.

Ø.	Ø.
Ø.	Ø.Ø8
Ø.	Ø.Ø8

Ø.	Ø.
Ø.	Ø.
Ø.	Ø.Ø8